Draft v 5.01
June 20, 2011

SEARCHING for a QCD MIXED PHASE at the NUCLOTRON-BASED ION COLLIDER FACILITY (NICA White Paper)

From: "T.D. Lee" <tdl@phys.columbia.edu>
To: "Sisakian A.N." <sisakian@jinr.ru>
Sent: Wednesday, January 14, 2009 7:01 PM
Subject: Comment on the goals of the NICA heavy ion collider

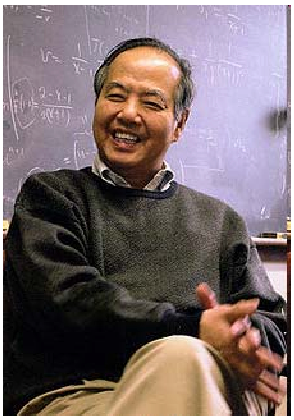

Dear Prof. Sissakian:

The NICA heavy ion collider will be a very major step towards the formation of a new phase of quark-gluon matter.

The goal of relativistic heavy ion physics is to modify the properties of the physical vacuum. Of particular interest is a possibility to create a phase of quark-gluon matter where some of the fundamental symmetries may be altered. Recent RHIC results indicate that there may be an evidence of parity violation (on an event-by-event basis) in heavy ion collisions at high energies. It would be of great importance to search for this phenomenon in the energy range covered by the NICA collider where a high baryon density is reached.

I am very much looking forward to the completion and future success of the NICA heavy ion collider. Warm regards and very best wishes,

T. D. Lee
--
T. D. Lee
University Professor
Dept. of Physics - MC 5208
Columbia University
New York, NY 10027

Foreword to the fifth Edition

The present fifth Edition of the NICA White Paper represents a milestone towards the realization of the NICA project. Besides new contributions and a revision of previous ones, in this Edition we have added a new Section "Editorial" which provides a summary of the basic parameters of the planned NICA accelerator facility, such as their beam characteristics and design parameters. This new Section also gives an overview on the physical phenomena which shall be investigated and the experimental observables which are suggested to reach this goal. Table 1.1 in Subsection 1.1 summarizes the most promising suggestions contained in the White Paper with reference to the chapters where more details are given. It shall be regarded as an important step towards a more detailed scientific programme for the NICA facility and shall help to identify the discovery potential of NICA in the context of the existing and planned heavy-ion collision experiments at RHIC, CERN and FAIR.

We hope that the present Edition of the NICA White Paper will prove useful for the further development of scientific collaborations for the NICA/MPD and BM@N experiments.

Yours sincerely,

D. Blaschke,
D. Kharzeev,
V. Matveev,
A. Sorin,
H. Stöcker
O. Teryaev,
I. Tserruya,
N. Xu

Foreword to the fourth Edition

The present fourth Edition of the NICA White Paper became necessary not only because newly submitted contributions had to be included to this open forum for the discussion of the "search for the quark-hadron mixed phase and QCD critical point". After the third Edition had been released in June 2010, an additional programme is being developed at the NICA facility for fixed target experiments with heavy ion beams extracted from the Nuclotron-N at energies up to $E_{\rm lab} = 5.5$ AGeV (start date: 2014). This programme was discussed, e.g., at the V$^{\rm th}$ Round Table Workshop "Physics at NICA" held on August 28, 2010, during the 6$^{\rm th}$ International Workshop on "Critical Point and Onset of Deconfinement" (Dubna) and at a dedicated Meeting on "Fixed target @ Nuclotron-N and SIS100 @ FAIR" (GSI Darmstadt, November 3, 2010). Links to these events are to be found on the NICA White Paper Wikipage

http://theor.jinr.ru/twiki-cgi/view/NICA/WebHome

Accordingly, we have introduced a new section for "Fixed target experiments" in the present Edition which contains already three new contributions.

Moreover, we have split from the big section 2 on "Phases of QCD matter at high baryon density" (which grew too big) a new section dedicated to "Hydrodynamics and hadronic observables" and reordered the contributions correspondingly.

Among the new contributions (marked in red) to this Edition the reader will find for the first time contributions on astrophysical constraints on dense matter and on lattice QCD, which put the NICA programme into a broader context. A separate contribution is devoted to the challenging new idea of a so-called "quarkyonic phase" and a triple point in the QCD phase diagram which directly concern the energy range of experiments planned at NICA.

With the present fourth Edition the NICA White Paper has grown to some maturity but it is still considered an open process and an invitation to the international heavy-ion physics community for collaborating with NICA and for discussing the physics of dense matter.

We are looking forward to your contribution!

Yours sincerely,

D. Blaschke,
D. Kharzeev,
A. Sorin,
O. Teryaev,
V. Toneev,
I. Tserruya

Foreword to the first Edition

Theoretical and experimental investigations of the QCD phase diagram belong to the most topical research directions in modern physics. The search for the quark-gluon plasma (QGP) at RHIC Brookhaven and CERN SPS has revealed first indications for rich physics going beyond the naive picture of a gas of quarks and gluons: a strongly coupled QGP (sQGP). Results from the energy scan program of the NA49 experiment, however, suggest that the physics of the onset of the hadron-to-quark matter transition should be expected at lower c.m. energies of the colliding heavy-ion systems. Therefore, new experimental programs are being developed which aim at investigations of the QCD phase diagram at lower temperatures and high baryon densities: low-energy RHIC, NA61 (SHINE), CBM @ FAIR Darmstadt and NICA-MPD in Dubna.

The Nuclotron-based Ion Collider fAcility (NICA) with its multi-purpose detector (MPD) has been defined as the new flagship of the Joint Institute for Nuclear Research (JINR) Dubna within the roadmap for the JINR development. Being the "CERN of the East", the JINR Dubna plans to provide with this instrument a dedicated collider experiment for exploring the high density region of the QCD phase diagram, thus filling a niche in the global plans.

In order to support the realization of heavy-ion collider facilities like NICA, it is important to continue the process of theory-experiment discussions which has been initiated with the now completed CBM White Book. As it has become clear during the preparations for the CBM experiment, it is of utmost importance to use the chance which a new experiment provides in order to stimulate this dialogue and to trigger the generation of new and the sharpening of known ideas on the phase structure of dense QCD and the possibilities for its experimental verification.

In this spirit, a series of Round Table discussions on the development of the NICA project has been organized, the next one on "Physics at NICA" to be held at JINR Dubna in the week of September 7 - 11, 2009.

In preparation of this event, a call for contributions to the physics programme at NICA has been issued in April 2009 and a Wiki-page has been created to provide a public forum making the submitted suggestions accessible to the community at:

http://theor.jinr.ru/twiki-cgi/view/NICA/WebHome

At the present stage, we have decided to assemble the submitted material into a unified document as a basis for the clarification of the key topics for the preparation of NICA and above mentioned experiments:

- Phases of dense QCD matter and conditions for their possible realization
- Characteristic processes as indicators of phase transformations
- Estimates for events and event rates
- Comparison to other experiments
- Interdisciplinary aspects, e.g. astrophysical constraints for dense matter phases

shall be continuously all interested at the Bogoliubov Laboratory for Theoretical Physics in Dubna (please, find attached the file with brief information on the NICA project) and invite you to participate in a discussion of the Physics potential of such a facility! As a forum for the discussions we will organize a Round Table on "Physics at NICA", to be held at JINR Dubna, tentatively in the week September 7 - 11, 2009. In preparation of this event, and

The recent developments in dense matter physics have shown that we must be prepared for the unexpected! Three examples:

- Only ten years ago, Frank Wilczek and Edward Shuryak with their groups have initiated the exploration of color superconducting quark matter which triggered an avalanche of papers with suggestions how the dense QCD phase diagram should look like and what consequences one could expect for the explanation of astrophysical phenomena. Unfortunately, up to now we don't know what dilepton spectrum we should expect from diquark annihilation in superconducting quark matter!

- Just two years ago, Rob Pisarski and Larry McLerran found out that in dense QCD chiral symmetry restoration may not be accompanied with deconfinement and suggested that in the yet unexplored high-density corner of the QCD phase diagram we shall find "quarkyonic matter", a quantum liquid of confined, but massless quarks! What observables shall identify such a phase once it gets "accidentally" created in a heavy-ion collision? We don't know yet.

- Last not least, Dmitry Kharzeev and collaborators suggested an observable effect from P-parity violation in heavy ion collisions - is this effect relevant for the exploration of dense matter phases?

We need to identify the challenges and the discovery potential of such machines like NICA, creating the densest forms of matter in terrestrial laboratories. It requires concerted efforts to understand the stuff which constitutes the interiors of neutron stars and governs fantastic astrophysical phenomena like supernova explosions and neutron star mergers, the possible origins for the mysterious gamma-ray bursts and cosmic rays. In order to support the process of construction or modification of heavy-ion collider facilities which would be suitable to study QCD phase transformations at high baryon densities in laboratory experiments (see Appendix for a sketch of the QCD phase diagram), we invite you to contribute with your expertise to a "White Paper" under the working title:

"Searching for the mixed phase of QCD matter at the Nuclotron-based Ion Collider fAcility".

In order to initiate the process and estimate the spectrum of items, we suggest that you draft your brainstorming ideas on just one or two pages and send them to the editors (nica@theor.jinr.ru). In the week April 12-18, we will assemble the ideas into topics on a Wiki Forum, which shall be maintained by the NICA group at JINR. We expect that the creation and feeding of such a forum accessible to all researchers involved in theoretical and experimental investigations of superdense QCD matter will prove successful whenever the actual status and potential of dense matter research shall be discussed or reported.

After another iteration of the available inputs during May, a first version of the "White Paper" shall be prepared by the NICA group, to be ready for presentation at the Program Advisory Committee on Particle Physics meeting beginning June in Dubna.

We are looking forward to your contribution!

Yours sincerely,

D. Blaschke,
D. Kharzeev,
A. Sissakian,
A. Sorin,
O. Teryaev,
V. Toneev,
I. Tserruya

Contents

1 **Editorial** . . . 11
1.1 Physical phenomena and relevant observables . . . 11
1.2 Parameters of the NICA accelerator facility . . . 12
2 **General aspects** . . . 16
2.1 MPD at the JINR NICA in the landscape of heavy ion projects
M. Gazdzicki . . . 16
2.2 Comments on the Mixed Phase Physics (MPP)
Nu Xu . . . 17
2.3 Experimental advantages of collider over fixed target
B. Mohanty . . . 18
2.4 Observables and open problems for NICA
E. Bratkovskaya[a] and W. Cassing[b] . . . 20
2.5 Exploring high-density baryonic matter: Maximum freeze-out density
J. Randrup[a] and J. Cleymans[b] . . . 21
2.6 Nuclear matter physics at NICA
Peter Senger . . . 23
3 **Phases of QCD matter at high baryon density** . . . 32
3.1 Comments on a phase diagram and fluctuations
M. Stephanov . . . 32
3.2 Search for manifestation of medium effects in dense, excited hadron-quark matter
D. Voskresensky . . . 34
3.3 Searching for evidence of spinodal decomposition
J. Randrup . . . 35
3.4 Supercooled quark-gluon phase?
Yu. Ivanov . . . 36
3.5 Rigorous investigation of surface tension and finite width of the QGP bags at NICA energies
K. Bugaev . . . 37
3.6 Isospin effects on phase transitions of hadronic to quark matter
M. Di Toro[a,b], V. Greco[a,b], B. Liu[c,d], and S. Plumari[2] . . . 39
3.7 Accessibility of dense QCD phases in heavy-ion collisions
D. Blaschke[a,b], F. Sandin[c,d], V. Skokov[b,e,f] and S. Typel[e,g] . . . 42
3.8 Transitional change to baryon-rich QCD matter at NICA energy
K. Fukushima . . . 44
3.9 Triple point and quarkyonic matter in the QCD phase diagram
L. McLerran[a], K. Redlich[b,c], D. Blaschke[b,d] . . . 45
3.10 Search for the QCD Critical Point at NICA
X. Luo[a,c], B. Mohanty[b], H.G. Ritter[c], N. Xu[c] . . . 47
3.11 Probing the hadron-quark mixed phase at finite temperature, baryon and isospin chemical potentials
G.Y. Shao[a], M. Di Toro[a,b], M. Colonna[a], S. Plumari[a,b], B. Liu[c,d], V. Greco[a,b], Y.X. Liu[e,f] 49
4 **Hydrodynamics and hadronic observables** . . . 63

4.1 Hadronic signals of non-equilibrium phase transition
B. Tomášik . . . 63
4.2 Scalar mesons properties at finite temperature and density at NICA energy
P. Costa[a] and Yu.L. Kalinovsky[b] . . . 63
4.3 Hadron abundances at high baryon density
H. Satz . . . 65
4.4 Directed flow as a signal of a liquid state of transient matter
S. M. Troshin . . . 66
4.5 Importance of third moments of conserved charges in relativistic heavy ion collisions
M. Asakawa . . . 73
4.6 Baryon Stopping in Heavy-Ion Collisions at $E_{\rm lab}$ = 2–160 GeV/nucleon
Yu.B. Ivanov[a,b] . . . 75
4.7 Statistical hadronization phenomenology in a low-energy collider
G. Torrieri[a,b] . . . 79
4.8 Flow scaling in a low energy collider: When does the perfect fluid turn on?
G. Torrieri[a,b] . . . 81
4.9 Dissipative hydrodynamics effects at NICA
L. Turko . . . 83
4.10 Hadronic Fluctuations, freeze-out conditions and the QCD (phase) transition line
F. Karsch[a,b] and C. Schmidt[c,d] . . . 85
4.11 Exploring hybrid star matter at NICA
T. Klähn[a], D. Blaschke[b,c], F. Weber[d] . . . 89
4.12 Testing Hadron Formation and Exotic Bound States in Heavy Ion Collisions at NICA
R. Bellwied[a], C. Markert[b] . . . 91
5 **Femtoscopy, correlations and fluctuations** . . . 98
5.1 Femtoscopic search for the 1-st order phase transition
R. Lednicky . . . 98
5.2 Brief arguments for studying azimuthally sensitive HBT
M. Lisa . . . 99
5.3 Physics at NICA-MPD: particle correlations
V. A. Okorokov . . . 101
5.4 Event-by-event fluctuations in nucleus-nucleus collisions
M. Gorenstein . . . 103
5.5 Flow and freeze-out in relativistic heavy-ion collisions at NICA
L. Bravina and E. Zabrodin . . . 103
5.6 Perspectives of anisotropic flow measurements at NICA
V. Korotkikh, I. Lokhtin, L. Malinina, S. Petrushanko, L. Sarycheva, A. Snigirev . . . 104
5.7 Fluctuations and non-equilibrium processes in collective flow
Takeshi Kodama . . . 105
5.8 The prospects for experimental study of directed, elliptic, and triangular flows in asymmetric heavy ion collisions at NICA energies
M. Bleicher[a,c], K. A. Bugaev[b], P. Rau[a,c], A. S. Sorin[d], J. Steinheimer[a,c] and H. Stöcker[a,e] 107
6 **Mechanisms of multi-particle production** . . . 114
6.1 My several thoughts on NICA
E. Levin . . . 114
6.2 Some issues in NICA-related research at LPI
I. Dremin and A. Leonidov . . . 115
6.3 Hydrokinetic analysis of space-time evolution and properties of strongly interacting matter formed at the NICA and FAIR energies
Yu. Sinyukov . . . 115
6.4 Open and hidden strangeness production
E. Kolomeitsev and B. Tomášik . . . 117
6.5 Chemical freeze-out and strangeness production study at NICA
F. Becattini . . . 118

6.6 MEMO production at high baryon densities
Marcus Bleicher[a,b], Jan Steinheimer[a,b] . . . 119
7 **Electromagnetic probes and chiral symmetry in dense QCD matter** . . . 123
7.1 Low-mass dileptons at NICA
I. Tserruya . . . 123
7.2 Dileptons at NICA
K. Gudima[a] and V. Toneev[b] . . . 124
7.3 Electromagnetic probes on NICA
Kh. Abraamyan and A. Friesen . . . 125
7.4 Solving the problem of anomalous J/ψ suppression at NICA MPD
A.B.Kurepin and N.S.Topilskaya . . . 127
7.5 Low energy J/ψ-hadron interactions
H. Satz . . . 128
7.6 J/ψ production in high energy nuclear collisions
P. Zhuang . . . 129
7.7 Soft photons at NICA
V. V. Avdeichikov[a], E. S. Kokoulina[a,b], A. Ya. Kutov[c], V. A. Nikitin[a], I. A. Rufanov[a] . 134
8 **Local $\mathcal{P}$ and $\mathcal{CP}$ violation in hot QCD matter** . . . 141
8.1 Topologically induced local $\mathcal{P}$ and $\mathcal{CP}$ violation in hot QCD matter
D. Kharzeev . . . 141
8.2 Magnetic effects in QCD vacuum: lattice view
P.V. Buividovich[a,b], M.N. Chernodub[b], E.V. Luschevskaya[b] and M.I. Polikarpov[c] . . . 142
8.3 Rich physics of non-central heavy-ion collisions
S. Voloshin . . . 143
8.4 Spontaneous $\mathcal{P}$-violation in dense matter accessible with NICA
A. Andrianov[a], V. Andrianov[a] and D. Espriu[b] . . . 144
8.5 On $\mathcal{CP}$ violation in heavy-ion collisions at the NICA energy
V. Skokov and V. Toneev . . . 146
8.6 Chiral vortaic effect and neutron asymmetries at NICA
O. Rogachevsky[a,b], A. Sorin[a,c] and O. Teryaev[a,c] . . . 148
9 **Cumulative processes** . . . 154
9.1 New forms of QCD matter and cumulative processes
A. Kaidalov . . . 154
9.2 The study of dense cold nuclear matter with cumulative trigger
A. Stavinskiy, O. Denisovskaya, Yu. Zaitsev, K. Mikhailov, P. Polozov, M. Prokudin, V. Stolin, R. Tolochek, S. Tolstoukhov and G. Sharkov . . . 155
10 **Polarization effects and spin physics** . . . 158
10.1 Polarization effects in heavy ions collisions at NICA
A. Efremov, O. Teryaev and V. Toneev . . . 158
10.2 Spin physics
A. Efremov, A. Nagaytsev, I. Savin, O. Shevchenko and O. Teryaev . . . 159
10.3 Polarization of Λ^0 hyperons in nucleus-nucleus collisions at MPD
V. Ladygin, A. Jerusalimov and N. Ladygina . . . 161
10.4 Possible effect of mixed phase and deconfinement upon spin correlations in the $\Lambda\bar{\Lambda}$ pairs generated in relativistic heavy-ion collisions
V.L. Lyuboshitz and V.V. Lyuboshitz . . . 163
11 **Related topics** . . . 169
11.1 Determination of the equation of state of dense matter
S. Fantoni[a], S. Gandolfi[b], A. Illarionov[c], F. Pederiva[c,d] and K. Schmidt[e] . . . 169
11.2 Relativistic nuclear fusion reactions and QED of strong fields: novel possibilities at the NICA facility
A. Kovalenko, A. Sissakian and A. Sorin . . . 170

11.3 Development of highly charged ion sources for NICA injector and its possible applications for nanofabrication and in medicine
D.E. Donets, E.D. Donets, E.E. Donets, V.V. Salnikov V.B. Shutov . . . 171
12 **Fixed Target Experiments** . . . 175
12.1 Measurement of Elementary Cross Sections
J. Aichelin[1], M. Bleicher[2], E. Bratkovskaya[2], C. Hartnack[1] . . . 175
12.2 Search for scaling onset in exclusive reactions with lightest nuclei at NUCLOTRON using fixed target.
Yu.N. Uzikov . . . 176
12.3 Measurement of strange particle production in the NICA fixed-target program
V. Friese . . . 178
12.4 Fixed target mode: correlations in relative 4-velocity space
V.A. Okorokov . . . 180

1 Editorial

1.1 Physical phenomena and relevant observables

The realization of the NICA project has been started at the Joint Institute for Nuclear Research (JINR) in Dubna as a flagship project in High Energy Physics. In addition to beams extracted from the Nuclotron (the existing accelerator of heavy ions) the project foresees the construction of a Nuclotron based Ion Collider fAcility (NICA) and a Multi-Purpose Detector (MPD).

With the energy range of $\sqrt{s_{\rm NN}} = 4 - 11$ GeV, the collider experiment will provide a unique possibility to explore properties of strongly interacting matter in a region of temperatures and baryon densities where the critical point (and possibly a triple point) is suspected in the QCD phase diagram (see the left panel of the Fig. 1.1). As it is indicated in a series of theoretical works (see, e.g., Cleymans and Randrup in the following Section), for heavy ion collisions within this energy range the highest possible baryon densities at freeze-out are reached (see the right panel of the Fig. 1.1).

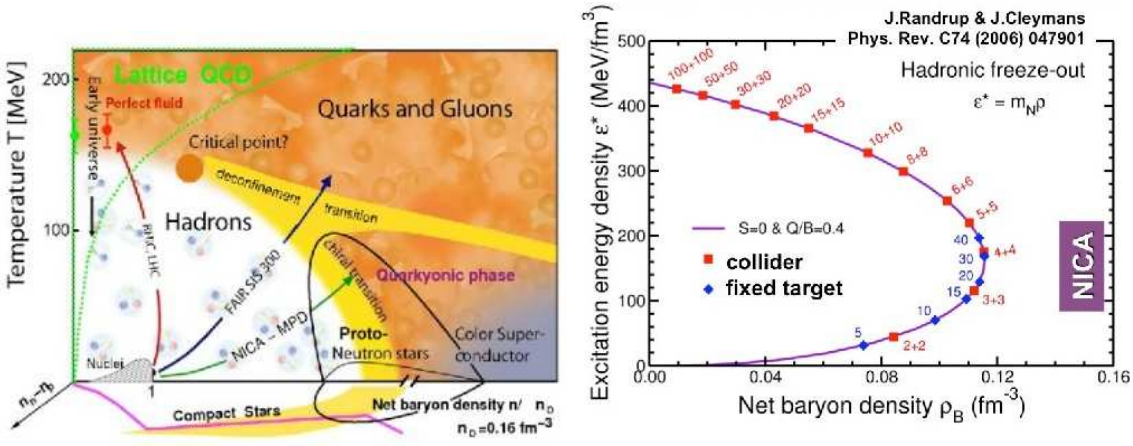

Figure 1.1: Left panel: QCD phase diagram. Right panel: Barion density in A + A collisions.

The experimental program aims at investigating physical properties and phenomena in hot and dense baryonic matter such as:

- in-medium modification of hadron properties (MMH)
- the nuclear matter equation of state (EoS);
- the onset of deconfinement (OD) and/or
- chiral symmetry restoration (CSR);
- signals of a phase transition (PT);
- the mixed phase and the critical end-point (CEP);
- possible local parity violation in strong interactions (LPV).

This shall be achieved by measuring of a large variety of observables under systematically changing conditions (energy, centrality, system size). An attempt to summarize the correlations between observables and physical phenomena is given in the Table 1.1. This table shall provide a basis for the development of the scientific program to be pursued at the NICA accelerator facility, with the BMN experiment (fixed target mode) and the MPD experiment (collider mode). For details on the technical parameters of these experiments, see the following Section.

Observables	Physical Phenomena							Reference in the White Paper
	MMH	EoS	OD	CSR	PT	CEP	LPV	
hadron and light nuclei yields	x	x	x	x				3.6, 3.9, 4.3, 3.11, 4.12
yields and spectra of multi-strange hyperons	x	x	x					2.6, 6.4, 12.3, 5.3
electromagnetic probes			x	x				7.1, 7.2, 7.3, 7.7
azimuthal charged particle correlations					x		x	8.1 - 8.6, 10.4
event-by-event (EBE) fluctuations						x		2.1, 2.6, 3.10, 5.4
EBE directed, elliptic and triangular flow of hadrons		x	x		x			4.4, 4.8, 5.8
higher moments of hadron distributions			x		x	x		3.10, 4.5, 4.6, 4.10
interferometric parameters		x			x			3.5, 5.1, 5.2, 5.5

Table 1.1: The correlations between observables and physical phenomena.

1.2 Parameters of the NICA accelerator facility

The Nuclotron is an existing accelerator facility of JINR in HEP put in operation in 1993. It is based on the unique technology of superconducting fast cycling magnets developed at JINR. The Nuclotron provides proton, polarized deuteron and multi-charged ion beams. The layout of the planned NICA facility and its components is shown in the Fig. 1.2

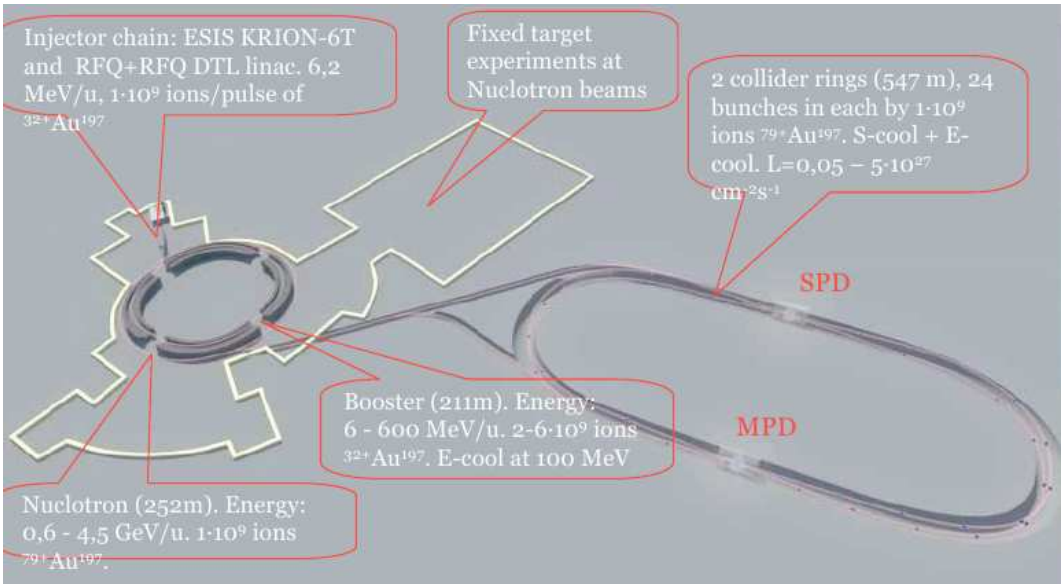

Figure 1.2: NICA facility and its components.

The maximum magnetic field of dipole magnets $B = 2.0$ T corresponds to the ion beam energies:

- 5.81 GeV/u for d (A = 2, Z = 1);
- 3.64 GeV/u for Xe (A = 124, Z = 42); and
- 4.56 GeV/u for Au (A = 197, Z = 79).

The new accelerator facility NICA includes:

- an injector complex providing wide spectrum of ions up to the heaviest one $^{197}Au^{32+}$ at the energy 6.2 MeV/u with an intensity $2 \cdot 10^9$;
- a booster accelerating ions up to 600 MeV/u;
- the Nuclotron continuing acceleration up to the maximum energy (4.5 GeV/u) and
- two storage rings with two interaction points (IP).

Beam	Intensities, particles per cycle				
	Energy	GSI (SIS18)	Nuclotron-M (2010)	Planned with Nuclotron-N (2012)	Planned with new ion source and booster (2014-2015)
p	4.5 GeV	$2 \cdot 10^{10}$	$8 \cdot 10^{10}$	$5 \cdot 10^{11}$	$5 \cdot 10^{12}$
d	2.2 GeV	$5 \cdot 10^{11}$	$8 \cdot 10^{10}$	$5 \cdot 10^{11}$	$5 \cdot 10^{12}$
^{4}He			$2 \cdot 10^9$	$3 \cdot 10^{10}$	$1 \cdot 10^{12}$
$d\uparrow$			$2 \cdot 10^8$	$7 \cdot 10^{10}$ (SPI)	$7 \cdot 10^{10}$ (SPI)
$^7Li^{6+}$			$7 \cdot 10^9$	$3 \cdot 10^{10}$	$5 \cdot 10^{11}$
$^{12}C^{6+}$	300 MeV	$7 \cdot 10^{10}$	$6 \cdot 10^9$	$3 \cdot 10^{10}$	$3 \cdot 10^{11}$
$^{24}Mg^{12+}$	300 MeV	$5 \cdot 10^{10}$	$7 \cdot 10^8$	$4 \cdot 10^9$	$5 \cdot 10^{10}$
$^{40}Ar^{18+}$	300 MeV	$6 \cdot 10^{10}$	$8 \cdot 10^6$	$2 \cdot 10^9$	$2 \cdot 10^{11}$
$^{56}Fe^{28+}$			$4 \cdot 10^6$	$2 \cdot 10^9$	$5 \cdot 10^{10}$
$^{58}Ni^{26+}$	300 MeV	$8 \cdot 10^9$			
$^{84}Kr^{34+}$	0.3-1 GeV	$2 \cdot 10^{10}$	$2 \cdot 10^5$	$1 \cdot 10^8$	$1 \cdot 10^9$
$^{124}Xe^{48/42+}$	0.3-1 GeV	$1 \cdot 10^{10}$	$1 \cdot 10^5$	$7 \cdot 10^7$	$1 \cdot 10^9$
$^{181}Ta^{61+}$	1 GeV	$2 \cdot 10^9$			
$^{197}Au^{65/79+}$		$3 \cdot 10^9$		$1 \cdot 10^8$	$1 \cdot 10^9$

Table 1.2: The modernization stages and the beams provided by the Nuclotron.

The ions are additionally stripped before the injection into the Nuclotron. The major parameters of the NICA collider are following:

- $B\rho_{\max} = 45$ Tm;
- vacuum in the beam chamber 10^{-11} Torr;
- maximum dipole field 2 T;
- kinetic energy from 1 GeV/u to 4.5 GeV/u for Au^{79+} ;
- zero beam crossing angle at IP;
- 9 m space for detector allocations at IP's;
- average luminosity for heavy ions $1 \cdot 10^{27}$ cm^{-2}s^{-1} (at 3.5 GeV/u).

For the modernization stages and the beams provided by the Nuclotron, see the Table 1.2.

The required Nuclotron upgrade has started in 2008 and will be fully completed by 2014. A booster and new linac will be put in operation. The overall construction schedule foresees that the storage ring and basic infrastructure facility should be available for the first ion collisions already in 2016.

The BMN Experiment

beam	p	d	^{7}Li	^{12}C	^{24}Ar	^{56}Fe	^{84}Kr	^{124}Xe	^{197}Au
intensity/s	$5 \cdot 10^{12}$	$5 \cdot 10^{12}$	$5 \cdot 10^{11}$	$2 \cdot 10^{11}$	$2 \cdot 10^{11}$	$5 \cdot 10^{10}$	$1 \cdot 10^{9}$	$1 \cdot 10^{9}$	$1 \cdot 10^{9}$

Table 1.3: A typical variety of possible beams and their intensities provided by the Nuclotron-NICA accelerator complex per cycle (5 s).

The energy of the extracted beams provided by upgraded Nuclotron-NICA will finally reach 5.81 GeV/u for typical values of A/Z = 2. A typical variety of possible beams and their intensities provided by the Nuclotron-NICA accelerator complex per cycle (5 s) is presented in the Table 1.3.

To realize the first stage of experiments at extracted beams with a fixed target a new set-up – BMN (Baryonic Matter at Nuclotron) will be constructed using an existing dipole magnet, tracking devices and other necessary parts for particle ID etc. The new silicon vertex detector will be constructed in cooperation with the partners from GSI (Darmstadt). Further details, such as the layout of the BMN detector and its components are presently under development. The NICA White Paper contributions shall assist in this process.

The MPD Experiment

The MPD experiment should be competitive and at the same time supplementary to the ones operating at RHIC, and those constructed in the framework of the FAIR project. The MPD will be installed at the first IP of NICA. The major sub-detectors of the MPD are (see Fig.1.3):

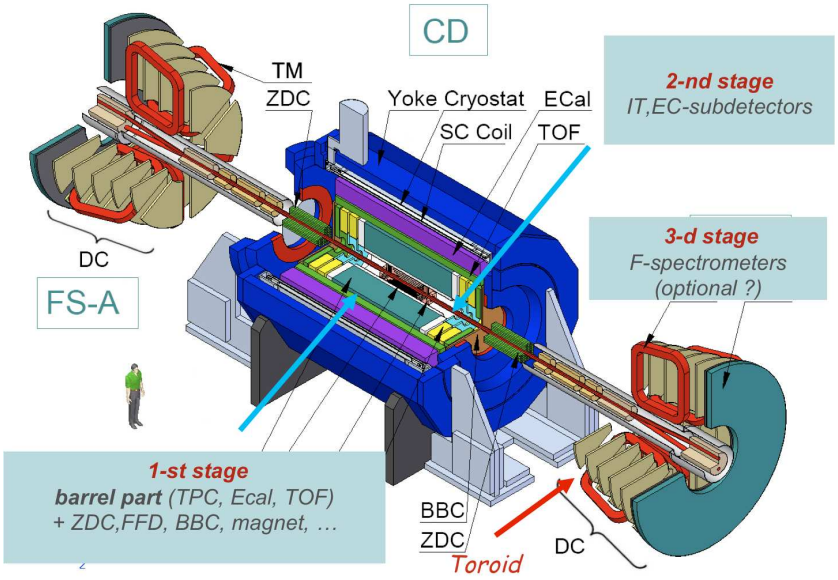

Figure 1.3: The MPD.

- a solenoidal superconducting magnet with a magnetic field of 0.5 T (5 m in diameter and 8 m in length);
- a time projection chamber (TPC);
- an inner tracker (IT);
- a time-of-flight (TOF) system;
- an electromagnetic calorimeter (ECAL);
- an end cap tracker (ECT) and
- two forward spectrometers based on toroidal magnets (optional).

Three stages are foreseen for putting MPD into operation. The first stage of operation involves magnet, TPC, TOF, ECAL (partially) and IT (partially), and should be ready for the first collision of beams in 2016.

The processes studied with MPD were simulated using the dedicated software framework (MpdRoot). This software is based on the object-oriented framework FairRoot and provides a powerful tool for detector performance studies, development of algorithms for reconstruction and physics analysis of the data. The evaluated rate in Au + Au collisions at $\sqrt{s_{\rm NN}} = 7.1$ GeV (10 % central interactions) taking into account the luminosity of $L = 10^{27}$ cm^{-2}s^{-1} is 7 kHz. More than ten working groups from 12 institutions are intensively working on sub-detector R&D, and on prototyping of all detector elements. Further detailed information could be found in the corresponding conceptual design report. It has been shown that the MPD is well optimized for the study of in-medium effects caused by high baryon densities, such as: changing particle properties in the hot and dense medium (broadening of spectral functions etc.), event-by-event dynamical fluctuations of strange to non-strange particle ratios, and others. These studies could be done with better precision than the one achieved at presently performed experiments. The simulations of the MPD experiment show that a high statistics of studied events could be accumulated (10^9 minimum bias events and 10^8 central events per week) which provide the best precision for femtoscopy studies with respect to RP correlation of multistrange particles. In ten weeks of running more than 10^7 of Ω-decays will be recorded.

Charged particles are reliably identified using both techniques: by measuring the dE/dx of tracks in the TPC, and by the TOF system. A sufficiently high resolution of vertex reconstruction has been obtained, as illustrated in the left panel of the Fig. 1.4.

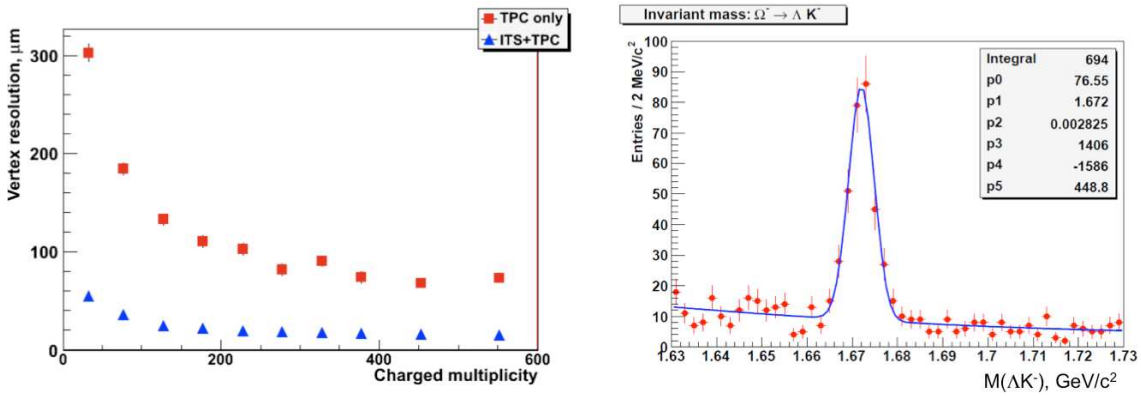

Figure 1.4: Left panel: The resolution of vertex reconstruction. Right panel: $\Omega \to \Lambda K^-$ decay reconstruction.

The right panel of this figure also shows the example of an $\Omega \to \Lambda K^-$ decay reconstruction implementing the full chain of simulations: central Au + Au collision generation at $\sqrt{s_{\rm NN}} = 7.1$ GeV; hyperon productions and decays; decay product detection and their reconstruction using necessary MPD subdetectors.

2 General aspects

The contributions in this section address the important question of the niche that will be occupied by the NICA project within the current and planned international effort on heavy ion research. The physics in the energy range of the NICA collider has been studied in the experiments at CERN SPS; this program will soon be extended at RHIC during the low energy scan, and then eventually at the FAIR facility. RHIC will work in the collider mode similarly to what is planned at NICA, whereas CERN and FAIR use the fixed target. The forthcoming experimental results from RHIC will help to identify even more precisely the most promising directions for research that would benefit from a higher beam luminosity at NICA and a dedicated detector design. Regarding the comparison to FAIR, the approaches taken by FAIR and NICA are complementary to each other – the fixed target at FAIR makes easier access to rare probes, whereas the collider set-up at NICA provides a symmetrical, uniform and energy-independent acceptance that is beneficial for the studies of various fluctuations and correlations.

2.1 MPD at the JINR NICA in the landscape of heavy ion projects

M. Gazdzicki

Institut für Kernphysik, University of Frankfurt, Frankfurt, Germany;
J. Kochanowski University, Kielce, Poland

A. MPD [1] at NICA together with **CBM** [2] at SIS-100/300 belong to the third generation of experiments planned to study nucleus-nucleus collisions at energies of the CERN SPS. Heavy ion physics in this energy range is very attractive for experimentalists and theorists mainly due to two reasons.

- First, following predictions of Ref. [3] the NA49 discovered a rapid change of the energy dependence of hadron production properties in central Pb+Pb collisions which starts at about $E_{\rm lab}$ =30 AGeV ($\sqrt{s_{\rm NN}} \approx$ 7.6 GeV) [4]. This result gives an evidence for the onset of deconfinement at the low CERN SPS energies. Clearly, the pilot NA49 study should be followed by systematic and precision measurements.

- Second, the critical point of strongly interacting matter may be located in the phase diagram region accessible in heavy ion collisions at energies larger than the energy of the onset of deconfinement ($\sqrt{s_{\rm NN}} \approx$ 7.6 GeV) [5]. Thus, measurements in this domain may lead to a discovery of the critical point.

B. The three generations of the experiments at energies of the CERN SPS are:

- NA49 at the CERN SPS. The pilot study of the energy dependence of hadron production properties in central Pb+Pb collisions, which resulted in the discovery of the onset of deconfinement [3]. The detector was designed for the study of hadron production at the top SPS energy and not optimized for the performed energy scan. Data were registered in the period 1999-2002.

- NA61 [6] at the CERN SPS and STAR/PHENIX [7] at the BNL RHIC. The second generation study will be performed with the beams and detectors originally designed for the top SPS and RHIC energies and subsequently upgraded/optimized for the new measurements, in particular for the study of event-by-event fluctuations. The basic goals are: systematic studies of the onset of deconfinement and search for the critical point. The two dimensional scans in the plane (system-size/centrality)-(energy) will be performed. Data will be registered in the period 2009-2014.

- MPD at the JINR NICA and CBM at the FAIR SIS-100/300. The third generation studies which are planned to be performed using dedicated accelerators and detectors. Due to the financial/technical constraints the maximum energy will be about $\sqrt{s_{\rm NN}} \approx 11$ GeV for MPD and $\sqrt{s_{\rm NN}} \approx 8$ GeV for CBM. In the latter case the event rate will be orders of magnitude higher than the NA61 and STAR/PHENIX one. The basic goals are precision studies of the properties of the dense confined matter and of the transition to the deconfined phase. The first data are expected in 2015.

C. The above information provokes **general comments** concerning the third generation projects.

- Planning and construction of the third generation projects starts well before the results of the second generation experiments are known. In particular, it may happen (as suggested by the first NA49 results [8]) that the critical point will be discovered close to the top SPS energy, $\sqrt{s_{\rm NN}} \approx 17$ GeV, i.e. above the maximum energies of NICA and SIS-300. It would be important to consider a possibility of future upgrades to higher energies.

- The performance of the second generation experiments is limited by the use of the facilities which were originally designed for other studies. This, in particular, negatively impacts event-by-event fluctuation and correlation measurements and excludes studies of low cross section processes. The third generation projects should be designed in order to overcome these limitations.

D. The third generation projects, MPD at the JINR NICA and CBM at the FAIR SIS-100/300 are to a large extend complementary. The fixed target collision geometry and a very high event rate make the CBM experiment ideal for the study of rare probes of dense confined matter. The collider collision geometry of the MPD project allows to have a complete and uniform acceptance. The designed maximum energy is significantly above the energy of the onset of deconfinement. These two features make the MPD project perfect for the study of fluctuation and correlation probes of the transition between confined and deconfined matter.

Clearly, there will be a significant overlap between the MPD and CBM measurements which will allow for important cross-checks of the final results.

E. A significant progress in comparison to the second generation experiments and complementarity with the CBM project will be achieved by the MPD at the JINR NICA providing the following.

The MPD detector will allow for:

- charged particle measurements in the full acceptance,

- measurements of proton and neutron spectators of both colliding nuclei,

- an almost unique particle identification in a a large acceptance. The scans in two dimensional planes, (system-size)-(energy) and (centrality)-(energy), will be performed.

2.2 Comments on the Mixed Phase Physics (MPP)

Nu Xu

Nuclear Science Division, Lawrence Berkeley National Laboratory, Berkeley, CA, USA

Number-of-quark scaling in event anisotropy (n_q-scaling of v_2)

In high-energy nuclear collisions at RHIC, the scaling of the event anisotropy v_2 for all hadrons has been observed providing a clear evidence for the formation of a partonic system in such collisions [9]. In order to reach the observed scaling, the system must have been in the state of deconfinement, and hadrons are then formed via coalescence [10, 11]. In case of hadron gas or mix-phase, on the other hand, the scaling will be violated. Results of simulations, for Au + Au collisions at $\sqrt{s_{\rm NN}} = 9$ GeV, from both partonic and hadronic system are shown in Fig. 2.1. Therefore the measurement of v_2 for (π, K, ρ, p, ϕ, Λ, Ξ, Ω) will provide info on the nature of the system created in the collision. It is important to point out that when the system at the mixed phase the expansion is stalled one expects a reduction of the strength of the collective flow. This has been predicted in Ref. [12]. For this study, the measurement of the v_1 (the direct flow) and v_2 for (π, K, p) and a function of the bombarding energy should be sufficient.

The measurement requires the capability for determine event plane, preferably at high rapidity range in order to avoid auto correlations and particle identification.

High order correlation of net-proton

Recent Lattice Gauge Theory (LGT) calculations [13, 14, 15] predicted a spike in quark susceptibility ratios χ_4/χ_2 at the finite values of temperature and chemical potential, see Fig. 2.2.

On the other hand, for a system with hadronic degrees of freedom, the ratio is expected to be one. *The secret of the degrees of freedom of the system is reflected by the ratio of susceptibilities.* In an experiment,

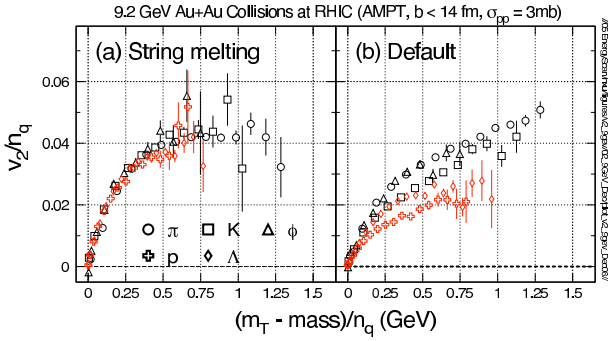

Figure 2.1: Number of quark scaled v_2 plotted as a function of the transverse mass (m_T-mass)/n_q, also scaled by n_q. Plot (a) and (b) represent partonic and hadronic system, respectively. It is clear that in the hadronic case no scaling in v_2 is observed in this simulation. The AMPT model [12] is used in the simulations.

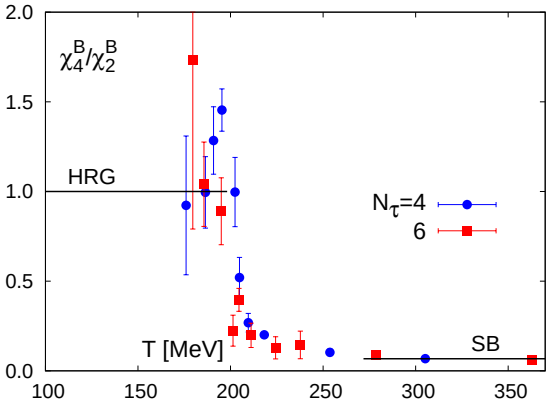

Figure 2.2: The ratio of the 4^{th} and 2^{nd} order cumulants of baryon number as a function of temperature. The value from hadronic gas model (HRG) is for the temperature range 100-200 MeV.

the ratio of the susceptibility can be readily constructed by the high order correlation function for conserved quantities in high-energy nuclear collisions. Baryon numbers are conserved in strong interactions. Simulations have shown that net-proton correlation function is a fair good representation of the net-baryons [16]. Note, at the critical point, the smallness (or disappearance) of the correlation length will lead to a large value of the quark susceptibility ratio. The systematic measurements of the net-charge and net-proton Kurtosis will provide info on the nature of the system.

Advantages for NICA

There is no comparison in terms of the control of systematic errors in a high-density tracking environment with the collider mode comparing with the fixed target experiment. In this sense, NICA provide a clear advantage compare to the proposed experiment CBM at FAIR. The possible shorting coming is the limitation of the luminosity with the collider. Therefore a careful selection of observable becomes more important. The above mentioned observables are, in my view, doable with the proposed collider.

2.3 Experimental advantages of collider over fixed target

B. Mohanty

Physics group, Variable Energy Cyclotron Center, Kolkata, India

Uniform acceptance for different particle species and for different beam energies in the same experimental setup

This is illustrated in Fig. 2.3 from the STAR experiment at the Relativistic Heavy-Ion Collidier in Brookhaven National Laboratory. The plot shows the uncorrected distribution of hadron transverse momentum versus rapidity within STAR Time Projection Chamber for three different beam energies and three types of hadron-pion, kaon and proton.

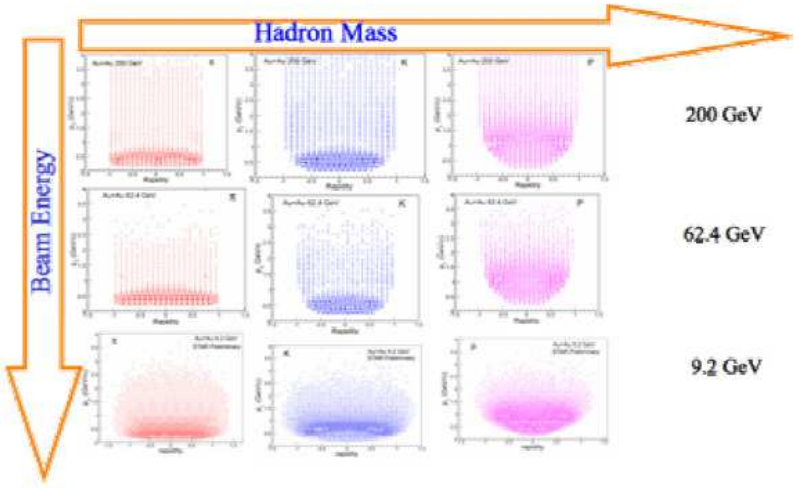

Figure 2.3: Acceptance for the collider mode [17]

Contrast this to similar plot from a typical fixed target experiment - NA49 at SPS, CERN Fig. 2.4. We can observe variation in acceptance for different hadrons at different beam energies.

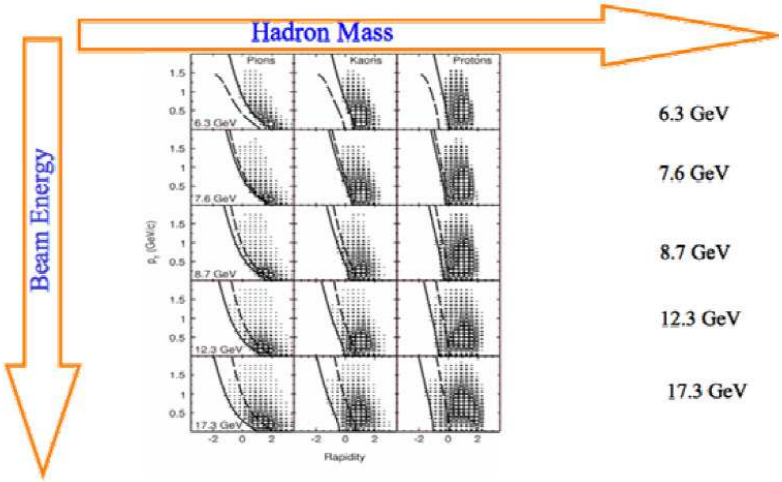

Figure 2.4: Acceptance in the fixed target mode [18]

For studies such as fluctuations (signatures for a phase transition and diverges at the QCD critical point) where having a correct knowledge of the acceptance is crucial for correct interpretation of results, it is desirable to have uniform acceptance at all beam energies for different hadrons.

Variation of particle density with beam energy

In a collider experiment: the variation of particle density with beam energy slower compared to fixed target experiments at similar colliding beam energies. This can be seen in Fig. 2.5, which shows the number of particles

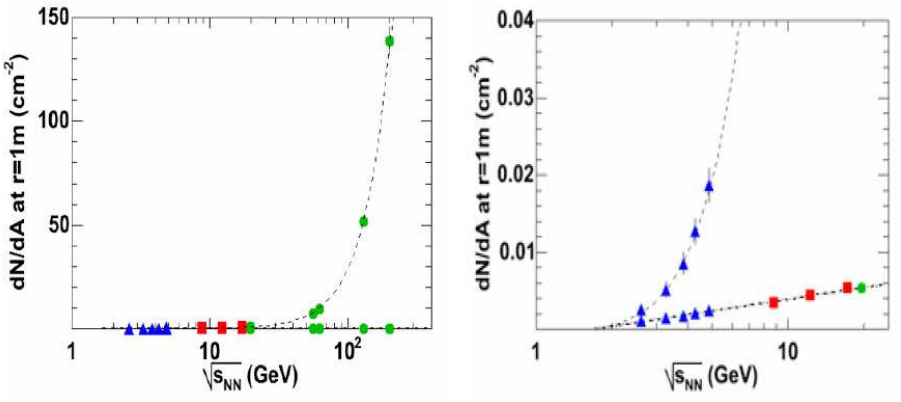

Figure 2.5: A number of particles per unit area at a distance of 1 meter from the collision point [19]. The low energy part of the left figure is zoomed in the right panel.

per unit area at a distance of 1 meter from the collision point [19]. A enlarged version of the figure is presented in the right panel, which clearly shows the difference in variation of particle density between collider and fixed target experiment.

A higher particle density affects the detector occupancy, which in turn could affect physics performance if not properly handled. A higher occupancy can lead to difficulties in reconstruction of tracks in the detector, also particle identification using techniques such as specific ionization energy loss, increase in double hit probability and space charge effects in tracking detectors.

One advantage which the fixed target experiments have over collider experiments is ability to reach higher luminosity for the same colliding beam energies.

2.4 Observables and open problems for NICA

E. Bratkovskaya[a] and W. Cassing[b]

[a] *Institut für Theoretische Physik, Universität Frankfurt;*
[b] *Institut für Theoretische Physik, Universität Giessen*

Recent efforts of the world-wide heavy-ion community have been made to develop the physical program of the future CBM experiment at FAIR. The results obtained directly apply for the NICA experimental program, too - cf. the CBM Physics Book [20].

The NICA and CBM facilities will provide a unique possibility to study nuclear matter under extreme conditions - at high baryon density and temperature - where according to lattice QCD the hadronic matter transforms to the strongly interacting quark-gluon plasma (sQGP). The different phases of the sQGP are not so well settled and there might be a mixed phase of partons and hadrons at higher baryon density, too. There are several indications for a critical endpoint in the QCD phase diagram - separating the cross over at low quark chemical potential μ_q from a first order phase transition at high μ_q, but a rigorous proof is not yet available. Ultimately, the experimental investigations at CBM and NICA should solve this issue.

However, the main difficulty of the problem is that the information about the initial sQGP stage of matter can only be obtained indirectly from the measurement of final (color neutral) hadronic observables. One should expect that a sQGP signal can be strongly distorted by the hadronization process itself as well as by (resonant) final state interactions of the hadrons. In order to subtract the "trivial" hadronic contribution from the sQGP signal, one needs nonequilibrium transport approaches for the phase transition from hadronic to partonic matter (Quark-Gluon-Plasma) on a microscopic level which include the partonic dynamics explicitly as well as the dynamics of hadronization and hadronic final state interactions.

The microscopic Parton-Hadron-String-Dynamics approach (PHSD) [21, 22] developed recently is based on a dynamical quasiparticle model (DQPM) matched to reproduce lattice QCD results in thermodynamic equilibrium [23, 24]. It includes a nontrivial partonic equation of state - in line with lattice QCD - as well as

covariant transition rates from partonic to hadronic degrees of freedom. Additionally PHSD incorporates the hadron and string dynamics which have been tested in the HSD approach for more than 15 years [25] in the energy range from about 100 AMeV to 21 ATeV.

A systematic analysis from the theoretical and experimental side for a large variety of observables - as a function of beam energy and centrality of the collision - will allow to study extensively the properties of hadronic/partonic matter and their phase transition.

The promising observables for NICA energies are considered to be:

- **Excitation function of particle yields and ratios:**
  Observation of a non-monotonic energy dependence of the particle yields and ratios as well as an enhancement of multi-strange particle production which can not be reproduced in hadron-based models [25, 26].

- **Transverse mass spectra and rapidity distributions:**
  Observation of a non-monotomnic increase/flattening of the excitation function for the inverse slope; global m_T-scaling of all mesons as a signal for chiral symmetry restoration. [26].

- **Collective flow:**
  Observation of strong collective flow v_2 and a "wiggle" in v_1 signals of non-hadronic nature of the initial pressure in the system; scaling of v_2 with quark content as a signal of the QGP as an approximately ideal liquid with low viscosity-to-entropy ratio [27].

- **Open and hidden charm:**
  Observation of an enhancement of D meson production due to a dropping mass in the hot and dense environment or a strong in-medium modification of the initial $c\bar{c}$ pair in the plasma phase; anomalous J/ψ suppression beyond the trivial "comover" or "QGP threshold melting" scenarios; ratio ψ'/ψ as a probe of charm equilibration; large v_2 as a signal of strong initial pressure of partonic nature [28].

- **Dileptons:**
  Observation of an enhancement of the dilepton rates - at low invariant masses - due to in-medium changes of the vector meson spectral functions as a signal of chiral symmetry restoration in the hot and dense matter; thermal dileptons from the QGP at intermediate invariant masses (1.2 GeV $<$ M $<$ 2.5 GeV) [29, 30].

- **Fluctuations and correlations:**
  Observation of strong fluctuations in the number of charged particles, baryon number, electric charge, transverse momenta p_T, K/π, K/p, p/π ratios etc. as well as correlations beyond the hadron based model predictions [31, 32].

2.5 Exploring high-density baryonic matter: Maximum freeze-out density

J. Randrup[a] and J. Cleymans[b]

[a] *Nuclear Science Division, LBNL, Berkeley, California, USA;*
[b] *Department of Physics, University of Cape Town, South Africa.*

Over the past decade a striking regularity has been established in heavy-ion collisions: From the lowest beam energies to the highest, the yields of various hadronic species are consistent with the assumption of chemical equilibrium [33, 16, 17, 19, 37]. Analyses of the experimentally obtained hadronic yield ratios at a variety of collision energies have shown that the data can be well reproduced within the conceptually simple statistical model that describes an ideal hadron resonance gas in statistical equilibrium. Furthermore, the extracted freeze-out values of the temperature T and the baryon chemical potential $\mu_{\rm B}$ exhibit a smooth and monotonic dependence on the collision energy and can be simply parametrized.

The beam energy thus plays a determining role for the thermodynamic properties of the final state in relativistic heavy-ion collisions. However, there is no simple relationship between the collision energy and the freeze-out value of the (net) baryon density: At low collision energies the freeze-out density increases with the energy, whereas it decreases when the collision energy is high due to the onset of nuclear transparency. Thus

there must exist a certain range of collision energies within which the freeze-out values of the net baryon density displays a maximum.

The optimal collision energy leading to this highest freeze-out density was discussed in [38] on the basis of the up-to-date results on the properties of the final state. It was pointed out there that since neither $\mu_{\rm B}$ nor T is subject to a conservation law they may be less suitable in a dynamical context. Furthermore, when a first-order phase transition is present, they become multivalued functions of the basic mechanical variables $\rho_{\rm B}$ (net baryon density) and ε (energy density) inside the mixed-phase region. It is therefore of interest to reexpress the thermodynamic variables in terms of those mechanical densities. Accordingly, we considered in [38] how the freezeout line appears when represented in terms of the basic baryon and energy densities, rather than chemical potential and temperature.

In [38], we presented the freeze-out line in terms of the net baryon density $\rho_{\rm B}$ and the energy density ε. We show below (in Fig. 2.6) the corresponding (ρ_B, ε^*) representation, where the "excitation energy density" $\varepsilon^* \equiv \varepsilon - n_{\rm N}\rho_{\rm B}$ is the energy density above the minimum value $m_{\rm N}\rho_{\rm B}$ dictated by the specified net baryon density. Thus ε^* has both compressional and thermal contributions.

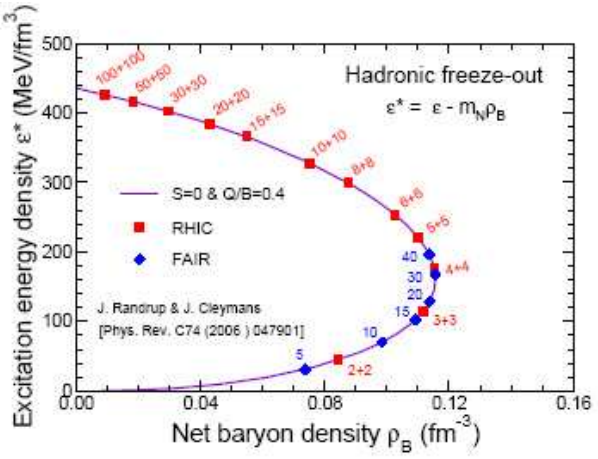

Figure 2.6: The hadronic freeze-out line in the $\rho_{\rm B} - \varepsilon^*$ phase plane as obtained from the values of $\mu_{\rm B}$ and T that have been extracted from the experimental data [16]. The calculation employs values of $\mu_{\rm Q}$ and $\mu_{\rm S}$ that ensure $< S >= 0$ and $< Q >= 0.4 < B >$ for each value of $\mu_{\rm B}$. Also indicated are the beam energies $E_{\rm lab}$ (in AGeV) for which the particular freeze-out conditions are expected at either a collider (red) or a fixed-target facility (blue).

The corresponding $(\rho_{\rm B,T})$ diagram, where T is the freeze-out temperature is perhaps more easily grasped and we show it in Fig. 2.7 below:

These novel representations of the freeze-out line bring out very clearly that there is a maximum value of the net baryon density: At the highest collision energies, freeze-out occurs for a negligible value of $\rho_{\rm B}$ and at an energy density of nearly one half GeV/fm^{-3}; then, in the range of $\mu_{\rm B}$ = 400 - 500 MeV (and a temperature of T = 140 - 130 MeV), the freeze-out line exhibits a backbend and approaches the origin. Thus, the net baryon density at freeze-out has a maximum value which amounts to about three quarters of the familiar nuclear saturation density of $\rho_0 \approx 0.16\ fm^{-3}$.

The fact that the freeze-out value of the net baryon density exhibits a maximum as the collision energy is being scanned suggests that the corresponding collision energy (range) is optimal for the exploration of compressed baryonic matter. This suggested optimal beam kinetic energy is 15 - 30 GeV per nucleon for a fixed-target configuration (such as FAIR at GSI), corresponding to $\sqrt{s_{\rm NN}}$ = 5.6 - 7.8 GeV for a collider (such as RHIC at BNL).

The results presented here should provide valuable guidance for establishing the desired capabilities of the contemplated NICA at JINR. In particular, our results suggest that freezeout densities all the way up to the maximum value could be explored at a collider facility delivering beam kinetic energies of up to $\approx$ 2.4 AGeV.

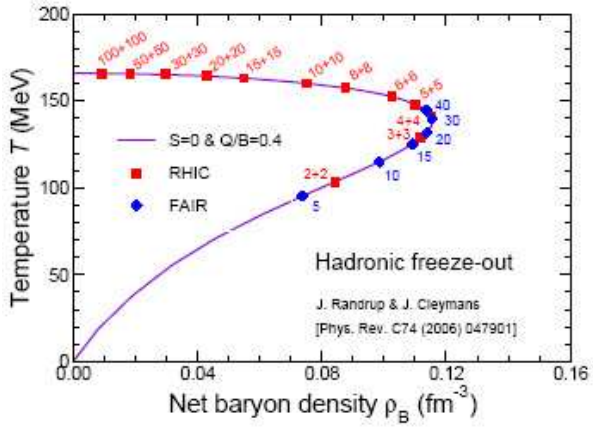

Figure 2.7: The hadronic freeze-out line in the $\rho_B - T$ phase plane as obtained from the values of μ_B and T that have been extracted from the experimental data [16]. The calculation employs values of μ_Q and μ_S that ensure $< S >= 0$ and $< Q >= 0.4 < B >$ for each value of μ_B. Also indicated are the beam energies (in AGeV) for which the particular freeze-out conditions are expected at either a collider (red) or a fixed-target facility (blue).

2.6 Nuclear matter physics at NICA

Peter Senger

GSI Helmholtzzentrum für Schwerionenforschung, D-64291 Darmstadt, Germany

The exploration of the QCD phase diagram is one of the most exciting and challenging projects of modern nuclear physics. In particular, the investigation of nuclear matter at high baryon densities offers the opportunity to find characteristic structures such as a first-order phase transition with a region of phase coexistence and a critical endpoint. The experimental discovery of these prominent landmarks of the QCD phase diagram would be a major breakthrough in our understanding of the properties of nuclear matter. Equally important is quantitative experimental information on the properties of hadrons in dense matter which may shed light on chiral symmetry restoration and the origin of hadron masses. Worldwide, substantial efforts at heavy-ion accelerators like RHIC/BNL and SPS/CERN are devoted to the clarification of these fundamental questions, and new dedicated experiments are planned at future facilities like CBM at FAIR in Darmstadt and MPD at NICA/JINR in Dubna. In this article the perspectives for MPD at NICA are discussed.

Exploring the phases of nuclear matter

Ordinary substances exist in different phases such as gas, liquid, and solid, depending on the temperature and pressure. A variation of these conditions may cause a transition from one phase to the other, and the boundaries between the different lines can be drawn in a diagram as function of temperature and pressure. These lines could meet at the triple point where several phases coexist. In general there is also a critical point where the distinct phase boundary between liquid and gas ends, and beyond which there is a continuous "crossover" between the two phases. The phase boundaries, the triple point and the critical point represent fundamental landmarks in the phase diagram of each substance.

Fig. 2.8 illustrates the possible phases of nuclear matter and their boundaries in a diagram of temperature versus net-baryon density. At moderate temperatures and densities, nucleons are excited to short-lived states (baryonic resonances) which decay by the emission of mesons. At higher temperatures, also baryon-antibaryon pairs are created. This mixture of baryons, antibaryons and mesons, all strongly interacting particles, is generally called hadronic matter, or baryonic matter if baryons prevail. At very high temperatures and/or baryon densities the hadrons melt, and the constituents, the quarks and gluons, form a new phase, the Quark-Gluon-Plasma (QGP). In the first microsecond after the big bang the early universe underwent a phase transition from the primordial matter consisting of quarks, antiquarks and gluons into hadronic matter. This confinement process happened at zero net-baryon densities i.e. at equal numbers of particles and anti-particles, where modern theory predicts a smooth crossover transition from partonic to hadronic matter. For larger net-baryon densities theory predicts the existence a critical endpoint, followed by a first-order deconfinement phase transition with a phase

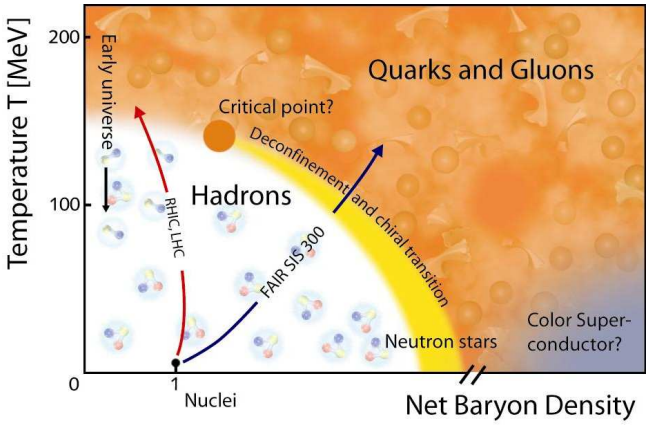

Figure 2.8: Sketch of the phase diagram of nuclear matter

coexistence region. High-density but rather cold nuclear matter is expected to exist in the core of neutron stars, and at very high densities correlated quark-quark pairs are predicted to form a color superconductor. A very fundamental but still open question is whether the deconfinement phase-transition coincides with the chiral phase-transition which is responsible for the generation of constituent quark masses, i.e. for the origin of the mass of the visible matter in our universe.

In the laboratory, hot and dense nuclear matter can be produced and studied in collisions between atomic nuclei at high bombarding energies. However, quantitative experimental information on the QCD phase diagram is still restricted to the freeze-out points of heavy-ion collisions as derived from statistical (thermal) model fits to measured particle yields and ratios [39]. The freeze-out points are shown in Fig. 2.9 as function of temperature T and baryon-chemical potential μ_B (full and open circles). A freeze-out temperature of T $\approx$ 160 MeV has been derived at very low values of μ_B from nucleus-nucleus collisions at the Relativistic Heavy Ion Collider (RHIC) at BNL . This number coincides with the critical temperature T_c found by lattice QCD calculations which varies between 150 and 180 MeV [40, 41]. The RHIC experiments made intriguing observations which support the picture that partonic degrees of freedom prevail in the early phase of the fireball evolution [42]. These studies will be continued at even higher energies at the Large Hadron Collider (LHC) at CERN.

It is worthwhile to note that the thermal model fits to the experimental data extract freeze-out temperatures which rise sharply up to beam energies of about 30 AGeV and then level off. The observation of a limiting freeze-out temperature is nontrivial, and may indicate a change of the degrees-of-freedom in the fireball which happens at FAIR (low SPS) beam energies. Around the same beam energy various structures in excitation functions have been observed by the NA49 experiment at the CERN-SPS [43]: the ratio of strange to non-strange hadrons exhibits a sharp peak, and the inverse slope parameters of the kaon transverse mass spectra (which are dominated by transverse flow) reach a plateau. Moreover, the dynamical fluctuations of the kaon-to pion ratio measured event-by-event increase with decreasing beam energy. Critical fluctuations are expected in the vicinity of the critical endpoint, like in macroscopic systems where the density fluctuations cause the phenomenon of "critical opalescence".

In Fig. 2.10 the freeze-out points are plotted as function of temperature and net-baryon density [38]. The numbers refer to either the total collision energy (from 2+2 to 100+100 AGeV)), or to laboratory kinetic energies for fixed target experiments (from 5 – 40 AGeV). The freeze-out density clearly exhibits a maximum at low CERN-SPS, NICA or FAIR energies indicating that beam energies between 30 and 40 AGeV (on fixed target), or total energies between $\sqrt{s_{\rm NN}} = 6$ and 10 AGeV are best suited to create the highest net-baryon densities in the laboratory.

In conclusion, the systematic and comprehensive exploration of the QCD phase diagram in the region of high net-baryon densities using novel observables will have a large discovery potential. In particular, future high-energy heavy-ion collision experiments such as CBM at FAIR or MPD at NICA will have to address the following fundamental questions:

- What is the equation-of-state of nuclear matter at neutron star densities (up to 6 ρ_0), and what are the relevant degrees-of-freedom at these densities?

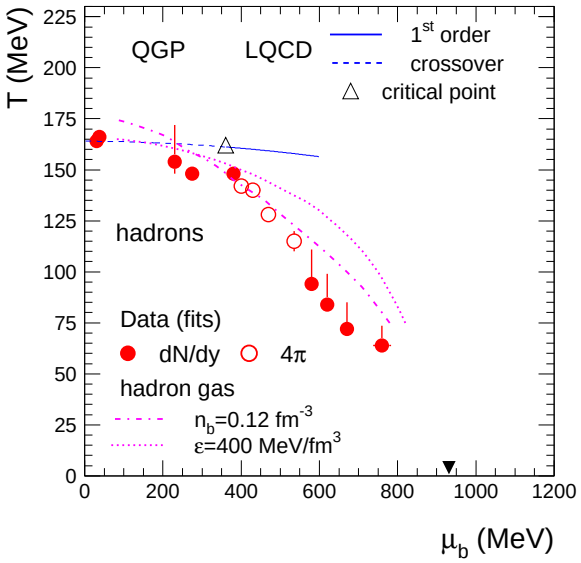

Figure 2.9: The QCD phase diagram as function of temperature and baryon chemical potential plane with chemical freeze-out points. The red dashed-dotted line corresponds to a constant total baryon density of n_b=0.12 fm^{-3}. The red dotted line represents a freeze-out curve for a hadron gas at constant energy density of ε = 500 MeV/fm^3. The black dashed line illustrates the location of a crossover transition as predicted by LQCD calculation, and the triangle represents the critical end point of a first order phase transition. Figure taken from [39].

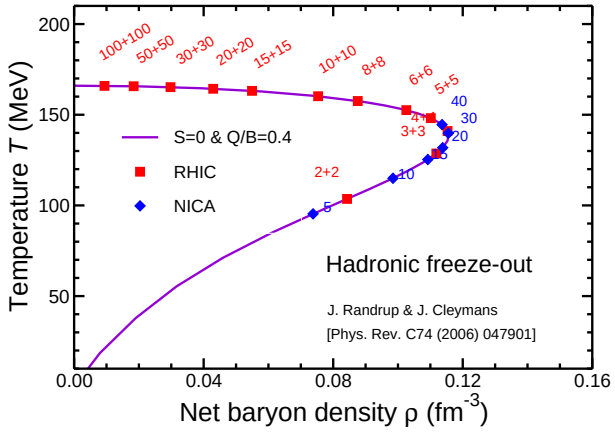

Figure 2.10: Chemical freeze-out curve as function of temperature and net-baryon density [38].

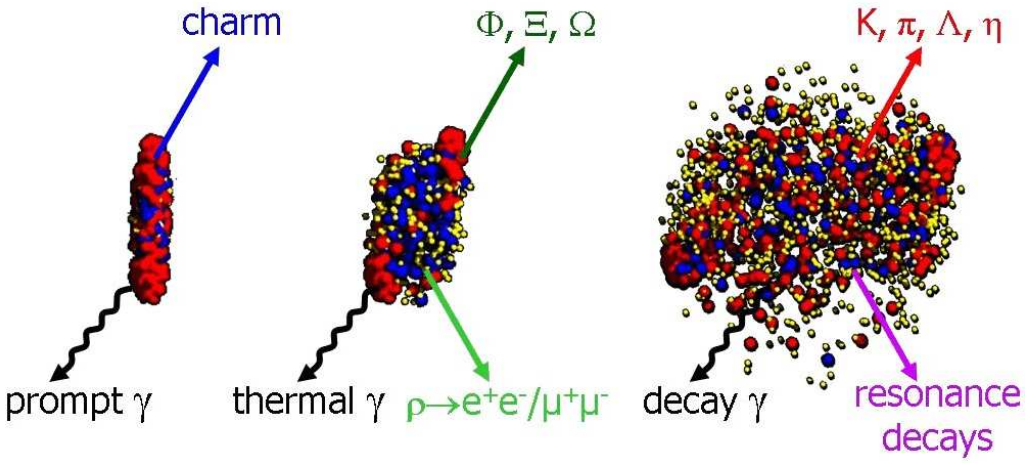

Figure 2.11: Sketch of the expansion phase of a U + U collision at a laboratory beam energy of 23 AGeV ($\sqrt{s_{\rm NN}}$ = 7 GeV) at different time steps: initial stage where the two Lorentz-contracted nuclei overlap (left), high density phase (middle), and final stage ("freeze-out") when all hadrons have been formed (right). Different particles are created in different stages of the collisions or escape from the interaction region at different times (see text). Almost 1000 charged particles are created in such a collision, most of them are pions.

- Are there structures in the QCD phase diagram such as a phase boundary between hadronic and partonic matter, a region of phase coexistence, a triple point or a critical endpoint ?
- Does strange matter exist in the form of heavy multi-strange short-lived objects?
- To what extent are the properties of hadrons modified in dense baryonic matter, and are there signatures for chiral symmetry restoration?

The theoretical understanding of nuclear matter properties at large net-baryon densities is still in its infancy. Therefore, the scientific progress in this field is mainly driven by new experimental results. This requires high-precision measurements of new experimental observables as discussed in the next section.

Observables in heavy-ion collisions

In order to explore the properties of dense baryonic matter one has to find observables which serve as diagnostic probes of the early stage of the fireball. One of these observables is the elliptic flow of hadrons which reflects the initial almond shaped collision volume in momentum space. This is particularly true for particles which do not suffer from rescattering like Ω hyperons or ϕ mesons because of their low hadronic cross sections. Moreover, heavy quarks are produced in hard processes which occur predominantly in the initial phase of the collision.

The emission time of various particle species is illustrated in Fig. 2.11 which depicts three snapshots of the evolution of a heavy-ion collision at NICA/FAIR energies. Particles containing charm quarks are expected to be created in the very first stage of the reaction, and, therefore, offer the possibility to probe partonic degrees-of- freedom. Vector mesons like ρ, ω and ϕ mesons are produced continuously via $\pi - \pi$ annihilation during the course of the reaction, and decay either again into mesons, or into a pair of leptons. The latter decay channel is suppressed by about 4 orders of magnitude (corresponding to the square of the electromagnetic coupling constant $(1/137)^2$). However, as leptons are not affected by final-state interactions, this decay offers the possibility to look into the fireball. In particular the short-lived ρ meson is a promising diagnostic probe of hot and dense nuclear matter. Due to their small hadronic cross sections, also multi-strange hyperons and ϕ mesons carry information on the dense phase of the collision, in particular via their collective flow. Finally, the bulk of the particles is emitted at densities below saturation density. Up to date, essentially these freeze-out probes have been measured in heavy-ion collisions at beam energies between 2 and 40 AGeV (on stationary target). In contrast, the messengers from the early and/or the high-density phase of the collision are produced very rarely, either because of the low cross section (charm) or because of the small branching ratios into lepton pairs (low-mass vector mesons). Therefore, a successful experimental program can only be realized with a combination of fast detector systems and high beam luminosity.

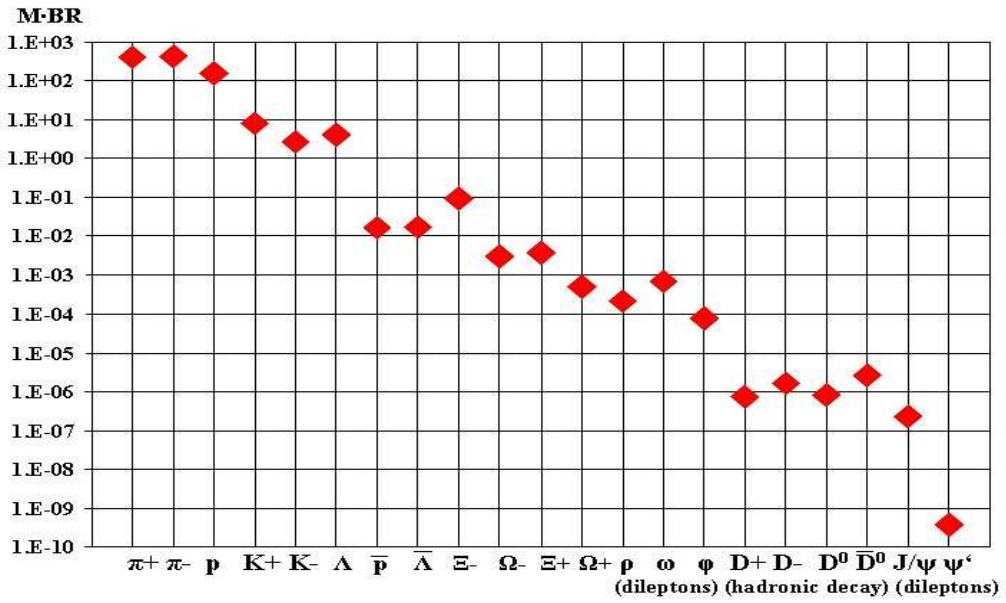

Figure 2.12: Particle multiplicities times branching ratio for central Au+Au collisions at 25 AGeV ($\sqrt{s_{\rm NN}} = 7.1$ GeV) as calculated with the HSD transport code [44] and the statistical model [45]. For the vector mesons (ρ, ω, ϕ, J/ψ, ψ') the decay into lepton pairs was assumed, for D mesons the hadronic decay into kaons and pions.

A successful future heavy-ion research program has to perform a comprehensive scan of observables, beam energies and collision systems. The observables should include low mass dilepton pairs, charmonia and open charm, but also collective flow of rare and bulk particles, correlations and fluctuations. The experimental goal is to measure these rare probes with high precision in spite of the very low multiplicities. Fig. 2.12 quantifies the notation "rare probes" in terms of the product of particle multiplicity times branching ratio. The points are calculated for central Au + Au collisions at 25 AGeV (or at $\sqrt{s_{\rm NN}} = 7.1$ GeV collider energy) using either the HSD transport code [44], or a thermal model assuming values for temperature and baryon chemical potential corresponding to a beam energy of 25 AGeV [45]. Mesons containing charm quarks are suppressed by about 9 orders of magnitude with respect to the pions (the ψ' meson is even more suppressed). The yield of lepton pairs from vector meson decays is about 6 orders of magnitude below the pion yield, similar to the yield of multi-strange hyperons.

Future experiments will have to be many orders of magnitude more sensitive than the ones which have been performed so far at AGS and low SPS energies. These experiments concentrated on the measurement of the most abundant hadrons which freeze out in the late and dilute stage of the collision. New insight will come from the measurement of multi-differential observables such as the elliptic flow of various particles as function of transverse momentum, and from the detailed analysis of rare diagnostic probes such as lepton pairs, multi-strange baryons and charmed hadrons.

Perspectives for NICA

The NICA energy range is ideally suited for the investigation of the equation-of-state of nuclear matter at neutron star core densities, and for the search for landmarks in the QCD phase diagram such as phase boundaries and critical/triple points. In order to characterize the properties of the fireball matter one has to measure the abundantly produced particles including their phase-space distributions and correlations, together with rare diagnostic probes like multi-strange particles, lepton pairs and charmed hadrons. The experimental challenge will be to identify these rare particles with high purity, and to collect samples with large statistics which is required for a multi-differential analysis.

Table 2.1 lists the multiplicities of the most important probes in minimum bias Au+Au collisions for two energies as calculated with the HSD transport model and the statistical model, and their yields which are estimated based on realistic detector and analysis efficiencies, and on the design NICA luminosity of of L=10^{27}cm^{-2}s^{-1}.

Particle (mass)	Multiplicity $\sqrt{s_{NN}}$ = 7.1 GeV	Multiplicity $\sqrt{s_{NN}}$ = 11 GeV	decay mode	BR	ε (%)	yield (s^{-1}) $\sqrt{s_{NN}}$ = 7.1 GeV	yield (s^{-1}) $\sqrt{s_{NN}}$ = 11 GeV	yield in 10 weeks $\sqrt{s_{NN}}$ = 7.1 GeV	yield in 10 weeks $\sqrt{s_{NN}}$ = 11 GeV
K^+ (494)	8	12	-	-	20	$9.6{\cdot}10^3$	$1.4{\cdot}10^4$	$5.8{\cdot}10^{10}$	$8.4{\cdot}10^{10}$
K^- (494)	2.6	5.6	-	-	20	$3.1{\cdot}10^3$	$6.7{\cdot}10^3$	$1.9{\cdot}10^{10}$	$4.0{\cdot}10^{10}$
ρ(770)	4.6	8	e^+e^-	$4.7{\cdot}10^{-5}$	2	$2.6{\cdot}10^{-2}$	$4.5{\cdot}10^{-2}$	$1.6{\cdot}10^5$	$2.7{\cdot}10^5$
ω(782)	7.6	13	e^+e^-	$7.1{\cdot}10^{-5}$	2	$6.5{\cdot}10^{-2}$	0.11	$3.9{\cdot}10^5$	$6.6{\cdot}10^5$
ϕ(1020)	0.24	0.4	e^+e^-	$3{\cdot}10^{-4}$	2	$8.6{\cdot}10^{-3}$	$1.4{\cdot}10^{-2}$	$5.2{\cdot}10^4$	$8.4{\cdot}10^4$
Ξ^-(1321)	0.16	0.2	$\Lambda\pi^-$	1	2	19	24	$1.1{\cdot}10^8$	$1.4{\cdot}10^8$
Ω^-(1672)	0.024	0.032	ΛK^-	0.68	2	1.9	2.9	$1.1{\cdot}10^7$	$1.7{\cdot}10^7$
D^0 (1864)	$7.5{\cdot}10^{-6}$	$7.5{\cdot}10^{-4}$	$K^+\pi^-$	0.038	2	$3.4{\cdot}10^{-5}$	$3.4{\cdot}10^{-3}$	200	$2{\cdot}10^4$
J/ψ (3097)	$2.4{\cdot}10^{-6}$	$5{\cdot}10^{-5}$	e^+e^-	0.06	10	$8.6{\cdot}10^{-5}$	$1.8{\cdot}10^{-3}$	520	$1.1{\cdot}10^4$

Table 2.1: Particle multiplicities and yields for minimum bias Au+Au collisions at energies of $\sqrt{s_{NN}}$ = 7.1 and 11 GeV (25 and 60 AGeV fixed target energy) as calculated with the HSD transport model and with the statistical model. The values have been calculated for central collisions, and then scaled down by 5 for minimum bias collisions. The yield estimates are based on the maximum NICA luminosity of L=10^{27}cm^{-2}s^{-1} corresponding to a reaction rate of 6 kHz for minimum bias Au + Au collisions.

The detector system should comprise the following components. The measurement of kaons, in particularly their separation from pions and protons, requires a magnetic field, a tracking detector like a Time-Projection-Chamber (TPC), and preferably a time-of-flight detector (TOF). Λ, Ξ, and Ω hyperons can be identified via the topology of their weak decays ($\Lambda \rightarrow p\pi$, $\Xi \rightarrow \Lambda\pi$, $\Omega \rightarrow \Lambda K$). Such a measurement requires tracking detectors inside a magnetic field. However, due to the short decay lengths of $c\tau$ = 7.89 cm (Λ), $c\tau$ = 4.91 cm (Ξ^-), and $c\tau$ = 2.46 cm (Ω^-) the track measurement should start close to the primary vertex where the track density is high. For this purpose, a high precision tracking detector based on Silicon micro-strip sensors would be the best choice. With a detector system in collider geometry it is very difficult to identify muons at midrapidity. Therefore, it would be preferable to add electron detectors such as a Ring Imaging Cherenkov (RICH) detector or an Electromagnetic Calorimeter (ECAL). Typically, in the NICA energy range on has to suppress the π yield by a factor of about 10^4 to see the electrons. If this cannot be achieved with RICH and ECAL one could add a Transition Radiation Detector (TRD) to identify electrons above 1 GeV. The rejection of physical background due to close electron pairs may require the use of a Hadron Blind Detector (HBD).

The identification of particles containing charm quarks poses a particular experimental challenge due the very low signal-to-background ratio at beam energies close to production threshold. Moreover, their yield would be very low even after 10 weeks of beam at highest luminosity, at least for beam energies where one expects the highest net-baryon densities to be produced (see Table 2.1). Therefore, the measurement of J/ψ and D mesons may be restricted to the highest NICA beam energies. Moreover, the identification of D mesons via their hadronic decay into pions and kaons (decay length of $c\tau$ = 123 μm for D^0, and $c\tau$ = 312 μm for $D^{\pm}$) would require the installation of an additional high-resolution low-mass micro-vertex detector.

Table 2.2 summarizes the major NICA physics cases, the corresponding observables and the required detector components. It turns out that the most interesting scientific questions can be tackled with a basic version of the MPD comprising a magnet, a TPC, a Silicon tracker, and a TOF detector. These measurements do not necessarily require the highest reaction rates as the production cross sections for strange particles are reasonably high. The electron detectors could possibly be part of an MPD upgrade program which could take place once NICA has reached the design luminosity.

The MPD/NICA project is part of a worldwide experimental research program which is devoted to the exploration of the QCD phase diagram at high net-baryon densities. This program was started about 30 years ago with pioneering experiments at the Bevalac at the LBL in Berkeley, and was continued at higher energies at AGS at BNL in Brookhaven and at the SPS at CERN. At the SPS, the fixed-target experiment NA61/SHINE is still taking data, mainly bulk particles like pions, kaons, and hyperons. At GSI/SIS18 the second generations

Physics case	**Observables**	**Detectors**
nuclear EOS at high densities	proton flow, Λ, Ξ, Ω	Silicon tracker, TPC, TOF
deconfinement phase transition, phase coexistence	excit. funct. of yield and flow of K, Λ, Ξ, Ω. e-by-e fluctuations	Silicon tracker, TPC, TOF
strange matter	multi-strange short-lived objects (decay into Λ, Ξ, Ω)	Silicon tracker, TPC, TOF
chiral phase transition, hadrons in dense matter	dileptons (e+e-)	HBD, RICH, TPC, TOF, ECAL, (TRD ?)

Table 2.2: The possible NICA physics cases, related observables, and detector requirements

experiments FOPI and HADES study nuclear matter properties at 2–3 time saturation density by measuring pions, strange particles and dileptons.

At RHIC, the energy scan program has been started mainly using the STAR detector with the goal to search for the critical endpoint. The scaling of the elliptic flow parameter v_2 with the number of constituent quarks as observed at RHIC is regarded as one of the most convincing signatures for partonic degrees-of-freedom prevailing in the early stage of the collision. Therefore, this signal should disappear at a certain beam energy when scanning down the energy. At the same energy, higher-order event-by-event fluctuations should appear indicating the location of the critical point. The statistical significance of these and other signals will be limited by the very low luminosity at RHIC injection energies. Moreover, the beam time available at RHIC for this kind of studies is very limited. In contrast, NICA is designed for high luminosities at the collision energies where high net-baryon densities are created and the MPD can run over long periods. This offers the possibility to perform systematic measurements of multi-differential observables, including particles with lower production cross sections. Extremely high beam intensities will be available at FAIR for the CBM experiment which is designed to measure bulk and rare probes with almost unlimited statistics [46]. In contrast to the fixed-target CBM, the collider experiment MPD has a uniform acceptance which is almost independent of the collision energy. Therefore, MPD at NICA and CBM at FAIR will be able to perform complementary measurements, covering different regions of phase space. Last but not least, the parallel development of two detector systems based on cutting-edge technology offers the opportunity of joint R&D activities which will be of large mutual benefit.

Bibliography

[1] A.N. Sissakian, A.S. Sorin and V.D. Toneev, *Proc. of the 33rd International Conference on High Energy Physics (ICHEP 06)*, (26 July - 2 August, Moscow 2006), p.421 [arXiv:nucl-th/0608032].

[2] P. Senger, T. Galatyuk, D. Kresan, A. Kiseleva and E. Kryshen, **PoS CPOD06,** 18 (2006).

[3] M. Gazdzicki and M. I. Gorenstein, Acta. Phys. Polon. **B 30,** 2705, (1999).

[4] C. Alt *et al.* (NA49 Collaboration), Phys. Rev. **C 77,** 024903, (2008) [arXiv:0710.0118].

[5] Z. Fodor and S. D. Katz, **JHEP 0404**, 050 (2004) [arXiv:hep-lat/0402006].

[6] N. Antoniou *et al.* (NA61/SHINE Collaboration), CERN-SPSC-2006-034.

[7] G.S.F. Stephans, *critRHIC: The RHIC low energy program*; nucl-ex/0607030.

[8] K. Grebieszkow *et al.* (NA49E Collaboration), *contributed talk at the Quark Matter 2009.*

[9] J. Adams, *et al.* (STAR collaboration), Nucl. Phys. **A 757,** 102, (2005).

[10] B.I. Abelev, *et al.* (STAR collaboration), Phys. Rev. Lett. **99,** 12301 (2007).

[11] R. J. Fries *et al.*, Phys. Rev. Lett. **90,** 202303 (2003) and references therein.

[12] C. Alt *et al.* (NA49 collaboration), Phys. Rev. **C 68,** 034903 (2003); [nucl-ex/0303001].

[13] M. Cheng et al., arXiv:0811.1006; M.A. Stephanov, arXiv:0809.3450.

[14] R.V. Gavai and S. Gupta, Phys. Rev. **D 71,** 114014, (2005).

[15] Y. Hatta and M. Stephanov, Phys. Rev. Lett. **91,** 102003 (2003).

[16] B. Mohanty, *private communication, 2009.*

[17] B. Mohanty, *talk at the Quark Matter 2009.*

[18] (NA49 Collaboration), arXiv:0808.1237.

[19] G. Roland, *talk at RHIC low energy running workshop, BNL*, March 2006.

[20] *CBM Physics Book, to be published.*

[21] W. Cassing and E.L. Bratkovskaya, Phys. Rev. **C 78,** 034919 (2008).

[22] W. Cassing, Eur. Phys. J. **ST 168,** 3, (2009).

[23] A. Peshier and W. Cassing, Phys. Rev. Lett. **94,** 172301, (2005).

[24] W. Cassing, Nucl. Phys. **A 791,** 365, (2007); **795**, 70, (2007).

[25] W. Cassing, E.L. Bratkovskaya, Phys. Rep. **308,** 65, (1999).

[26] E. L. Bratkovskaya et al., Phys. Rev. **C 69,** 054907, (2004).

[27] H. Stöcker et al., J. Phys. G. **31,** 929, (2005).

[28] O. Linnyk, E.L. Bratkovskaya and W. Cassing, Int. J. Mod. Phys. **E 17,** 1367, (2008).

[29] E. L. Bratkovskaya and W. Cassing, Nucl. Phys. **A 807,** 214 (2008);

[30] E.L. Bratkovskaya, W. Cassing and O. Linnyk, Phys. Lett. **B 67,** 428, (2009).

[31] V. P. Konchakovski *et al.*, Phys. Rev. **C 73,** 034902 (2006); **78**, 024906 (2008); **79**, 024907 (2009).

[32] V. P. Konchakovski *et al.*, Phys. Lett. **B 651,** 114 (2007).

[33] F. Becattini, J. Cleymans, A. Keränen, E. Suhonen, and K. Redlich, Phys. Rev. **C 64,** 024901, (2001).

[34] J. Cleymans, H. Oeschler, K. Redlich, and S. Wheaton, Phys. Rev. **C 73,** 034905, (2006).

[35] F. Becattini, J. Manninen, and M. Gazdzicki, Phys. Rev. **C 73,** 044905, (2006).

[36] J. Manninen and F. Becattini, Phys. Rev. **C 78,** 054901, (2008).

[37] A. Andronic, P. Braun-Munzinger, and J. Stachel, Phys. Lett. **B 673,** 142 (2009).

[38] J. Randrup and J. Cleymans, Phys. Rev. **C 74,** 047901, (2006).

[39] A. Andronic *et al.*, Nucl. Phys. **A 834,** 237, (2010)

[40] Y. Aoki *et al.*, **JHEP** 0906, 088, (2009); [arXiv:0903.4155].

[41] M. Cheng *et al.*, [arXiv:0911.3450 [hep-lat]]

[42] A. Adare et al. (PHENIX Collaboration), Phys. Rev. Lett. **98,** 162301, (2007)

[43] K. Grebieszkow (NA49 and NA61 Collaborations), Acta. Phys. Polon. **B 41,** 427, (2010); [arXiv:0911.1902 [nucl-ex]].

[44] E.L. Bratkovskaya, *private communication*

[45] A. Andronic, *private communication*

[46] http://www.gsi.de/fair/experiments/CBM/index_e.html

3 Phases of QCD matter at high baryon density

There has been an impressive progress in the understanding of the QCD phase diagram in recent years. This concerns in particular the phases at high baryon density: at low temperature, one expects the emergence of the color superconductivity phase. The classification in terms of large N_c (number of colors) behavior suggests the confined baryonic phase where the thermodynamic quantities scale proportionally to N_c (resembling for example the Skyrme crystal) – the "quarkyonic" phase. At high baryon density, the confined and deconfined phases are separated by a first order phase transition line that is expected to terminate at a chiral critical point. This critical point is likely located at a baryon density that is within the reach of the NICA collider. A number of related phenomena amenable to experimental observation are considered in this section. An interesting set of problems discussed here is related to the non-equilibrium and finite-size behavior in deconfined matter.

3.1 Comments on a phase diagram and fluctuations

M. Stephanov

University of Illinois, Chicago, USA

QCD phase diagram (contemporary view, Fig. 3.1**)**

- Models (and lattice) suggest crossover turns into first- order at some $\mu_{\rm B}$.
- Large $\mu_{\rm B}$ - Color Flavor Locked phase ("QCD ice").
- Crossover - "supercritica" fluid. Almost perfect. Strongly coupled. New methods needed.

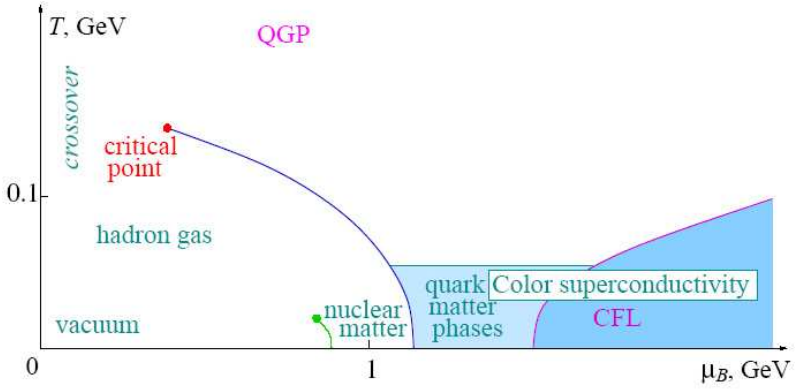

Figure 3.1: Phase diagram.

Location of the critical point vs freeze-out, Fig. 3.2
Needed:

- Energy-scan experiments:
  RHIC,
  NA61(SHINE)@SPS,
  CBM@FAIR/GSI,
  NICA
- Improve lattice predictions – understand systematic errors
- Understand critical phenomena in the dynamical environment of a heavy ion collision
  – understand background
  – develop optimal signatures.

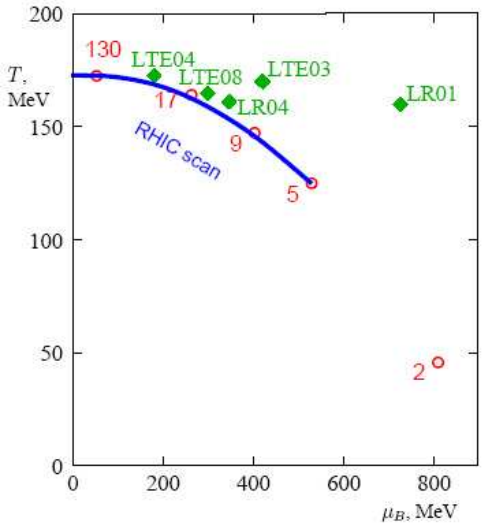

Figure 3.2: Estimates of a critical end point.

Fluctuation signatures, Fig. 3.3

- Experiments measure for each event: multiplicities $N\pi, N_p, ...$, momenta p, etc. These quantities fluctuate event-by-event.
  – Typical measure is standard deviation, e.g., $< (\delta N)^2 >$.
- What is the magnitude of these fluctuations near the critical point [39] ?
- *Universality* tells how it grows at the critical point: $< (\delta N)^2 > \sim \xi^2$.
  – Correlation length is a universal measure of the "distance" from the critical point. It diverges as $\xi \sim (\Delta\mu \text{ or } \Delta T)^{-2/5}$ as the critical point is approached.

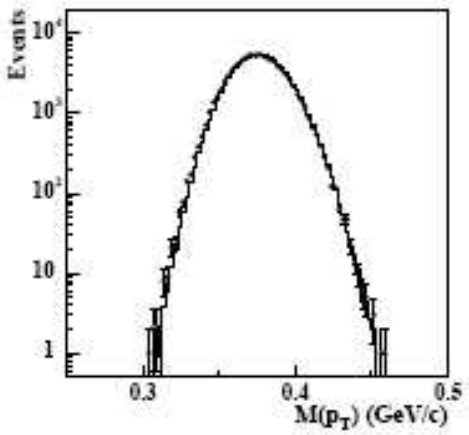

Figure 3.3: Transverse momentum fluctuation.

- Magnitude of ξ is limited by finite time/size effects: $\mathcal{O}(3 \text{ fm})$ – [2].
- "Shape" of the fluctuations can be also measured: non-Gaussian moments. As $\xi \to \infty$ fluctuations become more non-Gaussian.

- Higher cumulants show even stronger dependence on ξ [3]:

$$< (\delta N)^3 > \sim \xi^{4.5}, \quad < (\delta N)^4 > -3 < (\delta N)^2 >^2 \sim \xi^7$$

which makes them more sensitive signatures of the critical point.

Observables – theory comments

- Fluctuations:
  – Multiplicities –
  pro: larger signal – especially protons (coupled to critical mode);
  con: larger background (impact parameter fluctuations)
  – Ratios, mean $p_{\rm T}$ –
  pro: no impact parameter fluctuations;
  con: smaller signal.
  – Non-gaussian fluctuations (higher moments: skewness, kurtosis) –
  pro: strong dependence on ξ – large signal;
  con: difficult to estimate either signal or background.
  – Fluctuations from first- order transition (nonequilibrium)?
  pro: presumably more dramatic;
  con: difficult to predict – requires more detailed dynamic assumptions.
- Non-fluctuation observables: $\bar{p}/p$ – Asakawa-Bass-Möller-Nonaka; based on focusing – trajectories are "pulled" to larger $\mu_{\rm B}$ at earlier times + earlier freezeout of higher $p_{\rm T}$
- True critical point signal should show consistently in several observables.

3.2 Search for manifestation of medium effects in dense, excited hadron-quark matter

D. Voskresensky

Moscow Engineering Physics Institute, Russia

EoS and particle abundance. There are different possibilities for the behavior of the hadron masses, couplings, widths at finite temperature and density:

Following (partial) chiral symmetry restoration and the Brown-Rho scaling ideas, masses of hadrons and their coupling constants may decrease with increase of the density and the temperature. This behavior essentially affects particle occupations and the Equation of State (EoS). A rather appropriate EoS at $T = 0$ (fitted to the description of global properties of atomic nuclei and neutron stars) can be constructed at approximately the same suppression of masses and couplings (universal, or approximately universal suppression) [4]. Here one should stress necessity of *a simultaneous analysis of the relevant phenomena in different domains of nuclear physics (hadron scattering, atomic nuclei, neutron stars, heavy-ion collisions)* to construct an appropriate EoS, cf. [5]. Analysis of [6] shows that with mentioned approximately universal suppression the calculated pressure at large temperatures T proves to be much higher than that follows from the modern lattice calculations. Thus, if one believes the lattice data (for large temperatures, $T \gtrsim 170$ MeV), one should assume an additional suppression of the hadron couplings with the temperature at $T \sim T_c$, otherwise the phase transition to sQGP would not be energetically favorable. With suppressed couplings and masses the quasiparticle approximation proves to be operative in a broad temperature-density region at least for part of hadron species.

Opposite, in case when hadron couplings are assumed to be not decreased with the density and the temperature (strong coupling limit) the gap between upper and lower baryon continua may become blurred [7] with increase of the temperature. For $T \gtrsim T_{\rm bl}$ ($T_{\rm bl} \sim m_\pi$ at small baryon chemical potential) the abundance of baryon- antibaryon blurs (described by completely regular Green functions) is exponentially increased. Boson masses are diminished due to fermion blur - boson quasiparticle interactions. Some boson species may even undergo a hot boson condensation. The pressure increases substantially above that calculated on the lattice. If were so, one could expect a broad region of a hadron porridge of mesons and baryon blurs. Some of these hadron species can be melt into quark constituents leading to the state of strongly interacting hadron-quark porridge (a mixed phase).

Dynamics of the phase transition.

In assumption of the first-order hadron-sQGP phase transition in the vicinity of the endpoint all processes develop very slowly [8]. Thus in heavy ion collisions the expanding fireball may linger in the sQGP state, until $T(t)$ decreases well below the corresponding equilibrium value of the endpoint temperature. Far from the endpoint fluctuations may grow much faster provided the system reaches spinodal decomposition region. Appearing an aerosol mixture (a mixed phase) may manifest in observables. Ref. [8] also points on essential role of viscosity and finite size effects (surface tension) in the mixed phase preparing in the dynamics of the first-order phase transition. Fluctuations at the hadron-sQGP phase transition (at a finite baryon density) grow and dissolve, as if the fluid were effectively very viscous.

Critical fluctuations.

Analysis of [9] demonstrates that the fluctuation region (a mixed phase) at the color superconducting second-order phase transition at thermal equilibrium might be very broad ($0.5 \div 1.5\ T_c$) and thus, at least, some effects might be visible in heavy-ion collisions provided the critical temperature of the transition is sufficiently high. Although a critical slowing down effects smear effects of thermodynamical fluctuations, one may hope to observe some deviations in fluctuation effects compared to those from trivial statistical fluctuations.

Experiments with heavy-ions in a broad region of the beam energies (at a monotonous increase of the collision energy with a certain energy step) are welcome in order to distinguish above mentioned effects. One may hope to observe a non-monotonous behavior of different observables at a step-by-step increase of the collision energy in some energy interval.

3.3 Searching for evidence of spinodal decomposition

J. Randrup

Nuclear Science Division, Lawrence Berkeley National Laboratory, Berkeley, California, USA

The phase structure of strongly interacting matter forms a focal point for current theoretical and experimental investigations around the world. The Relativistic Heavy Ion Collider (RHIC) at BNL is preparing for a beam energy scan that aims to identify signals of the expected critical point and the CBM experiment at the future Facility for Antiproton and Ion Research (FAIR) at GSI will explore the properties of compressed baryonic matter in the deconfined phase as well as search for evidence of the expected confinement phase transition. The

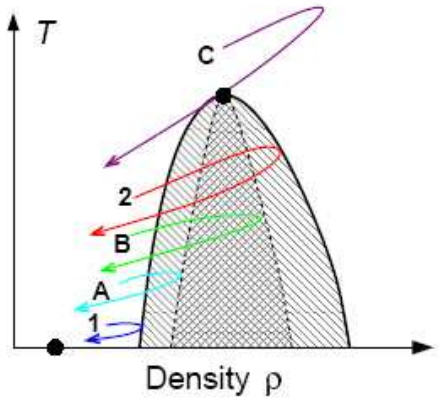

Figure 3.4: Dynamical phase trajectories for the most compressed matter produced at various threshold collision energies E_1, E_A, E_B, E_2, E_c. The solid curve shows the phase co-existence boundary: at a given temperature $T < T_c$, bulk systems at the densities $\rho_1(T)$ and $\rho_2(T)$ are in thermodynamic equilibrium; the lower and higher coexistence boundaries meet at the critical point (ρ_c, T_c); uniform matter is thermodynamically unfavored inside the coexistence region. The dashed curve shows the boundary within which uniform matter is mechanically unstable and entropy can be gained by infinitesimal irregularities.

contemplated Nuclotron-based Ion Collider Facility at JINR would complement those programs by focussing on collision energies where the bulk of the collision system receives maximum exposure to the mixed phase (these

relatively low collision energies can most likely not be provided by RHIC). Generally speaking, one may expect that the prospects for learning about the mixed phase would improve with the time spent by the bulk of the system inside the coexistence region of the phase diagram. Fig. 3.4 illustrates how this quantity develops with the collision energy.

A first-order phase transition is inherently accompanied by the phenomenon known as spinodal decompositon, a clumping with a characteristic spatial scale [10, 11]. Intuitively, one would expect that collision energies slightly below $E_{\rm B}$ would be optimal for maximizing the time spent by the phase trajectory inside the spinodal region. Such collisions, in turn, would presumably be most favorable for the spinodal instabilities to develop. Recent transport calculations of phase trajectories [12] suggest that this optimal beam energy is $E_{\rm lab} = 5 - 15$ AGeV for a stationary target setup, corresponding to a total beam energy of $1.8 - 2.8$ AGeV in a collider. [The precise values depend not only on the specific location of the spinodal phase boundaries, i.e. on the specific equation of state (which is still unknown), but also on the complications arising from the non-uniformity of the density and its time evolution.] Rough estimates indicate that collisions within a suitably tuned energy range may produce bulk matter that stays inside the mechanically unstable phase region sufficiently long for some degree of spinodal decomposition to develop [13]. However, reliable predictions cannot yet be made which underscores the need for identifying observable consequences of such a clumping.

3.4 Supercooled quark-gluon phase?

Yu. Ivanov

Kurchatov Institute, Moscow, Russia

A prime goal of planned experiments at NICA is search for onset of a phase transition to the quark-gluon phase. Presently theoretical models indicate that this should be a first-order phase transition. A phase transition, first of all, implies certain softening of the equation of state (EoS) as compared to a hadronic EoS without any transition. Therefore, experimental evidences of such softening can be viewed as a signal of the deconfinement transition. In fact, there are such evidences: directed flow data favor a steady softening of the EoS with increasing beam energy [14], proton rapidity distributions also require a softer EoS at lower SPS energies [15]. The above analysis was performed within a 3-fluid dynamical model [14]. At the same time, there is no model which, based on the same unique EoS (or mean-field interaction in kinetic models), reproduces all the body of available experimental data, from AGS to SPS energies, on such a "trivial" mechanical characteristics of nuclear collisions as proton rapidity distributions, transverse momentum spectra, directed and elliptic flows. It means that we do not quite well understand the global dynamics of nuclear collisions in this energy range. Hydrodynamical simulations with a EoS involving the first-order phase transition within the Maxwell construction do not help to improve this reproduction. A probable reason for these theoretical problems is that a phase transition occurs but the Maxwell construction is not applicable for its description in nuclear collisions at high incident energies. Indeed, the Maxwell construction implies adiabatically slow evolution of the matter, when seeds of the new phase have enough time to grow to their equilibrium value and thus form a mixed phase. As it was demonstrated in recent papers [8, 13], the rate of the fluctuation growth in the phase-transition region is very slow as compared with the collective evolution of the matter. Precisely this makes the Maxwell construction inapplicable. The slow growth of seeds of hadronic phase in the rapidly expanding quark-gluon matter may result in that the system pass by the mixed phase and directly gets into a phase of the supercooled quark-gluon matter. In particular, this supercooled matter will hadronize at lower temperatures and/or baryon densities than those predicted by thermodynamics based on the mixed-phase concept. Since growth of fluctuations in the supercooled state is already very fast, the hadronization of this supercooled quark-gluon matter has already an explosive character. This is an alternative scenario to the mixed-phase one which should be considered. The above scenario has its practical consequences. From the theoretical point of view:

- It is necessary to construct EoS's based on the concept of the supercooled quark-gluon matter rather than the corresponding mixed phase.
- It is necessary to adapt hydrodynamic models for work with such kind of EoS's.
- It is necessary to study fluctuations at the explosive hadronization of the supercooled matter and consider chances for these fluctuations to survive in the evolution of already hadronic phase to its freeze-out.

Note that while first steps in realization of the first two points have been already done [8, 13], the work on the last point has not been even started. From the experimental point of view:

- Excitation functions of such a conventional "mechanical" observables as rapidity distributions, transverse momentum spectra, directed and elliptic flows are required. A large body of such data is already available from experiments at AGS and SPS. However, in the range of lower SPS energies, which is most suspicious on the possible onset of deconfinement, these data are still fragmentary. NICA is going to well cover this energy range. These observables reflect softness of the EoS and hence are directly relevant to the search for a phase transition.

- Measurements of event-by-event fluctuations are required.

3.5 Rigorous investigation of surface tension and finite width of the QGP bags at NICA energies

K. Bugaev

Bogolyubov Institute for Theoretical Physics, Kiev, Ukraine

Extensive experimental and theoretical searches for the (tri)critical endpoint of the strongly interacting matter became one of the focal point of the modern nuclear physics. These searches are one of the primary goals of the planned low energy experimental programs at RHIC (BNL), SPS(CERN), NICA (Dubna) and FAIR (GSI). However, at present neither the Equation of State (EoS) of strongly interacting matter, nor the exact location of the deconfnement Phase Transition (PT) and/or cross-over are known. Moreover, on the one hand the lattice QCD simulations of different groups disagree with each other on the location of the (tri)critical QCD endpoint, and on the other hand the results of mean-field models are not informative. The commonly used Pisarski-Wilczek argument based on the universality properties is, strictly speaking, valid for the chiral restoration PT whereas for the deconfinement PT it might be irrelevant. Furthermore, such line of arguments does not explain the reason why, depending on the number of flavors, the finite masses of light quarks demolish the 1-st or 2-nd order PT at low baryonic densities and do not destroy it at high densities. Therefore, the searches for the physical cause that is responsible for a degeneration of the 1-st order deconfinement PT at high baryonic densities to a weaker PT at the (tri)critical endpoint and to a cross-over at low baryonic densities are of great importance for heavy ion phenomenology. Moreover, there exists a huge list of unanswered (and often ignored!) questions related to the following two main problems of modeling PT in finite systems which are probed in the nuclear laboratories:

- how the EoS with PT is modified in finite systems; and

- how the endpoint properties would look like in a finite system.

These problems are routed in the fact that, despite many progress reports, there are only a few general guesses how to define PT and the corresponding analogs of phases in finite systems while the rigorous treatment of this problem is at the initial stage of research [17].

It turns, however, out that investigation of the strongly interacting matter EoS based on the exactly solvable models [17, 18, 19, 20, 21] is vitally necessary for a success of NICA program. First of all the modern statistical model of the liquid-vapor PT teach us that the vanishing surface tension coefficient plays a crucial role in the (tri)critical endpoint existence [17]. This fact was put into the grounds of the Quark Gluon Bags with Surface Tension Model (QGBSTM) [18] which enable us to work out a unified statistical description of the 1-st and 2-nd order deconfinement PT with the cross-over. This model naturally explains that the reason for degenerating the 1-st order deconfinement PT into a weaker PT at the endpoint and into a cross-over at low baryonic densities is due to negative surface tension coefficient of the QGP bags at high energy densities [18]. It is shown that the QGBSTM has a tricritical point since the deconfined QGP phase must be separated from the cross-over QGP by another PT which is induced by the change of sign of the surface tension coefficient of large bags [18]. Very recently this model was developed further in order to generate the critical endpoint [19].

Despite the considerable success of the statistical models [17, 18, 19] discussed above and their remarkable features, all of them (and all other ones!) face two conceptual problems [20] that can be formulated as following:

- Why the QGP bags and/or strangelets are never directly observed in experiments?

- Why we do not observe more hadronic resonances with masses above 2.5 GeV?

These conceptual problems have been resolved recently [20] by the inclusion of the Gaussian width of the QGP bags which depends on the bag's volume. Such a model, the Finite Width Model (FWM), not only naturally generates the linear temperature dependence of the QGP pressure at low temperatures which is well known from the lattice QCD, but also it explicitly demonstrates that the large and/or heavy QGP bags can be regarded as the objects belonging to the Regge trajectories. Thus, at hight temperatures the average mass and width of the QGP bags behave in accordance with the upper bound of the Regge trajectory asymptotics (the linear asymptotics), whereas at low temperatures they obey the lower bound of the Regge trajectory asymptotics (the square root one) [20].

Counting all this I conclude that there are three main directions of research which will resolve two main problems of modeling a PT in finite systems and will help us to establish the leadership of NICA project both in theoretical and experimental studies compared to other low-energy programs (see the thorough discussions in [21]):

- **to drastically improve the exactly solvable models and rigorously extend them to finite systems**: to normalize the QGBSTM [18, 19] onto the existing lattice QCD data and reproduce the deviation of the QGP EoS from the Stefan-Boltzmann limit at zero baryonic densities; include the nonzero baryonic and strange chemical potentials into the QGBSTM inspired models [18, 19] and test them on the measured particle yield ratios; study the critical exponents of the QGBSTM [18, 19] and their possible modifications in finite systems on the basis of the Laplace-Fourier method [17]; investigate the influence of the Fisher index τ on the values of critical indices of the QGBSTM inspired models and the possible determination of τ value from the cluster scaling picture [21] emerging from the heavy ion collisions data; include the Lorentz contraction of the excluded volumes of light hadrons into the QGBSTM [18, 19], improve the existing Van der Waals extrapolations according to relativistic prescription, calculate the kinetic coefficients for hadronic matter and QGP bags below and above cross-over and determine the free parameters from the comparison with the AdS/CF results.

- **to study all aspects of the surface tension of the QGP bags**: generalize the Hills and Dales model [17] to the clusters with the continuous base of deformations and use it to estimate the surface entropy of the QGP bags; examine the bimodal [17] and monomodal [21] properties of finite QGP matter with positive and negative surface tension coefficient, respectively, to formulate possible signals of the deconfinement PT, the cross-over transition and surface-induced PT [18] in finite systems; study the volume-surface fluctuations of QGP bags in the grand canonical, canonical and microcanonical ensembles in order to reconstruct an actual surface tension coefficient of the QGP bags; investigate the HBT radii of highly nonspherical QGP bags above the cross-over and the HBT emission volume event-by-event fluctuations for soft photons and pions as the possible signals of negative surface tension coefficient; elucidate the surface tension coefficient of QGP bags from the LQCD data and establish the relation between the surface tension coefficient and the string tension one; study the in influence of shape deformations with positive heights (hills) on the fusion and decay rates of QGP bags to describe the kinetics and hydro-kinetics of the 1-st order PT in finite systems.

- **to investigate the role of the QGP bags finite width**: estimate the mean width of heavy hadronic resonances from the review of the Particle Data Group; consider the large N_c limit of the FWM and establish the connection between the FWM and the corresponding limit of the QCD and QCD inspired models; elucidate the width of QGP bags directly from the LQCD data of the metastable branch of the QGP EoS; work out a microscopic model of sequential decay of heavy QGP bags and find out the constraints on the width of these bags from the particle yields data measured in the collisions of elementary particles at high energies and from the nuclear collisions data on the early hadronizing particles; investigate the processes of melting and propagation of QGP bags in the dense and hot media in order to study the low energy jet evolution; combine all the features of the EoS found while completing the projects related to the surface tension of the QGP bags. A completion of this proposal will essentially advance the theoretical backup of NICA project and will allow us to formulate the firm signals of the mixed phase formation in finite systems.

3.6 Isospin effects on phase transitions of hadronic to quark matter

M. Di Toro[a,b], V. Greco[a,b], B. Liu[c,d], and S. Plumari[2]

[a] *Laboratori Nazionali del Sud, Catania, Italy*
[b] *University of Catania, Catania, Italy*
[c] *Center of Theoretical Nuclear Physics, National Laboratory of Heavy Ion Accelerator, Lanzhou, China*
[d] *Institute of High Energy Physics, Chinese Academy of Sciences, Beijing, China*

The phase transition of hadronic to quark matter at high baryon and isospin density is analyzed. Nonlinear relativistic mean field models are used to describe hadronic matter, and the MIT bag model is adopted for quark matter. The boundaries of the mixed phase and the related critical points for symmetric and asymmetric matter are obtained. Isospin effects appear to be rather significant. The binodal transition line of the (T, ρ_B) diagram is lowered in a region accessible to heavy ion collisions in the energy range of the NICA project. Some observable effects are suggested, in particular a "neutron distillation" mechanism. Theoretically a very important problem appears to be the suitable treatment of the isovector part of the interaction in effective QCD lagrangian approaches.

On the transition to a mixed hadron-quark phase at high baryon and isospin density

Several suggestions are already present about the possibility of interesting isospin effects on the transition to a mixed hadron-quark phase at high baryon density [22, 23, 24, 25]. This seems to be a very appealing physics program for the NICA project if heavy ion beams will be available with good intensities in the energy region $E_{\rm lab}$ =1 – 10 AGeV. The weak point of those predictions is the lack of a reliable equation of state that can describe with the same confidence the two phases, hadronic and deconfined. On the other hand this also represents a strong theory motivation to work on more refined effective theories for a strong interacting matter. The argument in favor of noticeable isospin effects on the hadron-quark transition at high density is very simple and can be easily derived from the Fig. 3.5, where we compare typical Equations of State for Hadron and Quark Matter (at zero temperature) for symmetric $\alpha \equiv \rho_n - \rho_p/\rho_B \equiv -\rho_3/\rho_B = 0$ and neutron matter ($\alpha = 1$). For the Hadron part we use a Relativistic Mean Field [26] result with non-linear terms and effective ρ-meson coupling for the isovector part, largely used to study isospin effects on meson production and collective flows [24, 27]. The energy density and the pressure for the quark phase are, respectively, given by the MIT Bag model [28] (two-flavor case):

$$\varepsilon = 3 \times 2 \sum_{q=u,d} \int \frac{d^3k}{(2\pi)^3} \sqrt{k^2 + m_q^2}\, (f_q + \bar{f}_q) + B \,, \tag{3.1}$$

$$P = \frac{3 \times 2}{3} \sum_{q=u,d} \int \frac{d^3k}{(2\pi)^3} \frac{k^2}{\sqrt{k^2 + m_q^2}}\, (f_q + \bar{f}_q) - B \,, \tag{3.2}$$

where B denotes the bag constant (the bag pressure), taken as a rather standard value from the hadron spectra (no density dependence), $m_{\rm q}$ is the quark mass, and $f_{\rm q}$, $\bar{f}_{\rm q}$ represent the Fermi distribution functions for quarks and anti-quarks. The transition to the more repulsive quark matter should appear around the crossing points of the two EoS. We see that such crossing for symmetric matter ($\alpha_{\rm H} = \alpha_{\rm Q} = 0$) is located at rather high density, $\rho_{\rm B} = \rho_{\rm Q} = 1$, while for pure neutron matter ($\alpha_{\rm H} = \alpha_{\rm Q} = 1.0$) the crossing is moving down to about three times ρ_0. Since we have a coexistence transition region we would expect to see some mixed phase effects already at relatively low density for asymmetric systems, easily reached in relativistic heavy ion collisions.

We note that the above argument is rather independent of the used Hadron EoS at high density, quite stiff in agreement with collective flow and kaon production data [6]. For the quark part the lack of explicit isovector interactions could represent a problem. In fact we can study in detail the isospin dependence of the transition densities [22, 23, 24]. The structure of the mixed phase is obtained by imposing the Gibbs conditions [30] for

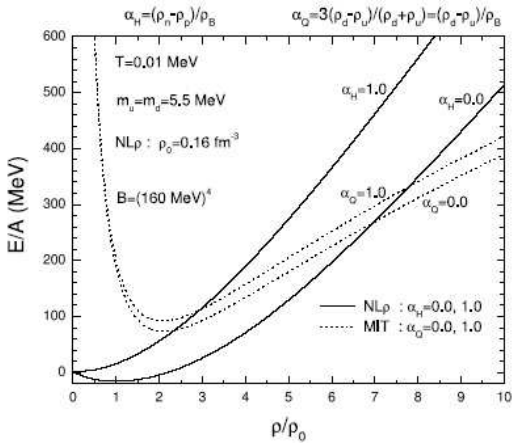

Figure 3.5: EoS of Symmetric/Neutron Matter: Hadron (NLρ), solid lines, vs. Quark (MIT-Bag), dashed lines. $\alpha_{\rm H,Q}$ represent the isospin asymmetry parameters respectively of the hadron,quark matter: $\alpha_{\rm H,Q}=0$, Symmetric Matter; $\alpha_{\rm H,Q}=1$ Neutron Matter.

chemical potentials and pressure and by requiring the conservation of the total baryon and isospin densities

$$\begin{aligned}
\mu_{\rm B}^H(\rho_{\rm B}^H,\rho_3^H,T) &= \mu_{\rm B}^Q(\rho_{\rm B}^Q,\rho_3^Q,T)\ ,\\
\mu_3^H(\rho_3^H,\rho_3^3,T) &= \mu_3^Q(\rho_3^Q,\rho_3^3,T)\ ,\\
P^H(\rho_{\rm B}^H,\rho_3^H,T) &= P^H(\rho_{\rm B}^Q,\rho_3^Q,T)\ ,\\
\rho_{\rm B} &= (1-\chi)\rho_{\rm B}^H+\chi\rho_{\rm B}^Q\ ,\\
\rho_3 &= -\alpha\rho_{\rm B}=(1-\chi)\rho_3^H+\chi\rho_3^Q\ ,
\end{aligned}\tag{3.3}$$

where χ is the fraction of quark matter in the mixed phase. In this way we get the binodal surface which gives the phase coexistence region in the (T,$\rho_{\rm B}$, ρ_3) space. For a fixed value of the total asymmetry $\alpha_T=\rho_3/\rho_{\rm B}$ we will study the boundaries of the mixed phase region in the (T, $\rho_{\rm B}$) plane. In the hadronic phase the charge chemical potential is given by $\mu_3=2E_{\rm sym}(\rho_{\rm B})\rho_3/\rho_{\rm B}$. Thus, we expect that critical densities rather sensitive to the isovector channel in the hadronic EoS. In general for each effective interactive lagrangian we can simulate the solution of the highly nonlinear system of Eqs.(3.3), via a minimization procedure, in order to determine the binodal boundaries and the final critical point (T_c, $\rho_{\rm Bc}$) of the mixed phase. Typical results for isospin effects

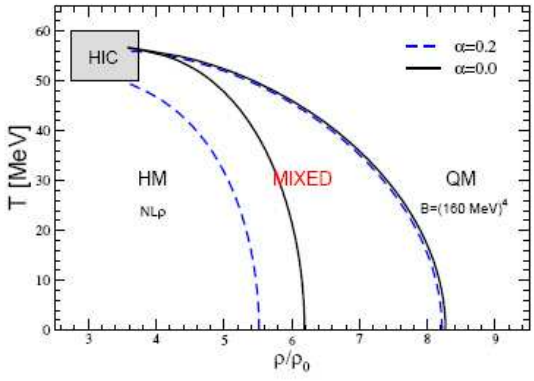

Figure 3.6: Binodal surface for symmetric (α =0.0) and asymmetric (α =0.2) matter. Hadron EoS from NLρ interaction. Quark EoS: MIT bag model with $B^{1/4}$=160 MeV. The grey region corresponds to the conditions reached in heavy ion collision simulations at few AGeV beam energies, see also Fig. 3.7.

on the binodal "surface" are presented in Fig. 3.6 for symmetric and asymmetric matter. For the hadron part we have started from a NLρ effective Lagrangian very close to other widely used relativistic effective models, e.g. see the GM3 of Ref. [30]. As expected, the lower boundary of the mixed phase is mostly affected by isospin effects. In spite of the relatively small total asymmetry, α =0.2, we clearly see a shift to the left of the first transition boundary, in particular at low temperature, and a relatively "early" critical point, around ($T = 53 \div 58$ MeV, $\rho_B = 2.5 \div 2.8\rho_0$), well within the reach of heavy ion collisions in the few AGeV range.

Collision simulations and NICA perspectives

In order to check the possibility of observing some precursor signals of a new physics even in collisions of stable nuclei at intermediate energies we have performed some event simulations for the collision of very heavy, neutron-rich, elements, using a consistent relativistic mean field approach with the same interactions [24, 27]. We have chosen the reaction $^{238}U + ^{238}U$ (average proton fraction Z/A = 0.39) at 1 AGeV and semicentral impact parameter $b = 7$ fm just to increase the neutron excess in the interacting region, see [24]. In Fig. 3.7 we report the evolution of momentum distribution and baryon density in a space cell located in the c.m. of the system. We see that after about 10 fm/c a local equilibration is achieved. We have a unique Fermi distribution and from a simple fit we can evaluate the local temperature (black numbers in MeV). We note that a rather exotic nuclear matter is formed in a transient time of the order of 10 fm/c with baryon density around $(3-4)\rho_0$, temperature 50 – 60 MeV, energy density 500 MeV fm^{-3} and proton fraction between 0.35 and 0.40, likely inside the estimated mixed phase region, close to the critical point. Which are the observable effects to look at if we enter and/or cross the mixed phase? A first expectation would be a general softening of the matter, due to the contribution of more degrees of freedom, with consequences on collective flows and particle/cluster production. For the latter point we can expect also a neutron distillation effect, a kind of *neutron trapping* in the quark phase, supported by statistical fluctuations as well as by a symmetry energy difference in the two phases, see Fig. 14 of Ref. [23]. In fact while in the hadron phase at high density we have a large neutron potential repulsion (in particular in the NLρ case), in the quark phase the neutron see only the much smaller kinetic contribution from the Fermi gas. If in a pure hadronic phase neutrons are quickly emitted or "transformed" in protons by inelastic collisions, when the mixed phase starts forming, neutrons are kept in the interacting system up to the subsequent hadronization in the expansion stage [24]. Observables related to such neutron "trapping" could be an inversion in the trend of the formation of neutron rich fragments and/or of the $\pi^-/\pi^+, K^0/K^+$ yield ratios for reaction products coming from high density regions, i.e. with large transverse momenta.

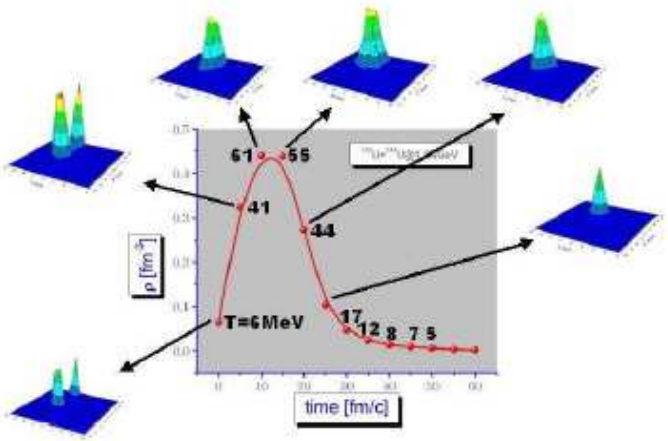

Figure 3.7: $^{238}U + ^{238}U$, 1 AGeV , semicentral collisions. Correlation between density, temperature (black values), momentum thermalization (3D plots), inside a cubic cell, 2.5 fm wide, in the center of mass of the system.

We note that all the above arguments, on the binodal boundaries of the mixed phase, on the critical point and on the neutron distillation are rather independent of the used Hadron EoS at high density, that should be relatively stiff in agreement with collective flow and kaon production data [6]. At variance for the quark sector there is the lack of explicit isovector interaction that could strongly affect the isospin effects on the location of the phase transition.

Isospin in effective partonic models

From the above discussion it appears extremely important to include the isospin degree of freedom in any effective QCD dynamics. A first approach can be supplied by a two-flavor NJL model [31] where the isospin asymmetry can be included in a flavor-mixing picture [32] via a Gap Equation like $M_i = m - i - 4G_1\Phi_i - 4G_2\Phi_j, i \neq j, (u,d)$, where the $\Phi_{u,d} =< \bar{u}u >, < \bar{d}d >$ are the two (negative) condensates and mu;d = m the (equal) current masses. Introducing explicitly a flavor mixing, i.e. the dependence of the constituent mass of a given flavor to both condensate, via $G_1 = (1-\alpha)G_0,\ G_2 = \alpha G_0$ we have the coupled equations

$$M_u = m - 4G_0\Phi_u - 4G_0(\Phi_u - \Phi_d) \tag{3.4}$$

$$M_d = m - 4G_0\Phi_u + 4(1-\alpha)G_0(\Phi_u - \Phi_d)\ . \tag{3.5}$$

For $\alpha = 1/2$ we go back to the usual NJL ($M_u = M_d$), while small/large mixing is for $\alpha \to 0/\alpha \to 1$, respectively. In neutron rich matter $|\Phi_d|$ decreases more rapidly due to the larger ρ_d and so $(\Phi_u - \Phi_d) < 0$. In the "realistic" small mixing case, see also [32, 33], we will get a definite $M_u > M_d$ splitting at high baryon density (before the chiral restoration). This expectation is nicely confirmed by a full calculation [34] of the coupled gap equations with standard parameters (same as in Ref. [32]).

All that can indicate a more fundamental confirmation of the $m_p^* > m_n^*$ splitting in the hadron phase, as suggested by the effective QHD model with the isovector scalar δ coupling, see [27, 35].

However such isospin mixing effect results in a very small variation of the symmetry energy in the quark phase. In fact this represents just a very first step towards a more complete treatment of isovector interactions in effective partonic models, and is of large interest for the discussion of the phase transition at high densities. We remind that confinement is still missing in these mean-field models. Stimulating new perspectives are open.

3.7 Accessibility of dense QCD phases in heavy-ion collisions

D. Blaschke[a,b], F. Sandin[c,d], V. Skokov[b,e,f] and S. Typel[e,g]

[a] *Institute for Theoretical Physics, University of Wrocław, Poland*
[b] *Joint Institute for Nuclear Research, Dubna, Russia*
[c] *Fundamental Interactions in Physics and Astrophysics, University of Liège, Belgium*
[d] *EISLAB, Luleå University of Technology, 971 87 Luleå, Sweden*
[e] *Gesellschaft für Schwerionenforschung mbH, Darmstadt, Germany*
[f] *Frankfurt Institute for Advanced Studies, Universität Frankfurt, Germany*
[g] *Excellence Cluster Universe, Technical University Munich, Garching, Germany.*

Theoretical studies of the QCD phase diagram have predicted a rich structure of nonperturbative phases under conditions of temperatures T below the deconfinement temperature $T_c \sim 180$ MeV found in lattice QCD studies [36] and baryochemical potentials $\mu_{\rm B}$ above $\sim m_{\rm N}$, where $m_{\rm N} = 939$ MeV is the nucleon mass. Of particular interest are the questions:

- How does the order and the location of the chiral phase transition depend on temperature, density, size and isospin asymmetry of the system?
- What is the nature of confinement and how does deconfinement occur?
- Can deconfinement and chiral symmetry restoration occur independent from each other at high densities? As a consequence, shall we expect massive deconfined quark matter or chirally symmetric but confined quark matter (quarkyonic matter)?
- Is dense quark matter (color) superconducting? Does confinement preclude color superconductivity? Is there a BEC or rather BCS phase of color superconductivity? What is the critical temperature? Can these phases be created in the laboratory?

The JINR Nuclotron and the Nuclotron-based Ion Collider fAcility (NICA) gives a unique opportunity to explore the above mentioned region of the phase diagram, and may thus complement alternative programs for systematic studies of heavy-ion collisons in the relevant range of collision energies $2 \leq E_{\rm lab} \leq 40$ AGeV. The energy scan program of the NA49 experiment has given indications for a phase change at $E_{\rm lab} \sim 30$ AGeV,

in particular from the peak ("horn") in the K^+/π^+ ratio. Experiments of the next generation (NA61-SHINE, low-energy RHIC, CBM and NICA) should, however, take into their focus the possibility that qualitatively new features could be found at still lower energies. This concerns in particular color superconducting quark matter phases like the 2SC phase and the recently conjectured quarkyonic phase [50]. As has been demonstrated in [37, 38] the coupling to the Polyakov loop increases the critical temperature for the 2SC phase to the order of the deconfinement temperature $T_{2SC} \sim 150$ MeV, see the left panel of Fig. 3.8. In that figure, we show a modern QCD model phase diagram based on a quark matter EoS from a three-flavor NJL model with selfconsistent quark masses and diquark gaps [39, 40, 41, 42], generalized here by the coupling to the Polyakov-loop potential to suppress unpysical quark degrees of freedom. The hadronic phase is modeled according to a density-dependent relativistic meanfield approach [43] which also describes the nuclear liquid-gas phase transition with a critical point, see the blue hatched region in Fig. 3.8 (left panel). The hadron-to-quark matter transition is obtained from the Maxwell construction with a mixed phase coexistence region shown by the turquoise hatched region. The unusual nose-like shape of this region is due to the Polyakov-loop potential which suppresses the quark pressure at finite temperatures below the deconfinement temperature, but not at $T = 0$. At low temperatures, the appearance of the diquark condensate shifts the chiral restoration transition to rather low densities, of the order of $(2-3)\ n_0$, $n_0 = 0.16$ fm^{-3}.

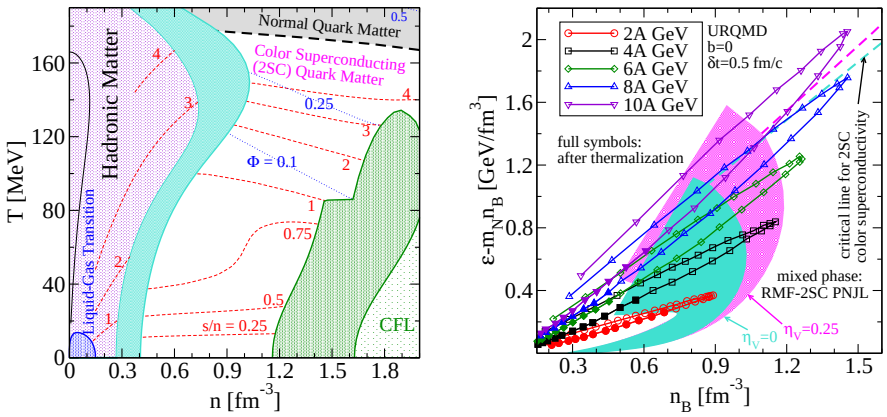

Figure 3.8: Left panel: QCD model phase diagram with mixed phase regions corresponding to the first order phase transitions: nuclear liquid-gas (blue), hadron - quark matter (turquoise), 2SC - CFL quark matter (green). The transition from color superconducting (2SC) quark matter to normal quark matter is of second order (dashed line). Right panel: trajectories of heavy-ion collisions at different energies in the excitation energy-density plane overlayed to the hadronic matter - 2SC quark matter mixed phase region of the model-QCD phase diagram. Hatched regions indicate the mixed phase for two parametrizations of the quark matter model, with ($\eta_V = 0.25$, magenta) and without ($\eta_V = 0$, turquoise) vector mean field. The dashed lines with corresponding colors denote the critical lines for 2SC color superconductivity of these parametrizations.

In order to answer the question of the accessibility of these new phases of dense QCD matter, we have examined the trajectories of the Lorentz contracted central region of central Au + Au collisions of given energies in the range $2 < E_{\rm lab} < 10$ AGeV from UrQMD simulations, see the right panel of Fig. 3.8. The hatched regions correspond to the mixed phase of hadronic and 2SC quarkyonic matter for two parametrizations of the PNJL model, with ($\eta_V = 0.25$, magenta) and without ($\eta_V = 0$, turquoise) vector mean field. The dashed lines with corresponding colors denote the critical lines for 2SC color superconductivity of these parametrizations. We conclude from this figure that for energies $4 < E_{\rm lab} < 8$ AGeV, which are in reach of the present Nuclotron facility already now, one may expect to enter the 2SC color superconducting quark matter phase with restored chiral symmetry and strong color correlations due to a low Polyakov-loop meanfield $\Phi < 0.25$, indicating a quarkyonic phase [95]. The exploration of the transition from color superconducting to normal quark matter and finally the ceasing of the mixed phase at the QCD critical point would require energies beyond 10 AGeV, aimed to be reached at NICA.

Finally, let us discuss two ideas for the experimental identification of the chiral restoration and the color superconductivity transition which should be considered when planning experiments and in particular when designing the MPD detector system.

- An enhancement of the two-photon invariant mass spectrum in the mass range $M_{2\gamma} \sim 300$ MeV, from the decay of the sigma meson which should become a long-lived "sharp" resonance when chiral symmetry gets restored and the dominant tw-pion decay channel gets closed [45, 46]. This signal shall also prevail in the hypothetic quarkyonic phase and more traditional estimates of the two-photon spectrum within the ordinary NJL model would have to be revised within the PNJL model.

- An enhancement of the lepton-pair invariant mass spectrum when approaching the critical temperature for color superconductivity from above (precursor effect [47]) which should eventually turn into a resonance-like structure when entering the 2SC phase, due to additional contributions to the diquark-antidiquark annihilation diagrams (generalized Aslamasov-Larkin and Maki-Thompson diagrams) containing anomalous propagator contributions.

In conclusion we would like to stress that our modern QCD model phase diagram suggests that new dense quark matter phases (color superconductor and quarkyonic matter) are accessible already at the present nuclotron energies and that both the study of the transition to normal quark matter and the vanishing of the mixed phase at the QCD critical endpoint will require higher energies than presently available at the Nuclotron but attainable at the NICA facility.

3.8 Transitional change to baryon-rich QCD matter at NICA energy

K. Fukushima

Yukawa Institute for Theoretical Physics, Kyoto University, Kyoto, Japan

The temperature T and the baryon chemical potential $\mu_{\rm B}$ at the chemical freeze-out are nicely determined by the Statistical Model. It is a tempting idea to associate the freeze-out curve unravelled in such a way with any of QCD phase transition. In fact both chiral and deconfinement transitions in QCD could crucially affect thermodynamic properties of the system and trigger the sudden freeze-out then.

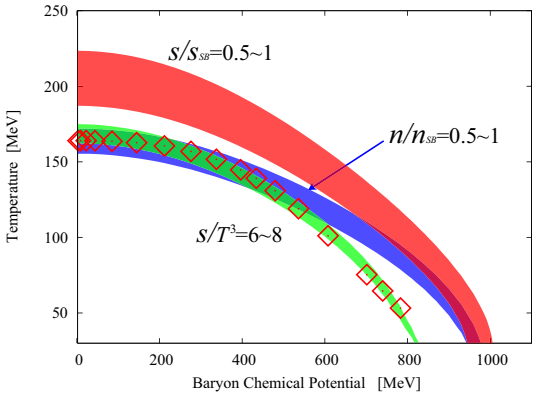

Figure 3.9: Thermodynamics from the Statistical Model by THERMUS [48]. The red and blue bands represent the regions where the entropy density s and the baryon number density n, respectively, normalized by the Stefan-Boltzmann value range from 0.5 to 1. The green band is the region in which s/T^3 takes a value from 6 to 8 so as to fit in with the freeze-out points represented by the red square dots.

One of the thermodynamic constraints that reproduce the freeze-out curve is the condition; $s/T^3 \approx 7$. The agreement is actually excellent as seen from Fig. 3.9. At the same time, as seen from Fig. 3.9, one may well consider that other conditions to detect the points where either the entropy density s or the baryon number density n rapidly increase lead to curves similar to the freeze-out one. Intuitively it should be rather natural to consider that not s/T^3 but s itself is a sensitive quantity to deconfinement. Let us try to fit the freeze-out curve by a condition to require that the entropy density itself is fixed.

Fig. 3.10 clearly shows that the constant-s cannot reproduce the freeze-out curve. It is interesting that the freeze-out curve suddenly drops down with a steeper slope than the constant-s curve. A possible interpretation for this is that a transitional change of the state of QCD matter occurs around $T \approx 150$ MeV and $\mu_{\rm B} \approx 400$ MeV

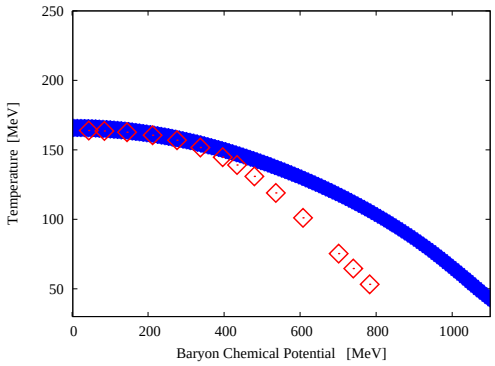

Figure 3.10: Blue band represents the thermodynamic constraint; $s = 4$ fm^{-3} and the freeze-out points are represented by the red square dots.

from where the deviation between the constant-s and freeze-out curves starts growing. It is quite interesting that this departing point corresponds to a collision with the energy $\sqrt{s_{\rm NN}} \approx 8$ GeV, which is just the NICA energy. Hence, it would be extremely intriguing to explore the character of QCD matter in this temperature and density region at NICA. It must be a special point.

A possible interpretation of this special point is the relevance of the triple-point-like region as depicted in Fig. 3.11 that presents a typical output from the PNJL model [95]. Here we see that the deconfinement transition is fairly flat and is to be interpreted as similar to the blue curve in Fig. 3.10. Therefore, in view of Figs. 3.10 and 3.11, the freeze-out points beyond $\mu_{\rm B} \sim 400$ MeV belong to some different physics, namely, a sudden jump in the baryon number in the system. If it is true, the collision energy $\sqrt{s_{\rm NN}} \approx 8$ GeV is a threshold above which abundant baryons can emerge. Such baryon dominant matter yet below deconfinement could be identified with so-called Quarkyonic Matter [49]. NICA would be an ideal facility to probe such an onset to enter the baryon-rich regime of QCD matter.

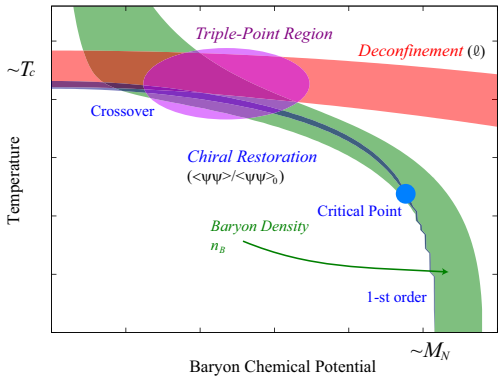

Figure 3.11: A typical example of the phase diagram from the PNJL model.

3.9 Triple point and quarkyonic matter in the QCD phase diagram

L. McLerran[a], K. Redlich[b,c], D. Blaschke[b,d]

[a] *BNL and Riken Brookhaven Center, Upton, NY, USA*
[b] *Institute for Theoretical Physics, University of Wrocław, Wrocław, Poland*
[c] *Theory Division, CERN, Geneva, Switzerland*
[d] *Joint Institute for Nuclear Research, Dubna, Russia*

Features of hadron production in relativistic nuclear collisions, mainly at CERN-SPS energies, may be explained by the existence of three forms of matter: Hadronic Matter, the Quark-Gluon Plasma, and a third

form introduced recently as Quarkyonic Matter [50]. It has been suggested [49] that these meet at a triple point in the QCD phase diagram. A schematic view of such a phase diagram is shown in the left panel of Fig. 3.12. If the transition(s) between the three phases are merely crossover(s), the triple point is only approximate. Some of the features explained by such a picture, both qualitatively and quantitatively, include the curve for the decoupling of chemical equilibrium (see the right panel of Fig. 3.12), along with the non-monotonic behavior of strange particle multiplicity ratios at center of mass energies $\sqrt{s}\lesssim$10 GeV (left panel of Fig. 3.13).

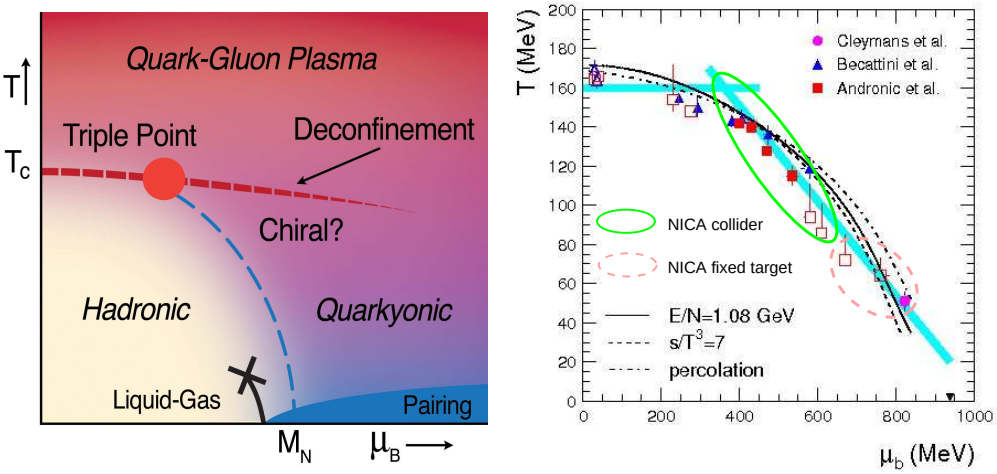

Figure 3.12: Left panel: The conjectured phase diagram of strongly interacting matter according to Ref. [49]. Right panel: Hadronic freeze-out temperatures and chemical potentials extracted by statistical model fits to experimental data on hadron production in heavy-ion collisions.

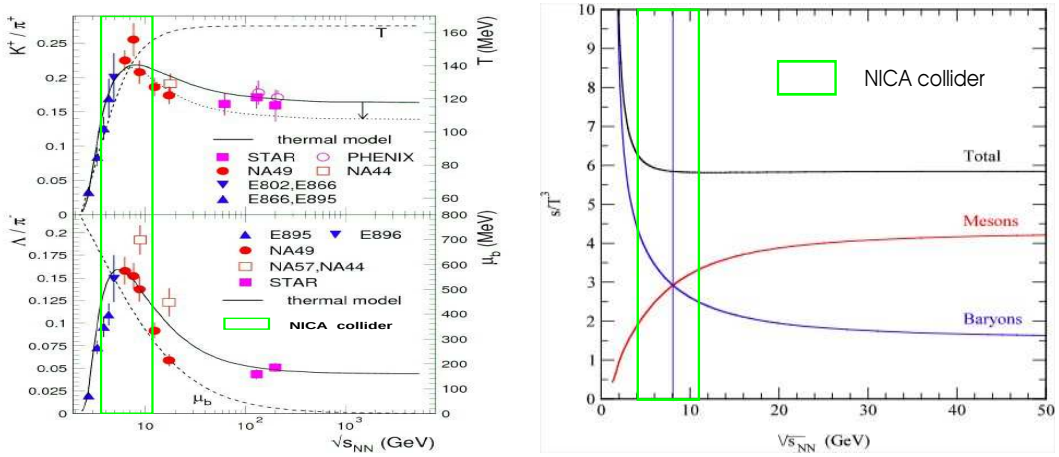

Figure 3.13: Left panel: Energy dependence of hadron yields relative to pions. Right panel: Baryonic and mesonic contributions to the entropy density as a function of the center of mass energy of heavy-ion collisions. When increasing the energy above that where the horn in the K^+/π^+ and Λ/π^+ ratios is observed, $\sqrt{s}\sim 10$ GeV, the system changes its character from baryon- to meson-dominated.

The energy range of the NICA facility at JINR Dubna will be ideally suited to provide more phenomenological evidence for the existence of the triple point and the characteristics of its underlying phase structure. This concerns heavy-ion collisions at both, the collider with the MPD experiment covering 4 GeV $\lesssim\sqrt{s}\lesssim$11 GeV (mirroring the fixed target CBM experiment at FAIR) and the fixed target experiments with the extracted Nuclotron beam of 2 AGeV $\lesssim E_{\rm lab}\lesssim$5.5 AGeV, filling the gap between GSI-SIS20 and AGS energies.

Let us explain the discovery potential of this facility related to the quarkyonic phase a bit more in detail.

According to the original motivation [50], and based on the large N_c limit of QCD, a new view of the QCD phase diagram emerges in the "quarkyonic" region where quarks are still confined like in the hadronic phase, but chiral symmetry is almost restored. A microscopic QCD-motivated approach for the simultaneous description of dynamical chiral symmetry breaking/restoration and confinement/deconfinement at finite temperatures and densities is still absent. Therefore, it is a challenge for theorists to develop approximative methods for characterizing the quarkyonic phase and its observable signatures.

Models of the Nambu-Jona-Lasinio (NJL) type may give valuable insights, in particular to the aspects of chiral dynamics in hot and dense matter. The absence of a confining interaction in this model can partly be remedied by the coupling to a Polyakov loop potential which effectively suppresses the unphysical appearance of quark degrees of freedom in the confinement domain [51, 52]. Polyakov-loop NJL (PNJL) models have been used to discuss the phase diagram [95], where for low temperatures and high densities one finds a chirally restored but confined phase [53], typically accompanied by a diquark condensate signalling color superconductivity [37, 133].

Most studies are restricted to homogeneous phases although the thermodynamically favored ground state at low temperatures generally is a chiral crystalline one characterized by an inhomogeneous order parameter (see Ref. [55] for a review on condensed matter aspects of dense QCD). Well-known example is the chiral density wave [56, 57]. Also in the $1+1$ dimensional NJL model, the Gross-Neveu (GN) model, an inhomogeneous (crystalline) phase exists which for the massless GN model (NJL_2) is a "chiral spiral" and a quite complete result for the phase diagram is known, see [58]. It has been shown that these results can be used to construct solutions of the $3+1$ dimensional NJL model with one-dimensional modulation of the chiral order parameter [59]. The phase structure of such a model bears similarities with the conjectured quarkyonic phase diagram of Fig. 3.12 in that it has three phases joining in the (tri-)critical point: two homogeneous ones (chirally symmetric and chirally broken) and the inhomogeneous chiral spiral phase which would stand for the quarkyonic one [60]. Such a view on the phase diagram got confirmed recently [61] and suggests that the quarkyonic phase could merely be an island covering the first-order transition which instead of ending in a critical point ends in a Lifshitz point [61].

What significance has the assumption of a one-dimensional modulation of the chiral order parameter for the QCD phase structure? For a chiral quark model with confining (Gribov-Zwanziger) Coulomb-gauge gluon propagator, the $3+1$ dimensional theory reduces to a gauge theory in $1+1$ dimensions with a local chiral condensate, spatially varying in one direction: the "Quarkyonic Chiral Spiral" [62]. The quarkyonic chiral spiral state which breaks chiral and translational invariance spontaneously forms patches on the quark Fermi sphere which increase in number with increasing quark density [63].

Unfortunately, no credible signals for the quarkyonic chiral spiral phase in heavy-ion collisions have been developed yet by theory. An *ad hoc* conjecture would suggest that baryon number fluctuations should emerge from the hadronization of this baryon-rich, inhomogeneous phase with spatially varying chiral condensate. Recently, Mócsy and Sorensen have examined the consequences of baryon-rich (like quarkyonic) bubble formation in an expanding in an expanding medium and showed how the tw-particle correlations vary in the transverse and longitudinal direction depending on assumptions for radial flow, bubble temperature and baryon emission time [64].

The NICA facility has an excellent opportunity to verify such conjectures experimentally. This would be a scientific discovery of great importance.

3.10 Search for the QCD Critical Point at NICA

X. Luo[a,c], B. Mohanty[b], H.G. Ritter[c], N. Xu[c]

[a] *Department of Modern Physics, University of Science and Technology of China, Hefei, China*
[b] *Variable Energy Cyclotron Center, Kolkata, India*
[c] *Lawrence Berkeley National Laboratory Berkeley, CA,USA*

Lattice QCD calculations predict that a cross-over from the hadronic phase to the Quark Gluon Plasma (QGP) phase occurs above a critical temperature for vanishing baryon chemical potential ($\mu_B = 0$). The corresponding cross-over temperature range has been estimated to be about 170 – 190 MeV [65, 66]. At large μ_B, QCD based model calculations indicate that the transition from the hadronic phase to the QGP phase is of first order. The end point of the first order phase transiton line is the QCD Critical Point [67, 68]. There are large theoretical uncertainties of its location and even its existence is not confirmed [69, 70, 71, 72].

Experimentally, we study the QCD phase diagram by high energy heavy ion collisions [73, 74, 75]. By tuning the collision energy, we can vary the baryon chemical potential in the region of interest.

The characteristic feature of a critical point is the increase and divergence of the correlation length (ξ) and of critical fluctuations. Recently, theoretical calculations have shown that higher moments of multiplicity distributions of conserved quantities, such as net-baryon, net-charge, and net-strangeness, are sensitive to the correlation length ξ [3].

In Lattice QCD calculations with $\mu_{\rm B} = 0$, higher order susceptibilities of the baryon number, which can be related to the higher order moments of the net-baryon multiplicity distributions, show a non-monotonic behavior near T_c [76]. A similar behavior is expected for the finite $\mu_{\rm B}$ region. Experimentally, it is hard to measure the net-baryon number while the net-proton number is measurable. Theoretical calculations show that fluctuations of the net-proton number can be used to infer the net-baryon number fluctuations at the critical point[77]. The NICA facility will cover the energy range from $\sqrt{s}$=4 GeV to 11 GeV at the collider and $E_{\rm lab}$ up to 5.5 AGeV for fixed target experiments. Therefore, we propose to study the energy dependence of kurtosis and skewness and other higher order moment products in order to search for the QCD critical point.

We introduce various moments definitions of the event-by-event multiplicity distributions: Mean, $M = < N >$, Variance, $\sigma^2 = < (\Delta N)^2 >$, Skewness, $S = < (\Delta N)^3 > / \sigma^3$, and Kurtosis, $\kappa = < (\Delta N)^4 > / \sigma^4 - 3$, where $\Delta N = N - < N >$. Skewness and Kurtosis are equal to zero for gaussian distributions. Thus, they are ideal probes to demonstrate the non-Gaussian fluctuations feature near the critical point, in particularly a sign change of the skewness or kurtosis may be a hint of that the system is evolving in the vicinity of the critical point [3, 78]. We have calculated the various moments of net-proton ($\Delta p = N_{\rm p} - N_{\bar{\rm p}}$) distributions from transport models. The kinetic coverage of protons and anti-protons used in our analysis is $0.4 < p_{\rm T} < 0.8$ GeV/c and $|y| < 0.5$. Fig. 3.14 (left panel) shows the number of participant ($N_{\rm part}$) dependence of moment

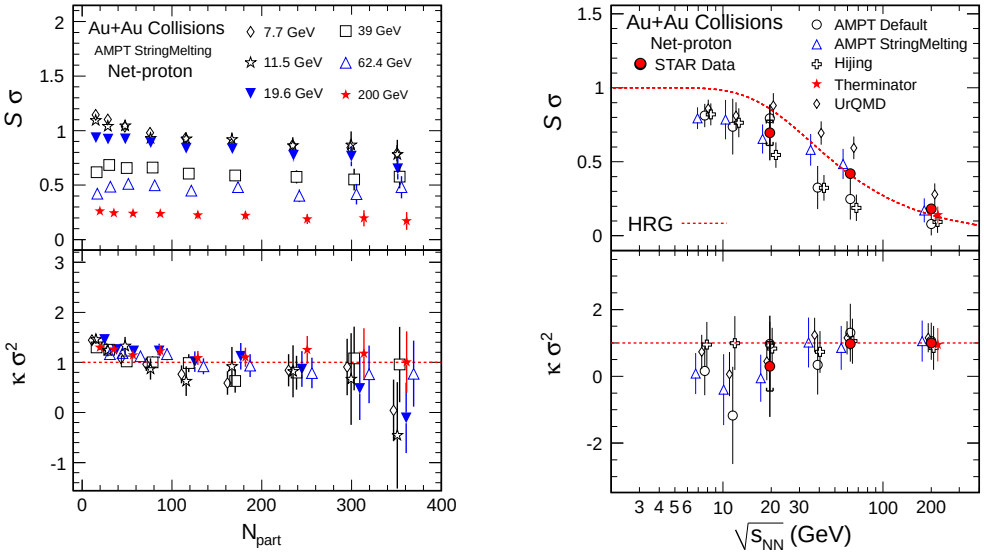

Figure 3.14: **Left panel:** Centrality dependence of moment products $S\sigma$, $\kappa\sigma^2$ of net-proton distributions for Au + Au collisions of various energies from AMPT String Melting model calculation. **Right panel:** Energy dependence of moment products $S\sigma$, $\kappa\sigma^2$ of net-proton distributions for Au + Au collisions of various models and STAR data.

products $S\sigma$, $\kappa\sigma^2$ of net-proton distributions from the AMPT string melting model for various energies. In Fig. 3.14 (right panel), the energy dependence of moment products $S\sigma$, $\kappa\sigma^2$ for most central net-proton distributions from STAR data [79] are compared with the results from various models. We see the data are in good agreement with the HRG model ($\kappa_{\rm B}\sigma^2_{\rm B} = 1$, $S_B\sigma_{\rm B} = tanh(\mu_{\rm B}/T)$) [80] and the thermal model (Therminator) results. A large deviation from constant as a function of $N_{\rm part}$ and collision energy for $\kappa\sigma^2$ may indicate new physics, such as critical fluctuations [3]. Recent lattice QCD calculations from [81] have shown that $\kappa\sigma^2$ non-monotonically depends on colliding energy in the neighbourhood of the critical point.

3.11 Probing the hadron-quark mixed phase at finite temperature, baryon and isospin chemical potentials

G.Y. Shao[a], M. Di Toro[a,b], M. Colonna[a], S. Plumari[a,b], B. Liu[c,d], V. Greco[a,b], Y.X. Liu[e,f]

INFN-Laboratori Nazionali del Sud, Catania, Italy;
Physics and Astronomy Dept., University of Catania, Italy;
IHEP, Chinese Academy of Sciences, Beijing, China
Theoretical Physics Center for Scientific Facilities, Chinese Academy of Sciences, Beijing, China
Department of Physics and State Key Laboratory of Nuclear Physics and Technology, Peking University, China;
Center of Theoretical Nuclear Physics, National Laboratory of Heavy Ion Accelerator, China

The exploration of the phase diagram of strongly interacting matter and search for the signals of the phase transition from hadronic to quark-gluon phase are very important in both theory and experiment. As a fundamental tool, lattice QCD provides us a framework for investigation of non-perturbative phenomena such as confinement and quark-gluon plasma formation at finite temperature and vanishing (small) chemical potential [82, 83, 84]. However, lattice QCD suffers the sigh problem of the fermion determinant with three color at finite μ. Although several approximation methods has been taken to try to evade this problem [67, 85, 86], the validity of lattice simulations at finite chemical potential is still limited in the region $\mu_{\rm q}/T < 1$. The results given with $\mu_{\rm q}/T > 1$ should be taken with care [87].

On the other hand, many phenomenological models [31, 25, 40, 42], as well as the more microscopic Dyson-Schwinger equations (DSEs) approach [88], have been proposed to give a completed description of QCD phase diagram. Among these effective models, the Nambu–Jona-Lasinio model (NJL) is a predominant one, which offers a simple illustration of chiral symmetry breaking and restoration, a key feature of QCD [89, 90, 91], and it presents a complicated phase diagram of color superconductivity at high density [92, 93]. One deficiency of the standard NJL model is that quarks are not confined. Recently, an improved version of the NJL model coupled to Polyakov loop (PNJL) has been proposed [94]. The PNJL model takes into both the chiral symmetry and (de)confinement effect, giving a good interpretation of lattice data at zero chemical potential and finite temperature, and make predictions in the region that cannot be reached in lattice calculation [52, 95, 96].

Most effective models, including the PNJL model, study the hadron-quark-gluon phase transition based on quark degrees of freedom. As a matter of fact, at low temperature and small chemical potential, the QCD dynamics is governed by hadrons. Therefore, it is natural to describe the strongly interacting matter with hadronic degrees of freedom at low T and small μ and quarks at high T and large μ. This picture can be realized in the two equation of state (Two-EoS) approach in which hadronic and quark phases are connected by Gibbs (Maxwell) criteria. This frame is widely used in describing the phase transition in the interior of compact star in weak equilibrium (e.g., [97, 98, 99, 100]). Recently, it has also been taken to explore the phase diagram of hadron-quark transition at finite temperature and density concerned with heavy-ion collision [23, 101, 102, 104, 103, 105]. Moreover, more attention was paid to asymmetric matter, and some observable effects have been already suggested in Ref. [23, 102].

We have studied the hadron-quark phase transition in the Two-EoS model by using the Relativistic Mean Field EoS for the hadron sector and various effective approaches for the quark phase, the static MIT-Bag model [102, 105], the NJL model [106] with the chiral dynamics and finally the extension to the Polyakov-Loop coupling (PNJL) [107] to include also the (de)confinement dynamics.

We obtain the phase diagrams of hadron–quark-gluon phase transition in $T - \rho_{\rm B}$ and $T - \mu_{\rm B}$ planes. The calculations show that some interesting signatures of the transition are very robust, in the sense that they appear for all the different quark EoS:

- The transition is of the first order at finite temperatures and chemical potentials.
- For isospin asymmetric matter the onset density of the mixed phase is much smaller than the one of symmetric matter. This appears important for the possibility of observations in heavy ion collisions at intermediate energies.
- The Isospin Distillation Effect, i.e. the isospin enrichement of the quark component in the mixed phase in the case of asymmetric matter, is always present, in particular at lower temperatures.

All that leads to some confidence about the possibility of an experimental confirmation.

Besides, the results show that the phase-transition region is greatly modified when both the chiral dynamics and (de)confinement effect are considered. The phase-transition at high T is more close to the result given by lattice calculation at small chemical potential. A Critical-End-Point (CEP) is found at $T \simeq 170\ MeV$ and baryon chemical potential $\mu_{\rm B} \simeq 600\ MeV$, i.e. at a quark chemical potential $\mu_{\rm q}/T_c \simeq 1$, in a region that could be tested by extended lattice calculations.

Hadron matter, quark matter and the mixed phase

In the Two-EoS model , the hadron matter at finite temperature and density/chemical potential is described by the non-linear Walecka model, the Relativistic Mean Field (RMF) effective theory which provides an excellent description of nuclear matter and finite nuclei as well as of of compressed matter properties probed with heavy ion collisions at high energies [23, 101, 108, 109]. The exchanged mesons include the isoscalar-scalar meson σ and isoscalar-vector meson ω (NL force, for isospin symmetric matter), isovector-vector meson ρ and isovector-scalar meson δ, ($NL\rho$ and $NL\rho\delta$ forces, for isospin asymmetric matter).

The quark matter at the same conditions is described by the MIT-Bag [102, 105], NJL [106] and PNJL [107] models. For the mixed phase between the pure hadronic and quark phase, the two phases are connected each other with the Gibbs conditions with the thermal, chemical and mechanical equilibriums.

Our aim is to compare mixed phase results obtained with different quark models but keeping the same hadron EoS. However we face a problem since while the microscopic NJL and PNJL approaches have no free parameters, in the MIT-Bag picture the Bag constant can be largely varied, in particular at high densities. Here we have chosen the Bag constant value in order to reproduce the same critical point at high chemical potential as in the NJL and PNJL cases (for isospin symmetric matter). From the systematic study reported in ref.[105] a good choice seems to be $B^{1/4} = 160\ MeV$.

Based on the conservations of baryon number and isospin during the strong interaction, the Gibbs conditions describing the phase transition can be expressed by

$$\begin{aligned}
&\mu_{\rm B}^H(\rho_{\rm B},\rho_3,T) = \mu_{\rm B}^Q(\rho_{\rm B},\rho_3,T)\\
&\mu_3^H(\rho_{\rm B},\rho_3,T) = \mu_3^Q(\rho_{\rm B},\rho_3,T)\\
&P^H(\rho_{\rm B},\rho_3,T) = P^Q(\rho_{\rm B},\rho_3,T),
\end{aligned} \tag{3.6}$$

where $\rho_{\rm B} = (1-\chi)\rho_B^H + \chi\rho_B^Q$ and $\rho_3 = (1-\chi)\rho_3^H + \chi\rho_3^Q$ are the total baryon density, isospin density of the mixed phase, respectively, and χ is the fraction of quark matter, The global asymmetry parameter α for the mixed phase is

$$\alpha \equiv -\frac{\rho_3}{\rho_{\rm B}} = \frac{(1-\chi)\rho_3^H + \chi\rho_3^Q}{(1-\chi)\rho_{\rm B}^H + \chi\rho_{\rm B}^Q} = \alpha^H\ |_{\chi=0} = \alpha^Q\ |_{\chi=1}, \tag{3.7}$$

which is determined by the heavy-ion source used in experiment.

Before showing detailed phase diagrams we can already predict the effects of chiral and (de)confinement dynamics on the quark pressure and then on the phase transition. The chiral symmetry restoration at finite temperature and low chemical potentials will largely increase the quark pressure leading to an End-Point for the pressure matching with the hadron part. When the confinement dynamics is added we will also get a reduction of the quark degrees of freedom and so in general the quark pressure will be reduced. This will imply the shift of the matching with the hadron pressure, and so also of the Critical-End-Point, to higher temperatures [107].

Numerical results and discussions

We present firstly the phase transition from hadronic to deconfined quark phase in $T-\rho_B$ plane for isospin symmetric matter in Figs. 3.15 (solid lines), 3.16 and 3.17 using the same NL hadron interaction and the MIT-Bag, NJL, PNJL respectively for the quark sector. In the Figs. 3.15 (dot-dashed lines), 3.18 and 3.19 the corresponding transition curves for isospin asymmetric matter with the global asymmetry parameter $\alpha = 0.2$. The same $NL\rho\delta$ interaction is used for the hadron matter.

For symmetric matter at a fixed T, the first order phase transition takes place with the same pressure and μ_B in both phases, but a jump in extensive variables, like density, energy density and entropy. In the mixed phase, the pressures of both phases keep unchanged and $\alpha = \alpha^H = \alpha^Q = 0$ for any quark fraction χ.

These features are quite different for the mixed phase in isospin asymmetric matter. For all the different quark EoS, MIT-Bag [23, 102, 105], NJL [106] and PNJL [107] we see a clear Isospin Distillation effect, i.e. a strong enhancement of the isospin asymmetry in the quark component inside the mixed phase, as reported in

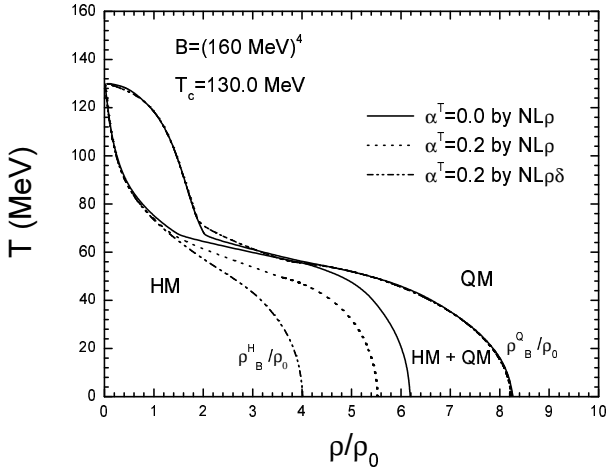

Figure 3.15: Phase diagram in $T-\rho_{\rm B}$ plane in the Two-EoS Hadron-MIT Bag model for isospin symmetric and asymmetric matter. $NL\rho$, $NL\rho\delta$ hadron interactions.

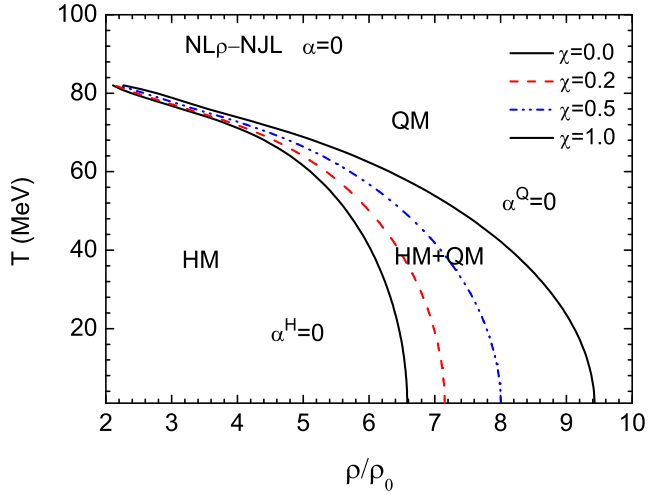

Figure 3.16: Phase diagram in $T-\rho_{\rm B}$ plane in the Two-EoS Hadron-NJL model for symmetric matter. NL hadron interaction.χ is the quark fraction in the mixed phase.

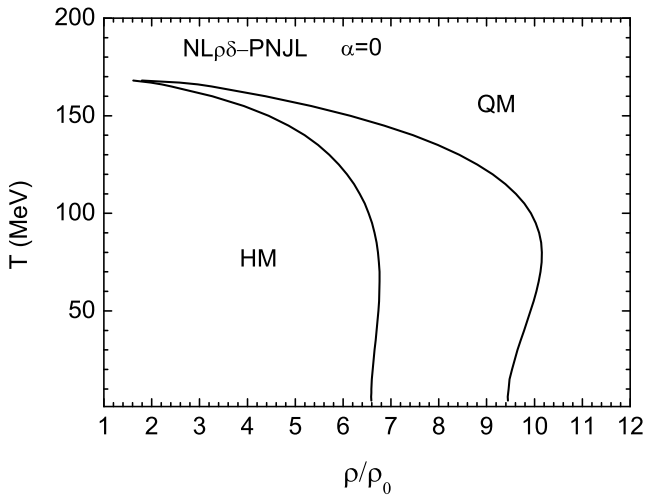

Figure 3.17: Phase diagram in $T-\rho_{\rm B}$ plane in the Two-EoS Hadron-PNJL model for symmetric matter. NL hadron interaction.

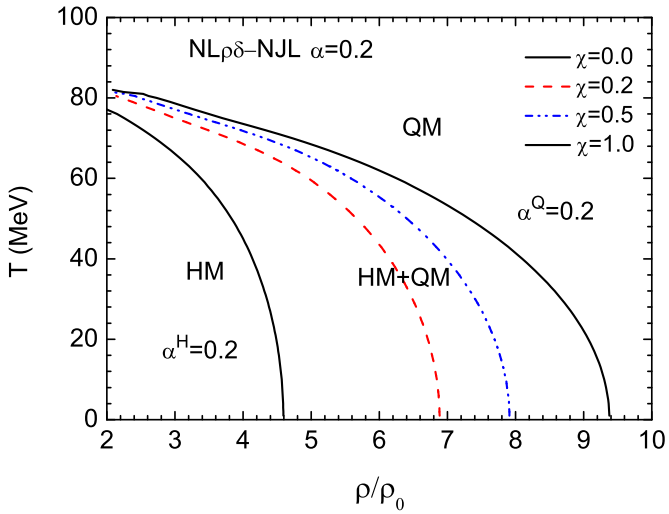

Figure 3.18: Phase diagram in $T-\rho_B$ plane in the Two-EoS Hadron-NJL model for asymmetric matter with the global asymmetry parameter $\alpha=0.2$. χ represents the fraction of quark matter. $NL\rho\delta$ hadron interaction.

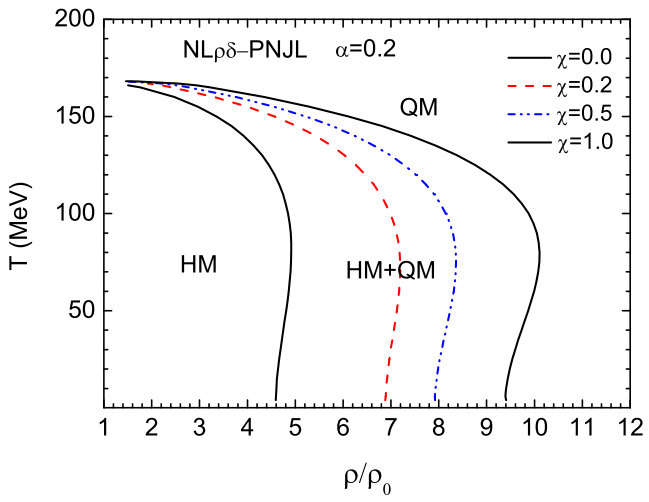

Figure 3.19: Phase diagram in $T-\rho_B$ plane in the Two-EoS Hadron-PNJL model for asymmetric matter with the global asymmetry parameter $\alpha = 0.2$. χ represents the fraction of quark matter. $NL\rho\delta$ hadron interaction.

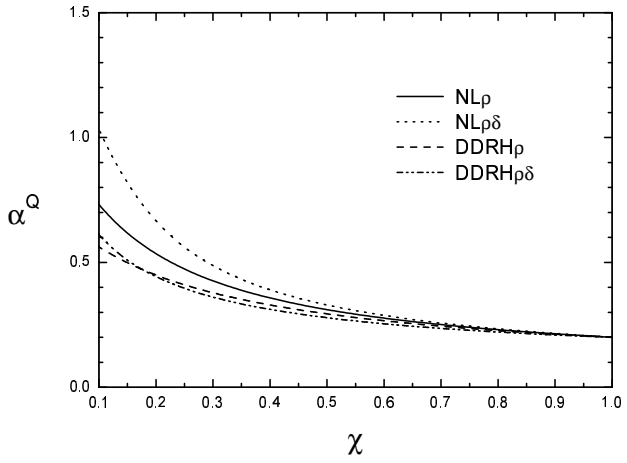

Figure 3.20: The behavior of local asymmetric parameter α^Q in the mixed phase at zero temperature in the Hadron-MIT Bag model. Dotted line: $NL\rho\delta$ hadron interaction. Global asymmetry $\alpha = 0.2$.

Figs. 3.20 (dotted line), 3.21, 3.22, where the asymmetry parameters in the two components are plotted vs. the quark fraction χ. As a consequence the pressure in the mixed phase keeps rising with χ, more rapidly for quark concentrations below 50 %, see details in [102, 106].

From Figs. 3.21, 3.22 we remark that this isospin enrichment of the quark phase is rather robust vs. the increasing temperature. This is important since color pairing correlations at low temperatures will decrease all symmetry energy effects [104].

Such behavior of the local asymmetry parameters will possibly produce some observational signals in the following hadronization during the expansion, see last Section.

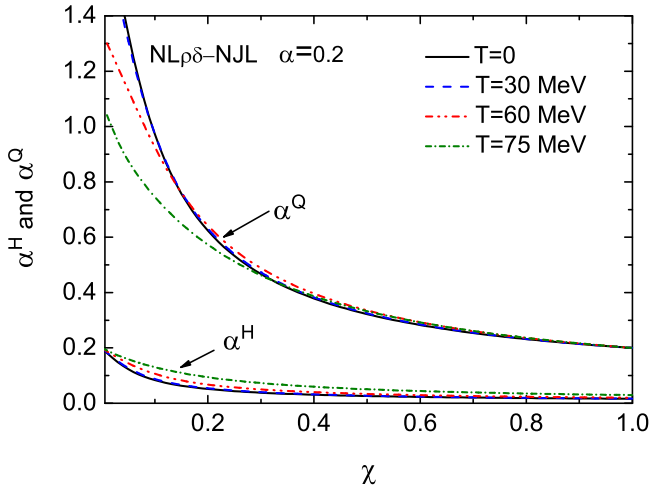

Figure 3.21: The behaviors of local asymmetric parameters α^H and α^Q in the mixed phase with several values of temperature. Hadron-NJL picture with $NL\rho\delta$ hadron interaction.

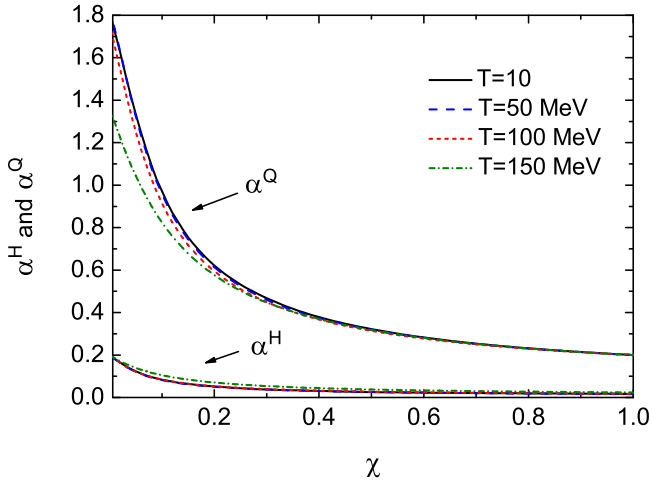

Figure 3.22: The behaviors of local asymmetric parameters α^H and α^Q in the mixed phase with several values of temperature. Hadron-PNJL picture with $NL\rho\delta$ hadron interaction.

We plot the $T-\mu_B$ phase diagrams in Figs. 3.23 (MIT-Bag quark EoS) and 3.24 (upper: Hadron-PNJL; lower: Hadron-NJL) for symmetric matter with the NL hadron interaction. In the Figs. 3.25 (Hadron-MIT Bag) and 3.26 (upper: Hadron-PNJL; lower: Hadron-NJL) the corresponding for asymmetric matter are shown.

Figs. 3.23, 3.24 clearly show that there is only one phase-transition line, not dependent on the quark fraction χ, in the $T-\mu_B$ plane. At variance, for asymmetric matter, the phase transition curve varies for different quark

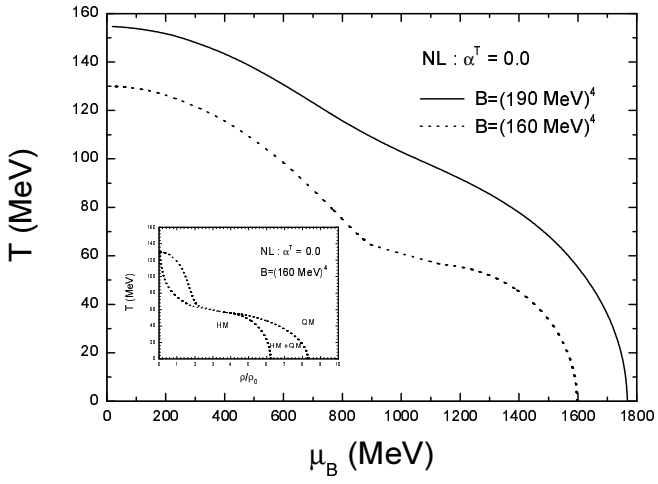

Figure 3.23: Phase diagram in $T - \mu_{\rm B}$ plane for symmetric matter. NL/Hadron-MIT-Bag picture.

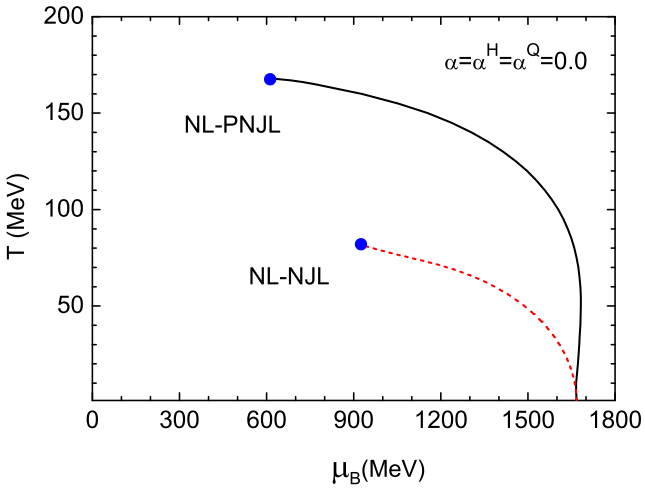

Figure 3.24: Phase diagram in $T - \mu_{\rm B}$ plane for symmetric matter. Upper: Hadron-PNJL. Lower: Hadron-NJL.

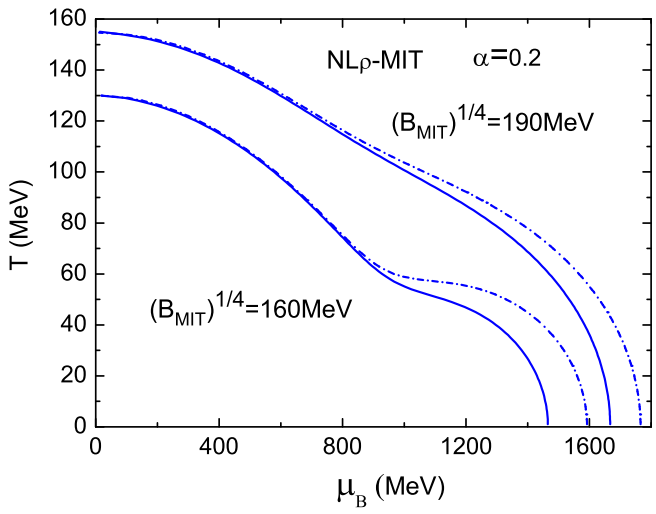

Figure 3.25: Phase diagram in $T-\mu_{\rm B}$ plane for asymmetric matter with the global asymmetry parameter $\alpha=0.2$. .$NL\rho\delta$/Hadron-MIT-Bag picture.

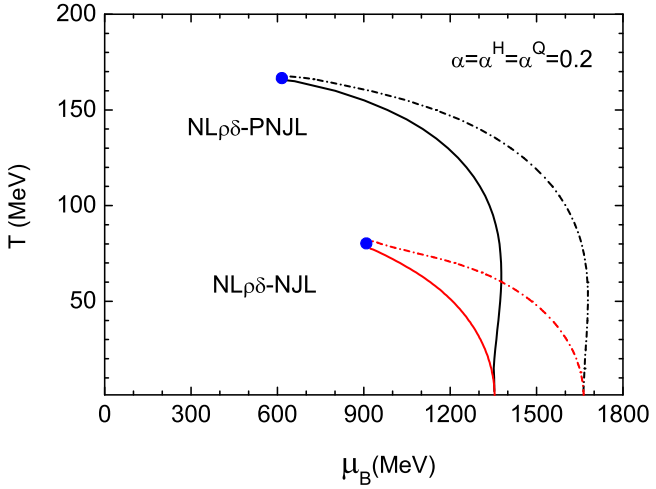

Figure 3.26: Phase diagram in $T-\mu_{\rm B}$ plane for asymmetric matter with the global asymmetry parameter $\alpha=0.2$. Upper: Hadron-PNJL; Lower: Hadron.NJL. $NL\rho\delta$ hadron interaction.

fraction χ. The two lines in Figs. 3.25, 3.26 are obtained with $\chi = 0$ and 1, representing the beginning and the end of hadron-quark phase transition, respectively.

In Figs. 3.24, 3.26 we compare the phase transition curves with the same hadron EoS and the two NJL/PNJL quark pictures. For the NJL model with only chiral dynamics, no physical solution exists when the temperature is higher than ~ 80 MeV. The corresponding temperature is enhanced to about ~ 166 MeV with the Hadron-PNJL model, which is closer to the phase transition temperature given by full lattice calculation at zero or small chemical potential [82, 83, 84].

Besides the critical end points given by the Hadron-PNJL model and Hadron-NJL model, the difference of the phase diagrams given by the two models is quite large, even at lower temperatures and chemical potentials. This can be qualitatively understood from the analysis of the quark pressures discussed at the end of Section II.

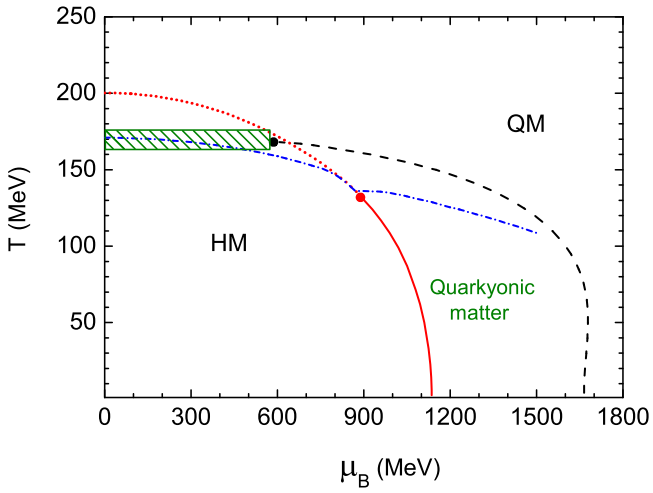

Figure 3.27: Phase diagrams of the PNJL model and the Two-EoS model

Finally in Fig.3.27 we present together the phase diagrams obtained by the PNJL pure quark model and the two EoS Hadron-PNJL approach. We find that the deconfined phase transition curve in the PNJL model is close to the one obtained in the Hadron-PNJL scheme at high temperature and intermediate chemical potential. At larger chemical potential, the deconfinement phase transition curve in the PNJL model is still at rather high temperature. This is naturally leading to the formation of a *quarkyonic* phase (chirally restored but still deconfined) [50], although the interpretation of the Polyakov Loop Φ as order parameter at low temperatures and large chemical potentials is not clear. In any case this is also a strong indication that presently we must rely on the Two-EoS approach for predictions in the region of interest for heavy ion experiments at intermediate energies, i.e. at high $\rho, \mu_{\rm B}$ and finite temperatures.

Summary and suggested observables In this study, the hadron-quark phase transition are investigated in the Two-EoS approach. We describe the hadron matter with nonlinear Walecka model and separately the quark matter with the MIT-Bag and the NJL(PNJL) models. We follow the Gibbs criteria to construct the mixed phase with baryon number and isospin conservations, likely reached during the hot and dense phase formed in heavy-ion collision at intermediate energies. The parameters in both models are fitted to give a good reproduction of the properties of nuclear matter, also at suprasaturation densities, and of lattice data at high temperature with zero/small chemical potential.

The phase diagrams for symmetric and asymmetric matter are explored in the $T - \rho_{\rm B}$ and $T - \mu_{\rm B}$ planes. In both Hadron-(P)NJL calculations we get a first order phase transition with a Critical-End-Point at finite temperature and chemical potential. In the PNJL case the CEP is shifted to larger temperatures and smaller chemical potential, to the $(166, 600)$ MeV point in the $(T, \mu_{\rm B})$ plane. This appears a nice indication of a decrease of the quark pressure when confinement is accounted for. Such result is particularly interesting since the CEP is now in the region of $\mu_{\rm q}/T_c \simeq 1$ (where μ_q is the quark chemical potential) and so it could be reached with some confidence by lattice-QCD complete calculations.

Isospin effects are almost negligible when we approach the CEP. At variance the calculation shows that the onset density of asymmetric matter is lower than that of symmetric matter. Moreover in the mixed phase of asymmetric matter, the decreasing of local asymmetry parameter α^H and α^Q with the increasing quark fraction χ may produce some observable signals. In particular we remark the noticeable isospin distillation mechanism (isospin enrichment of the quark phase) at the beginning of the mixed phase, i.e. for low quark fractions, that should show up in the hadronization stage during the expansion. We also see from Figs.3.20, 3.21 and 3.22 that this effect appears in all quark EoS models and it is still there even at relatively large temperatures, certainly present in the high density stage of heavy ion collisions at relativistic energies [23, 109].

Expected observables

A first expectation of the Isospin Distillation will be a kind of *neutron trapping* in the quark phase, supported by statistical fluctuations [23] as well as by the symmetry energy difference in the two phases [102]. In fact while in the pure hadron matter (neutron-rich) at high density we have a large neutron potential repulsion (in both $NL\rho$, $NL\rho\delta$ cases), in the quark phase the d-quarks see a smaller symmetry repulsion essentially only due to the kinetic contribution from the Fermi gas. As a consequence while in a pure hadronic phase neutrons are quickly emitted or "transformed" in protons by inelastic collisions [110], when the mixed phase starts forming, neutrons are kept in the interacting system, in the quark phase, where they can even thermalize, up to the subsequent hadronization in the expansion stage. Observables related to such neutron "trapping" could be

- (i). An inversion in the trend of emission of fast neutron rich clusters with increasing beam energy, to be seen in the n/p, $^3H/^3He$.. ratios at high kinetic energies;
- (ii). An enhancement of the production of isospin-rich nucleon resonances and subsequent decays, that can be evaluated via equilibrium statistical approaches [111];
- (iii). Related to the previous point, an increase of π^-/π^+, K^0/K^+ yield ratios for mesons coming from high density regions, to be selected via large transverse momenta, corresponding to a large radial flow.

If such kinetic selection of particles from the mixed phase can really be successful also other potential signatures would become available. One is related to the general softening of the matter, due to the contribution of more degrees of freedom, that should show up in the damping of collective flows [112].

The azimuthal distributions (elliptic flows) will be particularly affected since particles mostly retain their high transverse momenta escaping along directions orthogonal to the reaction plane without suffering much rescattering processes. Thus a further signature could be the observation, for the selected particles, of the onset of a quark-number scaling of the elliptic flow: a property of hadronization by quark coalescence that has been predicted and observed at RHIC energies, i.e. for the transition at $\mu_B = 0$ [113].

Finally, an evident feature of Figs. 3.15 (dot-dashed lines), 3.18, 3.19 is that the onset density of hadron-quark phase transition for asymmetric matter is much lower than that of the symmetric one, and therefore it will be easier to probe in heavy-ion collision experiments at intermediate energies.

All that support the possibility of an experimental observation in the new planned facilities, for example, FAIR at GSI-Darmstadt and NICA at JINR-Dubna, with realistic isospin asymmetries for stable/unstable beams.

Bibliography

[1] M. Stephanov, K. Rajagopal and E. Shuryak, Phys. Rev. **D 60,** 1140281, (1999); [hep-ph/9903292].

[2] B. Berdnikov and K. Rajagopal, Phys. Rev. **D 61,** 105017, (2000); [hep-ph/9912274].

[3] M. Stephanov, Phys. Rev. Lett. **102,** 032301, (2009); [arXiv:0809.3450].

[4] E.E. Kolomeitsev, D.N. Voskresensky, Nucl. Phys. **A 759,** 373, (2005).

[5] T. Klahn *et al.*, Phys. Rev. **C 74,** 035802, (2006).

[6] A.S. Khvorostukhin, V.D. Toneev and D.N. Voskresensky, Nucl. Phys. **A 791,** 180, (2007).

[7] D.N. Voskresensky, Nucl. Phys. **A 744,** 378, (2004); **812**, 158, (2008).

[8] V.V. Skokov and D.N. Voskresensky, [arXiv:0811.3868]; Nucl. Phys. **A 828,** 401, (2009); [arXiv:0903.4335].

[9] D.N. Voskresensky, Phys. Rev. **C 69,** 065209, (2004).

[10] R.A.L. Jones, *Soft Condensed Matter*, (Oxford University Press, 2002) [ISBN 0198505892].

[11] Ph. Chomaz, M. Colonna and J. Randrup, Phys. Rep. **389,** 263, (2004).

[12] I.C. Arsene *et al.*, Phys. Rev. **C 75,** 034902, (2007).

[13] J. Randrup, arXiv:0903.4736.

[14] V.N. Russkikh and Yu.B. Ivanov, Phys. Rev. **C 74,** 034904, (2006).

[15] Yu.B. Ivanov and V.N. Russkikh, **PoS CPOD07,** 008, (2007).

[16] Yu.B. Ivanov, V.N. Russkikh, and V.D. Toneev, Phys. Rev. **C 73,** 044904, (2006).

[17] K.A. Bugaev, Phys. Part. Nucl. **38,** 447, (2007)..

[18] K.A. Bugaev, Phys. Rev. **C 76,** 014903, (2007); Phys. Atom. Nucl. **71,** 1615, (2008).

[19] K.A. Bugaev, V.K. Petrov and G.M. Zinovjev, *The New Class of Exactly Solvable Models for the QCD Critical Endpoint* (in preparation).

[20] K.A. Bugaev, V. K. Petrov and G. M. Zinovjev, Europhys. Lett. **85**, 22002, (2009); [arXiv:0801.4869]; [arXiv:0807.2391]; K.A. Bugaev, [arXiv:0809.1023].

[21] K.A. Bugaev, *Testing the Influence of Surface Tension and Finite Width of QGP Bags on the QCD Matter Equation of State Properties at NICA Energies*, 2009 (in preparation).

[22] H. Muller, Nucl. Phys. **A 618,** 349, (1997).

[23] M. Di Toro, A. Drago, T. Gaitanos, V, Greco and A. Lavagno, Nucl. Phys. **A 775,** 102, (2006).

[24] M. Di Toro *et al.*, Progr. Part. Nucl. Phys. **62,**389, (2009).

[25] D. Toublan and J.B.Kogut, Phys. Lett. **B 605,** 129, (2005).

[26] B.D. Serot and J.D. Walecka, Adv. Nucl. Phys. **16**, 1 (1985).

[27] V. Baran, M. Colonna, V. Greco and M. Di Toro, Phys. Rep. **410,** 335, (2005).

[28] A. Chodos, *et al.*, Phys. Rev. **D 9,** 3471, (1974).

[29] P. Danielewicz, R.Lacey, W.G.Lynch, Science **298**, 1592 (2002)

[30] N.K. Glendenning, S.A. Moszkowski, Phys. Rev. Lett. **67,** 2414, (1991).

[31] Y. Nambu and G. Jona-Lasinio, Phys. Rev. **122,** 345, (1961); **124**, 246, (1961).

[32] M. Frank, M. Buballa and M. Oertel, Phys. Lett. **B 562,** 221, (2003).

[33] Guo-yun Shao et al., Phys. Rev. **D 73,** 076003, (2006).

[34] S. Plumari, Ph.D.Thesis, Univ.Catania 2008.

[35] B. Liu, V. Greco, V. Baran, M. Colonna, and M. Di Toro, Phys. Rev. **C 65,** 045201, (2002).

[36] A. Bazavov *et al.*, [arXiv:0903.4379 [hep-lat]].

[37] S. Roessner, C. Ratti and W. Weise, Phys. Rev. **D 75,** 034007, (2007); [hep-ph/0609281].

[38] D. Gomez Dumm, D. B. Blaschke, A. G. Grunfeld and N. N. Scoccola, Phys. Rev. **D 78,** 114021, (2008); [arXiv:0807.1660].

[39] D. Blaschke S. Fredriksson, H. Grigorian, A. M. Oztas and F. Sandin, Phys. Rev. **D 72,** 065020, (2005); [hep-ph/0503194].

[40] S.B. Ruester, V. Werth, M. Buballa, I. A. Shovkovy and D. H. Rischke, Phys. Rev. **D 72,** 034004, (2005); [hep-ph/0503184].

[41] H.J. Warringa, D. Boer and J.O. Andersen, Phys. Rev. **D 72,** 014015, (2005); [hep-ph/0504177].

[42] H. Abuki and T. Kunihiro, Nucl. Phys. **A 768,** 118 (2006); [hep-ph/0509172].

[43] S. Typel, Phys. Rev. **C 71,** 064301, (2005); [nucl-th/0501056].

[44] K. Fukushima, Phys. Rev. **D 77,** 114028, (2008); **78**, 039902, (2008); [arXiv:0803.3318].

[45] M.K. Volkov, E. A. Kuraev, D. Blaschke, G. Ropke and S. M. Schmidt, Phys. Lett. **B 424,** 235, (1998); [hep-ph/9706350].

[46] S. Chiku and T. Hatsuda, Phys. Rev. **D 57,** 6, (1998); [hep-ph/9706453].

[47] T. Kunihiro, M. Kitazawa and Y. Nemoto, **PoS CPOD07,** 041 (2007); [arXiv:0711.4429].

[48] S. Wheaton and J. Cleymans, Comput. Phys. Commun. **180**, 84 (2009).

[49] A. Andronic *et al.*, Nucl. Phys. **A 837,** 65 (2010); [arXiv:0911.4806.

[50] L. McLerran and R. D. Pisarski, Nucl. Phys. **A 796,** 83 (2007)

[51] K. Fukushima, Phys. Lett. **B 591,** 277, (2004).

[52] C. Ratti, M. A. Thaler and W. Weise, Phys. Rev. **D 73,** 014019, (2006).

[53] L. McLerran, K. Redlich and C. Sasaki, Nucl. Phys. **A 824,** 86 (2009).

[54] D. B. Blaschke, F. Sandin, V. V. Skokov and S. Typel, Acta Phys. Polon. Supp. **3**, 741 (2010).

[55] K. Rajagopal and F. Wilczek; arXiv:hep-ph/0011333.

[56] M. Kutschera, W. Broniowski and A. Kotlorz, Nucl. Phys. **A 516,** 566 (1990).

[57] E. Nakano and T. Tatsumi, Phys. Rev. **D 71,** 114006 (2005).

[58] G. Basar, G. V. Dunne and M. Thies, Phys. Rev. **D 79,** 105012, (2009).

[59] D. Nickel, Phys. Rev. **D 80,** 074025, (2009).

[60] D. Nickel, Phys. Rev. Lett. **103,** 072301 (2009).

[61] S. Carignano, D. Nickel and M. Buballa, Phys. Rev. **D 82,** 054009 (2010).

[62] T. Kojo, Y. Hidaka, L. McLerran and R. D. Pisarski, Nucl. Phys. **A 843,** 37 (2010).

[63] T. Kojo, R. D. Pisarski and A. M. Tsvelik, Phys. Rev. **D 82,** 074015, (2010).

[64] A. Mocsy and P. Sorensen, Phys. Lett. **B 690,** 135 (2010).

[65] Y. Aoki*et al.*, Nature **443**, 675(2006).

[66] M. Cheng, Phys. Rev. **D 74,** 054507, (2006).

[67] S. Ejiri, Phys. Rev. **D 78,** 074507, (2008).

[68] E. S. Bowman, J. I. Kapusta, Phys. Rev. **D 79,** 015202, (2009).

[69] M. A. Stephanov, Int. J. Mod. Phys. **A 20,** 4387, (2005).

[70] Z. Fodor *et al.*, **JHEP 0404**, 50 (2004).

[71] R. V. Gavai, S. Gupta, Phys. Rev. **D 78,** 114503, (2008);

[72] de Forcrand Philippe and O. Philipsen, Nucl. Phys. **B 642,** 290 (2002).

[73] J. Adams *et al.*, Nucl. Phys. **A 757,** 102 (2005).

[74] X. F. Luo *et al.*, Phys. Lett. **B 673,** 268 (2009).

[75] B. Mohanty, Nucl. Phys. **A 830,** 899, (2009).

[76] M. Cheng *et al.*, Phys. Rev. **D 79,** 074505, (2009).

[77] Y. Hatta and M. A. Stephanov, Phys. Rev. Lett. **91,** 102003, (2003).

[78] M. Asakawa, arXiv:0904.2089.

[79] M. M. Aggarwal *et al.* (STAR Collaboration), Phys. Rev. Lett. **105,** 022302, (2011).

[80] F. Karsch and K. Redlich, Phys. Lett. **B 695,** 136, (2011).

[81] R. V. Gavai and S. Gupta, arXiv:1001.3796.

[82] F. Karsch, E. Laermann, and A. Peikert, Nucl. Phys. **B 605,** 579 (2001).

[83] F. Karsch, Nucl. Phys. **A 698,** 199 (2002).

[84] M. Kaczmarek and F. Zantow, Phys. Rev. **D 71,** 114510, (2005).

[85] Z. Fodor, S.D. Katz, and C. Schmidt, JHEP **03**, 121 (2007).

[86] M. D'Elia and F. Sanfilippo, Phys. Rev. **D 80,** 014502 (2009).

[87] K. Fukushima and T. Hatsuda, Rep. Prog. Phys. **74**, 014001 (2011).

[88] Si-xue Qin, Lei Chang, Huan Chen, Yu-xin Liu, Craig D. Roberts, Phys. Rev. Lett. **106,** 172301 (2001).

[89] S. P. Klevansky, Rev. Mod. Phys. **64**, 649, (1992).

[90] T. Hatsuda and T. Kunihiro, Phys. Rep. **247,** 221 (1994).

[91] M. Buballa, Phys. Rep. **407,** 205 (2005).

[92] M. Huang and I. Shovkovy, Nucl. Phys. **A 729,** 835 (2003).

[93] M. Alford, A. Schmit, K. Rajagopal, and T. Schäfer, Rev. Mod. Phys. **80**, 1455 (2008), and refs. therein..

[94] K. Fukushima, Nucl. Phys. **B 591,** 277 (2004).

[95] W. J. Fu, Z. Zhang, Y. X. Liu, Phys. Rev. **D 77,** 014006 (2008).

[96] T. K. Herbst, J. M. Pawlowski, B-J. Schaefer, Phys. Lett. **B 696,** 58 (2011).

[97] N. K. Glendenning and J. Schaffner-Bielich, Phys. Rev. Lett. **81,** 4564 (1998); Phys. Rev. **C 60,** 025803 (1999).

[98] G. F. Burgio, M. Baldo, P. K. Sahu, and H.-J. Schulze, Phys. Rev. **C 66,** 025802 (2002).

[99] G. Y. Shao and Y. X. Liu, Phys. Rev. **C 82,** 055801 (2010).

[100] J. Xu, L. W. Chen, C. M Ko, and B. A. Li, Phys. Rev. **C 81,** 055803 (2010).

[101] H. Müller, Nucl. Phys. **A 618,** 349 (1997).

[102] M. Di Toro *et al.*, Phys. Rev. **C 83,** 014911 (2011).

[103] R. Cavagnoli, C.'Providência, and D. P. Menezes, [arXiv:1009.3596v1].

[104] G. Pagliara and J. Schaffner-Bielich, Phys. Rev. **D 81,** 094024 (2010).

[105] B. Liu, M. Di Toro, G.Y. Shao, V.Greco, C.W. Shen, Z.H. Li, [arXiv:1105.0555[nucl.th]].

[106] G. Y. Shao, M. Di Toro, B. Liu, M. Colonna, V. Greco, Y.X. Liu, S. Plumari, [arXiv:1102.4964], to be published in Phys. Rev. D (2011).

[107] G.Y. Shao, M. Di Toro, V. Greco, M. Colonna, B.Liu, Y.X. Liu, S. Plumari, *Phase diagrams in the Hadron-PNJL model*, in preparation.

[108] V. Baran, M. Colonna, V. Greco, M. Di Toro, Phys. Rep. **410,** 335 (2005)

[109] M. Di Toro *et al.*, Progr. Part. Nucl. Phys. **62,**389 (2009).

[110] G. Ferini, T. Gaitanos, M. Colonna, M. Di Toro. H.H. Wolter, Phys. Rev. Lett. **97,** 202301 (2006).

[111] G. Ferini, M. Colonna, T. Gaitanos, M. Di Toro, Nucl. Phys. **A 762,** 147 (2005).

[112] L. Csernai, D. Rohrich, Phys. Lett. **B 458,** 454 (1999).

[113] R.J. Fries, V. Greco V, P. Sörensen, Ann.Rev.Nucl.Part.Sci. **58** 177 (2008).

4 Hydrodynamics and hadronic observables

The rich structure of the QCD phase diagram at high baryon densities discussed in the previous section, suggests the possibility of a first order phase transition and the existence of a critical end point, eventually a triple point. This section is devoted to the discussion of the effects of a phase transformation in the evolving hot, dense hadronic system on the particle distributions. Critical behaviour and changes in the thermodynamical degrees of freedom shall be revealed in flow observables as well as in the higher moments of (measurable) distribution functions and their ratios. In particular the latter quantities can also be studied in lattice QCD simulations and thus providing a direct link between hadronic observables and *ab-initio* QCD theory.

4.1 Hadronic signals of non-equilibrium phase transition

B. Tomášik

Univerzita Mateja Bela, Banská Bystrica, Slovakia

As pointed out in Jorgen Randrup's contribution, NICA will operate in the regime likely near to and slightly below the critical point of QCD. There a first-order phase transition is expected. In quickly expanding systems this is accompanied with the appearance of spinodal decomposition. In this scenario, bulk fireball matter decays into droplets which evaporate hadrons. Droplets copy the original local expansion velocity of the bulk and recede from each other. Therefore, this would lead to clumps in momentum space: hadrons coming from the same droplet have similar velocities, while those coming from a different droplet have velocities grouped around a different mean. It is also important to realize that in each event the droplets will be in different positions. Therefore, each event will be described by different hadronic distributions.

Various observables have been proposed for the identification of such a scenario. In general, one would not be able to identify it in observables which are integrated over a large number of events, like e.g. hadronic spectrum. Instead, it is necessary to look at correlation and fluctuation signals. Many have been proposed: multiplicity fluctuations, mean p_{T} fluctuations, rapidity and azimuthal angle hadronic correlations, proton rapidity distributions, etc. A promising new way of analyzing data is the use of Kolmogorov-Smirnov (KS) test on a large number of event pairs. Generally, the test has been developed to measure, to what extent two sets of data are similar, i.e. resemble the same underlying probability density. If it is applied to a large number of event pairs then it is rather easy to decide whether the collection of test results corresponds to all events being described by the same distribution or whether there are some non-statistical differences between the events [1]. Recall that the latter can be caused by fragmentation.

The KS test is more sensitive to non-statistical differences between events than any other tool proposed so far. The advantage is that it is not constructed specifically to look at certain moment of the distribution function, but compares the whole empirical distributions. We should also stress that it does not focus exclusively on fragmentation, but indicates non-statistical fluctuations due to any mechanism. Once indicated with the help of the KS test, the exact cause must be identified by other means.

To perform the KS test, measured rapidities (angles, momenta, ...) of all hadrons must be available. It is not sufficient to have only filled histograms. This is the requirement on data reconstruction and analysis. We have checked that even a poor momentum resolution of the detector does not eliminate the signal completely [1]. Efficiency of the detector, which may be a function of the phase space position should also not influence the results qualitatively since it modifies the measurement the same way in all events. Careful Monte Carlo studies to check the last statement should be done, though.

4.2 Scalar mesons properties at finite temperature and density at NICA energy

P. Costa[a] and Yu.L. Kalinovsky[b]

[a] *Departamento de Física, Universidade de Coimbra, Coimbra, Portugal*
[b] *Laboratory for Information Technologies, JINR, Dubna, Russia*

Understanding the behavior of matter under extreme conditions is one of the most important task in physics of strong interactions. In the last years, major theoretical and experimental efforts have been dedicated to the physics of relativistic heavy-ion collisions, looking for signatures of the quark gluon plasma (QGP) formation.

A region of particular interest, that has been so far explored, is the $T - \mu_B$ phase boundary in order to try to explore different regions of the QCD phase diagram. The existence of the Critical End Point (CEP) in QCD was suggested in the end of the eighties, and its properties have been studied since then (for a review see [2]).

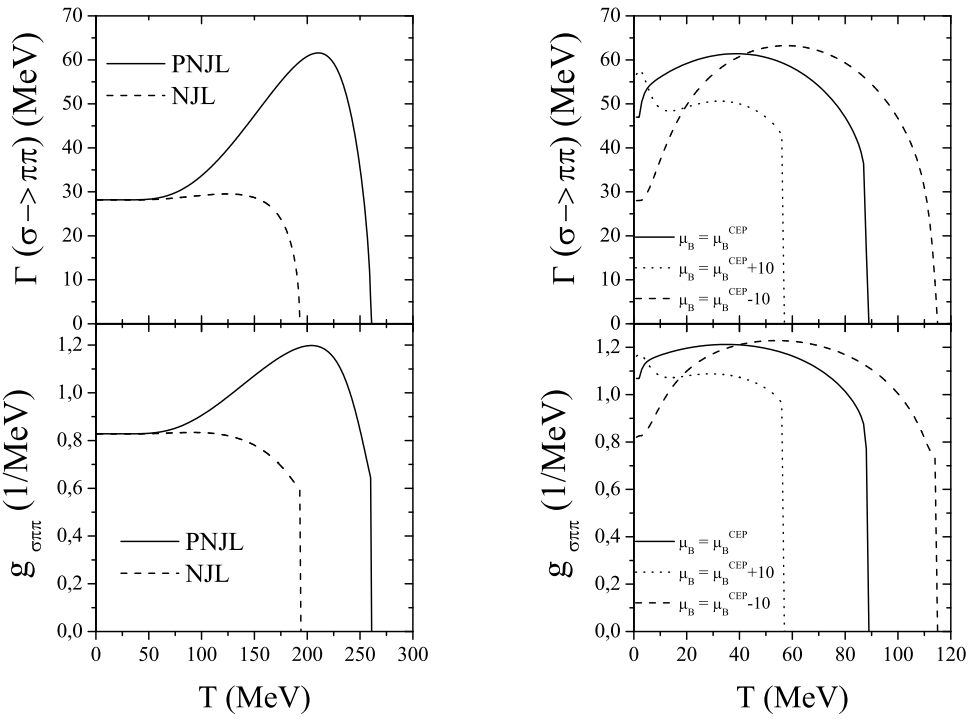

Figure 4.1: The temperature dependencies of decay width $\Gamma(\sigma \to \pi\pi)$ and interaction constant $g_{\sigma\pi\pi}$. These quantities are zoomed in the right panel to show their behavior in the vicinity of $\mu_{\rm CEP}$.

At the CEP the phase transition is of second order, belonging to the three - dimensional Ising universality class, and this kind of phase transitions is characterized by longwavelength fluctuations of the order parameter. As pointed out in [3], the critical region around the CEP is not point-like but has a very rich structure. This critical region is defined as the region where the mean field theory of phase transitions breaks down and nontrivial critical exponents emerge. The size of the critical region is important for future searches for the CEP in heavy ion collisions, particularly in the NICA energy.

It is also expected that experimental signatures peculiar to CEP can be observed through spectral changes in the presence of abnormally light σ mesons. The σ meson in a hot medium can decay through different processes like $\sigma \to \pi\pi$, $\sigma \to \gamma\gamma$, etc. Once the σ mass is so reduced around the chiral transition temperature, the σ meson cannot decay into two pions and thus the spectral function in the σ-channel must be significantly enhanced (the threshold point of the decay is defined by the mass equation $M_\sigma(T,\ \mu) = 2M_\pi(T,\ \mu)$). Using the resulting spectral functions it is possible to evaluated the multiplicity of diphoton emission [4].

In our project we aim to investigate the chiral phase transition and the CEP in quark matter. We perform our calculations in the framework of the two- and three-flavor NJL [5, 6, 7, 8] and PNJL models [9]. The generalized PNJL model plays the important role for explaining the equation of state and the critical behavior around the critical end point.

As an example, we present in Fig. 4.1 the $\sigma \to \pi\pi$ at the critical end point. When we are in the region of first order transition (from the chirally symmetric phase to the broken phase), the M_σ and M_π are discontinuous, so M_σ jumps up and M_σ jumps down. The σ decay starts not at the threshold, but at some value beyond the threshold. This means that the decay in the first - order transition region happens suddenly and the decay rate behaves like a step function as a function of the temperature.

When approaching to the critical endpoint from the first-order transition side, the jump of the mass difference disappear. The decay rate becomes continuous, while the coupling strength has still a jump.

4.3 Hadron abundances at high baryon density

H. Satz

Fakultät für Physik, Universität Bielefeld, Germany

Consider the medium formed in an energetic nucleus-nucleus collision. At low baryon density, the constituents of this medium are mostly mesons, and the dominant interaction is resonance formation; with increasing collision energy, different resonance species of increasing mass are formed, leading to a gas of ever increasing degrees of freedom. They are all of a typical hadronic size (with a radius $R_{\rm h} \simeq$1 fm) and can overlap or interpenetrate each other. For baryochemical potential $\mu_{\rm B} \simeq 0$, the contribution of baryons/antibaryons and baryonic resonances is relatively small, but with increasing baryon density, they form an ever larger section of the species present in the medium, and beyond some baryon density, they become the dominant constituents. Finally, at vanishing temperature, the medium consists essentially of nucleons.

For vanishing or low baryon number density, when the interactions are resonance dominated, the system can be described as an ideal gas of all possible resonance species [10, 11, 12], contained in an overall spatial volume V. The temperature of this gas is (for $\mu_{\rm B} \simeq 0$ and high collision energy) found to attain a universal value $T_{\rm H} \simeq$ 175 MeV, over a wide range of collision configurations, from e^+e^- annihilation to nucleus-nucleus interactions, and for all CMS collision energies above 10 – 20 GeV. For nuclear collisions at lower $\sqrt{s_{\rm NN}}$, applying the same resonance gas analysis leads to temperatures which become dependent on the baryochemical potential $\mu_{\rm B}$; they decrease for increasing $\mu_{\rm B}$ [13].

At high baryon density, however, the dominant interaction is non-resonant. Nuclear forces are short-range and strongly attractive at distances of about 1 fm; but for distances around 0.5 fm, they become strongly repulsive. The former is what makes nuclei, the latter (together with Coulomb and Fermi repulsion) prevents them from collapsing. The repulsion between a proton and a neutron shows a purely baryonic "hard-core" effect and is connected neither to Coulomb repulsion nor to Pauli blocking of nucleons. As a consequence, the volumes of nuclei grow linearly with the sum of its protons and neutrons. With increasing baryon density, the conceptual basis of a resonance gas thus becomes less and less correct, so that eventually one should encounter a regime of quite different nature.

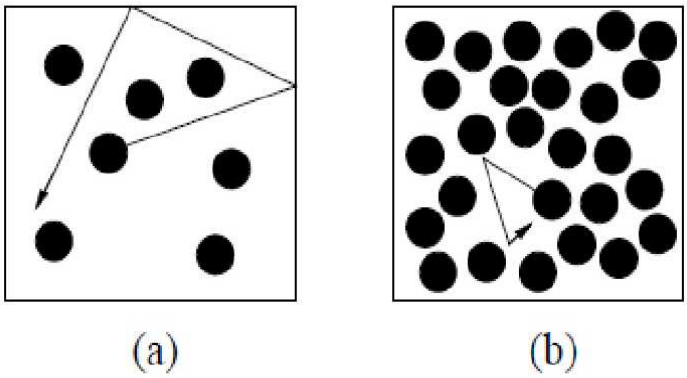

Figure 4.2: States of hard core baryons: full mobility (a), "jammed" (b).

It would seem very interesting to investigate experimentally, through a study of hadron abundances, this change of regimes. If NICA can reach large baryon densities and measure a variety of hadron species, this would appear to be a promising field of research.

In closing, we note that the conceptual differences of the low and the high baryon density regimes of the phase diagram for strongly interacting matter have recently been studied in terms of the underlying critical features [14]. While at low baryon density, hadron percolation leads to the universal chemical freeze-out temperature $T_{\rm H}$ specifying the species abundances, at high baryon density there occurs a "jamming" of nucleons: the mobility of baryons in the medium becomes strongly restricted by the presence of other baryons, leading to a jammed state, as shown in Fig. 4.2. A study of this region could thus help in the understanding of new, high baryon-density phenomena, which have also been discussed in the context of "quarkyonic matter" [15].

4.4 Directed flow as a signal of a liquid state of transient matter

S. M. Troshin

Institute for High Energy Physics, Protvino, Russia

Directed flow v_1, observable introduced for description of nucleus collisions is discussed. We consider a possible origin of the flow in hadronic reactions as a result of rotation of the transient matter and trace analogy with nucleus collisions. It is argued that the presence of directed flow can serve as a signal that transient matter is in a liquid state.

The deconfined state of transient matter found in the four major experiments at RHIC [16, 17, 18] reveals the properties of the perfect liquid, being strongly interacting collective state and therefore it was labelled as sQGP [19]. The nature of new form of matter discovered is not known, many different interpretations were proposed for the explanations of the experimental findings. The utmost significance of these experimental discoveries lies in the fact that the matter is strongly correlated and reveals high degree of the coherence when it is well beyond the critical values of density and temperature.

Important tools in the studies of the nature of the new form of matter are the anisotropic flows which are the quantitative characteristics of the collective motion of the produced hadrons in the nuclear interactions. With their measurements one can obtain a valuable information on the early stages of reactions and observe signals of QGP formation.

At the same time, the measurements of anisotropic flows and constituent quark scaling demonstrated an importance of the constituent quarks [20] and their role as effective degrees of freedom of the newly discovered state of matter. Of course the dynamics of strong interactions is the same for the hadron and nucleus collisions, and therefore the following question naturally arises, namely: To which extent, if at all, are the recent discoveries at RHIC relevant for hadronic interactions?

In this note we try to address in a model way one aspect of this broad problem, i.e. we discuss the role of the coherent rotation of the transient matter in hadron collisions as the origin of the directed flow in these reactions and stress that behavior of collective observable v_1 in hadronic and nuclear reactions would be similar and originates from the liquid state of transient matter.

The experimental probes of collective dynamics in AA interactions [20, 21], the momentum anisotropies v_n are defined by means of the Fourier expansion of the transverse momentum spectrum over the momentum azimuthal angle ϕ. The angle ϕ is the angle of the detected particle transverse momentum with respect to the reaction plane spanned by the collision axis z and the impact parameter vector $\mathbf{b}$ directed along the x axis. Thus, the anisotropic flows are the azimuthal correlations with the reaction plane. In particular, the directed flow is defined as

$$v_1(p_\perp) \equiv \langle \cos\phi \rangle_{p_\perp} = \langle p_x/p_\perp \rangle = \langle \hat{\mathbf{b}} \cdot \mathbf{p}_\perp/p_\perp \rangle \tag{4.1}$$

From Eq. (4.1) it is evident that this observable can be used for studies of multiparticle production dynamics in hadronic collisions provided that impact parameter $\mathbf{b}$ is fixed. Therefore we discuss hereabout directed flow v_1 in hadron collisions at fixed impact parameters and refer after that those considerations to the collisions of nuclei keeping in mind the same nature of the transient states in both cases. We amend the model [22, 23] developed for hadron interactions (based on the chiral quark model ideas) and consider the effect of collective rotation of a quark matter in the overlap region. We formulate a hypothesis on connection of the strongly interacting transient matter rotation with the directed flow generation.

Effective degrees of freedom and transient state of matter in hadron collisions

We assume that the origin of the transient state and its dynamics along with hadron structure can be related to the mechanism of spontaneous chiral symmetry breaking (χSB) in QCD [24], which leads to the generation of quark masses and appearance of quark condensates. This mechanism describes transition of the current into constituent quarks. The gluon field is considered to be responsible for providing quarks with masses and its internal structure through the instanton mechanism of the spontaneous chiral symmetry breaking. Massive constituent quarks appear as quasiparticles, i.e. current quarks and the surrounding clouds of quark–antiquark pairs which consist of a mixture of quarks of the different flavors. Quark radii are determined by the radii of the surrounding clouds. The quantum numbers of the constituent quarks are the same as the quantum numbers of current quarks due to the conservation of the corresponding currents in QCD.

Collective excitations of the condensate are the Goldstone bosons and the constituent quarks interact via exchange of the Goldstone bosons; this interaction is mainly due to pion field. Pions themselves are the bound

states of massive quarks. The interaction responsible for quark-pion interaction can be written in the form [25]:

$$\mathcal{L}_I = \bar{Q}[i\partial\!\!\!/ - M\exp(i\gamma_5\pi^A\lambda^A/F_\pi)]Q, \quad \pi^A = \pi, K, \eta. \tag{4.2}$$

The interaction is strong, the corresponding coupling constant is about 4. The general form of the total effective Lagrangian ($\mathcal{L}_{\rm QCD} \to \mathcal{L}_{\rm eff}$) relevant for a description of the non–perturbative phase of QCD includes the three terms [26]

$$\mathcal{L}_{\rm eff} = \mathcal{L}_\chi + \mathcal{L}_I + \mathcal{L}_C.$$

Here $\mathcal{L}_\chi$ is responsible for the spontaneous chiral symmetry breaking and turns on first.

To account for the constituent quark interaction and confinement the terms $\mathcal{L}_{\rm I}$ and $\mathcal{L}_{\rm C}$ are introduced. The $\mathcal{L}_{\rm I}$ and $\mathcal{L}_{\rm C}$ do not affect the internal structure of the constituent quarks.

The picture of a hadron consisting of constituent quarks embedded into quark condensate implies that overlapping and interaction of peripheral clouds occur at the first stage of hadron interaction. The interaction of the condensate clouds assumed to of the shock-wave type, this condensate clouds interaction generates the quark-pion transient state. This mechanism is inspired by the shock-wave production process proposed by Heisenberg [27] long time ago. At this stage, part of the effective lagrangian $\mathcal{L}_{\rm C}$ is turned off (it is turned on again in the final stage of the reaction). Nonlinear field couplings transform then the kinetic energy to internal energy [27, 28]. As a result the massive virtual quarks appear in the overlapping region and a transient state of matter is generated. This state consists of $\bar{Q}Q$ pairs and pions strongly interacting with quarks. This picture of quark-pion interaction can be considered as the origin for a percolation mechanism of deconfinement resulting in the liquid nature of the transient matter [29].

A part of the hadron energy carried by the outer condensate clouds being released in the overlap region goes to the generation of massive quarks interacting by pion exchange and their number was estimated as follows:

$$\tilde{N}(s,b) \propto \frac{(1-\langle k_{\rm Q}\rangle)\sqrt{s}}{m_{\rm Q}}\, D_c^{h_1} \otimes D_c^{h_2} \equiv N_0(s) D_{\rm C}(b), \tag{4.3}$$

where $m_{\rm Q}$ is the constituent quark mass and $\langle k_{\rm Q}\rangle$ the average fraction of hadron energy carried by the constituent valence quarks. The function D_c^h describes the condensate distribution inside the hadron h and b is the impact parameter of the colliding hadrons. Thus, $\tilde{N}(s,b)$ quarks appear in addition to $N = n_{h_1} + n_{h_2}$ valence quarks.

The generation time of the transient state $\Delta t_{\rm tsg}$ in this picture obeys to the inequality

$$\Delta t_{\rm tsg} \ll \Delta t_{\rm int},$$

where $\Delta t_{\rm int}$ is the total interaction time. The newly generated massive virtual quarks play a role of scatterers for the valence quarks in elastic scattering; those quarks are transient ones in this process: they are transformed back into the condensates of the final hadrons.

Under construction of the model for elastic scattering [22] it was assumed that the valence quarks located in the central part of a hadron are scattered in a quasi-independent way off the transient state with interaction radius of valence quark determined by its inverse mass:

$$R_{\rm Q} = \kappa/m_{\rm Q}. \tag{4.4}$$

The elastic scattering S-matrix in the impact parameter representation is written in the model in the form of linear fractional transform:

$$S(s,b) = \frac{1+iU(s,b)}{1-iU(s,b)}, \tag{4.5}$$

where $U(s,b)$ is the generalized reaction matrix, which is considered to be an input dynamical quantity similar to an input Born amplitude and related to the elastic scattering scattering amplitude through an algebraic equation which enables one to restore unitarity [30]. The function $U(s,b)$ is chosen in the model as a product of the averaged quark amplitudes

$$U(s,b) = \prod_{\rm Q=1}^{N} \langle f_{\rm Q}(s,b)\rangle \tag{4.6}$$

in accordance with assumed quasi-independent nature of the valence quark scattering. The essential point here is the rise with energy of the number of the scatterers like $\sqrt{s}$. The b–dependence of the function $\langle f_{\rm Q}\rangle$ has a simple form $\langle f_{\rm Q}(b)\rangle \propto \exp(-m_{\rm Q}b/\xi)$.

These notions can be extended to particle production with account of the geometry of the overlap region and properties of the liquid transient state. Valence constituent quarks would excite a part of the cloud of the virtual massive quarks and those quark droplets will subsequently hadronize and form the multiparticle final state. This mechanism can be relevant for the region of moderate transverse momenta while the region of high transverse momenta should be described by the excitation of the constituent quarks themselves and application of the perturbative QCD to the parton structure of the constituent quark. The model allow to describe elastic scattering and the main features of multiparticle production [22, 23, 31]. In particular, it leads to asymptotical dependencies

$$\sigma_{\rm tot,el} \sim \ln^2 s, \;\; \sigma_{\rm inel} \sim \ln s, \;\; \bar{n} \sim s^{\delta}. \tag{4.7}$$

Inclusive cross-section for unpolarized particles integrated over impact parameter $\mathbf{b}$, does not depend on the azimuthal angle of the detected particle transverse momentum. The s–channel unitarity for the inclusive cross-section could be accounted for by the following representation

$$\frac{d\sigma}{d\xi} = 4\int_0^{\infty} d\mathbf{b} \frac{I(s,\mathbf{b},\xi)}{|1-iU(s,\mathbf{b})|^2}. \tag{4.8}$$

The set of kinematic variables denoted by ξ describes the state of the detected particle. The function I is constructed from the multiparticle analogues $U_{\rm n}$ of the function U and is in fact an non-unitarized inclusive cross-section in the impact parameter space and unitarity corrections is given by the factor

$$w(s,b) \equiv |1-iU(s,b)|^{-2}$$

in Eq. (4.8). Unitarity modifies anisotropic flows. When the impact parameter vector $\mathbf{b}$ and transverse momentum $\mathbf{p}_\perp$ of the detected particle are fixed, the function $I = \sum_{n\geq 3} I_n$, where n denotes the number of particles in the final state, depends on the azimuthal angle ϕ between vectors $\mathbf{b}$ and $\mathbf{p}_\perp$. It should be noted that the impact parameter $\mathbf{b}$ is the variable conjugate to the transferred momentum $\mathbf{q} \equiv \mathbf{p}'_a - \mathbf{p}_a$ between two incident channels which describe production processes of the same final multiparticle state. The dependence on the azimuthal angle ϕ can be written in explicit form through the Fourier series expansion

$$I(s,\mathbf{b},y,\mathbf{p}_\perp) = I_0(s,b,y,p_\perp)[1+\sum_{n=1}^{\infty} 2\bar{v}_n(s,b,y,p_\perp)\cos n\phi]. \tag{4.9}$$

The function $I_0(s,b,\xi)$ satisfies the following sum rule

$$\int I_0(s,b,y,p_\perp)p_\perp dp_\perp dy = \bar{n}(s,b){\rm Im}U(s,b), \tag{4.10}$$

where $\bar{n}(s,b)$ is the mean multiplicity depending on impact parameter. The "bare" flow $\bar{v}_n$ is related to the measured flow v_n as follows

$$v_n(s,b,y,p_\perp) = w(s,b)\bar{v}_n(s,b,y,p_\perp).$$

In the above formulas the variable y denotes rapidity, i.e. $y = \sinh^{-1}(p/m)$, where p is a longitudinal momentum. Evidently, corrections due to unitarity are mostly important at small impact parameters, i.e. they provide an additional suppression of the anisotropic flows at small centralities, while very peripheral collisions are not affected by these corrections.

The geometrical picture of hadron collision at non-zero impact parameters described above implies that the generated massive virtual quarks in overlap region will obtain large initial orbital angular momentum at high energies. The total orbital angular momentum can be estimated as follows

$$L(s,b) \simeq \alpha b\frac{\sqrt{s}}{2}D_C(b). \tag{4.11}$$

The parameter α is related to the fraction of the initial energy carried by the condensate clouds which goes to rotation of the quark system and the overlap region, which is described by the function $D_{\rm C}(b)$, has an ellipsoidal form (Fig. 4.3). [h] It should be noted that $L \to 0$ at $b \to \infty$ and $L = 0$ at $b = 0$ (Fig. 4.4).

Rotating transient matter and directed flow in hadronic reactions

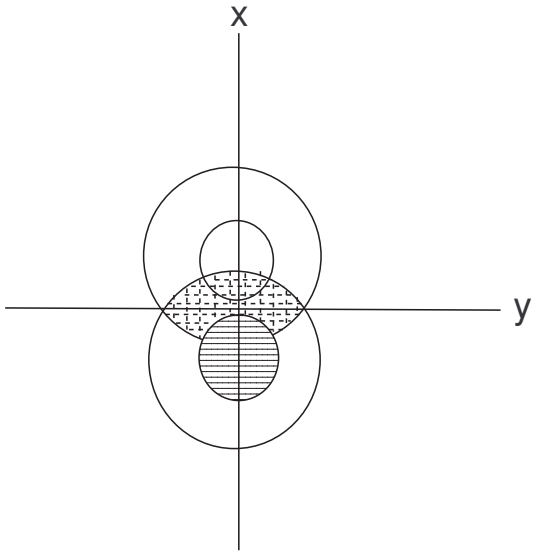

Figure 4.3: Schematic view in frontal plane of the hadron collision as extended objects. Collision occurs along the z-axis.

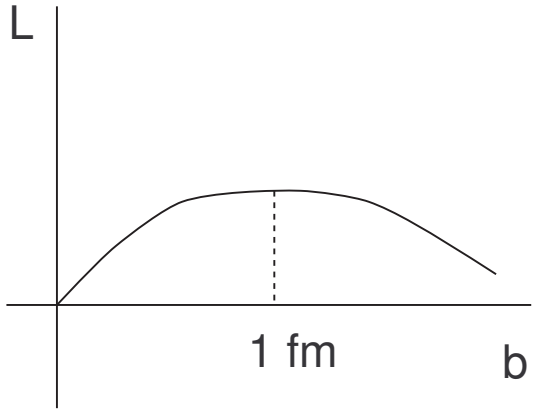

Figure 4.4: Qualitative dependence of the orbital angular momentum L on the impact parameter b.

Now we would like to discuss the experimental consequences of the described picture of hadron collisions. The important problem here is the experimental determination of the impact parameter **b**. To proceed that way the measurements of the characteristics of multiparticle production processes in hadronic collisions at fixed impact parameter should be performed with selection of the specific events sensitive to the value and direction of impact parameter. The determination of the reaction plane in the non-central hadronic collisions could be experimentally realizable with the utilization of the standard procedure[32, 33]. The relationship of the impact parameter with the final state multiplicity is a useful tool in these studies similar to the studies of the nuclear interactions. For example, in the Chou-Yang geometrical approac [34] one can restore the values of impact parameter from the charged particle multiplicity [35]. The centrality is determined by the fraction of the events with the largest number of produced particles which are registered by detectors (cf. [36]). Thus, the impact parameter can be determined through the centrality and then, e.g. directed flow, can be analyzed by selecting events in a specific centrality ranges. Indeed, the relation

$$c(N) \simeq \frac{\pi b^2(N)}{\sigma_{\rm inel}}, \tag{4.12}$$

between centrality and impact parameter was obtained [37] and can be extended straightforwardly to the case of hadron scattering. In this case we should consider $\bar{R}$ as a sum of the two radii of colliding hadrons and $\sigma_{\rm inel}$

as the total inelastic hadron-hadron cross–section. The centrality $c(N)$ is the centrality of the events with the multiplicity larger than N and $b(N)$ is the impact parameter where the mean multiplicity $\bar{n}(b)$ is equal to N.

At this point we would like to emphasize again the liquid nature of transient state. Namely due to strong interaction between quarks in the transient state, it can be described as a quark-pion liquid. Therefore, the orbital angular momentum L should be realized as a coherent rotation of the quark-pion liquid as a whole in the xz-plane (due to the aforementioned strong correlations between particles present in the liquid). It should be noted that for a given value of the orbital angular momentum L the kinetic energy has a minimal value if all parts of liquid rotate with the same angular velocity. We assume therefore that the different parts of the quark-pion liquid in the overlap region indeed have the same angular velocity ω. In this model the spin of the polarized hadrons has its origin in the rotation of the matter the hadrons consist of. In contrast, we assume rotation of the matter during intermediate, transient state of hadronic interaction.

Collective rotation of the strongly interacting system of the massive constituent quarks and pions is the main point of the proposed mechanism of the directed flow generation in hadronic and nuclei collisions. We concentrate on the effects of this rotation and consider directed flow for the constituent quarks supposing that directed flow for hadrons is close to the directed flow for the constituent quarks at least qualitatively.

The assumed particle production mechanism at moderate transverse momenta is the excitation of a part of the rotating transient state of massive constituent quarks (interacting by pion exchanges) by the one of the valence constituent quarks with subsequent hadronization of the quark-pion liquid droplets. Due to the fact that the transient matter is strongly interacting, the excited parts should be located closely to the periphery of the rotating transient state. Otherwise absorption would not allow the quarks and pions to leave the region (quenching). The mechanism is sensitive to the particular rotation direction and the directed flow should have opposite signs for the particles in the fragmentation regions of the projectile and target respectively. It is evident that the effect of rotation (shift in p_x value) is most significant in the peripheral part of the rotating quark-pion liquid and is to be weaker in the less peripheral regions (rotation with the same angular velocity ω), i.e. the directed flow v_1 (averaged over all transverse momenta) should be proportional to the inverse depth Δl where the excitation of the rotating quark-pion liquid takes place (Fig. 4.5) i.e.

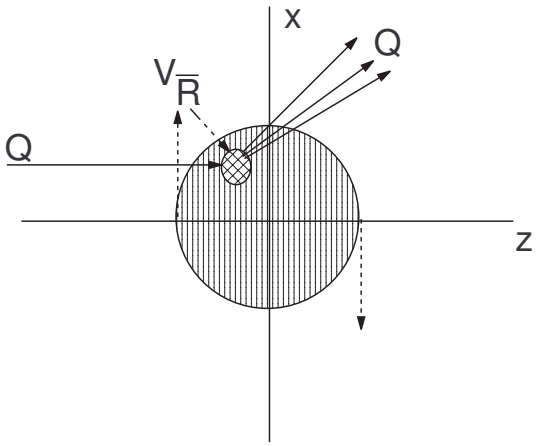

Figure 4.5: Interaction of the constituent quark with rotating quark-pion liquid.

$$|v_1| \sim \frac{1}{\Delta l} \tag{4.13}$$

In its turn, the length Δl is related to the energy loss of constituent valence quark in the medium due to elastic rescattering (quark-pion liquid) prior an excitation occurs, i.e. before constituent quark would deposit its energy into the energy of the excited quarks (those quarks lead to the production of the secondary particles), i.e. it can be assumed that

$$\Delta l \sim \Delta y,$$

where $\Delta y = |y - y_{\rm beam}|$ is the difference between the rapidities of the final particle and the projectile. On the other hand, the depth length Δl is determined by elastic quark scattering cross-section σ and quark-pion liquid

density n. Therefore, the averaged value of v_1 should be proportional to the particle density of the transient state and include the cross-section σ, i.e.

$$\langle |v_1| \rangle \sim \sigma n. \tag{4.14}$$

This estimate shows that the magnitude of the directed flow could provide information on the properties of the transient state. The magnitude of the observable v_1 (determined by the shift of transverse momentum due to rotation) is proportional to $(\Delta l)^{-1}$ in this mechanism and depends on the rapidity difference as

$$|v_1| \sim \frac{1}{|y - y_{\rm beam}|}. \tag{4.15}$$

It does not depend on the incident energy. Evidently, the directed flow $|v_1|$ decreases when the absolute value of the above difference increases, i.e. $|v_1|$ increases at fixed energy and increasing rapidity of final particle and it decreases at fixed rapidity of final particle and increasing beam energy. The dependence of $|v_1|$ will be universal for different energies when plotted against the difference $|y - y_{\rm beam}|$ (Fig. 4.6).

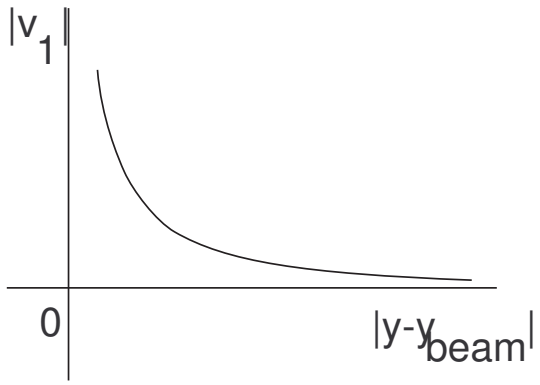

Figure 4.6: Universal dependence of directed flow on the rapidity difference.

The centrality dependence of $|v_1|$ is determined by the orbital momentum dependence L on the impact parameter, i.e. it should be decreasing towards higher and lower centralities. The decrease towards high centralities is evident: no overlap of hadrons or nuclei should be at high enough impact parameters. The decrease of v_1 towards lower centralities is a specific prediction of the proposed mechanism based on rotation since central collisions with smaller impact parameters would lead to slower rotation or its complete absence in the head-on collisions[1]. Thus, the qualitative centrality dependence of $|v_1|$ corresponds to Fig. 4.4.

Now we can consider the transverse momentum dependence of the directed flow $v_1(p_\perp)$ (integrated over rapidity) for constituent quarks. It is natural to suppose that the size of the region where the virtual massive quark Q comes from the quark-pion liquid is determined by its transverse momentum, i.e. $\bar{R} \simeq 1/p_\perp$. However, it is evident that $\bar{R}$ should not be larger than the interaction radius of the valence constituent quark $R_{\rm Q}$ (interacting with the quarks and pions from the transient liquid state). The production processes with high transverse momentum such that $\bar{R}$ is much less than the geometrical size of the valence constituent quark $r_{\rm Q}$ resolves its internal structure as a cluster of the non-interacting partons. Thus, at high transverse momenta the constituent quarks will be excited themselves and hadronization of the uncorrelated partons would lead to secondary particles with high transverse momenta and vanishing directed flow. If the production mechanism rendering to the constituent quark excitation is valid, then similar conclusions on the small anisotropic flows at large transverse momenta should be applicable for $v_n(p_\perp)$ with $n > 1$. Obviously, it should not be valid in the case of the polarized hadron collisions.

The magnitude of the quark interaction radius $R_{\rm Q}$ can be taken from the analysis of elastic scattering [22]; it has a dependence on its mass in the form (4.4) with $\kappa \simeq 2$, i.e. $R_{\rm Q} \simeq 1\ fm$ [2], while the geometrical radius of quark $r_{\rm Q}$ is about $0.2\ fm$. The size of the region[3], which is responsible for the small-$p_\perp$ hadron production, is large, valence constituent quark excites rotating cloud of quarks with various values and directions of their

[1] Of course, there is another reason for vanishing v_1 at $b = 0$, it is rotational invariance around collision axis.
[2] This is the light constituent quark interaction radius which is close to the inverse pion mass.
[3] For simplicity we suppose that this region has a spherically symmetrical form

momenta in that case. The effect of rotation will be averaged over the volume $V_{\bar{R}}$ and therefore $\langle \Delta p_x \rangle_{V_{\bar{R}}}$ and $v_1(p_\perp)$ should be small.

When we proceed to the region of higher values of $p_\perp^Q$, the radius $\bar{R}$ is decreasing and the effect of rotation becomes more prominent, the valence quark excites now the region where most of the quarks move coherently in the same direction with approximately equal velocities. The mean value $\langle \Delta p_x \rangle_{V_{\bar{R}}}$ and the directed flow, respectively, can have a significant magnitude and increase with increasing $p_\perp$. When $\bar{R}$ becomes smaller than the geometrical radius of constituent quark, the interactions at short distances start to resolve its internal structure as an uncorrelated cloud of partons. The production of the hadrons at such high values of transverse momenta is due to the excitation of the constituent quarks themselves and subsequent hadronization of the partons. The collective effects of rotating transient cloud in v_1 at large $p_\perp^Q > 1/r_Q$ will disappear as well as the directed flow of final particles. The value of transverse momentum, where the maximal values in the $p_\perp$-dependence of v_1 are expected, are in the region 1 GeV/c since $r_{\rm Q} \simeq 0.2\ fm$. The qualitative $p_\perp$-dependence of the directed flow is illustrated on Fig. 4.7.

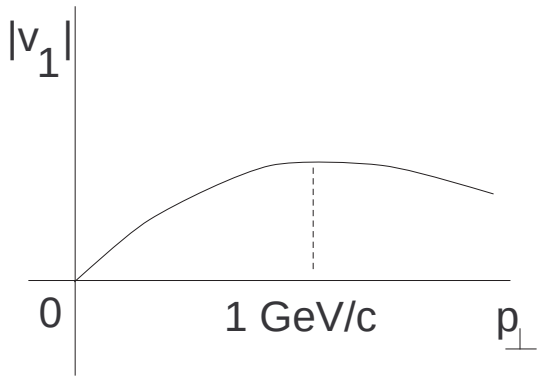

Figure 4.7: Qualitative dependence of directed flow on transverse momentum $p_\perp$.

Directed flow in nuclear collisions

Until now we considered hadron scattering and directed flow in this process, but a significant ingredient in this consideration was borrowed from the AA studies, namely we supposed that the transient matter is a strongly interacting one and it is the same in pp and AA reactions. Using the experimental findings of RHIC, we assumed, in fact, that it is a liquid consisting of massive quarks, interacting by pion exchange, and characterized by the fixed interparticle distances determined by the quark interaction radius. The assumption of the almost instantaneous, shock-wave type of generation of the transient state obtains then support in the very short thermalization time revealed in heavy-ion collisions at RHIC [18, 38]. The existence of massive quark matter in the stage preceding hadronization seems to be supported also by the experimental data obtained at CERN SPS [39].

The geometrical picture of hadron collision has an apparent analogy with collisions of nuclei and it should be noted that the appearance of large orbital angular momentum should be expected in the overlap region in the non-central nuclei collisions. And then due to the strongly interacting nature of the transient matter we assume that this orbital angular momentum realized as a coherent rotation of a liquid. Thus, it seems that underlying dynamics could be similar to the dynamics of the directed flow in hadron collisions.

We can go further and extend the production mechanism from hadron to nucleus case also. This extension cannot be straightforward. First, there will be no unitarity corrections for the anisotropic flows and instead of valence constituent quarks, as a projectile we should consider nucleons, which would excite a rotating quark liquid. Of course, those differences will result in significantly higher values of directed flow. But, the general trends in its dependence on the collision energy, rapidity of the detected particle and transverse momentum, should be the same. In particular, the directed flow in nuclei collisions as well as in hadron reactions will depend on the rapidity difference $y - y_{\rm beam}$ and not on the incident energy. The mechanism therefore can provide a qualitative explanation of the incident-energy scaling of v_1 observed at RHIC [40]. In the projectile frame the directed flow has the same values for the different initial energies. In Fig. 4.8 experimental data are shown along with the dependence

$$v_1 \sim (\eta - y_{\rm beam})^{-1}, \tag{4.16}$$

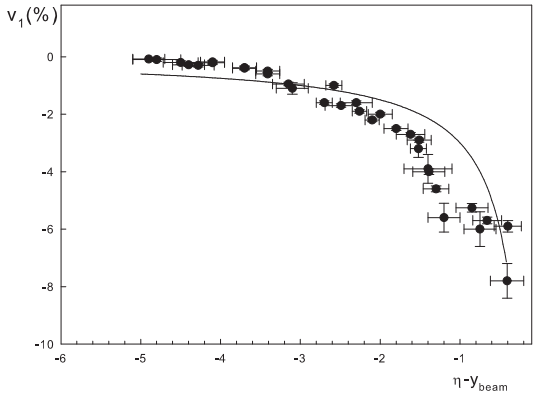

Figure 4.8: Dependence of directed flow on $\eta - y_{\rm beam}$ in Au+Au and Cu+Cu collisions at 62.4 GeV and 200 GeV at RHIC (preliminary data of STAR Collaboration [40])

where η is the pseudorapidity. This dependence reflects the trend in the experimental data and, therefore, the mechanism described in the previous section obtains an experimental justification, qualitatively, of course. In addition, we would like to note that the azimuthal dependence of the suppression factor $R_{\rm AA}$ found in the experiment PHENIX at RHIC [44] can also be explained by a rotation of the transient state. Since the correlations result from the rotation in this mechanism and therefore are maximal in the rotation plane, a similar dependence should be observed in the azimuthal dependence of the two-particle correlation function. The effect of rotation should be maximal for the peripheral collisions and therefore the dependence on ϕ should be steepest at larger impact parameter (or centrality) values. The discussed rotation mechanism should contribute to the elliptic flow too. However, since the regularities already found experimentally for v_1 and v_2 in nuclear interactions imply different dynamical origin for these flows, we should conclude that this mechanism does not provide a significant contribution to the elliptic flow.

Directed flow at the NICA and LHC energies and conclusion

Nowadays, with approaching start of the LHC, and planning of the NICA project at JINR Dubna it is interesting to predict what should be expected at such energies [45],[46] in particular: would deconfined matter produced in *pp* and A + A collisions be weakly interacting or will it remain to be a strongly interacting one as it was observed at RHIC in A + A collisions? In the latter case one can expect that the proposed rotating mechanism will be working at the LHC energies and at NICA and therefore the observed at RHIC incident-energy scaling in v_1 will remain to be valid also, i.e. directed flow plotted against the difference $y - y_{\rm beam}$ will be the same as it is at RHIC. However, if the transient matter at the LHC energies or at NICA will be weakly interacting, then one should expect the absence of the coherent rotation and the vanishing of the directed flow. This conclusion is valid provided that the rotation is the only mechanism of the directed flow generation. If it is so, vanishing directed flow can serve as a signal of a genuine quark-gluon plasma (gas of free quarks and gluons) formation.

I would like to thank Nikolay Tyurin, in collaboration with him the results described here were obtained. I am grateful to Oleg Teryaev for the interesting discussions and proposal to write this contribution for the NICA Project. I would like to aknowledge also many discussions with Laszlo Jenkovszky which were very helpful and interesting.

4.5 Importance of third moments of conserved charges in relativistic heavy ion collisions

M. Asakawa

Department of Physics, Osaka University, Toyonaka, Japan

Quantum chromodynamics (QCD) is believed to have a rich phase structure in the temperature (T) and baryon chemical potential ($\mu_{\rm B}$) plane. Lattice QCD calculations indicate that the chiral and deconfinement phase transitions are a smooth crossover on the temperature axis [47], while various models predict that the

phase transition becomes of first order at high density [48]. The existence of the QCD critical point is thus expected.

One may expect that the singularity at the critical point, at which the transition is of second order, may cause enhancements of fluctuations if fireballs created by heavy ion collisions pass near the critical point during the time evolution. Because of finite size effects and critical slowing down, however, such singularities are blurred and its experimental conformation may not be possible [49, 50].

Here we propose to employ *signs* of third moments of conserved charges around the averages, which we call, for simplicity, the third moments in the following, to infer the states created by heavy ion collisions. In particular, we consider third moments of conserved quantities, the net baryon and electric charge numbers, and the energy,

$$m_3(ccc) \equiv \frac{\langle (\delta N_c)^3 \rangle}{VT^2}, \quad m_3(\mathrm{EEE}) \equiv \frac{\langle (\delta E)^3 \rangle}{VT^5}, \tag{4.17}$$

where N_c with $c = \mathrm{B}, \mathrm{Q}$ represent the net baryon and electric charge numbers in a subvolume V, respectively, E denotes the total energy in V, $\delta N_c = N_c - \langle N_c \rangle$, and $\delta E = E - \langle E \rangle$. We also make use of the mixed moments defined as follows:

$$m_3(cc\mathrm{E}) \equiv \frac{\langle (\delta N_c)^2 \delta E \rangle}{VT^3}, \quad m_3(c\mathrm{EE}) \equiv \frac{\langle \delta N_c (\delta E)^2 \rangle}{VT^4}. \tag{4.18}$$

To understand the behaviors of these moments around the QCD phase boundary, we first notice that the moments Eqs. (4.17) and (4.18) are related to third derivatives of the thermodynamic potential per unit volume, ω, with respect to the corresponding chemical potentials and T. The simplest example is $m_3(\mathrm{BBB})$, which is given by

$$m_3(\mathrm{BBB}) = -\frac{\partial^3 \omega}{\partial \mu_\mathrm{B}^3} = \frac{\partial \chi_\mathrm{B}}{\partial \mu_\mathrm{B}}, \tag{4.19}$$

where the baryon number susceptibility, χ_B, is defined as

$$\chi_\mathrm{B} = -\frac{\partial^2 \omega}{\partial \mu_\mathrm{B}^2} = \frac{\langle (\delta N_\mathrm{B})^2 \rangle}{VT}. \tag{4.20}$$

The baryon number susceptibility χ_B diverges at the critical point and has a peak structure around there.

Since $m_3(\mathrm{BBB})$ is given by the μ_B derivative of χ_B as in Eq. (4.19), the existence of the peak in χ_B means that $m_3(\mathrm{BBB})$ changes its sign there. Although the precise size and shape of the critical region are not known, various models predict that the peak structure of χ_B well survives far along the crossover line. For also $m_3(cc\mathrm{E})$ and $m_3(c\mathrm{EE})$, a similar argument applies.

Once the negativeness of third moments is established experimentally, it is direct evidence of two facts: (1) the existence of a peak structure of corresponding susceptibility in the phase diagram of QCD, and (2) the realization of hot matter beyond the peak, i.e. the quark-gluon plasma, in heavy ion collisions. We emphasize that this statement using the *signs* of third moments is free from any theoretical ambiguities.

The range of μ_B/T where lattice simulations are successfully applied is limited to small μ_B/T with the present algorithms. In particular, thermodynamics around the critical point cannot be analyzed with the Taylor expansion method. In order to evaluate the qualitative behavior of the third moments in such a region, one has to resort to effective models of QCD. To make such an estimate, here we employ the two-flavor Nambu-Jona-Lasinio model [51, 52] with the standard interaction $\mathcal{L}_\mathrm{int} = G\{(\bar{\psi}\psi)^2 + (\bar{\psi} i \gamma_5 \tau_i \psi)^2\}$, where ψ denotes the quark field. For the model parameters, we take the values determined in Ref. [51]; $G = 5.5$ GeV^{-2}, the current quark mass $m = 5.5$ MeV, and the three-momentum cutoff $\Lambda = 631$ MeV. For the isospin symmetric matter, this model gives a first order phase transition at large μ_B.

The region where each moment becomes negative in the T-μ_B plane is shown in Fig. 4.9. One sees that all the moments become negative on the far side of the critical point as it should be, whereas the extent of the region depends on the channel. The figure shows that areas with $m_3(\mathrm{BBB}) < 0$ and $m_3(\mathrm{BBE}) < 0$ extend to much lower μ_B and much higher T than the critical point. This suggests that even if the critical point is located at high μ_B the negative third moments can be observed by heavy ion collision experiments. It should be, however, remembered that the results in Fig. 4.9, are obtained in an effective model. In particular, the model employed here gives the critical point at relatively low T and high μ_B [53]. If the critical point is at much lower μ_B, the areas with negative moments in Fig. 4.9 should also move toward lower μ_B and higher T.

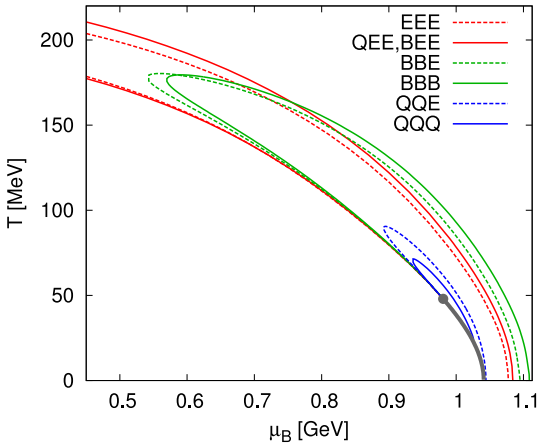

Figure 4.9: Regions where third moments take negative values in the T-$\mu_{\rm B}$ plane. The regions are inside the boundaries given by the lines.

It cannot be emphasized too much that it is essential to cover the entire phase space by changing colliding energy to draw a figure like Fig. 4.9 and get the full information on the QCD phase diagram. From this point of view, NICA project is as important as RHIC and LHC.

4.6 Baryon Stopping in Heavy-Ion Collisions at $E_{\rm lab}$ = 2–160 GeV/nucleon

Yu.B. Ivanov[a,b]

[a] *GSI Helmholtzzentrum für Schwerionenforschung GmbH, Darmstadt, Germany*
[b] *Kurchatov Institute, Moscow, Russia*

The degree of stopping of colliding nuclei is one of the basic characteristics of the collision dynamics, which determines the part of the incident energy of colliding nuclei deposited into produced fireball and hence into the production of secondary particles. The deposited energy in its turn determines the nature (hadronic or quark-gluonic) of the produced fireball and thereby its subsequent evolution. Therefore, a proper reproduction of the baryon stopping is of primary importance for the theoretical understanding of the dynamics of nuclear collisions. A direct measure of the baryon stopping is the net-baryon rapidity distribution. However, since experimental information on neutrons is unavailable, we have to rely on proton data.

Available data on the proton (at AGS energies) and net-proton (at SPS energies) rapidity distributions from central heavy-ion collisions are presented in Fig. 4.10. Only the midrapidity region is displayed in Fig. 4.10, since it is of prime interest in the present consideration. The data at 10 AGeV are repeated in the right panel of Fig. 4.10 in order to keep the reference spectrum shape for the comparison. The data are plotted as functions of a "dimensionless" rapidity $(y - y_{\rm cm})/y_{\rm cm}$, where $y_{\rm cm}$ is the center-of-mass rapidity of colliding nuclei. In particular, this is the reason why the experimental distributions are multiplied $y_{\rm cm}$. This representation is chosen in order to make different distributions of approximately the same width and the same height. This is convenient for comparison of shapes of these distributions. To make this comparison more quantitative, the data are fitted by a simple formula

$$\begin{aligned} \frac{dN}{dy} &= a\,(\exp\{-(1/w_s)\cosh(y - y_{cm} - y_s)\} \\ &+ \exp\{-(1/w_s)\cosh(y - y_{cm} + y_s)\}) \end{aligned} \tag{4.21}$$

where a, y_s and w_s are parameters of the fit. The form (4.21) is a sum of two thermal sources shifted by $\pm y_s$ from the midrapidity. The width w_s of the sources can be interpreted as w_s = (temperature)/(transverse mass), if we assume that collective velocities in the sources have no spread with respect to the source rapidities $\pm y_s$. The parameters of the two sources are identical (up to the sign of y_s) because we consider only collisions of identical nuclei. Results of these fits are demonstrated in Fig. 4.10.

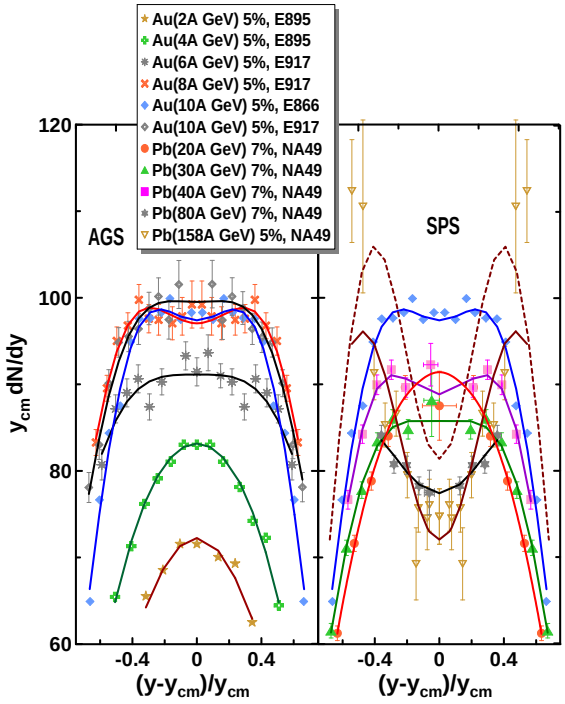

Figure 4.10: Rapidity spectra of protons (for AGS energies) and net-protons ($p - \bar{p}$) (for SPS energies) from central collisions of Au + Au (AGS) and Pb+Pb (SPS). Experimental data are from collaborations E802 [54], E877 [55], E917 [56], E866 [57], and NA49 [58, 59, 60, 61, 62]. The percentage shows the fraction of the total reaction cross section, corresponding to experimental selection of central events. Solid lines connecting points represent the two-source fits by Eq. (4.21). The dashed line is the fit to old data on Pb(158 AGeV)+Pb [58], these data themselves are not displayed.

The above fit has been done by the least-squares method. Data were fitted in the rapidity range $|y - y_{cm}|/y_{cm} < 0.7$. The choice of this range is dictated by the data. As a rule, the data are available in this rapidity range, sometimes the data range is even more narrow (40, 80 AGeV and new data at 158 AGeV [62]). We put the above restriction in order to treat different data in approximately the same rapidity range. Notice that the rapidity range should not be too wide in order to exclude contribution of cold spectators.

Inspecting evolution of the spectrum shape with the incident energy rise, we observe an irregularity. Beginning from the lowest AGS energy to the top one the shape of the spectrum evolves from convex to slightly concave at 10 AGeV. However, at 20 AGeV the shape again becomes distinctly convex. With the further energy rise the shape again transforms from the convex form to a highly concave one. In order to quantify this trend, we introduce a reduced curvature of the spectrum in the midrapidity defined as follows

$$\begin{aligned} C_y &\equiv \left(y_{\rm cm}^3 \frac{d^3N}{dy^3}\right)_{y=y_{\rm cm}} \Big/ \left(y_{\rm cm}\frac{dN}{dy}\right)_{y=y_{\rm cm}} \\ &= (y_{cm}/w_s)^2 \left(\sinh^2 y_s - w_s \cosh y_s\right). \end{aligned} \tag{4.22}$$

This curvature is defined with respect to the "dimensionless" rapidity $(y-y_{\rm cm})/y_{\rm cm}$. The factor $1/\left(y_{\rm cm}dN/dy\right)_{y=y_{\rm cm}}$ is introduced in order to get rid of overall normalization of the spectrum, i.e. of the a parameter in terms of fit (4.21). The second part of Eq. (4.22) presents this curvature in terms of parameters of fit (4.21).

Values of the curvature $C_{\rm y}$ deduced from fit (4.21) to experimental data are displayed in Fig. 4.11. The irregularity observed in Fig. 4.10 is distinctly seen here as a "zig-zag" irregularity in the energy dependence of $C_{\rm y}$.

Fig. 4.11 also contains $C_{\rm y}$ deduced from results of 3FD simulations with a hadronic equation of state (hadr. EoS) [65] and a EoS involving a first-order phase transition into the quark-gluon phase (2-ph. EoS) [66]. To obtain y_s and w_s, the 3FD spectra were also fitted by the form (4.21). The 3FD model with the hadronic EoS reasonably reproduces a great body of experimental data in a wide energy range from AGS to SPS, see Ref. [63]. Description of the rapidity distributions with the hadronic EoS is reported in Refs. [63, 64]. The reproduction of the distributions is quite good at the AGS energies and at the top SPS energies. At 40 AGeV the description is still satisfactory. However, at 20 and 30 AGeV the hadr.-EoS predictions completely disagree with the data,

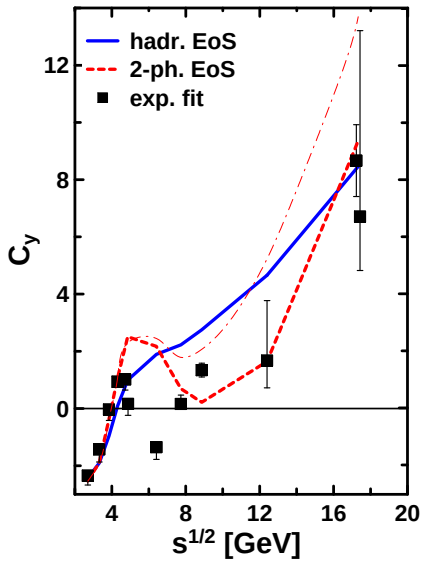

Figure 4.11: Midrapidity reduced curvature of the (net)proton rapidity spectrum as a function of the center-of-mass energy of colliding nuclei as deduced from experimental data and predicted by 3FD calculations with hadronic EoS (hadr. EoS) [65] and a EoS involving a first-order phase transition into the quark-gluon phase (2-ph. EoS) [66]. The thin dashed-dotted line demonstrates the effect of the 2-ph. EoS without changing the friction in the quark-gluon phase.

cf. [64]. At 20 AGeV instead of a bump at the midrapidity the hadronic scenario predicts a quite pronounced dip.

The 3FD simulations have been also done with a EoS involving a first-order phase transition into the quark-gluon phase (2-ph. EoS) [66]. In 2-ph. EoS the Gibbs construction was used for the mixed phase. These calculations well reproduce the AGS data up to the energy of 6 AGeV, where the purely hadronic scenario is realized. The data at the top SPS energy are also reproduced, which is achieved by a proper tune of the inter-fluid friction in the quark-gluon phase. Quality of the reproduction of above data is approximately the same as that with the hadronic EoS, as it is, e.g., seen from Figs. 4.11. However, at top AGS and lower SPS energies (8 – 80 AGeV), where the mixed phase turns out to be really important, the 2-ph. EoS completely fails. This failure cannot be cured by variations of neither the friction nor the freeze-out criterion.

However, the $C_{\rm y}$ curvature energy dependence in the first-order-transition scenario manifests qualitatively the same "zig-zag" irregularity (Fig. 4.11), as that in the data fit, while the hadronic scenario produces purely monotonous behaviour.

The baryon stopping depends on a character of interactions (e.g., cross sections) of the matter constituents. If during the interpenetration stage of colliding nuclei a phase transformation[4] of the hadronic matter into quark-gluonic one happens, one can expect a change of the stopping power of the matter at this time span. This is a natural consequence of a change of the constituent content of the matter because hadron-hadron cross sections differ from quark-quark, quark-gluon, etc. ones. This can naturally result in a non-monotonous behaviour of the shape of the (net)proton rapidity-spectrum at an incident energy, where onset of the phase transition occurs. The friction in the quark-gluon phase was tuned to reproduce the data at the top SPS energy. Naturally, it does not continuously match the friction in the hadronic phase.

However, if even the same friction is used in both phases, the calculated (with 2-ph. EoS) reduced curvature still reveals a "zig-zag" behaviour but with considerably smaller amplitude (see the thin dashed-dotted line in Fig. 4.11). This happens because the EoS in a generalized sense of this term, i.e. viewed as a partition of the total energy between kinetic and potential parts, also affects the stopping power. The friction is proportional to the relative velocity of the counter-streaming nuclei [63]. Therefore, it is more efficient when the kinetic-energy part of the total energy is higher, i.e. when the EoS is softer. The latter naturally results in a non-monotonous

[4]The term "phase transition" is deliberately avoided, since it usually implies thermal equilibrium.

evolution of the proton rapidity spectra with the energy rise.

Fig. 4.12 demonstrates that the onset of the phase transition in the calculations indeed happens at top-AGS–low-SPS energies, where the "zig-zag" irregularity takes place. Similarly to that it has been done in Ref. [69], the figure displays dynamical trajectories of the matter in the central box placed around the origin $\mathbf{r} = (0, 0, 0)$ in the frame of equal velocities of colliding nuclei: $|x| \leq 2$ fm, $|y| \leq 2$ fm and $|z| \leq \gamma_{\rm cm}$ 2 fm, where $\gamma_{\rm cm}$ is Lorentz factor associated with the initial nuclear motion in the c.m. frame. Initially, the colliding nuclei are placed symmetrically with respect to the origin $\mathbf{r} = (0, 0, 0)$, z is the direction of the beam. The ε-$n_{\rm B}$ representation is chosen because these densities are dynamical quantities and, therefore, are suitable to compare calculations with different EoS's. Subtraction of the $m_{\rm N} n_{\rm B}$ term is taken for the sake of suitable representation of the plot. Only expansion stages of the evolution are displayed, where the matter in the box is already thermally equilibrated. Nevertheless, the matter in the box still amounts to a minor part of the total matter of colliding nuclei. Therefore, only the minor part of the total matter undergoes the phase transition at 10 AGeV energy. As seen, the trajectories for two different EoS's are very similar at AGS energies and start to differ at SPS energies because of the effect of the phase transition.

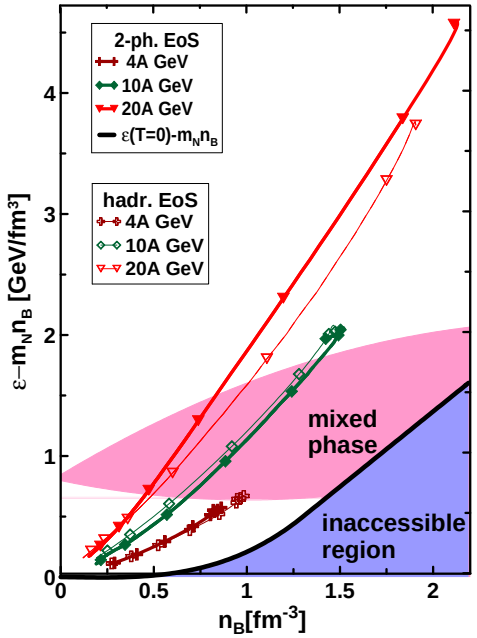

Figure 4.12: Dynamical trajectories of the matter in the central box of the colliding nuclei (4fm×4fm×$\gamma_{\rm cm}$4fm), where $\gamma_{\rm cm}$ is the Lorentz factor associated with the initial nuclear motion in the c.m. frame, for central ($b = 0$) collisions of Au+Au at 4 and 10 AGeV energies and Pb+Pb at 20 AGeV. The trajectories are plotted in terms of baryon density ($n_{\rm B}$) and the energy density minus $n_{\rm B}$ multiplied by the nucleon mass ($\varepsilon - m_{\rm N} n_{\rm B}$). Only expansion stages of the evolution are displayed for two EoS's. Symbols on the trajectories indicate the time rate of the evolution: time span between marks is 1 fm/c.

In conclusion, the experimentally observed baryon stopping may indicate (within the present experimental uncertainties) a non-monotonous behaviour as a function of the incident energy of colliding nuclei. This reveals itself in a "zig-zag" irregularity in the excitation function of a midrapidity reduced curvature of the (net)proton rapidity spectrum. Notice that the energy location of this anomaly coincides with the previously observed anomalies for other hadron-production properties at the low SPS energies [67, 70]. The 3FD calculation with the hadronic EoS fails to reproduce this irregularity. At the same time, the same calculation with the EoS involving a first-order phase transition into the quark-gluon phase (within the Gibbs construction) [66] reproduces this "zig-zag" behaviour, however only qualitatively. This non-monotonous behaviour of the baryon stopping is a natural consequence of a phase transition. The question why these calculations do not qualitatively reproduce the "zig-zag" irregularity deserves special discussion elsewhere. It is very probable that either the Gibbs and Maxwell constructions are inappropriate for the fast dynamics of the heavy-ion collisions or the phase transition is not of the first order.

It is somewhat suspicious that the "zig-zag" irregularity happens at the border between the AGS and SPS energies. It could imply that this irregularity results from different ways of selecting central events in AGS and SPS experiments. New data taken at the same acceptance and the same centrality selection in this energy range are highly desirable to clarify this problem. Hopefully such data will come from new accelerators FAIR at GSI and NICA at Dubna, as well as from the low-energy-scan program at RHIC. An advantage of NICA is that it covers precisely the whole energy range of the present interest. Therefore, the measurements can be taken with the same experimental conditions within the whole energy range. This will allow to confirm or reject the discussed experimental trend.

A report on this work in more detail can be found in [71].

4.7 Statistical hadronization phenomenology in a low-energy collider

G. Torrieri[a,b]

[a] *FIAS, J.W. Goethe Universität, Frankfurt A.M., Germany*
[b] *Department of Physics, Columbia University, New York, USA*

Fluctuation observables play an obvious primary role for searches of a lot of new physics planned at NICA. The most universal and model-independent signature of critical point physics is that fluctuations should spike close to the critical point [72] (a "remnant" of their divergence in the thermodynamic limit). Spinodal regions [73], triple points [74], color superconductivity transitions [75] etc. should also produce a qualitatively strong fluctuation enhancement. Before data can be compared to theory, however, two important issues need to be examined and clarified:

The first issue is the formulation of the fluctuation observable least affected by fluctuations not connected to the microscopic physics of the system, like initial state fluctuations and fluctuations due to limited detector acceptance. While an order-of-magnitude shift in fluctuations will probably be visible over a non-thermal background, the background could well overwhelm a smaller spike, especially, as is likely, if the onset of the critical point is also correlated with non-equilibrium dynamical effects.

The second issue is a thorough understanding of the fluctuations due to statistical mechanics *independently* of the critical point. Obviously, they form part of the background to any critical point signal. But more generally, fluctuations can be used to thoroughly constrain the free parameters in statistical models, and determine in what domain, in energy and system size, is statistical mechanics a valid description for particle production.

This task is important in and of itself: As an analogy from another field where fluctuations are crucial, Cosmic Microwave Background fluctuations have not yet yielded evidence of novel physics. Their use to constrain the dominant paradigm of cosmology, inflation, has however been invaluable enough to entitle the leaders of the COBE project to a Nobel Prize. The equivalent job in soft hadronic physics, using fluctuations to Gauge and constrain the statistical model of particle production, is far from being completed, and a low-energy collider is essential to complete it.

The idea of modeling the abundance of hadrons using statistical mechanics has a long history [76, 77, 78, 79]. In a sense, any discussion of the thermodynamic properties of hadronic matter (e.g. the existence of a phase transition and a critical point) *requires* that statistical mechanics be applicable to this system. Indeed, there is a consensus that statistical models can fit most particles from very high energies to energies comparable with NICA [80, 81, 82, 83, 84, 85, 86].

There are, however, several points of contention to this understanding: Some scientists [76] interpret the statistical model results in terms of nothing more than phase space dominance. If this is the case, the applicability of the statistical model has nothing to do with a genuine equilibration of the system,so using statistical mechanics inspired techniques to look for the critical point is useless. Others [74, 80] believe that the applicability of the statistical model is a sign of a phase transition, as the chemical equilibration of hadrons signals a regime in which multi-particle processes and high-lying resonances dominate.Still others [83] think that in soft QCD processes particles are "born in equilibrium", and the applicability of the statistical model to even smaller systems (itself controversial [87]) is a fundamental characteristic of QCD.

How can these scenarios be differentiated? One observable "at the heart" of statistical mechanics is event-by-event fluctuations. It is a fundamental principle of statistics that variances around averages scale a calculable way w.r.t. averages. In our context "Averages" are particle multiplicities per event and fluctuations are event-by-event fluctuations. For macroscopic systems, this principle ensures that fluctuations become negligible and

the expectation that the state of the system is the maximum entropy one is nearly certain to be realized. The typical event multiplicity, $\sim 100--1000$ particles is not enough for this to be the case, but, if statistical mechanics applies, one should still see that yields, fluctuations and higher cumulants scale in a way calculable from the partition function.

There are, however, some experimental issues specific to heavy ion collisions that need to be explored before this can be transformed into a quantitative test. "standard" fluctuation calculations assume that the volume stays constant. System size fluctuations due to initial geometry and dynamics obviously make this assumption invalid, and contaminate any straight-forward fluctuation observable.

The simplest way to eliminate system size fluctuations unrelated to statistical mechanics is to focus on fluctuations of *ratios* of particles ($\pi^+/\pi^-, p/\pi, K/\pi$, and so on). It can be shown that, at least in the thermodynamic limit, volume becomes a proportionality constant at the level of the partition function so that the scaled variance of a ratio is inversely proportional of the average, $\sigma_{N_1/N_2} \sim 1/\langle N_{1,2}\rangle$ and *strictly independent* of fluctuations in volume. This scaling, for *all yields* and *all fluctuations of ratios* is *specific* to statistical mechanics in the thermodynamic limit, *provided they are measured at the same value* with the same acceptance cuts. In other words, for all particles i, j, $\langle N_i\rangle\sigma_{N_i/N_j}$ is strictly independent of system size, and any dependence of it on $\sqrt{s}$ can be described by the same T and μ_B that *also* describe $\langle N_i\rangle/\langle N_j\rangle$. This is a very tight constraint, equivalent of using CMB fluctuations to tune inflationary cosmology models precisely [88]. Codes capable of doing this are already publically available [85, 86], but data to perform this kind of analysis reliably, for reasons explained below, is only available at high (top Relativistic Heavy Ion Collider) energy [88] (see Fig. 4.13 for the main result).

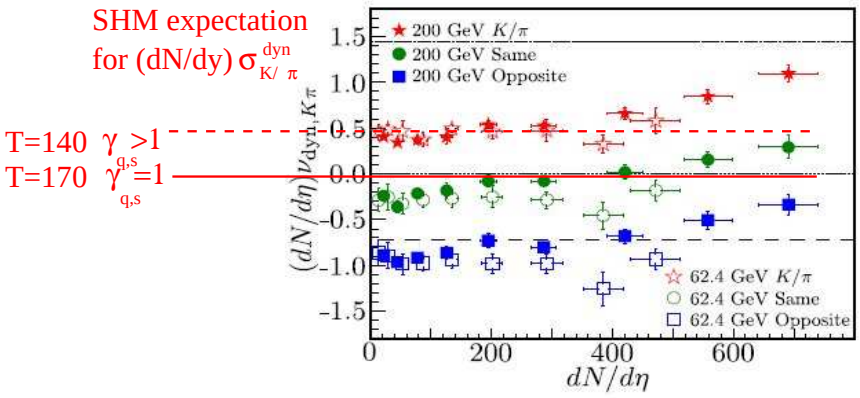

Figure 4.13: A comparison between statistical models and K/π fluctuation data at RHIC energies, see [88] for details.

The applicability and definition of the term "volume" is itself problematic in a dynamical quantum system. Statistical particle production *assumes* a volume, but leaves unexplained how this volume is defined, e.g. if acceptance cuts can be considered as "cuts in volume". If particles are created with a boost-invariant flow (spacetime and flow rapidity coincide) then cuts in rapidity are equivalent to cuts in volume (Fig. 4.14). To make such an approximation, however, the detector must be able to apply a simple rapidity cut for *all* particles at *all* energies under consideration, and to freely vary this cut to see how both the yield and the fluctuation scale. Only at a collider experiment capable of scanning in energy,such as NICA, can these criteria be satisfied. A different but related problem is the effect of particle misidentification, limited momentum resolution etc on fluctuation observables. These are much more difficult to model reliably than averages, and an observable needs to be constructed insensitive to them. Hence, the necessity of mixed event subtraction [86]. Such a mixed event subtraction is however most feasible in a collider, since a fixed target experiment has non-trivial energy dependent phase space cuts that make mixed event subtraction suspect.

Currently, the scaling of fluctuations at low energies is *not* understood [88]. Consequently, the relationship between fluctuation systematics and the structures seen in the *average* chemical properties of events (such as the "Kink" and the "horn" [67], suggesting deconfinement [70]) are ambiguus.

[89] has done a very useful job of showing that the scaling of fluctuations with $\sqrt{s}$ reflects, to a good approximation, that of yields. Of course, in the statistical model the scaling of $\sigma^{K/\pi}$ with $\langle K\rangle, \langle\pi\rangle$ in collisions

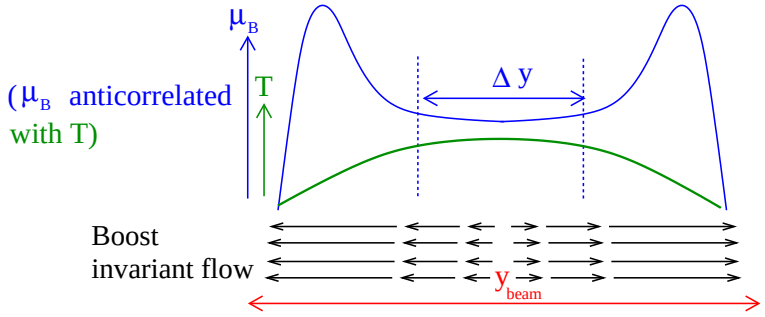

Figure 4.14: A schematic illustration of the Bjorken acceptance on fluctuations.

at different energies is more complicated than any of the models studied in [89], since it reflects changes in T, μ and possibly phase space occupancy γ [86] with $\sqrt{s}$.

It is impossible to go further with the data taken in [89], since the phase space cuts used to measure ratio fluctuations are highly particle and energy-specific. A quantitative separation between "statistical physics" and "detector acceptance" free of systematic errors is, therefore, impossible. To go further, measurements need to be made at mid-rapidity for all energies, with phase space cuts which are the same for all particles. The NICA accelerator is the idea laboratory where such measurements can be made.

If this program is successful, we will know the scaling of ratio fluctuations and abundances of π, K,protons and hyperons. Using the methods outlined in [88, 85, 86] it will be straightforward to understand in what energy and system size range does statistical particle production apply, how to temperatures, chemical potentials and phase space occupancies vary across energies and system sizes, and what is the relationship between the fluctuation systematics to the systematics of yields [67, 70]. Independently from the finding of the critical point or other new physics, this will be a crucial piece of knowledge for the study of hot QCD.

4.8 Flow scaling in a low energy collider: When does the perfect fluid turn on?

G. Torrieri[a,b]

[a] *FIAS, J.W. Goethe Universität, Frankfurt A.M., Germany*
[b] *Department of Physics, Columbia University, New York, USA*

A lot of attention, both in the academic and popular press, has been bestowed on the claim that the Relativistic Heavy Ion Collider (RHIC) has produced a "perfect fluid", of minimally low viscosity [17, 18, 90, 91, 92, 93].

This claim comes from the reasonably good description of the second Fourier component of flow (v_2, "elliptic flow") by ideal hydrodynamics [94, 95, 50, 97, 98, 99, 100], and by the under-prediction of v_2 when the viscosity over entropy density (η/s) in the calculation is not small, $\eta/s \geq 0.1$

Indeed, it is still a mystery why the matter created at RHIC has such a small viscosity w.r.t. the naive expectation. Proposed explanations range from strong field plasma instabilities [101] over strongly coupled theories captured by Gauge-gravity correspondence [93] to multi-particle microscopic reactions, partonic [102] or hadronic [103]. A conclusive link between RHIC hydrodynamics and microscopic QCD dynamics is, however, still missing.

Consequently, we do not know the temperature range at which the perfect liquid turns on, or *how* it turns on: Is it a phase transition to a strongly coupled quark-gluon phase, or is it a smooth descent of the mean free path from a dilute weakly interacting hadron gas limit to a gas of overlapping resonances to quarks?

Going further in our understanding is also hampered by the large number of "free" (or, to be more exact, poorly understood from first principles) parameters within the hydrodynamic model, initial conditions as well as transport coefficients: While the equation of state is thought to be understood from lattice simulations, the behavior of shear and bulk viscosity is quantitatively not known around T_c, where it is expected it could be non-trivial. The same goes for the large number of second-order transport coefficients. While we have some understanding of the initial transverse density of the system, we do not as yet have control over the degree of transparency: Is it closer to a Landau "firestreak" or transparent "Bjorken" pancakes that pass through

each-other leaving Hubble-expanding gas in between? How does the system move between these limits as the energy is varied? The thermalization time, and the amount of flow created before thermalization, are similarly unknown. All of these effects need to be understood before the transport coefficients can be determined without large systematic errors.

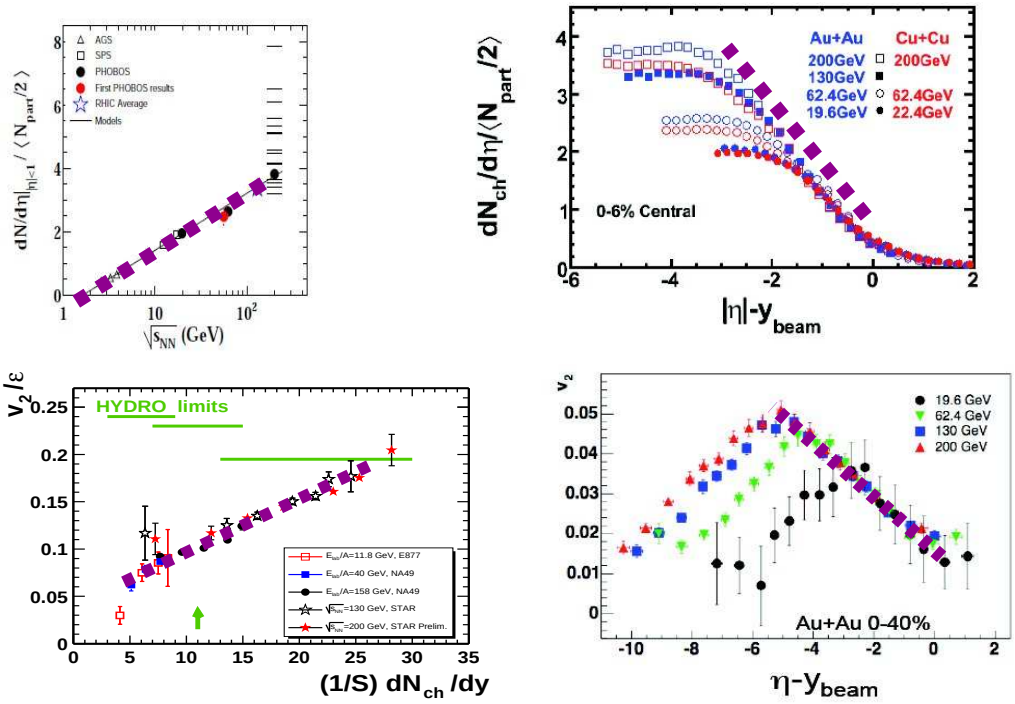

Figure 4.15: Top panels: The experimentally observed scaling of mid-rapidity dN/dy with $\sqrt{s}$ (left), as well as dN/dy away from mid-rapidity (right panel, known as limiting fragmentation). Bottom panel: elliptic flow normalized by eccentricity v_2/ϵ, integrated over rapidity (left panel) and as a function of rapidity (right panel, known as limiting fragmentation of v_2). All experimental plots from [104] and references therein, with the dashed line indicating the scaling trend.

A tool with the potential of overcoming these difficulties is scaling naturalness. Experiments have collected an extraordinary amount of flow data, encompassing a wide range of Energy,centrality, system size, rapidity, particle species and momentum. "Simple" patterns have been found [104], centered around the flow at different energies, system sizes and rapidities scaling with a few global dimensionless parameters (such as eccentricity and multiplicity density). This scaling is by no means natural when the flow is a function of many parameters, some set in the equilibrium phase and some not. Exploring which parameter combinations lead to the most natural scaling, therefore, could be used as a powerful tool to cut through the available parameter space.

What is remarkable is how well flow observables scale with $dN/(Sdy)$ (Fig. 4.15, bottom panel), the particle rapidity density normalized by the Glauber overlap area, over a wide range of energies and system sizes [105, 106]. $dN/(Sdy)$, in the Boost-invariant picture, is related to the initial particle density. In the absence of chemical potential, this is in turn related to the initial temperature. It is therefore natural to expect the scaling to hold to some extent. A non-trivial dependence of viscosity and speed of sound on temperature, and/or changes in initial transparency, however, are nearly certain to break the scaling [105, 106, 107].

The excellent scaling observed suggests that η/s, the speed of sound and the longitudinal structure of the system stay broadly the same in the energy range accessible to RHIC. The fact that multiplicity dN/dy scales so well both in rapidity and (top panels of Fig. 4.15, known as limiting fragmentation) and across energies (down to NICA energies, as the top panel in Fig. 4.15 shows) corroborates this conclusion, since strong changes in phase structure and viscosity, together with lumpy initial conditions, should lead to entropy generation.

A further, potentially much tighter constraint, is provided by the universal limiting fragmentation-like dependence of elliptic flow [107, 104] (Fig. 4.15 bottom-right panel). This seems to indicate that the transport

properties do not vary too much across rapidity in the RHIC domain, and that the initial conditions obey a "universal ansatz" largely independent of energy [107, 104]. It is to date unknown at what (lower) energy does the system experience a change in its collective properties or initial dynamics capable of breaking this scaling. Such a change could very well signal the transition of the system into the "fluid" phase.

Thus, the scaling of flow observables in a *low* energy accelerator could very well be crucial in understanding the collective properties of QCD matter. NICA is optimally configured for such a study, due to the fact that it is a collider, capable of performing rapidity and energy scans with minimal changes in the detectors acceptance. The NICA energy range is particularly interesting since, if one constructs the initial conditions from Bjorken flow and universal fragmentation, the initial temperature at mid-rapidity should approach the lattice critical temperature T_C close to the top NICA energy range[107] (Fig. 4.16 left panel,see [107] for details).

Given the limiting fragmentation observed in multiplicity and flow, a promising endeavor for low-energy measurements is to look for limiting fragmentation in other soft observables. In particular, it might be worthwhile to look for a similar limiting fragmentation in the average transverse momentum $\langle p_T \rangle$, a break of which could signal the "step" [49, 109] in rapidity space. $\langle p_T \rangle \sim T + m_\pi v_T^2$, and the transverse flow v_T should decrease significantly when the initial T is around T_c due to the dip of the speed of sound in the mixed phase regime. Similarly, rapidity dependence of $R_{\rm out}$ and $R_{\rm side}$ HBT radii could be used to check whether the scaling seen in *global* $R_{out,side} \sim \left(\frac{dN}{dy}\right)^{1/3}$ radii [110] is also local in rapidity. Such measurements will clarify whether the compressibility of the system does indeed change with rapidity, as its expected to in local thermal equilibrium where it mirrors the softness of the equation of state.

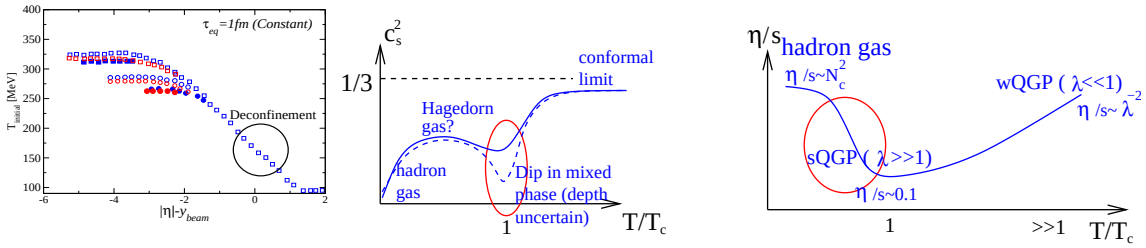

Figure 4.16: The initial temperature from limiting fragmentation (left) and the expected temperature dependence of speed of sound (center) and η/s (right), see [107] for details. The right panel shows qualitative expectations from scaling in number of colors N_c and 't Hooft coupling constant λ.

In conclusion, RHIC has shown the existence of a highly liquid phase in a regime where the initial temperature $\gg T_c$. It is however completely unclear when and how does this phase turn on, as RHIC has also shown the collective properties scale very well across energy, multiplicity and rapidity. A lower limit of this scaling could help us understand how hydrodynamics turns on in heavy ion collisions, and could well signal the transition from a weakly interacting hadron gas to strongly interacting QCD matter. For such a study, a collider capable of scanning in energy and rapidity, with the upper energy compatible with the lower energies studied at RHIC, would be optimal. NICA fulfills these criteria fully.

4.9 Dissipative hydrodynamics effects at NICA

L. Turko

Institute of Theoretical Physics, University of Wrocław, Poland

The NICA collider and the related MPD detector cover a very interesting energy range where crucial phenomena of phase transitions can take place. This is the region of the maximum net baryon density [111] available in heavy ion collision processes. The range of other expected parameters gives the possibility to observe phenomena such as the confinement-deconfinement and the chiral phase transition; it allows to test the equation of state at high baryonic density. The collider geometry provides also a better acceptance coverage than in the case of fixed target experiments.

These conditions should allow for a systematic treatment of fluctuations, correlations and higher order moments of physical quantities in a baryon-rich environment. It is also possible to study hydrodynamical flow properties with conservation laws and dissipative processes taken into account. The entropy of the QGP

phase at hadronization determines the observable particle multiplicity so it is important to take into account contributions due to particle production processes. Standard continuity equations are generalized to incorporate diffusion and particle production or chemical reactions. This results in a hydrodynamic model with dynamical chemical reactions and multi-fluid effects included. The equations have now the form

$$\partial_\mu \tilde{\rho}_i^\mu \equiv \partial_\mu(\rho_i^\mu + \triangle^{\mu\nu}\partial_\nu \mathcal{R}_i) = \mathcal{J}_i \ , \tag{4.23}$$

with $\triangle_{\mu\nu} \equiv g_{\mu\nu} - u_\mu u_\nu$, $g_{\mu\nu} = \mathrm{diag}(1,\text{-}1,\text{-}1,\text{-}1)$ being the flat space-time metric.

$\mathcal{R}$ is the diffusion term which is determined consistently [112, 113] with the Second Law of Thermodynamics. $\mathcal{J}_i$ are sources of particle production. They are determined by microscopic reaction cross sections. In the local rest frame one gets the gain and loss equation

$$\mathcal{J}_i = \sum_j [G_{i\leftarrow j}\rho_j - L_{j\leftarrow i}\rho_i] \ , \tag{4.24}$$

The entropy production in a dissipative relativistic fluid is given by:

$$\begin{aligned} T\partial_\mu s^\mu &= -\sum_i \mu_i \mathcal{J}_i - T^{-1}(\partial_\mu T)u_\nu \delta T^{\mu\nu} + (\partial_\mu u_\nu)\delta T^{\mu\nu} \\ &\quad + \sum_i (\mu_i + T\mathcal{L}_i)\partial_\mu \triangle^{\mu\nu}\partial_\nu \mathcal{R}_i + T\sum_i (\partial_\mu \mathcal{L}_i)\triangle^{\mu\nu}\partial_\nu \mathcal{R}_i \ , \end{aligned} \tag{4.25}$$

where T is the temperature, $u^2 = 1$, and we employed natural units $\hbar = c = k_B = 1$. The heat-flow four-vector is defined by

$$\mathcal{Q}_\mu \equiv \partial_\mu T - T u^\nu \partial_\nu u_\mu \, , \tag{4.26}$$

and the shear tensor is given by

$$\mathcal{W}_{\mu\nu} \equiv \partial_\mu u_\nu + \partial_\nu u_\mu - \frac{2}{3} g_{\mu\nu}\partial_\gamma u^\gamma \, . \tag{4.27}$$

The First Law of Thermodynamics implies

$$0 = T\partial_\mu \tilde{s}^\mu + \sum_i \mu_i(\mathcal{J}_i - \partial_\mu \triangle^{\mu\nu}\partial_\nu \mathcal{R}_i) + u_\nu \partial_\mu \delta T^{\mu\nu} \ , \tag{4.28}$$

with an auxiliary entropy four-current, $\tilde{s}^\mu \equiv s u^\mu$, and $\rho_i^\mu \equiv \rho_i u^\mu$.

The chemical potentials μ_i do not imply traditional chemical equilibrium as they are space and time dependent parameters here. They are related to the conservation of abelian charges such as the electric charge, the strangeness or the baryon number. In the case of a conserved abelian charge the corresponding chemical potential is written as

$$\bar{\mu} = \sum_i q_i \mu_i \, ,$$

where q_i denotes the charge of particles of species "i".

The proper entropy four-current is

$$s^\mu \equiv \tilde{s}^\mu + T^{-1}u_\nu \delta T^{\mu\nu} + \sum_i \mathcal{L}_i \triangle^{\mu\nu}\partial_\nu \mathcal{R}_i \ . \tag{4.29}$$

The condition of increasing entropy leads to constraints on the particle source terms $\mathcal{J}_i$ and the diffusion terms $\mathcal{R}$ and $\mathcal{L}$ [112]. The system is driven towards chemical equilibrium if

$$\sum_i \mu_i \mathcal{J}_i \leq 0 \ . \tag{4.30}$$

This condition is closely related to abelian charge conservation of the system.

The structure of the dissipative term $\delta T^{\mu\nu}$ compatible with $\partial_\mu s^\mu \geq 0$ is given as

$$\delta T^{\mu\nu} = \kappa(\triangle^{\mu\gamma}u^\nu + \triangle^{\nu\gamma}u^\mu)\mathcal{Q}_\gamma + \eta\triangle^{\mu\gamma}\triangle^{\nu\delta}\mathcal{W}_{\gamma\delta} + \zeta\triangle^{\mu\nu}\partial_\gamma u^\gamma \ , \tag{4.31}$$

where κ, η and ζ denote the coefficients of heat conductivity, shear viscosity, and bulk viscosity, respectively. The heat-flow is given by

$$\mathcal{Q}_\mu \equiv \partial_\mu T - T u^\nu \partial_\nu u_\mu \,, \tag{4.32}$$

and the shear tensor is

$$\mathcal{W}_{\mu\nu} \equiv \partial_\mu u_\nu + \partial_\nu u_\mu - \frac{2}{3} g_{\mu\nu} \partial_\gamma u^\gamma \,. \tag{4.33}$$

Also, the contribution to the entropy production involving $\mathcal{R}$ becomes nonnegative if one identifies

$$\mathcal{L}_i \equiv -\frac{\mu_i}{T} \quad , \quad \mathcal{R}_i \equiv \sum_j \sigma_{ij} \frac{\mu_j}{T} \quad . \tag{4.34}$$

The symmetric matrix σ consists of the mutual diffusion constants and has only nonnegative eigenvalues. The diffusion current

$$\vec{j}_i \equiv -\nabla \mathcal{R}_i = -\sum_j \frac{\sigma_{ij}}{T} (\nabla \mu_j - \frac{\mu_j}{T} \nabla T) \tag{4.35}$$

involves chemo- and thermo-diffusion contributions.

The entropy production in the relativistic fluid is now given as

$$\begin{aligned} T \partial_\mu s^\mu &= -\sum_i \mu_i \mathcal{J}_i - T \sum_{i,j} \sigma_{ij} (\partial_\mu \frac{\mu_i}{T}) \triangle^{\mu\nu} (\partial_\nu \frac{\mu_j}{T}) \\ &\quad - \frac{\kappa}{T} \mathcal{Q}_\mu \triangle^{\mu\nu} \mathcal{Q}_\nu + \frac{\eta}{2} \mathcal{W}^\beta_\alpha \triangle^\gamma_\beta \mathcal{W}^\delta_\gamma \triangle^\alpha_\delta + \zeta (\partial_\mu u^\mu)^2 \,. \end{aligned} \tag{4.36}$$

This allows us to specify conditions for particular freeze-outs encountered in high energy heavy ion collisions. A complete thermal equilibrium is reached when the entropy is not longer produced, i.e., when the condition $\partial_\mu s^\mu = 0$ is fulfilled.

Dissipative processes are mainly due to bulk and shear viscosities of resulting hadronic fluid and heavy flavor production before chemical equilibrium is reached. In the NICA energy range that would be strangeness production dominated by gluon fusion $g+g \to s+\bar{s}$, with much smaller contributions of light quarks annihilation processes $q + \bar{q} \to s + \bar{s}$. Gluons and light quarks can be treated as a heat bath for strange quarks. Local exact strangeness conservation leads to strong correlations. They can be measured as the event-by-event fluctuations of the number of $s\bar{s}$ pairs. An inclusion of production processes leads to the faster cooling of the fluid. The resulting "effective viscosity" decreases so the fluid becomes more and more "effectively perfect". Flow analysis performed at NICA would allow to look into this effective viscosity problem without influence of heavier flavors processes which lead to separate flavor-specific time scales.

4.10 Hadronic Fluctuations, freeze-out conditions and the QCD (phase) transition line

F. Karsch[a,b] and C. Schmidt[c,d]

[a] *Physics Department, Brookhaven National Laboratory, Upton, NY, USA*
[b] *Fakultät für Physik, Universität Bielefeld, Bielefeld, Germany*
[c] *Frankfurt Institute for Advanced Studies, Frankfurt am Main, Germany*
[d] *GSI Helmholtzzentrum für Schwerionenforschung, Darmstadt, Germany*

Critical behavior is signaled by long range correlations and an increasing size of fluctuations associated with the appearance of massless modes in the vicinity of a second order phase transition. Fluctuations of baryon number, electric charge as well as strangeness have been shown to be sensitive indicators for such critical behavior. In the exploration of the QCD phase diagram at non-zero temperature (T) and baryon chemical potential ($\mu_{\rm B}$) higher moments of baryon number fluctuations play a particularly important role. They will diverge on the chiral phase transition line $T_c(\mu_{\rm B}, m_{\rm q} \equiv 0)$. At physical values of the light and strange quark masses they may still be sensitive to the critical behavior in the chiral limit and may allow to characterize the crossover transition in strongly interacting matter.

It is the intention of this short note to point at some of the recent results on the analysis of charge fluctuations and the exploration of the QCD phase diagram obtained in the framework of lattice QCD calculations. This

short note only discusses results obtained with Taylor expansions. For a more general discussion of the QCD phase diagram and the specific problems with studies of non-zero density QCD on the lattice we refer to recent reviews on this topic [114].

Charge fluctuations

One approach to gain information on QCD at non-zero baryon chemical potential from lattice calculations is based on the usage of Taylor expansions. Within this approach actual numerical calculations are performed at vanishing chemical potential where a set of Taylor expansion coefficients is calculated. An expansion can be set up in terms of baryon ($\mu_{\rm B}$) as well as electric charge ($\mu_{\rm Q}$) and strangeness ($\mu_{\rm S}$) chemical potentials. The expansion coefficients of the resulting Taylor series are given in terms of moments of charges B, Q, S as well as their correlations [115]. The moments of charge fluctuations, $\delta N_{\rm X} \equiv N_{\rm X} - \langle N_{\rm X}\rangle$, with $X = B$, Q or S and their correlations are obtained from derivatives of the logarithm of the QCD partition function, *i.e.* the pressure,

$$\frac{p}{T^4} \equiv \frac{1}{VT^3} \ln Z(V,T,\mu_{\rm B},\mu_{\rm S},\mu_{\rm Q}) \; , \tag{4.37}$$

evaluated at $\mu_{\rm B,Q,S} = 0$,

$$\chi^{BQS}_{ijk} = \left. \frac{\partial^{i+j+k} p/T^4}{\partial \hat{\mu}_B^i \partial \hat{\mu}_Q^j \partial \hat{\mu}_S^k} \right|_{\mu=0} \; , \tag{4.38}$$

with $\hat{\mu}_{\rm X} \equiv \mu_{\rm X}/T$. While the first derivatives, *i.e.* baryon number, electric charge and strangeness densities, vanish for $\hat{\mu}_{\rm B,Q,S} = 0$, their moments and correlation functions with $i+j+k$ even are non-zero. The basic quantities are the quadratic and quartic and also sixth order charge fluctuations,

$$\begin{aligned} \chi_2^X &= \frac{1}{VT^3}\langle N_{\rm X}^2\rangle \\ \chi_4^X &= \frac{1}{VT^3}\left(\langle N_{\rm X}^4\rangle - 3\langle N_{\rm X}^2\rangle^2\right) \; , \\ \chi_6^{\rm X} &= \frac{1}{VT^3}\left(\langle N_{\rm X}^6\rangle - 15\langle N_{\rm X}^4\rangle\langle N_{\rm X}^2\rangle + 30\langle N_{\rm X}^2\rangle^3\right) \end{aligned} \tag{4.39}$$

Some results taken from [115] are shown in Fig. 4.17.

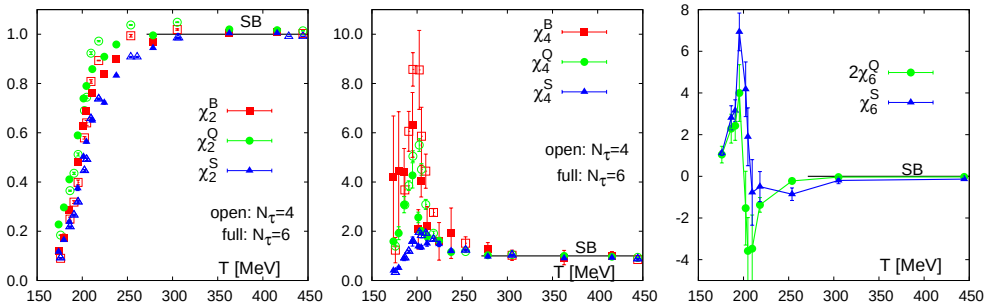

Figure 4.17: Quadratic and quartic fluctuations of baryon number, electric charge and strangeness. All quantities have been normalized to the corresponding free quark gas values. Also shown is the 6th order cumulant of electric charge and strangeness fluctuations without normalization.

Close to the chiral limit of QCD the temperature dependence of moments of charge fluctuations, in particular, higher moments of the baryon number fluctuation, are related to universal critical behavior. For QCD with two massless light quarks (u, d) this is expected to be controlled by critical exponents belonging to the universality class of the 3-dimensional, O(4) symmetric spin models. A consequence of this is that at vanishing baryon chemical potential the fourth moment of baryon number fluctuations will rise close to the transition temperature and will develop a cusp. The sixth order moment is the first moment that diverges in the chiral limit at the phase transition temperature. At non-zero values of the baryon chemical potential such a divergence will show up already in the third order moments. The strength of this divergence, however, will be proportional to $(\mu_{\rm B}/T)^3$

and thus will be difficult to isolate at small values of the baryon chemical potential,

$$\chi_k^B \sim \begin{cases} \left|\frac{T-T_c(0)}{T_c(0)}\right|^{2-\alpha-k/2} & , \text{ for } \mu_B/T = 0, \text{ and } k \text{ even} \\ \left(\frac{\mu_B}{T}\right)^k \left|\frac{T-T_c(\mu_B)}{T_c(0)}\right|^{2-\alpha-k} & , \ \mu_B/T > 0 \end{cases} , \tag{4.40}$$

with $\alpha < 0$ denoting the specific heat critical exponent, which is negative for the 3-d, $O(2)$ symmetric universality class.

Higher moments of charge fluctuations thus are expected to become increasingly sensitive to critical behavior. This also will show up in ratios of moments, χ_B^m/χ_B^n, which have the advantage of being independent of the interaction volume. A comparison with experimental results thus is much easier for ratios of moments rather then the moments themselves.

If matter created in heavy ion collisions is in equilibrium at the time of freeze-out, ratios of moments of charge fluctuations will reflect thermal properties at the freeze-out temperature. A first calculation of ratios of moments along the freeze-out line $T(\mu_B)$, which has been determined by comparing experimental results on particle abundances with results from a hadron resonance gas (HRG) model calculation [116], has been performed in [117]. In Fig. 4.18 we show the variation of a few ratios along the freeze-out line [118]. This calculation has been performed with an improved fermion action on lattice of temporal extent $N_\tau = 4$ and 6.

Calculations of the moments at non-zero baryon chemical potential are obtained from a Taylor expansion, which at present has to be interpreted with caution as these series unfortunately do not go beyond next-to-leading order. We note that results for these ratios agree quite well with HRG model calculations down to collision energies of $\sqrt{s_{\rm NN}} \simeq (20-30)$ GeV. At small values of the beam energy, which of course is the region of interest at NICA, deviations from the HRG model calculations show up. However, in this regime uncertainties in the lattice calculations are large. On the one hand there is need for a much more systematic analysis in order to get the continuum limit under control. On the other hand there clearly is also a need for the calculation of higher order corrections in the Taylor series as next-to-leading order corrections become larger than the leading order result at small $\sqrt{s_{\rm NN}}$, i.e. large values of $\mu_{\rm B}$. Here one has to worry about the convergence of the series, which of course is closely related to the determination of the location of a critical point in the QCD phase diagram. This too has been studied by using information on the ratio of moments of charge fluctuations.

We also note that HRG model calculations [119] for the ratios of moments shown in Fig. 4.18 are still in good agreement with experimental results [120] also at $\sqrt{s_{\rm NN}} \simeq 20$ GeV.

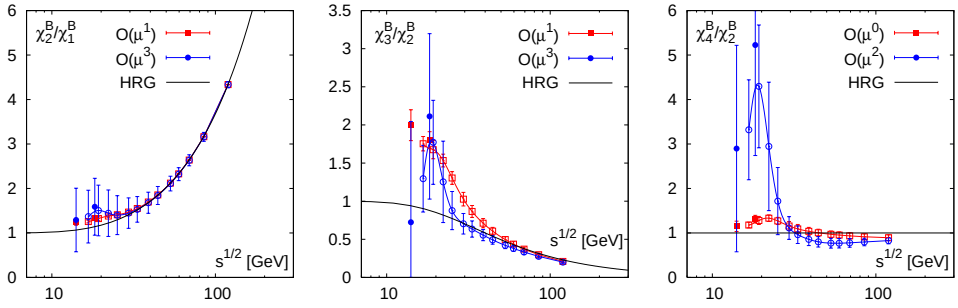

Figure 4.18: Shown are ratios of moments of net-baryon number fluctuations along the freeze-out curve, as a function of the center of mass energy $\sqrt{s_{\rm NN}}$.

Freeze-out curve and crossover line for the QCD transition

Closely related to the calculation of charge fluctuations in lattice QCD is the determination of the phase boundary of the chiral phase transition in the temperature and baryon chemical potential plane. In fact, ratios of moments $\chi_n^{\rm B}/\chi_{n+2}^{\rm B}$ provide estimates for the radius of convergence of the Taylor series of the pressure and may allow to determine a critical point in the QCD phase diagram at physical values of the quark masses [118, 122].

More rigorous results on the transition line at non-zero values of μ_B can be obtained for small $\mu_{\rm B}$ in the chiral limit, where the transition line corresponds to a true second order phase transition. Making use of universal scaling properties of the QCD phase transition in the chiral limit, the phase boundary can be determined to

leading order in the baryon chemical potential,

$$\frac{T_c(\mu_{\rm q})}{T_c} = 1 - \kappa_{\rm q} \left(\frac{\mu_{\rm q}}{T}\right)^2 + \mathcal{O}\left(\left(\frac{\mu_{\rm q}}{T}\right)^4\right) \ , \tag{4.41}$$

from a numerical study of the scaling properties of a mixed susceptibility [121]. Results from such a calculation are shown in Fig. 4.19. They indicate that for small values of the baryon chemical potential the dependence

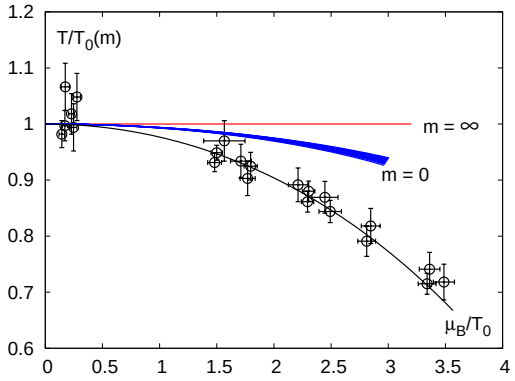

Figure 4.19: Phase boundary for the chiral phase transition in QCD with two massless quarks and a physical strange quark mass. Also shown are data for the freeze-out parameters in heavy ion collisions and the transition line for infinitely heavy quarks (pure gauge theory) which is independent of the chemical potential.

of the chiral phase transition temperature on the baryon chemical potential is rather weak. To what extent this signals that freeze-out occurs at a temperature smaller than the crossover transition in QCD with physical quark masses, still requires further investigations. At larger values of the chemical potential the freeze-out temperatures drop rapidly, which clearly cannot be described by a leading order expansion of $T_c(\mu_{\rm B})$. It has been speculated that this sudden drop may be signal an even richer phase structure of high density QCD [20]. The analysis of higher moments of charge fluctuations will be of great importance in clarifying the structure of the phase diagram in this regime.

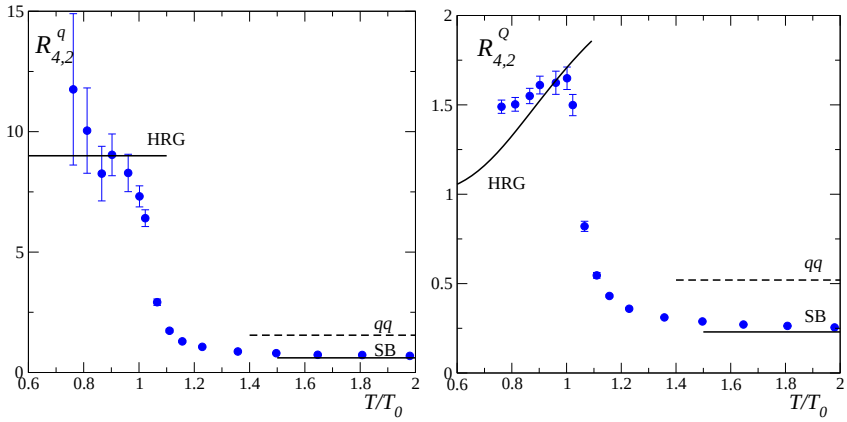

Figure 4.20: The ratio of quartic and quadratic moments of quark number fluctuations (left) [$n_{\rm q} \simeq 3n_{\rm B}$] and electric charge fluctuations (right) as function of temperature evaluated at vanishing baryon chemical potential. Shown in this figure is also an estimate for the high temperature value of these observables, if a significant di-quark component (qq) would contribute to the thermodynamics.

Studies of the phase diagram by NICA

The lattice results presented above and the discussion of the phase diagram in the high temperature, low chemical potential region will eventually form the rigorous background for our understanding of the phase diagram of strongly interacting matter. However, it will not be of direct applicability to the studies of the phase diagram in the energy range accessible at NICA. Experiments at NICA will probe a regime of high baryon number density in which the QCD transition, if at all it is a true phase transition, may well be of first order. In this high density regime direct lattice calculations will be difficult. Nonetheless current lattice results at least tell us that the study of ratios of higher moments of baryon number fluctuations may be of relevance also in this regime. The ratio of e.g. the quartic and quadratic moments of baryon number fluctuations are sensitive to properties of the relevant degrees of freedom that carry the baryonic charge. In Fig. 4.20 we show results from a calculation of ratios of quartic and quadratic moments of quark number and electric charge fluctuations, respectively, performed in a wide temperature range at $\mu_B = 0$ [124]. As one crosses the transition temperature this ratio drops rapidly, indicating the change from baryons ($B = 1$) to quarks ($B = 1/3$) as the dominant degrees of freedom that carry the baryonic charge. If freeze-out at NICA occurs in the mixed phase of a first order transition region one thus may speculate that this will be reflected in a drastic reduction of ratios such as χ_4/χ_2 over conventional values obtained for instance in calculations based on a hadron resonance gas model.

4.11 Exploring hybrid star matter at NICA

T. Klähn[a], D. Blaschke[b,c], F. Weber[d]

[a] *Institute for Theoretical Physics, University of Wrocław, Wrocław, Poland*
[b] *Joint Institute for Nuclear Research, Dubna, Russia*
[c] *Department of Physics, San Diego State University, USA*

Neutron stars (NS) provide valuable insights into the nature of nuclear matter at densities several times beyond nuclear saturation ($n_s \approx 0.16$ fm^{-3}) [125, 126, 127]. In particular any extreme (either small or large) value of measured neutron star observables, such as radius, mass, and temperature, is likely to improve our understanding of the properties of cold and dense matter substantially. A prime example underlining this statement is neutron star PSR J1614-2230, whose recently measured mass of (1.97 ± 0.04) M$_\odot$ makes him the heaviest neutron star ever observed with sufficient accuracy and confidence [128]. This measurement has direct consequences for the investiagtion of dense matter in terrestrial heavy-ion collision (HIC) experiments, as planned for NICA. The reason for this is the close relationship that exists between the stiffness of the equation of state (EoS) of symmetric nuclear matter and the highest NS mass supported by the associated EoS for neutron star matter, as illustrated in Figs. 1 and 2 in [127]. In that paper, a testing scheme, consisting of different constraints from astrophysical observations and HIC experiments, had been introduced and consistently applied to a given set of nuclear EoS. At the time of publication of Ref. [127], the most massive NS known was PSR J0751+1807. Its mass was ~ 2.1 M$_\odot$ but was affected by significant uncertainties. Therefore, a second, less strict mass constraint had been formulated, which demanded that the successful nuclear EoS reproduces at least a maximum neutron star mass of 1.6 M$_\odot$. All the EoS investigated back then passed this constraint. Due to the precision of the new mass measurement for PSR J1614-2230, we now update the overall result of this testing scheme (analogously to Table V in [127]). It is evident from Table 4.1 that only four (five) of the formerly eight nuclear EoS are still compatible with the upper (lower) mass value measured for PSR J1614-2230. An additional model for the nuclear EOS–the hybrid EOS "DBHF-NJL"–has been included in Table 4.1, which has several advantages over the purely hadronic EoS. Details about this EOS will be discussed below.

In summary, the important lesson that we learn from high NS masses, as measured for PSR J1614-2230, is that the EoS has to be 'rather stiff' or, conversely, can 'not be too soft' at ultra-high densities in order to be compatible with neutron star masses. In the following we point out how HIC experiments can contribute to constrain the behavior of the nuclear EoS further and, most importantly, provide most valuable information about the existence of quark matter in compact stars.

We focus here on two topics in HIC experiments which are relevant for determining the stiffness of nuclear matter at supersaturation densities and thus have direct implications for the astrophysics of compact stars: (i) strangeness production (see contribution by V. Friese) and (ii) transverse and elliptical particle flow.

According to the present status of the theory, subthreshold K^+ production at $E_{\rm lab} < 1.58$ AGeV appears to require a sufficiently soft equation of state (see [130] for a review) which is an interesting complement to the astrophysical requirement of sufficiently stiff equations of state demanded by the observations of high-mass

Model	$M_{\rm max} \geq 2.01\ M_\odot$	$M_{\rm max} \geq 1.93\ M_\odot$	$M_{DU} \geq 1.5\ M_\odot$	$M_{DU} \geq 1.35\ M_\odot$	4U 1636-536 (u)	4U 1636-536 (l)	RX J1856 (A)	RX J1856 (B)	J0737 (no loss)	J0737 (loss 1% $M_\odot$)	SIS+AGS flow	SIS flow+ K^+ prod.	No. of passed tests	(out of 6)
NLρ	−	−	−	−	−	−	−	−	−	−	+	+	1	1
NL$\rho\delta$	−	−	−	−	−	−	−	−	−	−	+	+	1	1
DBHF	+	+	−	−	+	+	−	+	−	+	−	+	2	5
DD	+	+	+	+	+	+	−	+	−	−	−	−	3	4
D^{3}C	+	+	+	+	+	+	−	+	−	−	−	−	3	4
KVR	−	−	+	+	−	∘	−	−	−	+	+	+	2	4
KVOR	+	+	+	+	−	+	−	−	−	∘	+	+	3	5
DD-F	−	+	+	+	−	+	−	−	−	+	+	+	2	5
DBHF+NJL	+	+	*	*	+	+	−	+	−	+	+	+	4	6

Table 4.1: Summary of results for the testing scheme suggested in [127], updated by the recently measured mass of PSR J1614-2230 ((1.97 ± 0.04) $M_\odot$) and supplemented by the hybrid EoS of Ref. [129] (last line), for which results are shown in Fig. 1. EoS not labeled in bold face fail to reproduce a NS mass of 2.01 $M_\odot$. Non-separated columns show the results for a strict (left) and weakened (right) interpretation of the corresponding constraint. The last column gives the total number of tests passed by a given EOS. (For details, see [127].)

neutron stars (see discussion above).

The analysis of flow data for experiments at different energies ($E_{\rm lab} = 0.4$ to 10 AGeV in Ref. [131]) put a constraint on the cold symmetric nuclear EoS, which represents a region in the nuclear pressure-density plane, $P(n)$, shown in Fig. 4.21.

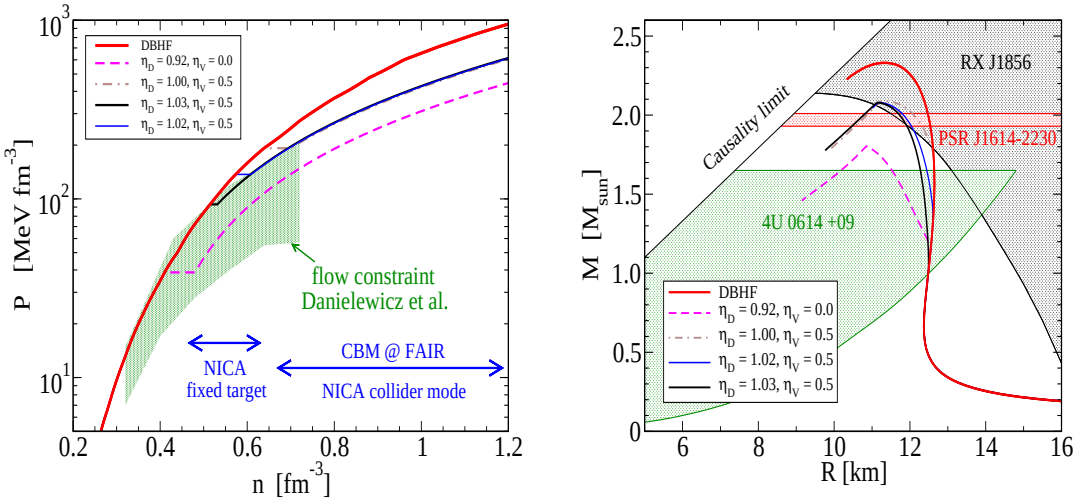

Figure 4.21: Left panel: Flow constraint [131] extracted from HIC experiments in the range $E_{\rm lab} = 0.4$ to 10 AGeV and estimated regions accessible at CBM and NICA experiments [132, 133]. Right panel: Sequences of compact star M-R relations obtained from solution of the Tolman-Oppenheimer-Volkoff [125, 126] equation for different EoS without (DBHF) and with deconfinement transition, as compared to NS constraints.

This constraint is readily applied to the isospin-symmetric part of any neutron star EoS and can therefore be used to derive upper bounds on the maximum mass of compact stars [127], as can be seen by comparing the left and right panels of Fig. 4.21.

From these far-reaching consequences of the latter constraint it is evident that an independent confirmation of this flow constraint is very important, both from the theroretical side as well as by providing sufficiently accurate flow data in the region of $E_{\rm lab} = 2$ to 5 AGeV (Nuclotron fixed-target range), where we suspect the deconfinement phase transition to occur, and just above the limits of the AGS data range, i.e. for $E_{\rm lab} = 10$ to 40 AGeV (CBM range or fixed-target equivalent of the NICA collider range).

According to the flow constraint, the *ab-initio* DBHF EoS for the Bonn-A nucleon-nucleon potential appears to be too stiff at densities above 3.5 times saturation density. Assuming the deconfinement phase transition to provide the softening of the high-density EoS just in this density range at the maximally tolerable stiffness of the Danielewicz et al. constraint would result in an upper limit for the maximum mass of compact stars at 2.1 $M_\odot$. This would be also compatible with the new mass constraint from PSR J1614-2230.

The quark matter EoS used here is the three-flavor color superconducting NJL model one with selfconsistently determined masses and diquark gaps [134] including a vector meson meanfield which entails a sufficient stiffening of the hybrid EoS [129] (a nonlocal, covariant generalization has been provided in Ref. [136]). Neglecting the latter term would result in too soft a hybrid EoS, conflicting with the new neutron star mass constraint (dashed lines in Fig 4.21. Moreover, if the diquark pairing interaction would be sufficiently reduced or even be neglected altogether so that no color superconducting phase can occur, the phase transition would occur at too high densities to be relevant for compact star structure.

Due to isospin asymmetry, in compact stars the deconfinement transition always occurs at lower baryon densities than in symmetric nuclear matter. There is another, indirect argument to expect a deconfinement phase transition in symmetric matter at densities not exceeding about 3 to 4 nuclear saturation densities. This relatively low critical density would correspond to a deconfinement transition in neutron star matter at low enough densities to avoid hyperon formation. In this way the problem could be eliminated that compact stars with hyperons in their interiors would have a too soft EoS to fulfill even much weaker maximum mass constraints than the new one, see Ref. [135].

In conclusion, the question of whether or not quark matter exists in compact stars is very challenging [137] and closely related to the question of deconfinement in heavy-ion collisions at the CBM [138, 139] and NICA facilities [133]. As we don't know a priori the coupling strengths in various interaction channels at high densities, it is important to verify the conjectured EoS in a heavy-ion collision experiment. The energies provided at the NICA facility (both, fixed target and collider) are perfectly suited for providing astrophysically relevant constraints such as to confirm or disprove the possibility that all neutron stars in the observed mass range between 1.23 and 2.01 $M_\odot$ are hybrid stars with color superconducting quark matter cores!

4.12 Testing Hadron Formation and Exotic Bound States in Heavy Ion Collisions at NICA

R. Bellwied[a], *C. Markert*[b]

[a] *Physics Department, University of Houston, USA*
[b] *Physics Department, University of Texas at Austin, USA*

Physics Motivation

The concept of formation time of hadrons in the chirally symmetric deconfined medium produced at RHIC and the LHC has been addressed by the authors in two recent publications [140, 141]. We have conjectured that the hadronization process through parton fragmentation in the deconfined medium is following the same time constraints than in the vacuum, since the hard parton does not thermalize with the system. A calculation based on light cone variables which takes into account not only the Lorentz-boost (inside-outside cascade), but also energy conservation in the medium (outside-inside cascade) shows that there is a finite probability that color-neutral pre-hadrons or bound states can form inside the medium, i.e. above the critical temperature and prior to bulk hadronization. These configurations carry all the necessary quantum numbers, but have not yet developed their full hadron wave function. Two dynamic hadronization scenarios are thus possible. Either these pre-hadron states are very massive (color-neutral resonance clusters or quasi-particles) and subsequently decay into hadronic ground states, or the resonant states of the ground states are formed off mass shell before gaining the necessary on-shell mass. In the second scenario the resonant state might decay with its chiral symmetry still partially restored.

In addition, at NICA, where the energy is lower than at RHIC but the particle density is considerably higher, it is conceivable that these bound states above the critical temperature are surviving states from the hadronic

phase since confined, but chirally symmetric, hadronic states (quarkyonic matter) were proposed recently as a new phase of matter at high baryo-chemical potential [15]. So rather than being formed through recombination of partons in deconfined matter these states survive the phase transition, i.e. they stay confined but their chiral symmetry is restored.

Based on either scenario we propose to actively search for color-neutral bound states around the phase transition in systems with high baryochemical potential but moderate critical temperature.

Model details

In momentum space, expressed through lightcone coordinates, the fragmentation of a parton of mass m_q into a hadron of mass m_h and a light secondary parton is represented through the lightcone $\Delta y^+ = \tau_{\rm form} + l_{\rm form}$ that is conjugate to the non-conserved lightcone momentum component $\Delta p^- = (p^-)_{\rm final} - (p^-)_{\rm initial}$ of the evolving system [141]:

$$\Delta y^+ \simeq \frac{1}{\Delta p^-} = \frac{z p^+}{m_h} \times 2 \left[m_h + \frac{\mathbf{k}^2}{(1-z)m_h} - \frac{z m_q^2}{m_h} \right]^{-1} \tag{4.42}$$

Here $|\mathbf{k}| \sim \Lambda_{\rm QCD} \sim 200\,{\rm MeV}/c$ is the deviation from collinearity and z is the fractional momentum $p^+_{\rm hadron}/p^+$. After further derivation the formation time reads:

$$\tau_{\rm form} = \frac{\Delta y^+}{1+\beta_q}\,, \quad \beta_q = \frac{p_{\rm q}}{E_{\rm q}}\,. \tag{4.43}$$

When compared to the lifetime of the QGP at the LHC we observe that for a wide range of momenta, hadron formation times are well within the anticipated lifetime of the plasma as shown in Fig. 4.22.

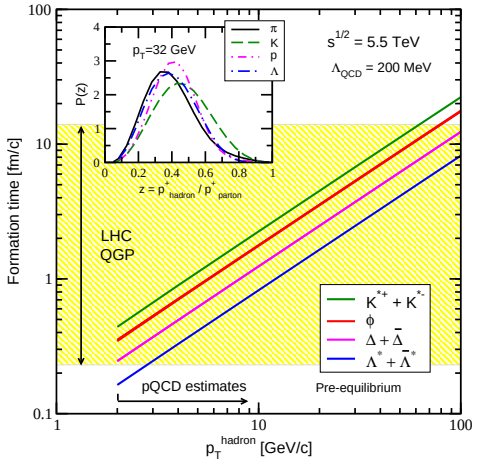

Figure 4.22: Transverse momentum dependence of resonance formation times at LHC energies. The shaded area represents the estimated QGP lifetime at the LHC. Insert shows the meson and baryon distributions P(z) at a fixed momentum (from [141]).

This will not necessarily be the case for NICA energies, where the lifetime of any plasma state is considerably smaller than at the LHC, but since it is anticipated that at least part of the system might contain chirally symmetric (quarkyonic) matter, the off-shell component of the color neutral states should be large, even if the lifetime of the system is small. In that case the argument does not need to be made on the basis of formation time of hadrons from deconfined partons, but rather on the survival probability of confined hadronic states in the chirally symmetric phase. One of the signatures of such a phase should be the measurement of chiral partners with similar or equal mass. Calculations of a common mass for the lowest lying chiral doublet beyond a first order phase transition have been performed in the framework of the PJNL model [142]. Fig. 4.23 shows the

predictions for the pion (π) and sigma (σ) masses above the chiral transition temperature for a baryochemical potential of 340 MeV.

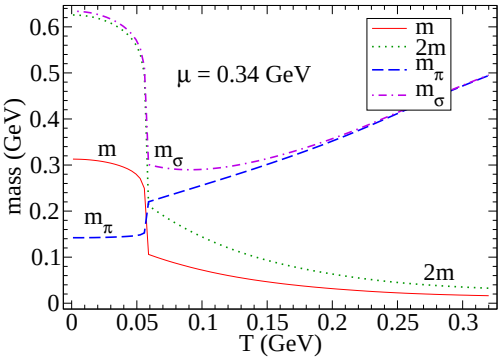

Figure 4.23: Masses of the π and σ as function of the temperature, together with the Hartree quark masses, in the PJNL model at $\mu = 0.34$ GeV. The chiral transition occurs at $T_c = 0.06$ GeV (from [142]).

The resulting chiral partner mass is around 250 MeV, with a remaining slight split between the states due to the finite current mass of the quarks, which explicitly breaks chiral symmetry. A mass peak at 250 MeV should be easily distinguishable from the π or σ on-shell masses.

Proposed measurements

The proposal is too look for the production of color-neutral bound states slightly above T_c in the region of high density. These bound states will be resonant states either above (quasi-particle clusters) or below (chirally symmetric color-neutral states) the known resonance spectrum. They exist either through formation in the deconfined phase or through survival in the confined phase above T_c. The aim is to prevent these states from undergoing medium modifications in the dense hadronic phase after hadronization of the bulk matter, and thus the most proficient way to search for such states is in the di-lepton spectrum. The mass region above the ϕ-meson but below the J/ψ, i.e. the continuum region, as well as the low mass di-lepton region below the ρ and above the π mass, are perfectly suited for such measurements. Beyond the occurrence of any distinct peaks in these regions, any reduction in relative strength or broadening of the pion peak compared to an unmodified cocktail calculation should also provide indications of chiral symmetry restoration for the case of the π,σ chiral doublet.

A dilepton spectrometer (e.g. a gas or silicon based tracking device combined with a time of flight detector) with 2π coverage in NICA collider mode is most appropriate for such measurements. The alternative would be to look for hadronic decay channels of high momentum chiral partners [2] in order to avoid effects due to hadronic re-interactions in the bulk medium, but the luminosity, and thus the sampled statistics of high momentum particles, might not be sufficient at NICA energies.

Bibliography

[1] I. Melo et al., arXiv:0902.1607.

[2] M. A. Stephanov, Prog. Theor. Phys. Suppl. **153**, 139 (2004); Int. J. Mod. Phys. **A 20,** 4385 (2005).

[3] Y. Hatta and T. Ikeda, Phys. Rev. **D 67,** 014028 (2003).

[4] K. Fukushima, Phys. Rev. **C 67,** 025203 (2003).

[5] P. Costa, M.C. Ruivo and Yu.L. Kalinovsky, Phys. Lett. **B 560,** 171 (2003).

[6] P. Costa, M.C. Ruivo, Yu.L. Kalinovsky and C.A. de Sousa, Phys. Rev. **C 70,** 025204 (2004);

[7] P. Costa, M.C. Ruivo, C.A. de Sousa and Yu.L. Kalinovsky, Phys. Rev. **D 70,** 116013 (2004);

[8] P. Costa, M.C. Ruivo, C.A. de Sousa and Yu.L. Kalinovsky, Phys. Rev. **D 71,** 116002 (2005).

[9] P. Costa, M.C. Ruivo, C.A. de Sousa and H. Hansen, Europhysics Letters **86**, 31001 (2009), [arXiv:0801.3616].

[10] E. Beth and G. E. Uhlenbeck, Physica **4**, 915 (1937).

[11] R. Dashen, S.-K. Ma and H. J. Bernstein, Phys. Rev. **187,** 345 (1969).

[12] R. Hagedorn, Nuovo Cim. Suppl. **3**, 147 (1965); Nuovo Cim. **56A**, 1027 (1968).

[13] P. Braun-Munzinger, K. Redlich and J. Stachel; Eds. R. C. Hwa and X.-N Wang *in Quark-Gluon Plasma 3*, (World Scientific, Singapore 2003).

[14] P. Castorina, K. Redlich and H. Satz, Eur. Phys. J. **C 59,** 67 (2009).

[15] L. McLerran and R. D. Pisarski, Nucl. Phys. **A 796,** 83 (2007), [arXiv:0706.2191].

[16] D. Rischke, G. Levin, eds, *Quark Gluon Plasma. New Discoveries at RHIC: A Case of Strongly Interacting Quark Gluon Plasma. Proceedings, RBRC Workshop, Brookhaven*, (Upton, USA, May 14-15, 2004), 2005, p. 169.

[17] J. Adams *et al.* (STAR Collaboration) Nucl. Phys. **A 757,** 102 (2005).

[18] K. Adcox *et al.* (PHENIX Collaboration), Nucl. Phys. **A 757,** 184 (2005).

[19] D. d'Enterria, [arXiv: nucl-ex/0611012].

[20] J.-Y. Ollitrault, Phys. Rev. **D 46,** 229 (1992); S.A. Voloshin, Nucl. Phys. **A 715,** 379 (2003).

[21] D. Molnar, [arXiv: nucl-th/0408044].

[22] S. M. Troshin, N. E. Tyurin, Phys. Rev. **D 49,** 4427 (1994).

[23] S. M. Troshin, N. E. Tyurin, J. Phys. G. **29,** 1061 (2003).

[24] J. D. Bjorken, Nucl. Phys. Proc. Supl. **B 25**, 253 (1992).

[25] D. Diakonov, [arXiv: hep-ph/0406043], JLAB-THY-04-12, Eur. Phys. J. **A 24,** 3 (2005);
D. Diakonov, V. Petrov, Phys. Lett. **B 147,** 351 (1984).

[26] T. Goldman, R. W. Haymaker, Phys. Rev. **D 24,** 724 (1981).

[27] W. Heisenberg, Z. Phys. **133**, 65 (1952).

[28] P. Carruthers, Nucl. Phys. **A 418,** 501 (1984).

[29] L. L. Jenkovszky, S. M. Troshin, N. E. Tyurin, [arXiv:0910.0796].

[30] A. A. Logunov, V. I. Savrin, N. E. Tyurin, O. A. Khrustalev, Teor. Mat. Fiz. 6, 157 (1971).

[31] S.M. Troshin, N.E. Tyurin, Int. J. Mod. Phys. **A 22,** 4437 (2007).

[32] S.A. Voloshin, [arXiv: nucl-th/0410089].

[33] S. A. Voloshin, A. M. Poskanzer, Phys. Lett. **B 474,** 27 (2000).

[34] T. T. Chou, C.-N. Yang, Int. J. Mod. Phys. **A 6,** 1727 (1987); Adv. Ser. Direct. High Energy Phys. 2, 510 (1988).

[35] T. T. Chou, C. N. Yang, Phys. Lett. **B 128,** 457 (1983); Phys. Rev. **D 32,** 1692 (1985).

[36] F. Antinori; Eds. A. Sissakian, G. Kozlov, E. Kolganova *Proc. of the XXXII International Symposium on Multiparticle Dynamics*, (Alushta, Crimea, Ukraine, September 2002), 77.

[37] W. Broniowski, W. Florkowski, Phys. Rev. **C 65,** 024905 (2002).

[38] J. Castillo (STAR Collaboration), Int. J. Mod. Phys. **A 20,** 4380 (2005).

[39] J. Zimányi, P. Lévai, T. S. Biró, *Heavy Ion Phys.* 17, 205 (2003); J. Phys. G. **31,** 711 (2005).

[40] G. Wang (STAR Collaboration), J. Phys. G. **34,** 1093 (2007), [arXiv: nucl-ex/0701045].

[41] B.B. Back et al., (PHOBOS Collaboration), Phys. Rev. Lett. **97,** 012301 (2006).

[42] A.H. Tang (STAR collaboration), J. Phys. G. **31,** S35 (2005).

[43] J. Adams *et al.*, (STAR Collaboration), Phys. Rev. **C 73,** 034903 (2006).

[44] V. S. Pantuev, [arXiv:hep-ph/0604268].

[45] S. Abreu *et al.*, [arXiv:0711.0974].

[46] A.N. Sissakian *et al.*, (NICA Collaboration),J. Phys. G. **36,** 064069 (2009).

[47] T. Hatsuda, J. Phys. G. **34,** S287 (2007)

[48] M. A. Stephanov, PoS **LAT2006**, 024 (2006).

[49] B. Berdnikov and K. Rajagopal, Phys. Rev. **D 61,** 105017 (2000)

[50] C. Nonaka and M. Asakawa, Phys. Rev. **C 71,** 044904 (2005)

[51] T. Hatsuda and T. Kunihiro, Phys. Rep. **247,** 221 (1994)

[52] T. Kunihiro, Phys. Lett. **B 271,** 395 (1991)

[53] M. Asakawa and K. Yazaki, Nucl. Phys. **A 504,** 668 (1989)

[54] L. Ahle *et al.* (E802 Collaboration), Phys. Rev. **C 60,** 064901 (1999).

[55] J. Barrette *et al.* (E877 Collaboration), Phys. Rev. **C 62,** 024901 (2000).

[56] B. B. Back *et al.*, (E917 Collaboration), Phys. Rev. Lett. **86,** 1970 (2001).

[57] J. Stachel, Nucl. Phys. **A 654,** 119 (1999).

[58] H. Appelshäuser *et al.* (NA49 Collaboration), Phys. Rev. Lett. **82,** 2471 (1999).

[59] T. Anticic *et al.* (NA49 Collaboration), Phys. Rev. **C 69,** 024902 (2004).

[60] C. Alt *et al.* (NA49 Collaboration), Phys. Rev. **C 73,** 044910 (2006).

[61] C. Blume (NA49 Collaboration), J. Phys. G. **34,** S951 (2007).

[62] H. Strobele (NA49 Collaboration), [arXiv:0908.2777 [nucl-ex]].

[63] Yu.B. Ivanov, V.N. Russkikh, and V.D. Toneev, Phys. Rev. C **73**, 044904 (2006).

[64] Yu.B. Ivanov and V.N. Russkikh, PoS(CPOD07)008 (2007), [arXiv:0710.3708 [nucl-th]].

[65] V.M. Galitsky and I.N. Mishustin, Sov. J. Nucl. Phys. **29**, 181 (1979).

[66] A.S.Khvorostukhin, V.V.Skokov, K.Redlich, and V.D.Toneev, Eur. Phys. J. **C 48,** 531 (2006).

[67] C. Alt *et al.* (NA49 Collaboration), Phys. Rev. **C 77,** 024903 (2008).

[68] C. Alt *et al.* (NA49 Collaboration), Phys. Rev. **C 68,** 034903 (2003).

[69] I.C. Arsene, *et al.*, Phys. Rev. **C 75,** 034902 (2007).

[70] M. Gazdzicki and M. I. Gorenstein, Acta. Phys. Polon. **B 30,** 2705 (1999), [arXiv:hep-ph/9803462].

[71] Yu.B. Ivanov, [arXiv:1001.0670 [nucl-th]], to be published in Phys. Lett. B.

[72] M. A. Stephanov, K. Rajagopal and E. V. Shuryak, Phys. Rev. Lett. **81,** 4816 (1998), [arXiv:hep-ph/9806219].

[73] I. N. Mishustin, [arXiv:hep-ph/0512366].

[74] A. Andronic *et al.*, Nucl. Phys. **A 837,** 65 (2010), [arXiv:0911.4806 [hep-ph]].

[75] D. B. Blaschke, F. Sandin, V. V. Skokov and S. Typel, Acta Phys. Polon. Supp. **3**, 741 (2010), [arXiv:1004.4375 [hep-ph]].

[76] E. Fermi, Prog. Theor. Phys. **5**, 570 (1950).

[77] I. Pomeranchuk Proc. USSR Academy of Sciences (in Russian) **43**, 889 (1951).

[78] L. D Landau, Izv. Akad. Nauk Ser. Fiz. **17** 51-64 (1953).

[79] R. Hagedorn Suppl. Nuovo Cimento **2**, 147 (1965).

[80] P. Braun-Munzinger, D. Magestro, K. Redlich and J. Stachel, Phys. Lett. **B 518,** 41 (2001)

[81] J. Cleymans, H. Oeschler, K. Redlich and S. Wheaton, [arXiv:hep-ph/0607164].

[82] J. Letessier, J. Rafelski (2002), *Hadrons quark - gluon plasma, Cambridge Monogr.*, Part. Phys. Nucl. Phys. Cosmol. **18**, 1, and references therein

[83] F. Becattini, P. Castorina, A. Milov and H. Satz, Eur. Phys. J. **C 66,** 377 (2010), [arXiv:0911.3026 [hep-ph]].

[84] J. Cleymans, B. Kampfer, M. Kaneta, S. Wheaton and N. Xu, Phys. Rev. **C 71,** 054901 (2005)

[85] G. Torrieri, S. Steinke, W. Broniowski, W. Florkowski, J. Letessier Comput. Phys. Commun. **167**, 229 (2005), [arXiv:nucl-th/0404083].

[86] G. Torrieri, S. Jeon, J. Letessier and J. Rafelski, Comput. Phys. Commun. **175**, 635 (2006), [arXiv:nucl-th/0603026].

[87] K. Redlich, A. Andronic, F. Beutler, P. Braun-Munzinger and J. Stachel, J. Phys. G. **36,** 064021 (2009), [arXiv:0903.1610 [hep-ph]].

[88] G. Torrieri, R. Bellwied, C. Markert and G. Westfall, [arXiv:1001.0087 [nucl-th]].

[89] V. Koch and T. Schuster, [arXiv:0911.1160 [nucl-th]].

[90] I. Arsene *et al.* (BRAHMS Collaboration), Nucl. Phys. **A 757,** 1 (2005)

[91] B. B. Back *et al.*, Nucl. Phys. **A 757,** 28 (2005)

[92] M. Gyulassy and L. McLerran, Nucl. Phys. **A 750,** 30 (2005), [arXiv:nucl-th/0405013].

[93] E. Shuryak, Progr. Part. Nucl. Phys. **53,**273 (2004), [arXiv:hep-ph/0312227].

[94] P. F. Kolb and U. W. Heinz, [arXiv:nucl-th/0305084].

[95] U. W. Heinz and P. F. Kolb, Nucl. Phys. **A 702,** 269 (2002).

[96] D. Teaney, J. Lauret and E. V. Shuryak, [arXiv:nucl-th/0110037].

[97] P. Romatschke and U. Romatschke, Phys. Rev. Lett. **99,** 172301 (2007).

[98] P. F. Kolb, U. W. Heinz, P. Huovinen, K. J. Eskola and K. Tuominen, Nucl. Phys. **A 696,** 197 (2001), [arXiv:hep-ph/0103234].

[99] W. Broniowski, M. Chojnacki, W. Florkowski and A. Kisiel, [arXiv:0801.4361 [nucl-th]].

[100] T. Hirano and K. Tsuda,Nucl. Phys. **A 715,** 821 (2003)

[101] J. Randrup and S. Mrowczynski, Phys. Rev. **C 68,** 034909 (2003), [arXiv:nucl-th/0303021].

[102] O. Fochler, Z. Xu and C. Greiner, Phys. Rev. Lett. **102,** 202301 (2009) [arXiv:0806.1169 [hep-ph]].

[103] J. Noronha-Hostler, J. Noronha and C. Greiner, Phys. Rev. Lett. **103,** 172302 (2009), [arXiv:0811.1571 [nucl-th]].

[104] W. Busza (PHOBOS Collaboration), [arXiv:0907.4719 [nucl-ex]].

[105] G. Torrieri, [arXiv:0911.4775 [nucl-th]].

[106] H. Song and U. W. Heinz, Phys. Rev. **C 78,** 024902 (2008), [arXiv:0805.1756 [nucl-th]].

[107] G. Torrieri, Phys. Rev. **C 76,** 024903 (2007), [arXiv:nucl-th/0702013].

[108] L. Van Hove, Phys. Lett. **B 118,** 138 (1982).

[109] P. Seyboth *et al.* (NA49 Collaboration), Acta. Phys. Polon. **B 36,** 565 (2005).

[110] M. Lisa, AIP Conf. Proc. **828**, 226 (2006), [arXiv:nucl-ex/0512008].

[111] J. Randrup and J.Cleymans, Phys. Rev. **C 74,** 047901 (2006)

[112] H-Th. Elze, J. Rafelski and L. Turko, Phys. Lett. **B 506,** 123 (2001)

[113] L. Turko, J. Phys. G. **35,** 044019 (2008)

[114] S. Gupta, PoS(Lattice 2010) 007, [arXiv:1101.0109 [hep-lat]].

[115] M. Cheng *et al.*, Phys. Rev. **D 79,** 074505 (2009), [arXiv:0811.1006 [hep-lat]].

[116] A. Andronic, P. Braun-Munzinger, K. Redlich and J. Stachel, Phys. Lett. **B 571,** 36 (2003), [arXiv:nucl-th/0303036].

[117] R. V. Gavai and S. Gupta, [arXiv:1001.3796 [hep-lat]].

[118] C. Schmidt, Net-baryon number fluctuations in (2+1)-flavor QCD, arXiv:1007.5164 [hep-lat].

[119] F. Karsch and K. Redlich, Phys. Lett. **B 695,** 136 (2011), [arXiv:1007.2581 [hep-ph]].

[120] M. M. Aggarwal *et al.* (STAR Collaboration), Phys. Rev. Lett. **105,** 022302 (2010), [arXiv:1004.4959 [nucl-ex]].

[121] O. Kaczmarek *et al.*, Phys. Rev. **D 83,** 014504 (2011), [arXiv:1011.3130 [hep-lat]].

[122] R. V. Gavai and S. Gupta, Phys. Rev. **D 78,** 114503 (2008), [arXiv:0806.2233 [hep-lat]].

[123] A. Andronic, D. Blaschke, P. Braun-Munzinger *et al.*, Nucl. Phys. **A 837,** 65-86 (2010), [arXiv:0911.4806 [hep-ph]].

[124] C. R. Allton, M. Doring, S. Ejiri *et al.*, Phys. Rev. **D 71,** 054508 (2005), [hep-lat/0501030].

[125] F. Weber, *Pulsars as astrophysical laboratories for nuclear and particle physics*, (IOP Publishing, Bristol, 1999).

[126] N. K. Glendenning, *Compact Stars*, (Springer, New York, 2000).

[127] T. Klähn *et al.*, Phys. Rev. **C 74,** 035802 (2006), [arXiv:nucl-th/0602038].

[128] P. Demorest, T. Pennucci, S. Ransom, M. Roberts and J. Hessels, Nature **467**, 1081 (2010), [arXiv:1010.5788 [astro-ph.HE]].

[129] T. Klähn *et al.*, Phys. Lett. **B 654,** 170 (2007) [arXiv:nucl-th/0609067].

[130] C. Fuchs, Progr. Part. Nucl. Phys. **56,**1 (2006).

[131] P. Danielewicz, R. Lacey and W. G. Lynch, Science **298**, 1592 (2002), [arXiv:nucl-th/0208016].

[132] I. C. Arsene *et al.*, Phys. Rev. **C 75,** 034902 (2007), [arXiv:nucl-th/0609042].

[133] D. B. Blaschke, F. Sandin, V. V. Skokov and S. Typel, Acta Phys. Polon. Supp. **3**, 741 (2010) [arXiv:1004.4375 [hep-ph]].

[134] D. Blaschke, S. Fredriksson, H. Grigorian, A. M. Öztas and F. Sandin, Phys. Rev. **D 72,** 065020 (2005), [arXiv:hep-ph/0503194].

[135] M. Baldo, G. F. Burgio and H. J. Schulze,]arXiv:astro-ph/0312446].

[136] D. B. Blaschke, D. Gomez Dumm, A. G. Grunfeld, T. Klähn and N. N. Scoccola, Phys. Rev. **C 75,** 065804 (2007) [arXiv:nucl-th/0703088].

[137] M. Alford, D. Blaschke, A. Drago, T. Klähn, G. Pagliara and J. Schaffner-Bielich, Nature **445**, E7 (2007), [arXiv:astro-ph/0606524].

[138] D. Blaschke, T. Klähn and F. Weber, "Constraints on the High-Density Nuclear Equation of State from Neutron Star Observables," in: *Astronomy and Relativistic Astrophysics – New Phenomena and New States of Matter in the Universe*, (Word Scientific, 2010), p. 31, [arXiv:0808.1279 [astro-ph]].

[139] D. Blaschke, T. Klähn and F. Weber, "Compact star constraints on the high-density equation of state," in: *Strongly Interacting Matter - The CBM Physics Book*, Lecture Notes in Physics **814**, (Springer, 2011), p. 158.

[140] R. Bellwied, C. Markert, Phys. Lett. **B 691,** 208 (2010).

[141] C. Markert, R. Bellwied, I. Vitev, Phys. Lett. **B 669,** 92 (2008).

[142] H. Hansen *et al.*, Phys. Rev. **D 75,** 065004 (2007).

5 Femtoscopy, correlations and fluctuations

Femtoscopy, HBT correlations and event-by-event fluctuations reveal important information about the space-time history of the hot deconfined matter, and can help to understand the nature of the phase transition at high baryon density. Indeed, if the phase transition is of the first order, it should reveal itself through a number of observables discussed in this section, in particular, through the transverse momentum asymmetry of identified hadrons. Event-by-event fluctuations are also expected to provide a signature of the chiral critical point addressed in the previous section.

5.1 Femtoscopic search for the 1-st order phase transition

R. Lednicky

Joint Institute for Nuclear Research, Dubna

Since the pioneering papers of Kopylov and Podgoretsky, it is well-known that the width of the two-particle correlation function in the out-direction (parallel to the pair transverse velocity) is sensitive to the duration of particle emission (see, e.g., [1, 2, 3]). In the case when the hot and dense system created in the collision process passes through the quark-gluon (partonic) phase back to the hadronic phase according to the 1-st order phase transition, the latent heat and the related soft equation of state is expected to substantially increase the emission duration [4, 5, 6]. The corresponding increase of the out Gaussian radius of the two-pion correlation function or, the increase of the ratio of the out and side radii, has not been however observed experimentally. Instead, the measured out and side radii appear to be nearly equal and almost constant in a wide energy range from AGS, SPS up to the highest RHIC energies.

Assuming the scenario with the first order phase transition taking place somewhere in the AGS-SPS energy region, one can explain the lack of the signal of increased emission duration in the measured Gaussian radii by the two following reasons (besides the effects of flows and resonance decays - both decreasing the ratio of the out to side radii - underestimated or neglected in the original calculations within ideal hydrodynamics):

- according to the Parton-Hadron-String-Dynamics transport calculations, a dramatic decrease of the partonic phase with the decreasing energy is expected, the most of the energy being carried out by the large hadronic corona; particularly, the maximal partonic energy fraction during the evolution of the system created in the central Pb+Pb collisions at $E_{\rm lab}$ =20 and 158 AGeV is estimated on the level of $\sim 10\%$ and $\sim 40\%$, respectively [7];
- in the presence of two or more essentially different characteristic radii (time scales), the single-(3D)Gaussian fit of the correlation function is dominated by the smaller scales even if the contribution of the larger ones is of comparable size (the large space-time separations of the particle emitters leading mainly to a decrease of the correlation strength parameter lambda) [8].

The femtoscopic search for the first order phase transition thus requires sufficiently high statistics allowing one to perform the multiparametric 2D-(3D-)Gaussian or Hamp function fits of the multidimensional correlation functions (with up to 8 parameters taking into account two sets of the three radii and the corresponding fractions) or, to apply the imaging techniques, for a systematic study of the energy dependence of the contribution of different space-time scales. The multidimensional analysis is important to disentangle e.g. the effect of resonances (contributing to non-Gaussian tails in all directions) from the emission duration effect (absent in the side direction).

The first attempts of such an analysis have been done for two-pion correlation functions measured in central heavy ion collisions at the top SPS and RHIC energies [9, 10]. The non-Gaussian tails observed in the out and side directions can be mainly explained by resonance decays while the one in the longitudinal direction is nearly consistent with the Bjorken longitudinal flow. At the same time, the finite exponential emission duration of 2 fm/c and 4 fm/c (corresponding to the 1.4 times larger r.m.s. width of the exponential distribution of the proper lifetime, i.e. - to the 1.4 times larger r.m.s. width of the original Blast Wave Gausssian distribution characterized by the same duration parameters) is required to fully describe the non-Gaussian tails in the out and longitudinal directions found in the RHIC and SPS data, respectively.

A similar analysis of the lower energy heavy ion data on correlation functions of various particle species already available and planned to be measured in future experiments is obviously called for. The analysis of

correlation functions of various particle species (including nonidentical particles) is important to better control the contribution of the non-lifetime effects (resonance decays, flows, rescatterings etc.) to the non-Gaussian tails. The simultaneous search for other signals of the first order phase transition or the critical point (e.g., the decrease of transverse flow or increased fluctuations) is required having in mind a tiny size of the expected effects. Such a detailed and complex study will require high statistics and precise data with a good particle identification which will hopefully be provided by the future dedicated NICA and FAIR facilities.

5.2 Brief arguments for studying azimuthally sensitive HBT

M. Lisa

Ohio State University, USA

It is well known that collective flow carries important and characteristic information about the bulk sector - i.e. the non-perturbative sector - of a heavy-ion collision. Transport calculations (e.g. Kolb and Heinz) repeatedly predict telltale signatures of flow observables as a function energy density, if a threshold from confined to deconfined matter is crossed. Beyond the existence of threshold, detailed excitation functions should reveal

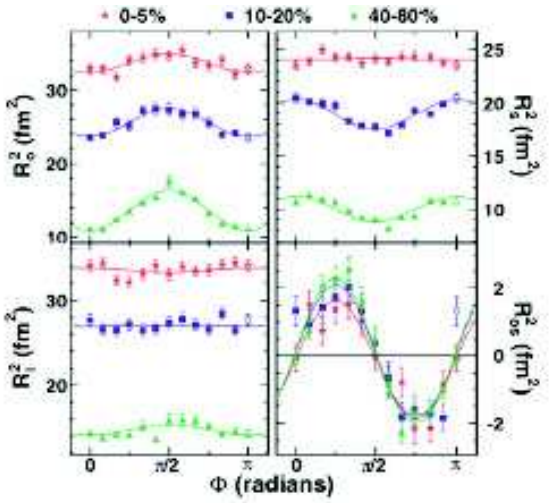

Figure 5.1: HBT radii relative to the 2nd-order event plane in Au + Au collisions at $\sqrt{s_{\rm NN}}$ =200 GeV [14].

important thermodynamic quantities, like any quasi-latent heat or the speed of sound associated with the transition. Common measures of flow include $p_{\rm T}$ spectra (radial flow), and momentum anisotropy (directed and elliptic flow).

But momentum-only observables tell only half of the story of collective flow. The bulk response of the system has a non-trivial structure in both space and time and femtoscopic studies are required to extract this information [21]. Just the $p_{\rm T}$ dependence of azimuthally-integrated HBT radii gives access to the geometric substructure generated by *radial* flow (e.g. [12]), HBT measured relative to the first- and second-order event plane are the spatial analogs of directed and elliptic flow [12, 13], respectively, and contain important information not accessible in momentum space alone. As explained below, these measurements can be sensitive to a "softening" in the equation of state, related to a first-order phase transition, or even rapid crossover.

STAR has measured oscillation of pion HBT radii relative to the second-order event plane (Fig. 5.1) [14]. In addition to the overall size of the source, these reveal the transverse *shape*, which is found to be extended out of the reaction plane at freezeout (the stage probed by HBT). It is, however, less anisotropic (equivalently, more round) than the initial source defined by the overlap of the colliding nuclei at finite impact parameter, reflecting the evolution over time in preferential in-plane expansion.

The anisotropy has been measured at a few lower energies, as well. Since the lifetime of the system and elliptic flow increase with energy, one naively expect that, for a fixed initial anisotropy, the freezeout anisotropy becomes less and less out-of-plane extended and may even become in-plane extended (as predicted [15] for example at

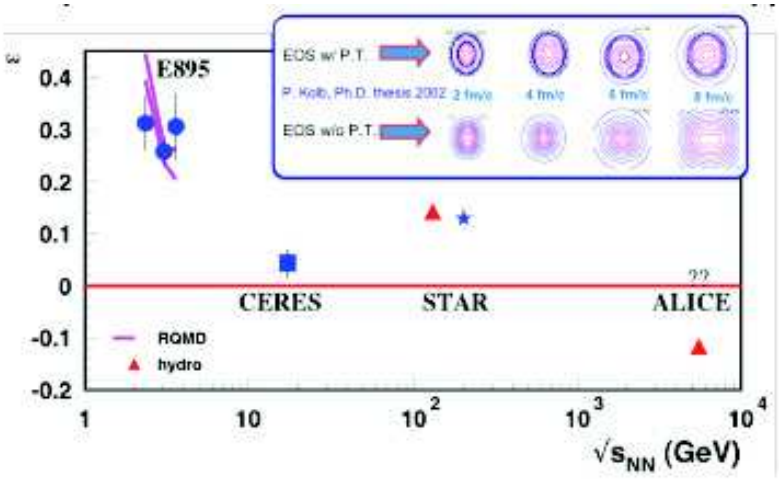

Figure 5.2: Freezeout anisotropy from 2nd-order oscillations of HBT radii. Inset shows hydro evolution of source shape for an equation of state with (upper) and without (lower) softening due to finite latent heat [16].

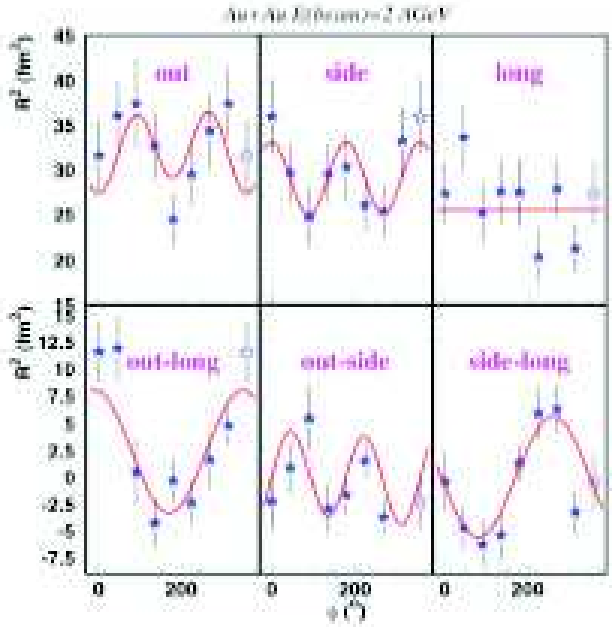

Figure 5.3: HBT radii measured in very low energy ($E_{\rm lab}$ =2 GeV) Au+Au collision at AGS [19], versus the first-order reaction plane. Note that there are now six HBT radii and ϕ is defined over the entire range $0-2\pi$. Lines indicate a fit corresponding to a tilted three-dimensional emission ellipse in coordinate space [13].

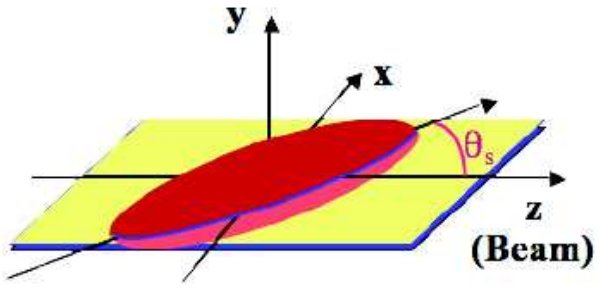

Figure 5.4: The emission source generated at midrapidity may be tilted - in coordinate space - relative to the beam direction [13]. This tilt is revealed in the first order oscillations of the "out-long" and "site-long" cross-terms HBT radii. See Fig. 5.3.

LHC). However, Fig. 5.2 shows instead an intriguing non-monotonic behavior. A possible explanation may be as follows: at low energies (say $E_{\rm lab}$ =3 – 10 AGeV) a stiff equation of state of a hadronic system generates a large pressure pushing the system quickly towards a round shape. But at some energy (say 20 AGeV), a threshold energy required to generate a phase transition is crossed, characterized by a finite latent heat. This generates a "soft point" in the equation of state and the push towards a round state is stalled briefly. As the energy increases beyond this threshold, the time spent in the "soft state" grows, and the "out-of-plane-ness" at freezeout *grows* with energy until some point (say 70 AGeV). Then, at even higher energy, the system spends most of its time in the (stiff) QGP phase, and "out-of-plane-ness" again decreases with energy with no further non-monotonic behaviour. This would be the direct analog of non-monotonic excitation function of v_2 originally predicted by ideal hydro model with softening due to a phase transition [17]. The signal in v_2 has not been observed perhaps because increasing viscous effect at lower energies smears the structure. However, the spatial anisotropy probed by HBT is weighted in the time evolution differently, so may retain sensitivity to the softest point. Fig. 5.2 represents one of very rare bulk-sector probes with a non-monotonic excitation function. Especially given its potential to probe the long sought "soft point", this excitation function cries out to be mapped.

Measuring correlations relative to the *first*-order event plane gives even more unique geometrical information. In particular, if one approximates the spatial configuration of freezeout system as an ellipse, on can extract the angle between its major axis and the beam direction. This "tilt" angle [13] is the spatial analog of the so called "flow angle" [18] formally used to characterized directed flow. It is however, much larger ($\sim 40^o$ at AGS energies [19], compared to flow angles $< 2^o$) and may even have an opposite sign. Simultaneous measurement of both anisotropies provide unique insight on the nature and physics behind the directed flow at lower energies, Fig. 5.3. At RHIC energies, the directed flow becomes even more important, since here we are studying the *bulk* response of the system at the very earliest stages of the collision. Crossing a threshold to a phase transition will generate a "wiggle" in the directed flow at midrapidity, as the system spends most of relevant time (keeping in mind that very small time window to generate directed flow is of order of the crossing time) in the "soft" state. This same physics scenario is predicted to generate non-trivial fingerprint on coordinate-space configuration (of which the tilt angle is the dominant component) [20]. The geometry Fig. 5.4 will probe the physics *behind* the "third component" of flow generating the v_1 wiggle [20, 21].

5.3 Physics at NICA-MPD: particle correlations

V. A. Okorokov

National Research Nuclear University MEPhI, Moscow, Russia

Correlation measurements allow us to get unique information about space-time structure of strong interaction. Moreover study of collective effects is promising tool for investigation of fundamental symmetries and invariances in QCD matter. The requirements for MPD general design suppose reliable identification of various types of charged particles. Thus the detector geometry and characteristics allow us to investigate collective

effects via wide set of correlation measurements.

Azimuthal correlations

The heavy ion investigations at all facilities prove the importance of study of correlations with respect to the reaction plane (flows) for understanding of early stages of final state evolution. Moreover the azimuthal correlation measurements are the promising tool for investigation of fundamental symmetries in hot and dense strongly interacting matter [7, 25, 24, 26]. Recent investigations at high energies at STAR/RHIC indicate at possible topology-induced local parity violation in strong interactions [27, 28]. This effect is an integral part of QCD and it is dominated by non-trivial topology structure of QCD vacuum. Effect of fundamental symmetry violation can serve as a signature of deconfinement state formation and chiral symmetry restoration. It seems QCD vacuum contains high irregular field con-figurations [29]. The features of geometry of these configurations may influence on the fundamental symmetry breaking in particular on the local parity violation in hot strongly interacting matter. Event-by-event charge asymmetry with respect to the reaction plane is observable signature of strong parity violation in heavy ion collisions [30]. There are significant theoretical uncertainties in dependences of effect value on beam energy, atomic number of colliding nuclei etc. so far [24]. The preliminary estimates and general theoretical expectations indicate that the magnetic field at intermediate energies is larger significantly that that for high energy domain [31]. The first correlator calculations show the increasing of experimental observable with energy decreasing for some choice of initial time. But the theoretical estimates never expect decreasing correlator value (as long as deconfinement state of matter is formed) with collision energy decreasing. Some of important characteristics of TPCs for STAR and MPD project are shown in Table 5.1. One can see that the TPC MPD characteristics are suitable for study of fundamental symmetries in hot and dense strongly interacting matter via correlation techniques. Therefore the investigation of topology-induced local parity violation effect can be important task for collectivity / correlation part for physics program of NICA-MPD project.

Characteristic	Main tracker (TPC)	
	NICA/MPD (requirements)	RHIC/STAR
Sizes, cm (TL x IR x OR)	$300 \times 20 \times 110$	$420 \times 50 \times 200$
Rapidity range	$\|\eta\| \leq 1.0$	$\|\eta\| \leq 1.8$
P_t range, GeV/c (ident.)	0.1 -? 3.0	0.1 -? 1.0
dE/dx resolution	$\approx 6\%$	$\approx 7\%$
Momentum resolution	$< 2.5\%$	2 – 3 %
Tracking efficiency	$> 90\%$	80 – 90 %
Two-track resolution	< 5 MeV/c (≈ 1 cm)	0.8 (is) / 1.3 (os) cm
Rate capability	≈ 10 kHz	≈ 0.1 - 1 kHz

Table 5.1: Some characteristics of main trackers for MPD and STAR.

Femtoscopy

Femtoscopy is one of the important experimental tasks for first stage of NICA-MPD project. It seems the AGS/SPS have measured the energy range 3 – 17 GeV in detail for identical charged pion pair. The new experimental data with high statistics are important for resolving radii discrepancy in energy range under study. Perhaps, such data can be useful for detail study of freeze-out geometry which can be high irregular in general. Investigation of correlation peak structure and influence of resonances on the pion correlations could be considered as some additional item for NICA-MPD pion femtoscopy. Study of heavier identical meson (kaons) and baryon (lambdas) correlations, correlations of non-identical particle pairs [32, 33] can be one of the focuses and significant part of NICA-MPD femtoscopy program. Study for identical kaon HBT interferometry can be considered as important physical point because of, in particular, very poor sample of experimental data at intermediate energies [34]. Neutral strange particle (Λ, K^0) HBT correlations can be considered as useful tool for study of space-time evolution and size of baryon-rich final state. Moreover, the $\Lambda\Lambda$ correlations can be used for search of exotic states in QCD, for example, H dibaryons [35]. The non-identical particle correlations with kaons (charged and neutral) allow us to obtain information about space-time asymmetry of particle emission, final state interaction, some exotic objects as well as kaonic atoms. Study of femtoscopy correlations for non-identical particle pairs includes correlations with baryons. Possibly, the study of correlations with particles heavier than kaons/lambdas will be some difficult at NICA-MPD because of low corresponding multiplicities.

But even available particle types give us wide additional opportunities for femtoscopy program.

5.4 Event-by-event fluctuations in nucleus-nucleus collisions

M. Gorenstein

Bogolyubov Institute for Theoretical Physics, 03680 Kiev, Ukraine

The energy dependence of most hadron observables demonstrates rapid non-monotonic changes in the SPS energy range. This suggests the onset of the deconfinement in nucleus-nucleus A + A collisions at $E_{\rm lab} = 30$ AGeV [36]. The experimental study of event-by-event fluctuations in A + A collisions gives a unique possibility to reveal a new physical information about the transitions between different phases of the QCD matter. The interest in the study of fluctuations in strong interactions is motivated by expectations of anomalies in the vicinity of the onset of deconfinement [37, 38]. In particular, a critical point of strongly interacting matter may be signaled by a characteristic power-law pattern in fluctuations [39]. The measurements require a large (ideally full) acceptance tracking detector and a precise control of collision centrality. It is also recommended to identify charged hadrons (pions, kaons and protons) on an event-by-event basis, which would allow to study baryon number and strangeness fluctuations as well as the fluctuations of the particle number ratios. Recent theoretical results on event-by-event fluctuations within the statistical and transport models can be found in [40, 41, 42]. From the experimental point of view the NICA energy range seems to be ideal for these measurements. This is because a moderate particle multiplicity and their relatively broad angular distribution simplifies efficient detection of all produced charged particles. Up to now only results in a very limited acceptance at high energy A + A collisions are available.

5.5 Flow and freeze-out in relativistic heavy-ion collisions at NICA

L. Bravina and E. Zabrodin

Department of Physics, University of Oslo, Oslo, Norway

One of the observables especially sensitive to the changing of the equation of state (EOS) is the collective flow [18, 43]. The softening of the EOS in the proximity of the QCD phase transition [4, 21, 44] should be seen in the excitation functions of the transverse directed flow of baryons. Its experimental observation would be an important discovery, and an unambiguous signal for the transition to QGP. In microscopic models [45, 46, 47, **?**, 49] the softening of the directed flow [50] of nucleons in semi-peripheral collisions was found at energies from AGS and higher. The origin of the disappearance is traced to nuclear shadowing (or screening). Since the effect is stronger for a light S + S system [45, 46, 47, 48], it can be distinguished from the similar phenomenon caused by the quark-gluon plasma formation. In the latter case the disappearance of the flow due to the softening of the equation of state should be most pronounced in collisions of heavy ions.

Some results on the development of anisotropic flow of pions and protons at 40 AGeV have been reported in [51]. The data demonstrate significant softness of the directed flow v_1^p accompanied by the collapse of the elliptic flow v_2^p at the midrapidity range. Several microscopic models cannot reproduce this feature, which can be taken as another evidence of the QGP formation [21]. Here we would like to mention that the trend predicted in the QGSM calculations [45, 46] is similar to that obtained experimentally. Therefore, further microscopic study of this phenomenon at 20 – 40 AGeV is necessary to make any conclusive statements.

The formation and evolution of the anisotropic flow is closely related to the freeze-out of particles. It was found [52, 53] that the freeze-out picture, predicted by the microscopic models for heavy ion collisions at AGS and SPS energies, is quite different from the one, adopted in fluid dynamical models. Even for the most heavy systems particle emission takes place from the whole space-time domain available for the system evolution, but not from the thin freeze-out hypersurface.

Pions are continuously emitted from the whole volume of the reaction and reflect the main trends of the system evolution. Nucleons in heavy ion collisions at both AGS and SPS initially come from the surface region. Therefore, nucleons with large rapidity show a small longitudinal size of the emitting source, while particles from the midrapidity region indicate a large longitudinal size and lifetime of the source. For both reactions there is a separation of the elastic and inelastic freeze-out. Particles which have a small interaction cross section leave the system earlier than those with a large cross section. Thus, the observed interferometric time average

depends on the particle species and on the relative momentum of the pair and so does the correlation function (see also [54]).

It appears that particles with large transverse momenta p_t are predominantly produced at the early stages of the reaction. They are emitted from a spatial domain with small longitudinal and large transverse dimensions. The low p_t-component is populated mainly by the decay products of resonances. This explains naturally the increasing source sizes with decreasing p_t, as observed in HBT interferometry.

The shapes of the emitting sources are far from Gaussians, and the τ -scaling, that is often used in the parameterizations, is not confirmed. Therefore, more realistic source shapes and freeze-out criteria should be used in the analysis of HBT interferometric data. These findings are supported by the results of Ref. [55], in which the HBT correlators of both identical and nonidentical pions are shown to depend strongly on the pion production scenario. The problem with several different emitting sources for hadrons is quite complex and requires further theoretical analysis.

5.6 Perspectives of anisotropic flow measurements at NICA

V. Korotkikh, I. Lokhtin, L. Malinina, S. Petrushanko, L. Sarycheva, A. Snigirev

D.V. Skobeltsyn Institute of Nuclear Physics;
M.V. Lomonosov Moscow State University, Moscow, RUSSIA

Measurements of collective flow phenomena are one of the important tools for studying the properties of the dense matter created in relativistic heavy ion collisions (such as the equation of state EoS, formation conditions, etc.). In non-central collisions of two nuclei the beam direction and the impact parameter vector define a reaction plane for each event. The azimuthal anisotropy of particle production with respect to the reaction plane is an important signature of the physics dynamics at early stages of non-central heavy ion collisions [56, 57]. An initial nuclear overlap region has an almond form at non-zero impact parameter. If the produced matter interacts and thermalizes, pressure is built up within the almond shaped region leading to anisotropic pressure gradients. This pressure pushes against the outside vacuum and the matter expands collectively. The expansion is fastest along the largest pressure gradient, i.e. along the shortest axis of the almond. The result is an anisotropic azimuthal angle distribution of the detected particles. One can expand this azimuthal angle distribution in a Fourier series. The second coefficient of the expansion v_2 is often called the elliptic flow and it is expected to be the dominant contribution in the relativistic domain of heavy ion energies. According to the typical hydrodynamic scenario, the values $v_2(p_{\rm T})$ at relatively low transverse momenta ($p_{\rm T} < 2$ GeV/c) are determined mainly by the internal pressure gradients of an expanding fireball during the initial high density phase of the reaction. The ideal hydrodynamics predicts non-monotonic $\sqrt{s_{\rm NN}}$-dependence of v_2 as a result of EoS softening near the critical temperature of quark-hadron phase transition [58].

The elliptic flow was measured in a wide range of heavy ion beam energies (AGS, SPS, RHIC). Besides the integral elliptic flow, differential measurements of v_2 (e.g. as a function of particle transverse momentum $p_{\rm T}$ for various hadron species) are of a great interest. In particular, one of the most striking features of the RHIC experimental data for Au+Au collisions at $\sqrt{s_{\rm NN}} = 200$ and 62.4 GeV per nucleon pair is a so-called constituent quark scaling approximate independence of $v_2/n_{\rm q}$ as a function of $p_{\rm T}/n_{\rm q}$ on hadron species up to $p_{\rm T}/n_{\rm q} \sim 1$ GeV/c (where $n_{\rm q}$ is a number of constituent quarks for the given hadron type), which can be explained in terms of the elliptic flow formation on a partonic level [59]. The breaking such scaling at lower energies may carry the information about changes in properties of a created dense matter. In particular, decrease of the baryon flow and increase of the meson flow are predicted as the signal of a first order quark-hadron phase transition in the presence of critical point [21, 60]. Since at SPS energies the energy dependence of v_2 for baryons is not established, the better measurements (including $p_{\rm T}$ -dependence of v_2 up to high $p_{\rm T} \sim (2-3)$ GeV/c) are required for SPS energy range.

It is expected that the high-accuracy and high-luminosity measurements of differential anisotropic flow for various hadron types over full NICA energy range will provide important constraints on the early dynamics of heavy ion reactions under the conditions where a first order quark-hadron phase transition may occur. We estimated the statistical reach for elliptic flow measurements at NICA with HYDJET++ heavy ion event generator [61]. For NICA energies, input parameters of the model were tuned using SPS and recent low-energy RHIC data. We have found that for MPD acceptance, the statistical $p_{\rm T}$ reach up to $p_{\rm T}/n_{\rm q} = 1$ GeV/c ($p_{\rm T} = 3$ GeV/c for protons and $p_{\rm T} = 2$ GeV/c for pions and kaons) is expected to be achieved within first million

minimum bias Au+Au events at the NICA energy $\sqrt{s_{\rm NN}} = 9$ GeV per nucleon pair. It corresponds to the "first day" physics at designed NICA luminosity. Thus at long time scale measurements, the statistical error in differential v_2 determination (hopefully not only for pions, kaons and protons, but also for other identified hadrons like ρ, ω and ϕ mesons Λ, Σ and Ω baryons) is expected to be much less than the systematic uncertainties. The latter needs to be investigated in the future using different wide-spread flow analysis methods.

5.7 Fluctuations and non-equilibrium processes in collective flow

Takeshi Kodama

Instituto de Física, Universidade Federal do Rio de Janeiro, Caixa, Rio de Janeiro, Brazil

Dissipative hydrodynamics has been applied to relativistic heavy ion collisions to understand the viscous nature of the matter produced by relativistic collision of heavy nuclei. Several works have been done to extract the shear viscosity from the experimental data of the collective flow parameter v_2 [62, 63, 64]. Now the hydrodynamic approach is widely accepted as an essential tool to describe the flow dynamics of relativistic heavy ion collisions.

On the other hand, a hydrodynamic description of heavy ion collisions requires many external inputs such as the equation of state, transport coefficients, initial condition and freeze out mechanism. They are exactly what we want to extract from the experimental data applying the hydrodynamic model analysis. Unfortunately (or fortunately), these external "parameters" are all entangled in a complicated way in the final state physical observables. This means that each of any single type of experimental data alone, e.g., particle spectra, collective flow, etc., is not sufficient to specify quantitatively the required information directly from them. Therefore, correlations among the observables, especially those reflect the (estimated) geometrical information of the initial condition like the centrality are invoked to determine, for example, the viscosity coefficients.

One important factor in relativistic hydrodynamics is the relaxation time. To keep the causality and stability of the system, a finite value of the relaxation time related to the viscosity is mandatory. However, this new parameter increases the uncertainty of the hydrodynamic approach. For example, we know that the shear viscosity η/s takes different value in QGP and hadronic phases, and it even depends on the temperature(see Fig. 5.5). This is the same for the relaxation time, τ_Π. Even though, due to the interplay between the effects of viscosity and relaxation time (a large relaxation time reduces the effect of shear viscosity), it is possible to fit the behavior of collective flow in terms of one unique (constant) effective shear viscosity per entropy, $\eta_{\rm eff}/s$ shown by the grey line in Fig. 5.5 [65].

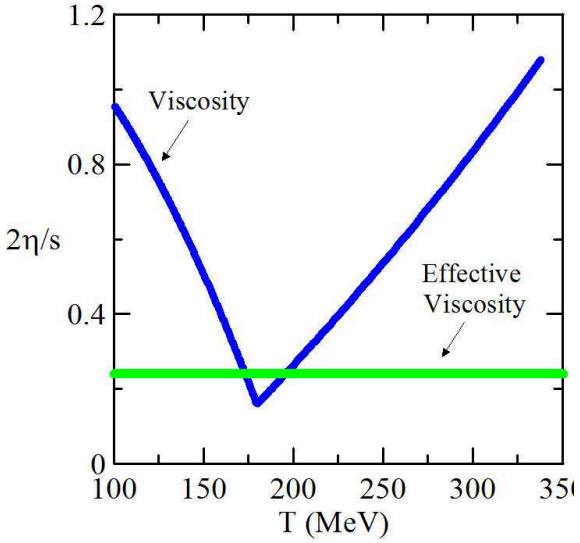

Figure 5.5: Shear viscosity as function of temperature. In spite of the large temperature dependence (black line), the same behaviour of the final values of collective flow parameter can be obtained with a constant (and relatively small) effective shear viscosity (grey line) [65].

The value of effective viscosity depends critically on the evolution of the system. Specifically, this value is affected by the time span for which the system remains in different phases. For the LHC energies, for example, we would expect a different value for the effective viscosity since the system will stay longer in the quark gluon plasma phase. It is thus quite important to study the behaviour of collective flow as function of energy. We further expect that the finite value of baryon chemical potential, $\mu_{\rm B}$, also changes the behaviour. Therefore, the study of these quantities near the first order phase transition domain will reveal more exclusive information on transport coefficients.

In addition to the above mentioned correlations among inclusive observables, a very important information can be obtained by studying event by event (EbyE) fluctuations [66, 67]. There are many origins of EbyE fluctuations but within a hydrodynamical scenario, we may classify them in three categories: fluctuations in the initial condition (IC), dynamical fluctuations due to the hydrodynamical instabilities, and the fluctuations in hadronization stage. In conventional hydrodynamic models, these fluctuations are usually neglected. For example, the initial conditions for the hydrodynamic expansion are usually parametrized as smooth distributions of thermodynamic quantities and four velocity. However, in the case of relativistic heavy ion collisions, the system is relatively small compared to the inhomogeneity scale so that important event-by-event fluctuations are expected in the IC of the real collisions. Moreover, each set of ICs should presents strongly inhomogeneous structure [68].

Fluctuations of observables also happen due to hydrodynamical instabilities such as turbulences. This may take place when the system passes through the phase boundary and meet the instabilities of order parameters [69, 70]. In particular, at the mixed phase the sound velocity vanishes, so that any inhomogeneity in the velocity field easily generates shocks. At the same time, the relaxation time becomes very large, and when this becomes comparable to the hydrodynamic time scale, the hydrodynamical description may loose its validity. This is because hydrodynamic equations are usually considered as a theory where the local thermodynamical equilibrium is attained. There, we may expect some new features of the collective dynamics, specifically associated with the first order phase transition such as nucleation or spinodal instabilities [71]. These dynamics depend crucially on the coarse-graining scale for the hydrodynamics. Therefore, we need observables sensitive to the small coarse-graining scale of the collective flow.

Another origin of fluctuations comes from the final stage of hydrodynamics, where the observed hadrons are emitted from the fluid. The most common (because it is simple) way to treat this is use the Cooper-Frye formula applied to a sharp freeze-out hyper surface. Recent calculations include the final state interactions of hadrons using the hadronic cascade codes like rQMD[72, 73]. These hadronization process also induces dynamical and statistical fluctuations. Furthermore, if one considers the emission of hadrons from any space time point, EbyE fluctuations also changes according to the kinematical domain (continuous emission mechanism) [74, 75].

One should note that several very different physical scenarios within the hydrodynamical approaches (e.g. smooth initial conditions vs. bumpy initial conditions, single shear viscosity vs. temperature dependent viscosity plus corresponding relaxation time, etc.) can give rise somewhat equally good results in reproducing several sets of observables with suitable choices of parameters. In a way, one may say that the hydro signature is "robust", but on the other hand, this could be a synonym of "insensitive". Recent sophisticated studies, with the combination of adequate initial condition, equation of state and final state interactions, show that most of collective features of the data are well reproduced, even solving the HBT puzzle [76]. Nevertheless, we are still not able to say that these are unique description of the real situation.

With respect to this point, one should remind an important point of the collective flow. We usually say that the hydrodynamic description is valid *only* when the local thermal equilibrium is attained. This is because, by using the assumption of local thermal equilibrium, we introduce the equation of state to describe the pressure as function of density to close the hydrodynamic equations. However, is the inverse of this statement true? That is, does the use of thermodynamical relations really imply the local thermal equilibrium? Unfortunately, the answer is NO, in general. To prove this, we need just find any counter example. As is well-known, for a massless relativistic gas, any *isotropic* momentum distribution leads to the ideal massless equation of state, $\varepsilon = 3p$, irrespective of its energy distribution. More generally, this relation holds for any traceless energy and momentum tensor, if the system is locally isotropic. This means that the use of such an equation of state does not mean at all that the system is in thermal equilibrium.

There exist indeed another situations where the equations of state are valid but their microscopic energy states do not follow the Boltzmann distribution [77, 78]. In such cases, the equations of hydrodynamics can be viewed simply as a coarse-grained (in time and space) effective theory for conserved quantities such as energy

and momentum tensor and charge currents. They are essentially a set of continuity equations for these effective conserved quantities, complemented with the "so-called" equation of state and time evolution equation for the off-diagonal elements of the energy and momentum tensor to close the system. In this vision, it is dangerous to exclude from the beginning any other possibilities than the equation of state and transport coefficients calculated from the real thermal equilibrium, such as those of the lattice QCD calculations. The exclusion should be done using the experimental data. Some people explores the so-called non-extensive statistical approach [80, 81, 82, 83]. If this is the case, it would be possible that the effective equation of state that we should use in hydrodynamical analysis does not necessarily be that of the Lattice QCD calculations, and so the transport coefficients.

To clarify these aspects, more observables related directly to genuine hydrodynamical modes, such as shock waves or density waves should be explored [84], without introducing any prejudice for the equation of state and transport coefficients. In this direction, two or more particle correlations in the EbyE analysis are good candidates and some interesting interpretation of double peaks in azimuthal two particle correlations is being studied [85, 86]. In addition, the study of the behavior of universal signatures, such as scaling phenomena is extremely important[87].

There exist still several fundamental questions for the hydrodynamical description of relativistic heavy ion collisions, especially around the domain where the first order phase transition occurs. Thus, more extensive and precise studies, both experimental and theoretical, are required for the determination of properties of the fluid. The NICA program certainly will give a crucial contribution to a large advance of understandig the dynamics of QCD matter near the first order phase transition domain when combined with the energy scan program at the RHIC [88].

5.8 The prospects for experimental study of directed, elliptic, and triangular flows in asymmetric heavy ion collisions at NICA energies

M. Bleicher[a,c], K. A. Bugaev[b], P. Rau[a,c], A. S. Sorin[d], J. Steinheimer[a,c] and H. Stöcker[a,e]

[a] *Frankfurt Institute for Advanced Studies (FIAS), Frankfurt, Germany*
[b] *Bogolyubov Institute for Theoretical Physics, National Academy of Sciences of Ukraine, Ukraine*
[c] *Institut für Theoretische Physik, Goethe-Universität, Frankfurt, Germany*
[d] *Joint Institute for Nuclear Research (JINR), Dubna, Russia*
[e] *GSI Helmholtzzentrum fur Schwerionenforschung, Darmstadt, Germany*

Introduction.

The experimental study of strongly interacting matter has reached a decisive moment: it is hoped that the low energy heavy ion collisions programs performed at the CERN SPS and the BNL RHIC and two new programs that are planned to begin in a few years at NICA (JINR, Dubna) and FAIR (GSI, Darmstadt) will allow the heavy ion community to locate the mixed phase of the deconfinement phase transition and to discover a possible (tri)critical endpoint [89, 90]. The major experimental information is provided by the measurements of particle yields, one particle momentum spectra, two particle correlations, and the Fourier components of the collective hadronic flow [96] known as v_1-coefficient (directed flow), v_2-coefficient (elliptic flow) and v_3-coefficient (triangular flow). Although the great success of experiments at the BNL RHIC and at the CERN LHC proved the high efficiency of modern experimental methods, their results also clearly demonstrated that the heavy ion collisions programs at RHIC, SPS, NICA and FAIR energy range are not simpler and they require further development of both new experimental approaches and far more sophisticated theoretical models in order to reach their goals. Therefore, in view of new opportunities opening with the Nuclotron program Baryonic Matter@Nuclotron (BMN) [89, 90] which will start at JINR (Dubna) in 2014, we would like to address here some new physical issues that can be studied at laboratory energies of 2–5 AGeV for a wide range of colliding nuclei in the fixed target mode. In future, they can further be investigated at the accelerators of new generation like NICA (JINR, Dubna) and FAIR (GSI, Darmstadt) at a center of mass energy up to 11 AGeV.

This range of energies was thoroughly investigated in the past at the GSI SIS and the BNL AGS experiments, but only for symmetric, i.e. A + A, nuclear collisions. In this paper we demonstrate by using the Ultrarelativistic Quantum Molecular Dynamics transport model UrQMD [4, 29] that one of the major tasks of the low energy programs at JINR and GSI could be a systematic study of directed, elliptic, and triangular flows for non-central asymmetric nuclear collisions (ANC), i.e. for non-central $A + B$ reactions with $1 \ll B \ll A$ (see Fig. 5.6).

This aspect of heavy ion physics was not yet systematically explored. Until today there were only a few works reported for ANC [93, 94, 95]. Moreover, these works were completed before a systematic investigation of the Fourier components [96] of hadronic flow was proposed. Only recently there appeared the first predictions for this energy range in Ref. [97] which also studied the influence of high density Mach shock waves formed in ANC on the resulting spatial particle and cluster distribution. Using the comprehensive analysis of the v_1, v_2 and v_3 Fourier-coefficients of the azimuthal particle distributions obtained in [98] for non-central ANC, here we argue that a comprehensive experimental study of ANC can help us to essentially improve our understanding of the hadronic matter equation of state at high densities. In addition, under certain conditions, highest baryonic charge densities can be reached in these experiments [97], what could help clarifying the question, whether the mixed quark-hadron phase [89, 90, 99] or the predicted chiral quarkyonic phase [99] can be formed in this energy range.

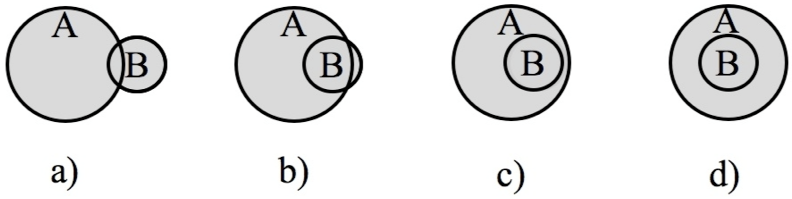

Figure 5.6: Schematic picture of an asymmetric nuclear collision of nuclei A (large circle) with B (small circle) shown in the transverse plane. The common area of two nuclei is shown for very peripheral collisions (panel a)), for semi-peripheral collisions (panels b) and c)) and for the most central collision (panel d)). Clearly, for semi-peripheral collisions the effect of the shadowing of particle motion to the right hand side of the nucleus B is very weak.

The unusual features of ANC.

ANC have some history since they were suggested long ago (see, for instance, [93, 100, 101]), but in those days the analysis of Fourier coefficients of the azimuthal particle distributions was not even suggested. Since that time the analysis of the Fourier coefficients $v_1, v_2, ...$ has become a powerful tool of experimental studies of the evolution process of symmetric heavy ion collisions at high energies [102, 103, 104]. Thus, the quark scaling of the v_2 dependence on the transverse momentum p_T [104] clearly demonstrated the partonic source of elliptic flow of hadrons at RHIC energies, while the triangular flow is reflecting the correlations that appear at the early stage of collisions [105].

A principally new element of the ANC compared to symmetric nuclear collisions is the formation of strong and asymmetric gradients of energy density and baryonic density at the initial stage of the collision process along with a stronger flow from the target towards the projectile for a specific choice of the impact parameter values. In contrast to symmetric collisions, in ANC the reflection symmetry between the left nucleus A and the right nucleus B (see panels a)-c) in Fig. 5.6) is broken from the very beginning. This leads to an entirely different shape and location of the overlap region between the colliding nuclei which, in its turn, results in different flow patterns compared to symmetric collisions. Indeed, if the impact parameter value is close to $b_{ANC} \approx 1.1\,\text{fm} \cdot (A^{\frac{1}{3}} - B^{\frac{1}{3}}) \pm 1$ fm (see the panels b) and c) of Fig. 5.6) and if the size of the target nucleus is chosen close to $B^{\frac{1}{3}} \approx \frac{1}{2}A^{\frac{1}{3}}$, then there is sufficient room to vary the impact parameter in the experiment and to select values close to b_{ANC} using an event-by-event analysis. In this case ANC allow us to scan the interior of the target nucleus as well as to study in detail the variety of surface phenomena such as the surface formation of light nuclear fragments like deuterons, tritons, and helium nuclei, the emission of high p_T pions, the isospin dependence of hadron surface emission, and so on.

The discussion of new possibilities opened up by ANC can be found in [98]. In Figs. 5.7-5.9 we show a few results on the directed, elliptic, and triangular flow coefficients obtained by the UrQMD transport model containing in medium potentials [106, 107, 108] which was thoroughly tested on the available data in a wide range of collision energies. The left panel of Fig. 5.7 shows the energy and centrality dependence of the v_1^{AS} coefficient for all charged particles at longitudinal midrapidity in the equal velocity frame of the colliding Ne and Au nuclei. Such a system is convenient to compare the results with both the data obtained in the symmetric nuclear collisions. As one can see from Fig. 5.7 the v_1^{AS} coefficient of charged particles is essentially non-zero

at $|y| < 0.1$ for ANC, whereas it is zero for $y = 0$ in the symmetric case since it is an odd function of the center of mass rapidity. The right panel of Fig. 5.7 shows the v_1^{AS} coefficient of charged particles found for the configuration that contains a fluctuating high density spot in the target nucleus [98].

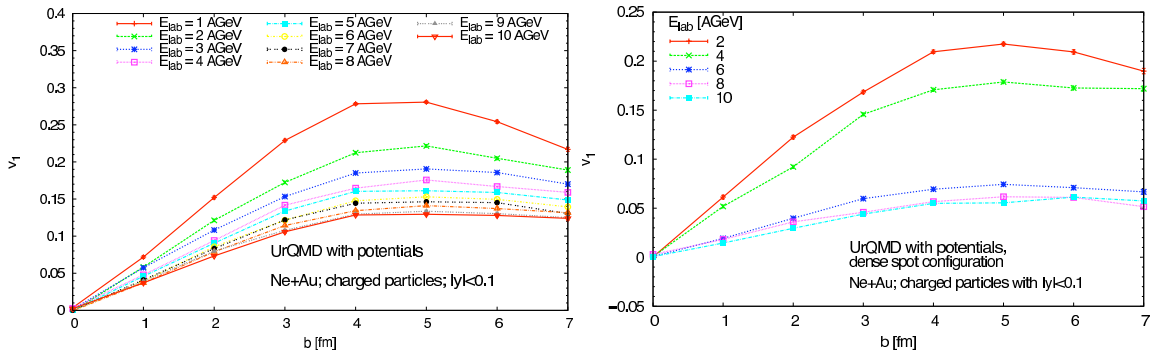

Figure 5.7: Energy and centrality dependence of the v_1^{AS} coefficient of charged particles from Ne+Au collisions as calculated with the UrQMD model with potentials for the standard initialisation (left panel) and with a fluctuating high density spot in the target nucleus (right panel). For more details see the text.

An existence of high density fluctuations in ordinary nuclei is debated for a long time [109, 110] along with their possible applications in the context of the heavy ion reactions [111, 112]. Here we would like to draw attention to this issue and to demonstrate the influence of the high density fluctuations on the v_1^{AS}, v_2^{AS}, and v_3^{AS} coefficients for ANC. To estimate this effect, we randomly put 20 nucleons from the Au-nucleus in a narrow Gaussian distribution inside of the ordinary Monte Carlo sampled nucleus. This gives us a fluctuating dense spot initial configuration. Such an assumption is far from the extremely high densities discussed with respect to flucton [109, 112]. The dense spot is fixed in the center of the Au target with an offset in x-direction of half of the impact parameter in order to make sure the Ne projectile always hits the high density region. Thus, for all impact parameters below 12 fm there is an overlap of the dense spot with Ne-nucleus. The right panel of Fig. 5.7 shows the non-monotonic energy dependence which indicates [98] the change of regimes from the dominance of the target break up process at $E_{lab} = 2 - 4$ AGeV to a strong compression and more intense thermalization of the reaction zone for $E_{lab} \geq 5$ AGeV.

In Figs. 5.8 and 5.9 we also show the v_2^{AS} and v_3^{AS} coefficients calculated for ANC with and without the fluctuating dense spot in the target. These figures show that the 50 % reduction of the directed flow for the dense spot configurations at $E_{\rm lab} \geq 4$ AGeV does not lead to a dramatic change of the corresponding elliptic, and triangular flows at these energies.

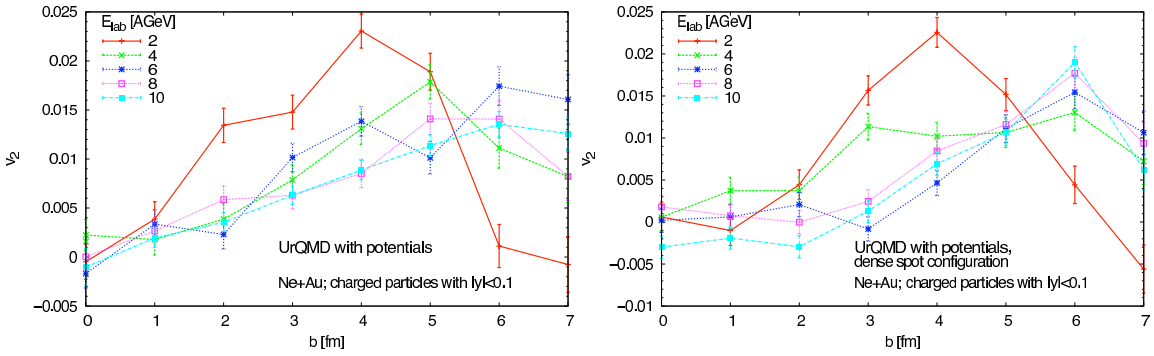

Figure 5.8: Energy and centrality dependence of the v_2^{AS} coefficient of charged particles found by the UrQMD model for the asymmetric Ne + Au collision with the dense spot (right panel) and without it (left panel).

Conclusions and perspectives.

Our analysis of the v_1^{AS}, v_2^{AS} and v_3^{AS} coefficients from ANC revealed [98] that they have a richer and more complicated structure compared to symmetric collisions. Also we find that these flow patterns are very sensitive

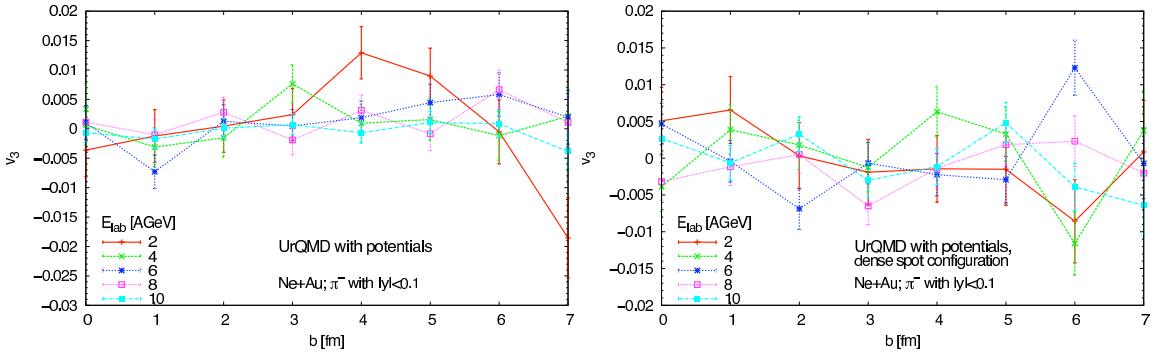

Figure 5.9: Energy and centrality dependence of the v_3^{AS} coefficient of negative pions found by the UrQMD model for the asymmetric Ne+Au collision with the dense spot (right panel) and without it (left panel).

to the details of the employed interaction which can be used both for fine tuning of the transport codes and for elucidation of the essential features of the hadron interaction in the medium.

Therefore, one can hope that a systematic study of the directed, elliptic and, perhaps, triangular flows of strange particles would provide us with the information about the modification of the strange particle interaction with the dense hadronic media that exhibits strong density gradients.

Perhaps, it is reasonable to expect, that in the BMN program energy range the impact parameter dependence of the triangular flow coefficient v_3^{AS} will be uncorrelated (or weakly correlated) to that one of the v_2^{AS}-coefficient even for the semi-peripheral collisions. Such a conclusion is based on the triangular flow pattern developed at highest RHIC energies, where the proportionality of v_2^S and v_3^S is established both experimentally [105] and theoretically [113], and it indicates long-range rapidity correlations occurring at the initial stage due to the color flux tube. Then one can expect that the appearance of such correlations in ANC with the dense spot initial state can signal a possible color flux tube formation.

Furthermore, for the semi-peripheral ANC one can expect the appearance of a sizable flow of deuterons, tritons, ^{3}He and ^{4}He nuclei in the out-of-plane direction [97] which are born during the crush of a narrow layer of nucleus A that surrounds the reaction zone from above and below of the reaction plane (see panels b) and c) of Fig. 5.6). We hope that the investigation of such a flow will allow us to study the dynamical and statistical aspects of nuclear cluster formation.

There is also a hope to identify the case of (partial) chiral symmetry restoration without deconfinement by studying the recently suggested chiral vortaic effect [26] which can be stronger in ANC due to large density gradients [114].

Bibliography

[1] G. I. Kopylov and M. I. Podgoretsky, Sov. J. Nucl. Phys. **15**, 656 (1973).

[2] G. I. Kopylov, Phys. Lett. **B 50,** 472 (1974).

[3] M. I. Podgoretsky, Sov. J. Part. Nucl. **20**, 266 (1989).

[4] D. H. Rischke and M. Gyulassy, Nucl. Phys. **A 608,** 479 (1996).

[5] J. W. Harris and B. Muller. Ann. Rev. Nucl. Part. Sci. **46**, 71 (1996).

[6] A. Bass, M. Gyulassy, H. Stoecker, and W. Greiner, J. Phys. G. **25,** R1 (1999).

[7] W. Cassing and E. Bratkovskaya, *Talk at the Symposium on The Physics of Dense Baryonic Matter*, (Darmstadt, March 9-10, 2009); https://www.gsi.de/ documents/FOLDER-9871235706286.html .

[8] R. Lednicky and M. I. Podgoretsky, Sov. J. Nucl. Phys. **30**, 432 (1979).

[9] C. Alt *et al.*, (NA49 Collaboration), [arXiv:0809.1445].

[10] S. Afanasiev *et al.*, (PHENIX Collaboration), Phys. Rev. Lett. **100,** 232301 (2008).

[11] M. A. Lisa, S. Pratt, R. Soltz and U. Wiedemann, Ann. Rev. Nucl. Part. Sci. **55**, 357 (2005).

[12] F. Retiere and M. A. Lisa, Phys. Rev. **C 70,** 044907 (2004).

[13] M. A. Lisa, U. Heinz and U. Wiedemann, Phys. Lett. **B 489,** 287 (2000).

[14] J. Adams *et al.*, (STAR Collaboration), Phys. Rev. Lett. **90,** 12307 (2004).

[15] U. Heinz and B. Kolb, Phys. Lett. **B 542,** 216 (2002).

[16] M. A. Lisa and S. Pratt, [arXiv:0811.1352].

[17] U. Heinz and B. Kolb, Phys. Lett. **B 469,** 557 (1999).

[18] W. Reisdorf and H. G. Ritter, Ann. Rev. Nucl. Part. Sci. **47**, 663 (1997).

[19] M. A. Lisa *et al.*, (E895 Collaboration), Phys. Lett. **B 496,** 1 (2000).

[20] J. Brachman *et. al.*, Phys. Rev. **C 62,** 024909 (2000), [nucl-th/9908010].

[21] L. P. Csernai and R. Rohrich, Phys. Lett. **B 458,** 458 (1999), [nucl-th/9908034].

[22] H. Stoecker, Nucl. Phys. **A 750,** 121 (2005).

[23] D. Kharzeev, Phys. Lett. **B 633,** 260 (2006).

[24] D. E. Kharzeev *et al.*, Nucl. Phys. **A 803,** 227 (2008).

[25] V. A. Okorokov, [0809.3130 [nucl-ex]].

[26] O. Rogachevsky, A. Sorin and O. Teryaev, Phys. Rev. **C 82,** 054910 (2010), [arXiv:1006.1331 [hep-ph]].

[27] B. I. Abelev *et al.*, Phys. Rev. Lett. **103,** 251601 (2009).

[28] B. I. Abelev *et al.*, Phys. Rev. **C 81,** 054908 (2010).

[29] D. E. Kharzeev, *private communications.*

[30] S. A. Voloshin, Phys. Rev. **C 70,** 057901 (2004).

[31] V. A. Okorokov, [0908.2522 [nucl-th]].

[32] R. Lednicky *et al.*, Phys. Lett. B373, 30 (1996).

[33] R. Lednicky, [arXiv : nucl-th/0112011]; [nucl-th/0212089].

[34] V.A. Okorokov, Proceedings of the XVIII International Baldin Seminar on High Energy Physics Problems, Dubna. V.II, 101 (2008). Eds. by A.N. Sissakian, V.V. Burov, A.I. Malakhov.

[35] C. Greiner, B. M?ller, Phys. Lett. **B 219,** 199 (1989).

[36] M. Gazdzicki and M. I. Gorenstein, Acta. Phys. Polon. **B 30,** 2705 (1999); M. I. Gorenstein, Phys. Atom. Nucl. **71**, 1594 (2008).

[37] M. Gazdzicki, M. I. Gorenstein and S. Mrowczynski, Phys. Lett. **B 585,** 115 (2004);

[38] M. I. Gorenstein, M. Gazdzicki and O. S. Zozulya, Phys. Lett. **B 585,** 237 (2004).

[39] M. Stephanov, K. Rajagopal and E. Shuryak, Phys. Rev. **D 60,** 1140281 (1999) [hep-ph/9903292].

[40] M. I. Gorenstein, Phys. Part. Nucl. **39,** 1102 (2008).

[41] V. P. Konchakovski, B. Lungwitz, M. I. Gorenstein and E. L. Bratkovskaya Phys. Rev. **C 78,** 024906 (2008), [arXiv:0712.2044]].

[42] M. I. Gorenstein, M. Hauer, V. P. Konchakovski, E. L. Bratkovskaya, Phys. Rev. **C 79,** 024907 (2009), [arXiv:0811.3089].

[43] H. Stoecker and W. Greiner, Phys. Rep. **137,** 277 (1986).

[44] C. M. Hung and E. V. Shuryak, Phys. Rev. Lett. **75,** 4003 (1995).

[45] L. V. Bravina, A. Faessler, C. Fuchs and E. E. Zabrodin, Phys. Rev. **C 61,** 064902 (2000).

[46] E. E. Zabrodin, C. Fuchs, L. V. Bravina and A. Faessler, Phys. Rev. **C 63,** 034902 (2001).

[47] L.V. Bravina, Phys. Lett. **B 344,** 49 (1995).

[48] L.V. Bravina, E.E. Zabrodin, A. Faessler and C. Fuchs, Phys. Lett. **B 470,** 27 (1999).

[49] M. Bleicher and H. Stoecker, Phys. Lett. **B 546,** 309 (2002).

[50] S. Voloshin and Y. Zhang, Z. Phys. **C70**, 665 (1996).

[51] C. Alt *et al.*, (NA49 Collaboration), Phys. Rev. **C 68,** 034903 (2003).

[52] L. V. Bravina *et al.*, Phys. Lett. **B 354,** 196 (1995); Nucl. Phys. **A 594,** 425 (1995).

[53] L. V. Bravina, I. N. Mishustin, J. P. Bondorf, A. Faessler and E. E. Zabrodin, Phys. Rev. **C 60,** 044905 (1999).

[54] F. Gastineau and J. Aichelin, Phys. Rev. **C 65,** 014901 (2002).

[55] A. Makhlin and E. Surdutovich, Phys. Rev. **C 59,** 2761 (1999).

[56] J.-Y. Ollitrault, Phys. Rev. **D 46,** 229 (1992).

[57] H. Sorge, Phys. Rev. Lett. **82,** 2048 (1999).

[58] P. Kolb, J. Solfrank and U. Heinz, Phys. Rev. **C 62,** 054909 (2000).

[59] S. A. Voloshin, J. Phys. Conf. Ser. **9**, 276 (2005).

[60] E. Shuryak, [hep-ph/0504048].

[61] I. P. Lokhtin, L. V. Malinina, *et al.*, Comput. Phys. Commun. **180**, 779 (2009).

[62] M. Luzum and P. Romatschke, Phys. Rev. **C 78,** 034915 (2008), **79**, 039903 (2009).

[63] H. Song and U. Heinz, Nucl. Phys. **A 830,** 287 (2009)

[64] G. S. Denicol, T. Kodama, T. Koide and Ph. Mota, Phys. Rev. **C 2009** 80 064901, A. Monnai and T. Hirano, Phys. Rev. **C 80,** 054906 (2009).

[65] G. S. Denicol, T. Kodama and T. Koide, [arXiv: nucl-th/1002.2394v1] .

[66] S. Jeon and V. Koch; eds. R.C. Hwa and X.-N. Wang *Quark-Gluon Plasma 3*, (World Scientific, Singapore) [arXiv:hep-ph/0304012v1].

[67] S. A. Voloshin, V. Koch, H. G. Ritter, Phys. Rev. **C 60,** 024901 (1999).

[68] R. P. G. Andrade *et al.*, Phys. Rev. Lett. **101,** 112301 (2008); Acta. Phys. Polon. **B 40,** 931 and 993 (2009) [arXiv:hep-ph/0901.2849v1].

[69] C. E. Aguiar, E. S. Fraga and T. Kodama, J. Phys. G. **32,** 179 (2006), [arXiv:nucl-th/0306041v2].

[70] K. Paech, H. Stoecker and A. Dumitru, Phys. Rev. **C 68,** 044907 (2003); K. Paech and A. Dumitru, Phys. Lett. **B 623,** 200 (2005).

[71] A. Mocsy and P. Sorensen, Phys. Lett. **B 690,** 135 (2010), [arXiv:nucl-th/0908.3983v2].

[72] T. Hirano, J. Phys. G: Nucl. Part. Phys. **30**, S845 (2004).

[73] K. Werner *et al.*, J. Phys. G: Nucl. Part. Phys. **36**, 064030 (2009), [arXiv:nucl-th/0907.5529v2].

[74] F. Grassi, Y. Hama and T. Kodama, Phys. Lett. **B 355,** 9 (1995).

[75] S. V. Akkelin, Y. Hama, Iu. Karpenko and Yu. M. Sinyukov, Phys. Rev. **C 78,** 034906 (2008), [arXiv:nucl-th/0804.4104v4]

[76] K. Werner *et al.*, [arXiv:1004.0805v1[nucl-th]]; S. Pratt, Nucl. Phys. **A 830,** 51 (2009), [arXiv:nucl-th/0907.1094].

[77] J. Berges, S. Borsanyi and C. Wetterich, Phys. Rev. Lett. **93,** 142002 (2004), [arXiv:hep-ph/0403234]

[78] C. Tsallis, J. Stat. Phys. **52**, 479 (1988).

[79] A. S. Parvan, T. S. Biro, [arXiv:1003.5630v1 [cond-mat.stat-mech]]

[80] G. Wilk and Z. Wlodarczyk, Phys. Rev. Lett. **84,** 2770 (2000).

[81] T. Osada, Phys. Rev. **C 81,024907** (2010), [arXiv:nucl-th/0911.2303v2]

[82] T. S. Biro, G. Purcsel and K. Urmossy, Eur. Phys. J. **A 40,** 325 (2009).

[83] A. Adare *et al.* (PHENIX collaboration), [arXiv:1005.3674v1[hep-ex]] .

[84] C. Sasaki, B. Friman and K. Redlich, J.Phys.G: Nucl. Part. Phys. **35**, 104095(2008)

[85] J. Takahashi et al., Phys. Rev. Lett. 103, 242301 (2009) [arXiv:nucl-th 0902.4870v2].

[86] R. Andrade, F. Grassi, Y. Hama and W.-L. Qian, [arXiv:0912.0703v3 [nucl-th]] .

[87] G. Torrieri, *Flow scaling in a low energy collider: When does the perfect fluid turn on?'*, this volume.

[88] G. Odyniec (STAR collaboration), J. Phys. G: Nucl. Part. Phys. **35**, 104164 (2008).

[89] A. N. Sissakian, A. S. Sorin, M. K. Suleymanov, V. D. Toneev and G. M. Zinovjev, Phys. Part. Nucl. Lett. **5**,1 (2008).

[90] NICA White Paper v.3.3, Chapter I, http://theor.jinr.ru/twiki/pub/ NICA/WebHome/

[91] S. A. Bass *et al.*, Prog. Part. Nucl. Phys. **41**, 255 (1998).

[92] M. Bleicher *et al.*, J. Phys. G. **25,** 1859 (1999).

[93] H. G. Baumgardt *et al.*, Z. Phys. **A273** , 359 (1975).

[94] J. Gosset *et al.*, Phys. Rev. Lett. **62,** 1251 (1989).

[95] B. Adyasevich *et al.*, Nucl. Phys. B (Proc. Suppl.) **16**, 419 (1990).

[96] S. Voloshin and Y. Zhang, Z. Phys. C **70**, 665 (1996).

[97] P. Rau, J. Steinheimer, B. Betz, H. Petersen, M. Bleicher and H. Stöcker, [arXiv:1003.1232 [nucl-th]].

[98] M. Bleicher, K.A. Bugaev, P. Rau, A.S. Sorin, J. Steinheimer, H. Stöcker, [arXiv:1106.xxxx [nucl-th]].

[99] for a discussion and estimates see D. Blaschke, F. Sandin, V. Skokov and S. Typel, *NICA White Paper* v.3.3, http://theor.jinr.ru/twiki/pub/ NICA/WebHome/ and refences therein.

[100] H. Stöcker, J. A. Maruhn and W. Greiner, Z. Phys. A **293**, 173 (1979).

[101] H. Stöcker, J. A. Maruhn and W. Greiner, Phys. Rev. Lett. **44,** (1980) 725.

[102] J. Y. Ollitrault, Nucl. Phys. **A 638,** 195 (1998) and references therein.

[103] see R. Stock, J. Phys. **G 30**, (2004) S633 and references therein.

[104] S. S. Adler *et al.*, (PHENIX Collaboration), Phys. Rev. Lett. **91,** (2003) 182301.

[105] B. Alver and G. Roland, Phys. Rev. **C 81,** 054905 (2010).

[106] Q. -f. Li, Z. -x. Li, S. Soff, M. Bleicher, H. Stoecker, J. Phys. **G32** , 151 (2006).

[107] Q. -f. Li, Z. -x. Li, S. Soff, M. Bleicher, H. Stoecker, J. Phys. **G32** , 407 (2006).

[108] H. Petersen, Q. Li, X. Zhu and M. Bleicher, Phys. Rev. **C 74,** 064908 (2006).

[109] D. I. Blokhintsev, ZhETP **6**, 995 (1958).

[110] A. Bohr and B. Mottelson, *"Nuclear Structure", Benjamin Press*, (New York, 1975), Vol.2.

[111] D. Seibert, Phys. Rev. Lett. **63,** 136 (1989).

[112] A. Stavinskiy *et al.*, *NICA White Paper v.3.3*, http://theor.jinr.ru/twiki/pub/NICA/WebHome/

[113] H. Petersen, G.-Y.Qin, S. A. Bass and B. Müller, [arXiv:1008.0625v2 [nucl-th]].

[114] D. E. Kharzeev and D. T. Son, [arXiv:1010.0038v1 [hep-ph]].

6 Mechanisms of multi-particle production

The mechanism by which the energy of the colliding hadrons or nuclei is converted into the final-state particles is a long-standing problem in physics. There has been significant progress in understanding this mechanism at high energies, where the strong color fields inside the colliding hadrons or nuclei play an important role. The systematics of data on hadron production shows that such an approach formulated in terms of gluons and quarks applies starting from the c.m.s. energy of 15 GeV. Below that energy, the dynamics of multi-particle production should probably be described in terms of some effective low-energy degrees of freedom. The deviations from the trends established earlier at higher energies at RHIC and SPS should provide an important clue to this dynamics. An important part of the NICA program is the physics of high multiplicity events, which are expected to give an access to QCD in the high parton density regime even at a moderate energy. It will be very interesting to explore the evolution of the produced system towards freeze-out through a possible mixed phase, as discussed in this section. A detailed study of multi-particle production in the energy range of the NICA collider will thus contribute to the understanding of Quantum Chromo-Dynamics in the non-perturbative domain.

6.1 My several thoughts on NICA

E. Levin

Department of Particle Physics, Tel Aviv University, Tel Aviv, Israel

First, I would like to state clear why I think that we need the nucleus-nucleus collider for the intermediate range of energy. My own experience in describing the ion-ion collision at RHIC taught me that starting from $W = \sqrt{s} \approx 17\ GeV$ we can expect that the best theoretical approach to ion-ion interaction is the QCD cascade in terms of quark and gluons, while at low energies the successful description has been given in terms of hadron cascade. The intermediate energies are needed just to study the transition from hadron cascade to the QCD one.

Having this idea in mind, I think that the NICA project has one shortcoming and one advantage.

The shortcoming is obvious: the upper energy is too low. Indeed, in our paper [1] we showed that starting with $W = 17\ GeV$ we can describe the data on multiplicity using the QCD approach based on saturation of the gluon density and on Colour Glass Condensate (CGC). Therefore, I believe that we need the accelerator which will cover the range: $2 \div 20\ GeV$, From this point of view the upper energy of NICA ($W = 12\ GeV$ is too low.

The advantage is the fact that it is a new machine and we can adjust construction to our specific goals. As I have mentioned the most interesting phenomena occur at large parton densities where the CGC gives the effective theory to describe the QCD cascade. We have explored two ways to penetrate the region of high parton density: the high energy scattering (Tevatron, HERA and coming LHC) and ion-ion collisions (RHIC and LHC).

However, there is another way to enter this region: to measure the events with high hadron multiplicities. The density of hadrons as well as partons are expected to be high in these events and, therefore we can expect to see all high-density QCD predictions.

The second key question that NICA can shed the light is the thermodynamic equilibrium. The data show that the spectrum of the produced particle behaves as $\exp(-E/T)$ where E is the energy of the particle. This spectrum is an indication that we reach the equilibrium. However, the real thermodynamic equilibrium means that all correlations have the same exponential behaviour or very small. I have not found any systematical study of correlation for ion-ion collisions. I believe that NICA can provide the first of this study.

Summarizing, I see two major goals for NICA:

- Study the high multiplicity events to penetrate into the kinematic region suitable for high density QCD: roughly speaking we have to do the multiplicity of the order of multiplicities in high energies, say $W > 15\ GeV$.
- Systematic study of particle correlations to find out whether we have the stage of thermodynamic equilibrium in ion-ion collisions.

Frankly speaking I have only preliminary list of possible experiments which I want to share with you.

- The p_T distribution in high multiplicity events. We expect that the typical transverse momentum $Q_s^2 \propto \rho$ where ρ is the density of partons (particles) in the transverse plane. Therefore, we expect that the mean p_T increases for larger values of ρ.

- The rapidity distribution in high multiplicity events. The KLN approach [2] predicts the rapidity distribution at different and large multiplicities and these formulae can give us the first estimates for what we can expect in ion-ion collisions at this energies. However much work is needed to take into account the effect of rather low energies.

- The azimuthal angle correlations. Qualitatively, CGC leads to the suppression of azimuthal angle correlations for particle with transverse momenta close to the saturation momentum ($p_T \approx Q_s$) since the transverse momentum of the detected particle can be compensate by several particles with the transverse momentum Q_s. In our paper we suggest several way to measure this effect. As far as I know the best way is to measure the correlation between particles with sufficiently large difference in rapidity [3]. The main idea to measure these correlations as a function of the multiplicity is to observe how the number of uncorrelated pair increases with the value of multiplicity.

- One of interesting features of ion-ion collisions is the existence of a hydrodynamical stage in the final state (for some time after collision). I am sure that the measurement of the elliptic flow (v_2 as a function of the multiplicity) will clarify the question how hydro works and at what distances and time.

Certainly this is not full list of the interesting experiments, but at this stage of planning it is enough to think about.

6.2 Some issues in NICA-related research at LPI

I. Dremin and A. Leonidov

P. Lebedev Physics Institute, Moscow, Russia

One of the crucial characteristics of dense strongly interacting matter created in heavy ion collisions is a collective flow of final hadrons. To quantify the amount of flow present in collisions at given energy it is very important to make a careful subtraction of rescattering effects that are present already in proton-nucleus collisions and can mimic some part of collective flow. In fact a model based on parametrizing effects of transverse rescattering in terms of transverse rapidity [4, 5] was shown to provide a very good description of transverse and longitudinal hadron spectra for different hadron types (with an interesting exception of kaons). One can argue that a more natural description of the effects of transverse broadening is to use transverse momentum, not transverse rapidity as a variable quantifying an amount of this rescattering. To analyze this issue one has to work out a corresponding version of the model of [4, 5]. This work is currently underway.

In a more distant perspective our group is planning to study several issues directly related to the main object of experimental studies at NICA, the mixed baryon-rich phase of QCD:

- Kinetic description of fluctuations in the expanding mixed phase. Comparative analysis of baryonless and baryon-rich case.

- Possible role of gluon junctions in the physics of mixed phase.

- Microcanonical description of the physics of mixed phase.

6.3 Hydrokinetic analysis of space-time evolution and properties of strongly interacting matter formed at the NICA and FAIR energies

Yu. Sinyukov

Bogolyubov Institute for Theoretical Physics, Kiev, Ukraine

The phase evolution of strongly interacting matter created at the NICA and FAIR energies is expected to occur near the bondary of the first order phase transition and possibly in vicinity of the critical QCD point. The initially hot and dense matter, produced in A+A collisions, cools down and loses density because of fast

expansion, and passes, therefore, all the thermodynamic phases crossing, possible, phase boundary. The lifetime of such a system is around 10 fm/$c = 10^{-22}$ sec. The information about evolution and properties of the matter can be extracted only from one- and multi-particle momentum spectra for different particle species. The hadrons appears as a result of their gradual liberalization from the interacting matter, this process lasts, typically, a half of the total lifetime of the created finite system [6, 7]. So, the peculiarities and distinctive properies of observables related to characteristics of the new states of matter have to be analysed only within the reliable approach allowing one to describe correctly the evolution, particle emission and spectra formation from the system undergoing the phase transition during its fast expansion.

Hydrodynamic models gives possibility to describe the space-time evolution of the system basing on the hypothesis of local thermalization and energy-momentum conservation low. The microscopic properties of the matter, including complicated kinetics of the possible phase transition, are encoded then only in corresponding equation of state - it is the main advantage of the hydrodynamic models. At the same time, the application of this approach to finite explosively expanding systems faces difficulties since the particles are emitted continuously and so, especially at the later stage, the system is not in local equilibrium. So, the standard Landau/Cooper-Frye prescription, treating the spectra formation as the result of a sudden transition from an ideal fluid to an ideal gas that corresponds to instant switching of very big value of particle cross section in perfect fluid to zero value, is too rough approximation [6, 7]. The hybrid models [8] that match hydrodynamics with cascade models, like UrQMD, collide with problem of causality [9]. Our description of particle emission and spectra formation is based on the hydrokinetic approach (shortly HKM - Hydro-Kinetic Model) [6, 10] that initially has been applied for the systems with the cross-over type of equation of state and zero or small baryonic densities at the RHIC energies [11, 12, 13]. The HKM method is based on an analysis of the kinetic equations in terms of probabilities of particles to escape from the hydrodynamically expanding system consisting of these particles. It deals with non-locally equilibrium distribution functions and accounts for a back reaction of the emitted particles on the system evolution.

To simulate the hadron emission and spectra formation at the NICA and FAIR energies we are planning to develop the theoretical basis allowing include into the HKM the modified properties of hadrons in the strongly interacting medium with high baryonic density. The non-equilibrium effects, connected with continuous hadron emission, and viscosity are taken into account in a generalized relaxation time approximation [6, 13]. The local hydrodynamic variables evolve according to hydrodynamic equations of ideal fluid with sources/sinks in the right hand side [6] and account for a possible phase transition and critical QCD point. The corresponding numerical code serves then as an effective tool for calculation of the one- and multi-particle hadronic spectra depending on the properties of the formed matter and initial conditions at the energies of NICA and FAIR.

Collective flows in expanding matter, that are reflected in the spectra of emitting hadrons, depend essentially on properties of super-dense states of the strongly interacting matter, e.g., on its equation of state. A few types of flows are marked out in the experimental analysis: radial flow (isotropic component) and elliptic one - azimuthally asymmetric flows, which appears due to the almonds-like form of the initial interacting region of two nuclei in non-central collisions. We plan to provide a detail study of both types of flows, the transverse momentum spectra and its azimuthal anisotropy as well as the two-particle Bose-Einstein correlation functions. The latter contain main information as for space and time scales of the systems formed in relativistic A + A collisions.

Definitive aim of the hydrokinetic study for NICA and FAIR energies is a search for "anomalies" in spectra and correlation functions which become apparent when the phase trajectory of evolving system passes in vicinity of the critical point or crosses the boundary of the first order phase transition, as well as a search of signatures of in-medium modification of hadron spectral function in hot and dense strongly interacting nuclear surrounding.

The hydro-kinetic approach, which directly accounts for particle interaction inside the matter, allows one to calculate and compare the spectra and correlations for hadrons with different cross-sections, including the particles with "open" and "hidden" charm having a relatively small cross-sections. Because a value of cross-section affect essentially probabilities of the particle emission, it allows one to study varied temporal "slices" of the hadronic matter associated with the different temperatures using corresponding particle species. Such an investigation of the spectra and correlations of particles with different cross-sections is also important because the hadron cross-section in dense medium is different from those which is in the vacuum. This allows one to study off-vacuum modifications of the hadron properties in dense strongly interacting medium. The method can be a useful supplement to the CBM program of an analysis of an influence of the dense medium on hadron properties based on a study of short-lived vector mesons which decay inside the medium on free-emitted lepton pairs.

6.4 Open and hidden strangeness production

E. Kolomeitsev and B. Tomášik

Univerzita Mateja Bela, Banská Bystrica, Slovakia

Since a long time an enhancement of strangeness production in heavy ion collisions has been considered as a signal for quark-gluon plasma formation. The discovery of the sharp peak of K^+/π^+ multiplicity ratio for collisions at beam energy of 30 AGeV is interpreted as a signal for QGP formation, since purely hadronic models without a deconfinement phase transition were not able so far to reproduce the peak. Mainly two quantities are decisive for how much strangeness is produced in a collision: available energy and time. Clearly, more energy increases the rates for production of strange particles. Furthermore, in an environment with under-represented strangeness the abundance of strange particles grows with time.

In Ref. [15] we argued that the peak can be explained as a combination of two effects:

- due to an increase of the collision energy more energy becomes available for strangeness production that enhance the strangeness production;
- the lifespan of the fireball decreases with a collision energy increase, this can lead to the sharp decrease of that ratio.

The physics picture behind the second assumption is that nuclear stopping is stronger at lower energies and expansion is mainly built up from pressure. This takes some time. On the other hand at higher collision energy transparency regime is reached and the longitudinal expansion is, to a large amount, due to original motion of the nuclei. Thus expansion may be quick. The fireball disintegrates when the energy density drops below some critical value, depending also on the expansion speed. Alternatively, one can argue that at higher collision energy the expansion also starts from higher initial (energy) density and might need longer time to drop to its freeze-out value. Hence, the lifetime as a function of collision energy results from two competing effects: the initial energy density which increases with $\sqrt{s_{\rm NN}}$ and tends to prolong the lifetime, and the stopping power which decreases with $\sqrt{s_{\rm NN}}$ and leads to a shortening of the lifetime.

The quantitative question how the fireball lifetime depends on $\sqrt{s_{\rm NN}}$ is non-trivial and cannot be answered conclusively with the present theoretical studies at hand.

The practical results of [15] is that the K^+/π^+, K^-/π^- and Λ/π ratios can be qualitatively described if the the fireball lifetime varies from 15 – 20 fm at the collision energies E = 11.6 AGeV to 25-30 fm at $E_{\rm lab}$ = 30 AGeV and decreases gradually down to 15 fm between 30 and 80 AGeV. We have to note that the obtained lifetimes are sizeably longer than that follow from the hydrodynamical calculations, e.g., [14]. The observed amount of strangeness can hardly be produced during the shorter time unless there is some mechanism to enhance the in-medium production rates, which is operative even at the lower collision energies below an expected phase transition region.

So there is a need in more detailed and thorough study of strangeness production in heavy ion collision which can reveal some details of collision dynamics. For complete reconstruction of the strangeness production dynamics it is mandatory to measure not only strange mesons, but also hyperons. A sensitive test of strangeness production mechanism is also the measurement of multistrange baryons (Ξ, Ω).

Another messenger of the strangeness dynamics in heavy-ion collision is ϕ meson of which the dominant component is a spin-one bound state of s and $\bar{s}$ quarks. The ϕ meson production is an important part of the study program of different nucleus-nucleus collision experiments in the whole range of collision energies: at the AGS, the SPS, RHIC, and even at deeply subthreshold energies at the SIS. As the longest-living vector meson, the ϕ is considered to be a good probe of the collision dynamics: it would decay mainly outside the fireball and the daughter hadrons would be weakly affected by rescattering. The dominant hadronic decay is $\phi \to \bar{K} K$, hence, the production of ϕ's interplays with the production of strange mesons in nucleus-nucleus collisions.

In [**?**] we propose a new mechanism of ϕ meson production in nucleus-nucleus collisions—the catalytic reactions on strange particles, e.g., $\pi Y \to \phi Y$ and $\bar{K} N \to \phi N$. These reactions are OZI-allowed and their cross section can be by an order of magnitude larger than the cross section of conventional OZI-suppressed ϕ production reactions $\pi N \to \phi N$ and $N\Delta \to \phi N$, etc, considered so far. These reactions require only one strange

particle in the entrance channel and therefore are less suppressed than the strangeness coalescence reactions, $K\bar{K} \to \phi$ and $KY \to \phi N$ in collisions where strangeness is statistically suppressed. Comparison of the rates of ϕ production in the catalytic reactions and in the $\pi N \to \phi N$ reaction shows that the former can be competitive in collisions with the maximal temperature above 110 MeV and the collision time $\gtrsim$ 10 fm. The efficiency of catalytic reactions increases if some strangeness is presented in the fireball right in the beginning after the first most violent nucleon-nucleon collisions and if the fireball lifetime is longer. Thus the ϕ meson production can serve as a timer for a nucleus-nucleus collision.

Summarizing, we suggest that the NICA/MPD research program should put some emphasize on the strange particle production, including *hyperons*, and the ϕ mesons. Important complementary information on the production mechanisms can be extracted from the centrality dependence of the particle yields.

6.5 Chemical freeze-out and strangeness production study at NICA

F. Becattini

University of Florence, Italy

Chemical freeze-out in relativistic heavy ion collisions has been studied systematically from few to few hundreds GeV/s in the nucleon-nucleon centre-of-mass energy [16, 17, 18]. The picture that has emerged from such studies is that of a regular behaviour of the parameters which determine the state of the source, i.e. temperature and baryon-chemical potential: a steep increase (decrease) of temperature (baryon-chemical potential) in the

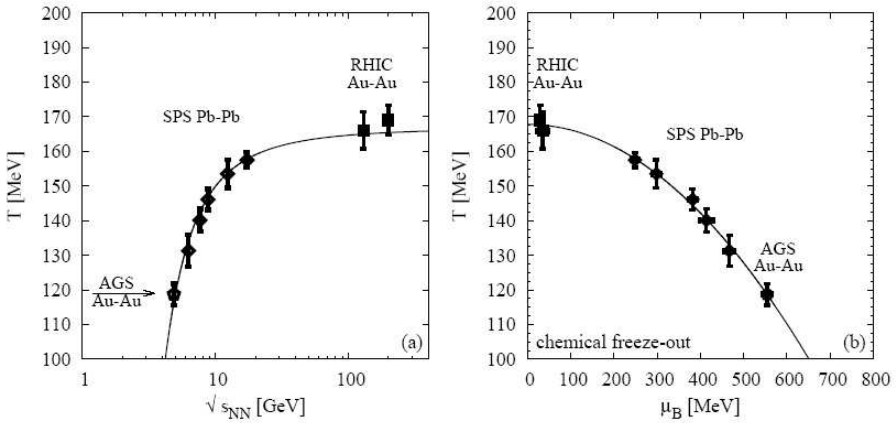

Figure 6.1: Chemical freeze-out temperature as a function of center-of-mass energy in central heavy-ion collisions at AGS, SPS and RHIC (from Ref. [19]).

low energy region followed by a saturation at large energy (see Fig. 6.1). Moreover, it has been observed that also a strangeness undersaturation parameter γ_S is needed to describe the final abundances of hadrons. This parameter also shows a regular behaviour slowly increasing from $\simeq 0.65$ to 1 going from $\sqrt{s_{\rm NN}} = 4.5$ GeV to 200 GeV (see Fig. 6.2). By studying the behaviour of strange particle production as a function of centrality in high-energy heavy-ion collisions, it has been recently argued [20, 21] that the appearance of γ_S is geometrical in origin. Namely, the apparent undersaturation of strangeness might be the effect of single nucleon-nucleon collisions taking place in the outer rim of the colliding nuclei overlapping region, coexisting with a central fully equilibrated hadron gas possibly originated from the quark-gluon plasma (core-corona effect [22, 23, 24]). If this was the case, the intriguing question arises whether this superposition is able to account for strangeness undersaturation also in the few GeV/s energy range. Particularly, whether and where a fully equilibrated hadron gas sets in, as its formation could be related to the onset of deconfinement itself. The data which has been collected so far in heavy ion collisions are not sufficient to provide a definite answer to this question and especially in the range $\sqrt{s_{\rm NN}} = 2.6$ GeV. It is therefore crucial to collect and analyze a wealthy data in a new generation of experiments to assess these phenomenological issues which could be decisive in our understanding of the production of the quark-gluon plasma in nuclear collisions. Some analyses seem to indicate that the

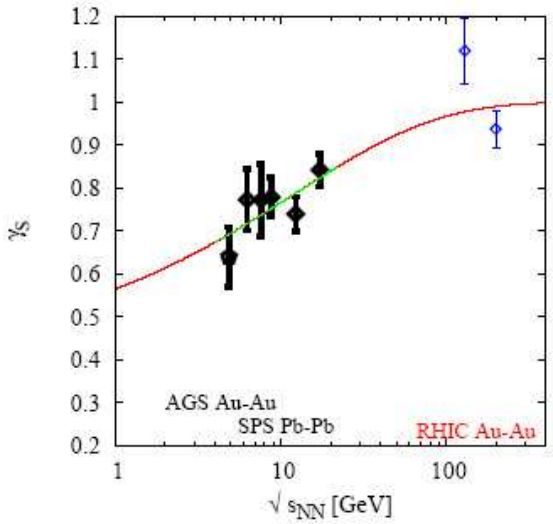

Figure 6.2: γ_S parameter as a function of NN centre-of-mass energy in nuclear collisions.

thermodynamical parameters of the source at very low energy (SIS) follow the general trend [25], however it is not clear whether the hadron-resonance gas model in its zero-order formulation, with non-resonant interaction neglected, can be safely applied at temperatures as low as 100 MeV. The collection of experimental data at low energies will certainly be very important to elucidate this issue.

6.6 MEMO production at high baryon densities

Marcus Bleicher[a,b], *Jan Steinheimer*[a,b]

[a] *Institut für Theoretische Physik, Johann Wolfgang Goethe-Universität, Frankfurt am Main, Germany;* [b] *Frankfurt Institute for Advanced Studies (FIAS), Johann Wolfgang Goethe-Universität, Frankfurt am Main, Germany*

The production of multi-strange meta-stable objects (MEMOs) in Pb+Pb reactions around 30 AGeV is explored in a coupled transport-hydrodynamics model [26]. In addition to making predictions for yields of these particles we are able to calculate particle dependent rapidity and momentum distributions. We argue that this energy regime is the optimal place to search for multi-strange baryonic object (due to the high baryon density, favoring a distillation of strangeness).

Massive heavy-ion reactions provide an abundant source of strangeness. More than 50 hyperons and about 30 Anti-Kaons (i.e. $K^- + \overline{K^0}$ carrying the strange quark) are produced in central collisions of lead nuclei at the CERN-SPS low energy program and before that at the AGS. In the near future, NICA and FAIR will start to investigate this energy regime closer with much higher luminosity and state-of-the-art detector technology. This opens the exciting perspective to explore the formation of composite objects with multiple units of strangeness so far unachievable with conventional methods.

For the microscopic+macroscopic calculation, the Ultra-relativistic Quantum Molecular Dynamics Model (UrQMD) is used to calculate the initial state of a heavy ion collision for a subsequent hydrodynamical evolution [27, 4, 29]. This has been done to account for the non-equilibrium dynamics in the very early stage of the collision. In this configuration the effects of event-by-event fluctuations of the initial state are naturally included. The coupling between the UrQMD initial state and the hydrodynamical evolution proceeds when the two Lorentz-contracted nuclei have passed through each other.

$$t_{\text{start}} = \frac{2R}{\sqrt{\gamma^2 - 1}} \tag{6.1}$$

Cluster	Mass [GeV]	Quark content
He^4	3.750	$12q$
H^0	2.020	$4q+2s$
α_q	6.060	$12q+6s$
$\{\Xi^-,\Xi^0\}$	2.634	$2q+4s$
$\{4\Lambda\}$	4.464	$8q+4s$
$\{2\Xi^-,2\Xi^0\}$	5.268	$4q+8s$
${}^{5}_{\Lambda}He$	4.866	$14q+1s$
${}^{6}_{\Lambda\Lambda}He$	5.982	$16q+2s$
${}^{7}_{\Xi^0\Lambda\Lambda}He$	7.297	$16q+2s$
$\{2n,2\Lambda,2\Xi^-\}$	6.742	$12q+6s$
$\{2\Lambda,2\Xi^0,2\Xi^-\}$	7.500	$8q+10s$
$\{d,\Xi^-,\Xi^0\}$	4.508	$8q+4s$
$\{2\Lambda,2\Xi^-\}$	4.866	$6q+6s$
$\{2\Lambda,2\Sigma^-\}$	4.610	$8q+4s$

Table 6.1: Properties of all considered multibaryonic states (see also [35] for decay systematics).

After the UrQMD initial stage, a full (3+1) dimensional ideal hydrodynamic evolution is performed using the SHASTA algorithm [30, 31]. For the results presented here an equation of state for a hadron-resonance gas without any phase transition is used [32]. The EoS includes all hadronic degrees of freedom with masses up to 2 GeV, which is consistent with the effective degrees of freedom present in the UrQMD model. One should note that we apply a purely hadronic EoS, for energy densities where a transition to the QGP is expected (see also [33] for details on the model and comparison of extracted particle yields to data). Final particle (and MEMO) multiplicities are mainly sensitive on the degrees of freedom at chemical freezeout which is reflected in the hadronic EoS. Dynamical observables such as momentum and rapidity spectra are more sensitive on the underlying dynamics. In addition, a phase transition could catalyse a strangeness destillation process further enhancing MEMO production. However, studying the effects of a phase transition on MEMO production is left subject of future investigations.

The hydrodynamic evolution is stopped, if the energy density of all cells drops below five times the ground state energy density (i.e. ~ 730 MeV/fm^3). This criterion corresponds to a T-$\mu_{\rm B}$-configuration where the phase transition is expected - approximately $T = 170$ MeV at $\mu_{\rm B} = 0$. The hydrodynamic fields are mapped to particle degrees of freedom via the Cooper-Frye equation on an isochronous hyper-surface.

$$E\frac{dN}{d^3p} = \int_\sigma f(x,p)p^\mu d\sigma_\mu \quad \text{with} \quad \mathrm{d}\sigma_\mu = (\mathrm{dx}^3,\tilde{0}) \tag{6.2}$$

Here $f(x,p)$ are the boosted Fermi or Bose distributions corresponding to the respective particle species. Inputs for these distributions are the masses and chemical potentials of the desired particles. For our calculation we assumed the mass of a MEMO to be the sum of the masses of all hadrons it is composed of. Similarly the total chemical potential is the sum of the constituents, and is composed of baryon and strange-quark chemical potentials $\mu_{\rm B}$ and μ_s.

The particle vector information is then transferred back to the UrQMD model, where rescatterings and the final decays are performed using the hadronic cascade. Using this parametrisation of the model one obtains a satisfactory description of data in a energy regime of 1 – 160 AGeV. A more detailed description of the hybrid model including parameter tests and results for multiplicities and spectra can be found in [33].

To calculate the multiplicities of MEMOS in the NICA/FAIR energy region, we employ the introduced hybrid approach to heavy ion collisions. Thus, the fluctuating initial state produced in UrQMD, is coupled to a (3+1) dimensional hydrodynamics evolution. When the energy density drops below $5\epsilon_0(\sim 730\mathrm{MeV/fm}^3)$ the freeze-out is performed and MEMOs and strangelets are produced according to the Cooper-Frye description (6.2). As distinctive inputs for the distribution functions, the chemical potentials $(\mu_{\rm s},\mu_{\rm B})$ and masses of the MEMOs enter as discussed above. Final state interactions of these MEMOs are neglected for the present study. Table 6.1. gives the properties of all multibaryonic states considered in our analysis. They are the most promising and stable candidates.

Fig. 6.3 provides the total multiplicities per degeneracy factor of various types of MEMOs and strangelets in central Pb + Pb reactions at $E_{\rm lab} = 30A$ GeV. The yields obtained are in good comparison to the statistical model analysis [34], which is describing strange cluster production at AGS energies.

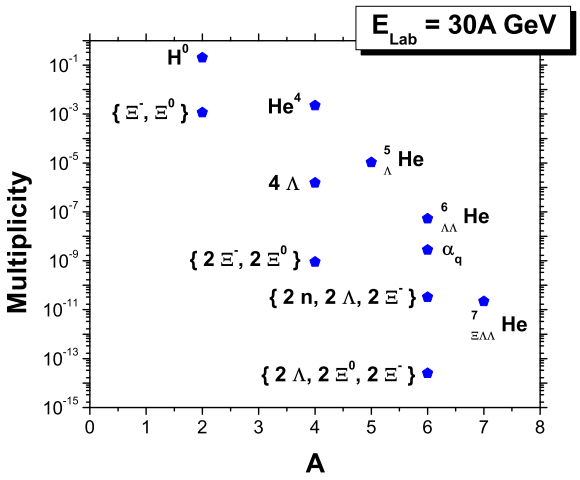

Figure 6.3: Multiplicities of various types of MEMOs and strangelets in central Pb+Pb reactions at $E_{\rm lab} = 30A$ GeV from the hybrid approach.

We have presented results for the thermal production of MEMOs in nucleus-nucleus collisions from a combined micro+macro approach at $E_{\rm lab} = 30$ AGeV. The excitation functions for various MEMO multiplicities show a clear maximum in this energy regime making NICA and FAIR the ideal place to study the production of these exotic forms of multistrange objects.

This work has been supported by GSI and Hessian initiative for excellence (LOEWE) through the Helmholtz International Center for FAIR (HIC for FAIR). We would like to thank Dr. Jürgen Schaffner-Bielich for fruitful discussions. Computational resources were provided by the Center for Scientific Computing (CSC).

Bibliography

[1] D. Kharzeev, E. Levin and M. Nardi, Phys. Rev. **C 71,** 054903 (2005), [hep-ph/0111315].

[2] D. Kharzeev and M. Nardi, Phys. Lett. **B 507,** 121 (2001), [nucl-th/0012025]; **523**, 79 (2001), [nucl-th/0108006]; **561**, 93 (2003), [hep-ph/0210332].

[3] D. Kharzeev, E. Levin and L. McLerran, Nucl. Phys. **A 748,** 627 (2005), [hep-ph/0403271].

[4] A. Leonidov, M. Nardi and H. Satz, Nucl. Phys. **A 610,** 124 (1996).

[5] A. Leonidov, M. Nardi and H. Satz, Z. Phys. **C74**, 535 (1997).

[6] S. V. Akkelin, Y. Hama, Iu. Karpenko and Yu. M. Sinyukov. Phys. Rev. **C 78,** 034906 (2008).

[7] Yu. M. Sinyukov, S. V. Akkelin and Iu. A. Karpenko. Acta. Phys. Polon. **B 40,** 1025 (2009).

[8] S. A. Bass *et al.*, Progr. Part. Nucl. Phys. **41,**225 (1998).

[9] K. A. Bugaev, Phys. Rev. Lett. **90,** 252301 (2003).

[10] Yu. M. Sinyukov and S. V. Akkelin, Y. Hama, Phys. Rev. Lett. **89,** 052301 (2002).

[11] N. Armesto, *et al.*, J. Phys. G: Nucl. Part. Phys. **35**, 054001 (2008).

[12] Yu. M. Sinyukov, S. V. Akkelin and Iu. A. Karpenko, Physics of Atomic Nuclei, **71**, 1619 (2008).

[13] Yu. M. Sinyukov, Iu. A. Karpenko and A. V. Nazarenko, J. Phys. G: Nucl. Part. Phys. **35**, 104071 (2008).

[14] Yu. B. Ivanov, V. N. Russkikh, and V. D. Toneev, Phys. Rev. **C 73,** 044904 (2006).

[15] B. Tomasik and E. E. Kolomeitsev, [arxiv:nucl-th/0512088]; Eur. Phys. J. **C 49,** 115 (2007), [nucl-th/0610041].

[16] J. Cleymans, H. Oeschler, K. Redlich, and S. Wheaton, Phys. Rev. **C 73,** 034905 (2006).

[17] F. Becattini, J. Manninen, and M. Gazdzicki, Phys. Rev. **C 73,** 044905 (2006).

[18] A. Andronic, P. Braun-Munzinger and J. Stachel, Phys. Lett. **B 673,** (2009) 142.

[19] J. Manninen and F. Becattini, Phys. Rev. **C 78,** 054901 (2008).

[20] F. Becattini and J. Manninen, J. Phys. G. **35,** 104013 (2008);

[21] F. Becattini and J. Manninen, Phys. Lett. **B 673,** 19 (2009).

[22] P. Bozek, Acta. Phys. Polon. **B 36,** 3071 (2005).

[23] K. Werner, Phys. Rev. Lett. **98,** 152301 (2007).

[24] V. S. Pantuev, JETP Lett. **85**, 104 (2007).

[25] R. Averbeck, R. Holzmann, V. Metag and R. S. Simon, Phys. Rev. **C 67,** 024903 (2003).

[26] J. Steinheimer, M. Mitrovski, T. Schuster, H. Petersen, M. Bleicher and H. Stoecker, Phys. Lett. **B 676,** 126 (2009), [arXiv:0811.4077 [hep-ph]].

[27] J. Steinheimer, M. Bleicher, H. Petersen, S. Schramm, H. Stocker and D. Zschiesche, Phys. Rev. **C 77,** 034901 (2008), [arXiv:0710.0332 [nucl-th]].

[28] S. A. Bass *et al.*, Progr. Part. Nucl. Phys. **41,**255 (1998); Progr. Part. Nucl. Phys. **41,**225 (1998), [arXiv:nucl-th/9803035].

[29] M. Bleicher *et al.*, J. Phys. G. **25,** 1859 (1999), [arXiv:hep-ph/9909407].

[30] D. H. Rischke, S. Bernard and J. A. Maruhn, Nucl. Phys. **A 595,** 346 (1995), [arXiv:nucl-th/9504018].

[31] D. H. Rischke, Y. Pursun and J. A. Maruhn, Nucl. Phys. **A 595,** 383 (1995); **596**, 717 (1996), [arXiv:nucl-th/9504021].

[32] D. Zschiesche, S. Schramm, J. Schaffner-Bielich, H. Stoecker and W. Greiner, Phys. Lett. **B 547,** 7 (2002), [arXiv:nucl-th/0209022].

[33] H. Petersen, J. Steinheimer, G. Burau, M. Bleicher and H. Stocker, Phys. Rev. **C 78,** 044901 (2008), [arXiv:0806.1695 [nucl-th]].

[34] P. Braun-Munzinger and J. Stachel, J. Phys. G. **21,** L17 (1995), [arXiv:nucl-th/9412035].

[35] J. Schaffner-Bielich, R. Mattiello and H. Sorge, Phys. Rev. Lett. **84,** 4305 (2000), [arXiv:nucl-th/9908043].

7 Electromagnetic probes and chiral symmetry in dense QCD matter

Dileptons and photons provide a powerful penetrating probe of dense QCD matter. They have been extensively and productively used at RHIC and SPS. Because of the small electromagnetic interaction cross sections, dileptons and photons do not suffer from final state interactions even in a dense medium and deliver unique information about the properties of QCD matter throughout its space-time history. The thermal electromagnetic radiation reveals the temperature of the hot QCD matter. The studies of low-mass dileptons allow access to the properties of dense hadronic matter, and are sensitive to the restoration of chiral symmetry as discussed in this section. The top NICA energy $\sqrt{s_{\rm NN}}$ =11 GeV opens a way to investigate heavy-mass dileptons from J/ψ decays near the threshold. The density of baryons is known to affect the chiral symmetry restoration in a very significant way; therefore the study of electromagnetic probes at NICA energies where a very high baryon density will be achieved would be very valuable.

7.1 Low-mass dileptons at NICA

I. Tserruya

Weizmann Institute of Science, Rehovot, Israel

Dileptons (e^+e^- or $\mu^+\mu^-$ pairs) are an important and powerful tool to diagnose the hot and dense matter produced in relativistic heavy-ion collisions. They play a crucial role in the study of the Quark-Gluon Plasma, the state of matter predicted by lattice QCD numerical calculations and characterized by the deconfinement of quarks and gluons and the restoration of chiral symmetry, the latter being crucial to explore the generation of the hadron masses.

The interest in this probe was first emphasized by Shuryak [1]. Due to their large mean-free-path, dileptons do not suffer from final state interactions and once produced they can escape unaffected to the detector carrying information about the conditions and properties of the medium at the time of production.

The interest is in the detection of radiation emitted in the form of real or virtual photons by the medium in thermal equilibrium. Such radiation is a direct fingerprint of the matter formed. Two well distinct sources are considered:

The thermal radiation emitted by the QGP in the early phase of the collision through quark annihilation ($q\bar{q} \rightarrow l^+l^-$) serves as a proof of deconfinement and provides a direct measurement of the plasma temperature. Theory has singled out dileptons in the mass range $m_{l^+l^-} = (1-3)$ GeV/c^2 as the most appropriate window to observe the thermal radiation from the QGP phase. The challenge is to identify it.

The thermal radiation emitted by the high-density hadron gas in the later phase of the collision through pion annihilation ($\pi^+\pi^- \rightarrow \rho \rightarrow \gamma^* \rightarrow l^+l^-$) contributes primarily to the low-mass region, ($m_{l^+l^-} \leq 1$ GeV/c^2) around and below the ρ mass. This component must always be present since ultimately the system ends in the hadronic phase. It has been identified in the enhancement of low-mass dileptons discovered at the SPS in the mid-nineties primarily by the CERES experiment and later confirmed and studied with much higher precision by the NA60 experiment [2, 3].

The enhancement of low-mass dileptons triggered a huge theoretical activity stimulated mainly by interpretations based on in-medium modifications of the intermediate ρ meson with a possible link to chiral symmetry restoration (CSR). (For a recent theoretical review see [4]). The SPS results motivated also new experiments aiming at precise spectroscopic studies of the vector meson resonances, ρ, ω, and ϕ, to explore in-medium modifications of their spectral properties (mass and width). This topic is of interest in its own right and more so because these modifications could shed light into the behavior of the resonances close to the chiral restoration boundary. The ρ meson with its short lifetime, $\tau \sim 1.3$ fm/c, and its strong coupling to the $\pi\pi$ channel is best suited in this context, making it the most sensitive signal for in-medium modifications and the best probe for CSR. (For a recent review on the experimental results see [5]).

The physics potential of dileptons is confirmed by the wealth of interesting results obtained so far and by the relatively large number of experiments focusing on their study. The energy range covered by the planned NICA facility, $\sqrt{s_{\rm NN}} = (4-11)$ GeV, is unique in several respects. It fills a very important gap where no dilepton measurements exist, providing a crucial complement to the measurements at lower (DLS and HADES) and higher (SPS and RHIC) energies. This is a very promising energy range with considerable discovery potential.

All measurements of dileptons at high energies (SPS and RHIC) have revealed an enhancement with respect to the expected yield from hadronic sources, in particular an enhancement was observed at all SPS energies down to 40 AGeV. The DLS puzzle, referring to the enhancement of low-mass electron pairs originally reported by the DLS experiment at 1 – 2 AGeV, could be close to a solution with the recent HADES results on elementary p+p and p+d collisions indicating no enhancement of low-mass e^+e^- pairs in C+C collisions but rather a mere superposition of nucleon-nucleon collisions. There is no compelling evidence to invoke any new source of dileptons or any in-medium modification of the light vector mesons in this light system and at this low energy. This implies an onset of the low-mass dilepton enhancement somewhere in the energy range of 2 – 40 AGeV. It is interesting to note that this is almost the same energy range where the QCD critical point is being looked for. The NICA facility is thus ideally suited to search not only for the QCD critical point but also for the onset of the low-mass dilepton enhancement.

In the many-body approach of Rapp and Wambach [6] the mid-rapidity baryon density plays a crucial role in explaining the low-mass dilepton enhancement. The interpretation invokes pion annihilation $\pi^+\pi^- \to \rho \to \gamma^* \to l^+l^-$ with the intermediate ρ broadened by its scattering off baryons. The importance of baryons prompted the CERES experiment to perform a measurement of low-mass electron pairs at 40 AGeV. An enhancement was indeed observed but the experimental uncertainties were too high for a more elaborate analysis. In the energy range covered by NICA, the mid rapidity baryon density is expected to reach a maximum and thus the NICA facility will allow to measure low-mass dileptons under optimal conditions

Our present knowledge of the QCD phase diagram shows a critical end point at a baryon chemical potential of about $\mu_B = 400$ MeV with a smooth cross over at lower values and a first order phase transition at larger values. Again NICA's planned energy range is ideally suited to explore this region.

7.2 Dileptons at NICA

K. Gudima[a] and V. Toneev[b]

[a] *Institute of Applied Physics, Cishineu, Repubica of Moldova;*
[b] *Joint Institute for Nuclear Research, Dubna, Russia*

Due to weak interaction, dileptons play an exceptional role among different probes providing information on a state of highly compressed and hot nuclear matter formed in relativistic heavy ion collisions. Generally, a dilepton yield depends on both global properties of matter constituents (hadrons and/or quarks, gluons) defined by the equation of state and individual constituent properties related to their in-medium modification. The analysis of the e^+e^- invariant mass spectra from central Pb + Au collisions at the bombarding energy $E_{\rm lab} = 158$ AGeV, measured by the CERES Collaboration, for certain shows an excess radiation in the range of invariant dilepton masses $0.2 \lesssim M \lesssim 0.7$ GeV. Observation of an enhancement of the dilepton rates - at low invariant masses - due to in-medium changes of the vector meson spectral functions as a signal of chiral symmetry restoration in the hot and dense matter. Various scenarios of hadron modification were proposed. However, low statistics, insufficient mass resolution, and large signal/background ratio in the CERES experiments did not allow one to discriminate these scenarios, in particular those based on the Brown-Rho scaling hypothesis [7] assuming a dropping ρ mass and on a strong broadening as found in the many-body approach by Rapp and Wambach [6].

However, recent highly precise NA60 [3] results for $\mu^+\mu^-$ pair production in In+In (158 AGeV) collisions have showed a good agreement with Rapp's theoretical predictions within the many-body approach but do not confirm the expected dropping mass scenario of Brown and Rho. We hope that dimuon measurements in the NICA energy range may clarify this situation.

The main Brown-Rho objection to this interpretation is the validity of the vector dominance. In more general theory of the hidden chiral symmetry [8] the vector dominance is valid only at small temperature while in the measured In-In collisions mainly high-temperature states are populated [9].

In Fig. 7.1 the dimuon invariant mass distributions are presented for two limiting energies of colliding Au ions. These spectra are calculated within the Quark-Gluon String Model [10, 11, 12] with applying the NICA acceptance. Contributions of channels which are taken into account are shown in figure. Note that no in-medium effects are implemented in these calculations. About 90% of ρ-mesons decay inside the interacting system and therefore should undergo medium influence. Thus, these results may be considered as a reference point for future analysis of muon data.

We expect that at $\sqrt{s_{\rm NN}}$ =11 GeV the broadening of ρ-meson spectral function and an enhancement of the

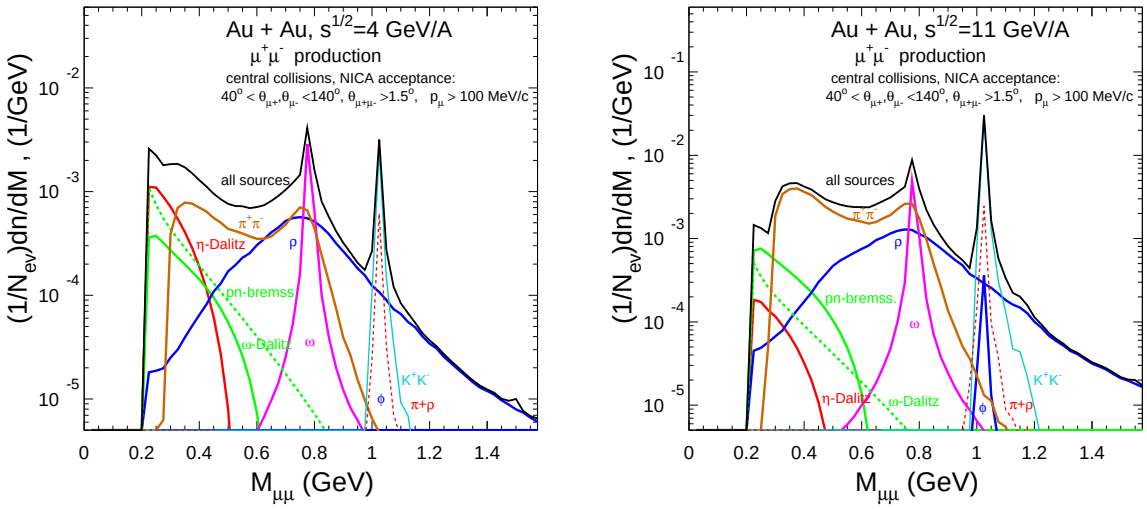

Figure 7.1: Invariant mass spectra of $\mu^+\mu^-$ pairs created in central Au+Au collisions at $\sqrt{s_{\rm NN}}$ = 4 and 11 GeV. Contributions of different dimiuon sources are plotted. The NICA acceptance used is shown in figures.

dilepton rates at low invariant masses, similarly to the case of In - In (158 AGeV) collision, should be observed. But at $\sqrt{s}_{\rm NN}$ =4 GeV the temperature of populated states will be essentially lower and there is a chance for manifestation of the dropping mass scenario as a direct signal of the partial chiral symmetry restoration.

7.3 Electromagnetic probes on NICA

Kh. Abraamyan and A. Friesen

Joint Institute for Nuclear Research, Dubna, Russia

Diphoton production

The two-photon decay of light mesons represents an important source of information. In particular, the $\gamma\gamma$ decay of light scalar mesons was considered as a possible tool to deduce their nature. Also the scalar-isoscalar sector is question at issue presently, since more states are known (including possible glueball candidates) than can be fitted into a single multiplet. Unfortunately, the existing experimental information from $\pi\pi$ scattering has many conflicting data sets at intermediate energies and no data at all close to the interesting threshold region. For many years this fact has made very hard to obtained conclusive results on $\pi\pi$ scattering at low energies or in the sigma region. Interest in the investigation of the photon pair production is bound up with a set of problem:

- To clarify the nature and further investigations of the resonance observed in the invariant mass spectrum of $\gamma\gamma$-pairs in dC-interactions at 2.75 GeV/c per nucleon and dCu-interactions at 3.83 GeV/c per nucleon (see Fig. 7.2) [13].
- To search for some features in the invariant mass spectrum of $\gamma\gamma$-pairs in the interval of 270 – 750 MeV bounding up with the chiral symmetry restoration [14].
- Due to hidden strangeness of η-mesons ($s\overline{s}$ component), comparison η and π^0-productions allows to clarify the mesons production mechanism. The indication on the difference between π^0- and η-mesons production mechanisms was obtained from the comparison of the mesons spectra in the near-threshold region (the PHOTON-2 experiments [15]).

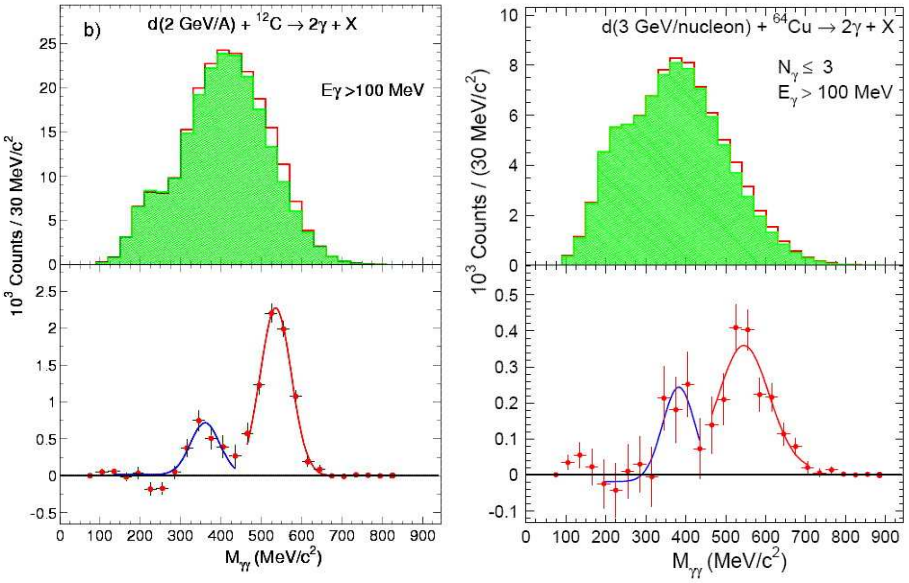

Figure 7.2: Invariant mass distributions of $\gamma\gamma$ pairs without (upper panels) and with (bottom panels) the background subtraction. The left and right figures are obtained for the dC- and dCu-interactions at 2.75 GeV/c and 3.83 GeV/c per nucleon respectively. The curves are the Gaussian approximation of experimental points.

- Investigations of π^0-mesons is of interest in view of the NICA possibilities. The scan of the π^0 spectra in the nuclear-nuclear collision allows one to detect signals of the π-condensate state: the pion vacuum breaking at the strong QCD field in dense nuclear matter.

The NICA advantages

The collider NICA allows one to scan the energy and mass dependence of the resonance production in ion collisions.

To solve above problems a calorimeter with large acceptance and high resolution is needed (in consisting of MPD or as a separate setup), our investigations show that the hexagonal crystal calorimeter meets the requirements. The increasing of the calorimeter acceptance allows to study the invariant mass spectra of $\gamma\gamma$ pairs in a wide range at different energies and transverse momenta of pairs (that means different production mechanisms).

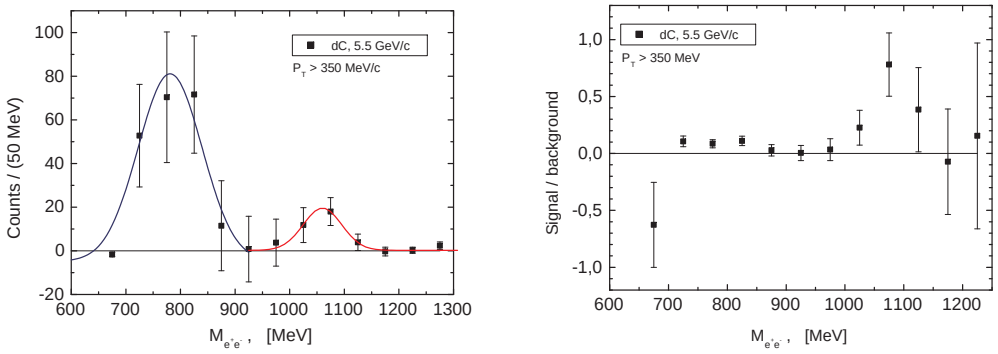

Figure 7.3: Invariant mass distributions of e^+e^- pairs after the background subtraction (left) and signal to background ratio in the reaction $d + C \to e^+e^- + X$ at 2.75 GeV/c per nucleon (right). The curves are the Gaussian approximation of experimental points.

Dilepton production

A possibility of vector mesons detection by e^+e^--decay is shown in Fig. 7.3. The experiment was carried out on the internal Nuclotron beam by the multichannel lead-glass calorimeter with the hexagonal prism modules with length 14 R.L. and the inscribed circle diameter 17.5cm. Emission angles of $e^+(e^-)$ are in the range $20^\circ \div 30^\circ$, opening angles of e^+e^- pairs are $42^\circ \div 66^\circ$. These parameters can be useful for determination of the optimal calorimeter configuration.

7.4 Solving the problem of anomalous J/ψ suppression at NICA MPD

A.B.Kurepin and N.S.Topilskaya

Institute Nuclear Physics, Troizk, Russia

The dissociation of heavy quark resonances by colour Debye screening in a deconfined nuclear matter [16] is one of the possible signature of Quark Gluon Plasma formation in high energy heavy ion collisions.

The absorption of charmonia states at its passing through the ordinary nuclear matter was found by mass dependence in proton-nucleus collisions at the CERN SPS in the NA38 experiment [17]. However in lead-lead collisions an additional anomalous absorption was observed by the NA50 experiment [18, 19] and proposed that it is due to the colour screening in the compressed nuclear matter. Later in some theoretical models the NA50 data were interpreted as the results of charmonia and comover interactions in cold nuclear matter.

However, the experimental results obtained at SPS for indium-indium collisions by the NA60 experiment [20] and at RHIC for gold-gold collisions [21] have shown that the problem is much more complicated.

The amount of anomalous suppression depends on the value of normal absorption. A suppression of J/ψ production (decreasing of J/ψ production cross section per nucleon with increasing the atomic number A) was observed by the NA38 experiment in pA-collisions and in collisions of light ions up to S – U collisions at 200 GeV per nucleon. The results of this experiment were explained by normal nuclear absorption of pre-resonance $c\bar{c}$-state in nuclear matter [17, 22]. The cross section for the absorption process, $\sigma_{\rm abs}$, was the same for all nuclei within the range of errors.

The NA50 experiment measured the charmonium production in Pb + Pb collisions at 158 GeV per nucleon [18, 19] and in proton-nucleus collisions at 400 and 450 GeV [23, 24, 25]. The normal suppression of J/ψ in proton- nucleus reactions and "anomalous" enhanced suppression was observed in central lead-lead collisions. The suppression grows with increasing centrality. The value of normal nuclear absorption of J/ψ per nucleon was obtained from analysis of proton-nucleus data at 400 and 450 GeV assuming a weak energy dependence and in terms of the Glauber model the value of $\sigma_{\rm abs}$ was 4.2 0.5 mb.

However the recent measurements of pA-collisions at 400 and 158 GeV in the NA60 experiment shows that the energy dependence of $\sigma_{\rm abs}$ is not weak and that it is very important to measure charmonium production in $p+p$, p + A and A + A collisions in the same kinematical domain. The values $\sigma_{\rm abs}(400\ GeV) = 4.3\pm0.8\pm0.6$ mb is in agreement with NA50 results but the appropriatwe value at low energy is different $\sigma_{\rm abs}(158\ GeV) = 7.6\pm0.7\pm0.6$ mb. The In + In collisions measured in the NA60 experiment at 158 GeV per nucleon show small "anomalous" J/ψ suppression $< 10\%$ for central In + In events with this new value of $\sigma_{\rm abs}(158\ GeV)$, while for central Pb + Pb collisions "anomalous" suppression is still near 30%. If anti-shadowing effect (which is very model dependent and previously considered to be important only at high parton density conditions) of EKS model in In + In and Pb + Pb collisions is taken into account. Practically normal, cold nuclear matter J/ψ suppression in In + In collisions and still "anomalous" J/ψ suppression is observed in the most central Pb + Pb collisions [26].

Recent PHENIX experiment at RHIC observed J/ψ suppression in Au + Au and Cu + Cu collisions at $\sqrt{s_{\rm NN}}$ =200 GeV in nucleon-nucleon center-of-mass system [21, 27]. At these energies the results show that the J/ψ suppression at mid-rapidity is of the same order as the suppression at SPS energies for Pb + Pb and is the same for different systems at RHIC. But for forward rapidity range the suppression is stronger.

There are no theoretical models which could explain all the data. Different energy intervals between AGS, SPS, RHIC and LHC are very important to study the mechanism of quarkonium production and suppression, to investigate medium effects and conditions of Quark Gluon Plasma formation.

It is not clear if this problem could be solved at LHC energies, since the multiple charmed production could compensate the effect of color screening. Therefore we can assume that the explanation of anomalous charmonia states suppression could be found at lower energies. It is planned for SIS300 at FAIR, but it is not possible at SIS100 where for heavy ion experiments charmonia production is below threshold.

In conclusion, the measurements of charmonia states production are very important at MPD NICA where the appearance of mixed phase is expected. Although it is not easy to obtain the proton-nuclei data in the collider experiment, the problem could be solved by measurements of the energy dependence for charmonia production in heavy ions collisions at different centralities. The strong effect could be seen near the critical point.

7.5 Low energy J/ψ-hadron interactions

H. Satz

Fakultät für Physik, Universität Bielefeld, Germany

The suppression of J/ψ production has been proposed as a signal for the deconfinement of the medium produced in high energy nuclear collisions [16]. This implies that collisions in a confined thermal medium, i.e., in matter consisting of mesons of thermal momenta, cannot dissociate a J/ψ. To make such considerations quantitative, one first has to calculate the cross-section for the gluon-dissociation of a J/ψ , a QCD analogue of the photo-effect. This can be carried out using the operator product expansion [28, 29], and the result is

$$\sigma_{g-J/\psi} \simeq \frac{1}{m_c^2} \frac{(k/\Delta E_\psi - 1)^{3/2}}{(k/\Delta E_\psi)^5} \ , \tag{7.1}$$

where $\Delta E_{J/\psi} = 2M_D - M_\psi$, k denotes the gluon momentum and m_c the charm quark mass. The corresponding cross-section for the hadron dissociation is then obtained by convoluting the gluon-dissociation cross-section (7.1) with the hadronic gluon distribution function $g(x)$, which for J/ψ -meson interactions leads to

$$\sigma_{g-J/\psi} \simeq \sigma_{\rm geom}(1 - \lambda_0/\lambda)^{5.5} \tag{7.2}$$

with $\lambda \simeq (s - M_\psi^2)/M_\psi$ and $\lambda_0 \simeq (M_{\rm h} + \Delta E_\psi)$. Here $\sigma_{\rm geom} = \pi r_{J/\psi}^2 \simeq 2$ mb is the geometric J/ψ cross-section and $M_{\rm h}$ denotes the mass of the incident meson. In Fig. 7.4, we compare the two dissociation cross-sections (7.1) and (7.2) as function of the incident and pion momentum, respectively.

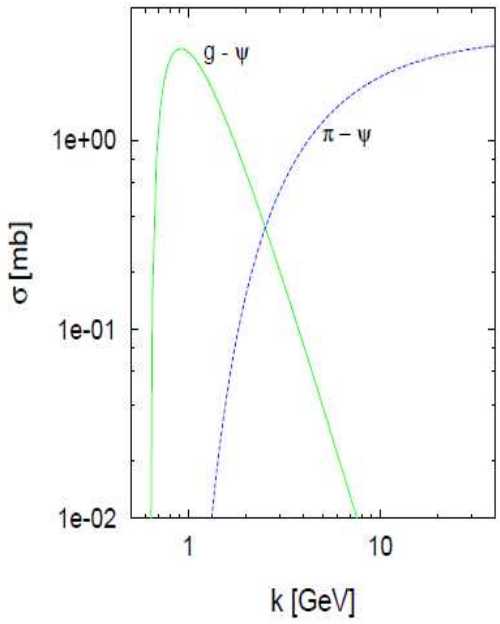

Figure 7.4: Gluon and hadron J/ψ dissociation cross-sections [29].

This result shows that typical thermal gluon momenta near 1 GeV produce a large dissociation cross-section, whereas hadron momenta in a thermal range (up to 1 – 2 GeV) still lead to a vanishingly small cross-section. In other words, the J/ψ should survive in confining media. This assertion is testable experimentally, by studying if slow charmonia in normal nuclear matter suffer significant dissociation.

Such experiments have been proposed for the CERN-SPS [30], but were never carried out, since they would have required major re-arrangements of the NA50 set-up. Studies at Fermilab and at HERA-B do provide some first hints that the inelastic J/ψ -nucleon cross-section indeed decreases for the slowest J/ψ's in nuclear matter accessible there [27].

The argumentation presented so far was based on OPE calculations [28, 29], which become exact in the large quark mass limit $m_{\rm q} \to \infty$. It is not clear if the charm quark mass really satisfies this condition, and so the dissociation cross section in J/ψ-hadron collisions has been discussed in other approaches, in particular on the basis of meson exchange reactions, leading to much larger values [31, 32]. A possible threshold enhancement has also been discussed. A conclusive experimental study would therefore provide important basic information.

7.6 J/ψ production in high energy nuclear collisions

P. Zhuang

Physics Department, Tsinghua University, Beijing, China

In 1986, Matsui and Satz [16] proposed J/ψ suppression as a signature for the deconfinement phase transition in relativistic heavy-ion collisions. Since the mass of heavy quarks (charm and bottom) is much larger than typical secondary (thermal) excitations of the system created in nuclear collisions, $m_{\rm c,b} \gg T$, they are mainly produced through initial hard processes. Therefore, the background for theoretically calculating heavy flavor production is rather solid and the study of J/ψ production can yield important information on the properties of the quark-gluon plasma (QGP) formed in the early stage of nuclear collisions.

Since $c\bar{c}$ pairs are created via hard processes, the J/ψ yield in p + A collisions should be proportional to the number of binary nucleon-nucleon interactions. However, from the experimental findings in p + A and light nuclear collisions, there exists already J/ψ suppression, the so-called "normal" nuclear suppression induced by multiple scattering between J/ψ (or its pre-resonance state) and spectator nucleons. In addition to the nuclear absorption, the primordially produced charmonia suffer an "anomalous" suppression when they pass though the hot and dense medium created in heavy-ion collisions [33, 34].

The number of charm quarks created in the initial stage of heavy-ion collision increases substantially with collision energy. While a small production of charm quarks at SPS energy is expected (about ∼0.2 in central Pb + Pb), there are more than 10 $c\bar{c}$ pairs produced in a central Au + Au collision at RHIC (at $\sqrt{s_{\rm NN}}$ =0.2 TeV), and the number is probably over 200 in heavy-ion collisions at LHC (at $\sqrt{s_{\rm NN}}$ = 5.4 TeV). The large number of uncorrelated $c\bar{c}$ pairs in the QGP can recombine to form charmonia (primarily J/ψ's). Obviously, this regeneration will enhance the J/ψ yield, and the momentum spectra of the total final state J/ψ's may be quite different from the one with only initial production. The J/ψ initial production, continuous regeneration, nuclear absorption and anomalous suppression are schematically illustrated in Fig. 7.5.

Normal and anomalous suppression

Proton-nucleus p + A collisions are believed to be a good measure of normal (nuclear) J/ψ suppression. Suppose the projectile proton collides with a nucleon at $(\mathbf{b}; z)$ (characterizing the transverse and longitudinal positions) in the target nucleus and produces a J/ψ or its pre-resonant state on a very short time scale. On its way out the nucleus, the produced J/ψ collides inelastically with spectators. From the comparison with the SPS data, the average nuclear absorption cross section at SPS energy is extracted at $\sigma_{\rm abs} = 6.5 \pm 1.0$ mb, similar for both J/ψ and J/ψ'. The inelastic J/ψ+nucleon cross section (3.5±0.8 mb) is significantly less than the above value, and the inelastic cross section for ψ' is almost four times the value for J/ψ. The most recent analysis of NA50 data exhibits some of this trend, with $\sigma_{\rm abs} = 4.1 \pm 0.5$ mb and 8.2± 1.0 mb for the J/ψ and ψ', respectively. This indicates that the $c\bar{c}$ states suffering from nuclear absorption have already (at least partially) evolved into their final states, even tough the role of pre-resonant states could still be present.

Note that the effect of nuclear absorption depends strongly on the passing time $d_t = 2R_{\rm A} = sinh\ Y_{\rm B}$ of the two colliding nuclei, where $R_{\rm A}$ is the radius of the nuclei and $Y_{\rm B}$ is their rapidity in the center-of-mass frame. While at SPS energy the collision time is about 1 fm/c and normal suppression is large, the cold nuclear matter effect in extremely high-energy nuclear collisions should be small, due to the small collision time, e.g., $d_t \sim 0.1$

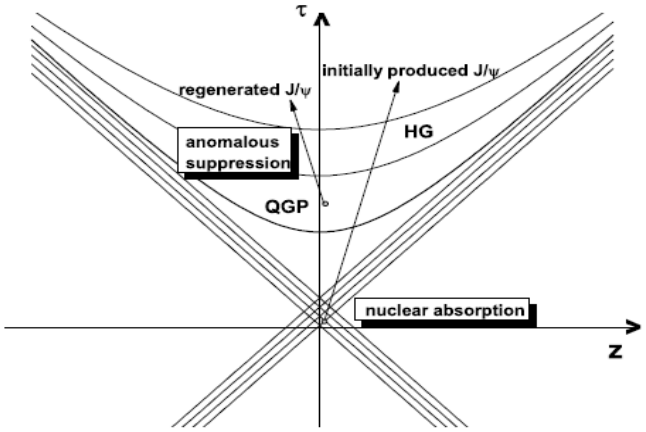

Figure 7.5: A schematic illustration of J/ψ production and suppression in relativistic heavy ion collisions.

fm/c at RHIC and 1/200 fm/c at LHC.

While the nuclear absorption mechanism can well account for the experimental data in p + A and light nuclear collision systems at SPS energy, the experiments with heavy nuclear projectile and target (Pb + Pb and In + In) show that the suppression of J/ψ (and ψ') in semi-/central collisions goes well beyond normal nuclear absorption [35], see Fig. 7.6. This phenomenon, called "anomalous" J/ψ suppression, is considered as one of the most important experimental results in relativistic heavy-ion collisions at SPS. Various theoretical approaches have been put forward to explain the anomalous suppression [36, 37, 29, 38, 39, 40].

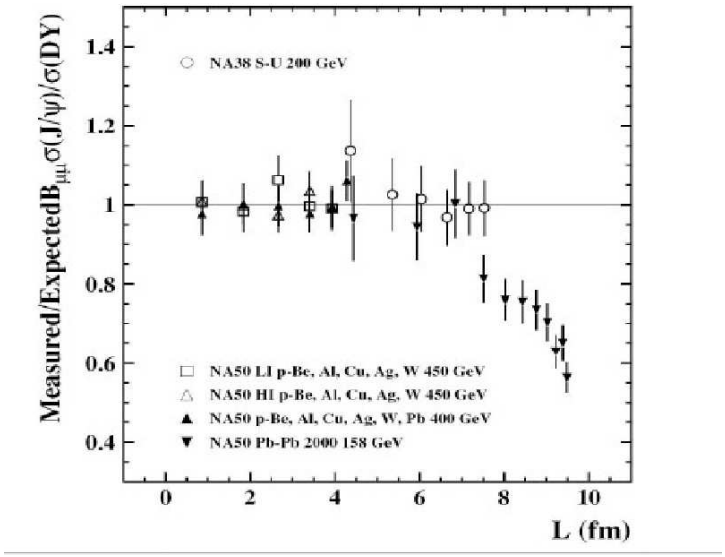

Figure 7.6: The J/ψ anomalous suppression at SPS energy. The figure is taken from Ref.[35].

The first mechanism is based on the original prediction of Matsui and Satz [16]: the Debye screening effect in the QCD medium created in the early stage of nuclear collisions leads to J/ψ melting. The properties of the charmonium states in QGP and in vacuum are very different. In particular, it is currently an open question whether the free energy, $F = U - TS$, or the internal energy is the appropriate quantity to be identified with a heavy-quark potential suitable for use in Schrödinger or Lippmann-Schwinger equation. In any case, due to the weakening of the potential with increasing temperature, the resonant states of $c\bar{c}$ dissociate at some Mott temperature $T_{\rm d}$. If the maximum temperature of the medium produced in heavy nuclear collisions

reaches the Mott temperature, the Debye screening effect results in the anomalous charmonium suppression. Recent lattice calculations of charmonium spectral functions in the deconfined phase suggest that the J/ψ can survive up to temperatures of $T_{\rm d} \simeq 1.6. - 2T_c$ (T_c: critical temperature of the deconfined phase transition), while the excited states ψ' and χ_c disappear around T_c. Employing the heavy-quark potential extracted from the lattice calculation, the potential models generally support the above results from the spectral function analysis, even though no quantitative conclusions on the dissociation temperatures have been reached yet. A common conclusion from the lattice-based calculations is that, different charmonium states correspond to different dissociation temperatures. This leads to the sequential dissociation model of describing anomalous charmonium suppression: With continuously increasing temperature of the fireball, ψ' will melt first, then χ_c dissociate and finally J/ψ disappears. Considering the fact that about 40% of the final state J/ψ's originate from the decay of ψ' and χ_c in $p+p$ and p + A collisions, the anomalous J/ψ suppression in Pb + Pb collisions at SPS is associated with the dissociation of ψ' and χ_c in the produced fireball. A precise measurement on ψ' and especially on χ_c yield in the future can help to check the sequential model. Along similar lines, J/ψ suppression in hot and dense medium has been described in a general threshold model without considering microscopic dynamics. In the hot and dense part of the fireball where the density of the system $n_{\rm p}$ is larger than a critical value n_c, all the J/ψ's are absorbed by the matter, and those J/ψ's outside the region suffer only normal suppression. The threshold density n_c in this model is a parameter, e.g., taken as the maximum $n_{\rm p}$ in S+U collisions at SPS (where no anomalous suppression is observed). If the matter with $n_{\rm p} > n_c$ is QGP, the critical density n_c can be considered as the threshold value to create QGP.

The above analysis based on the Debye screening effect is typically based on the simplifying assumption of a constant temperature in connection with a sharp transition of the inelastic charmonium widths from zero (stable below $T_{\rm d}$) to infinity (dissolved above $T_{\rm d}$). However, the volume of the produced fireball in relativistic heavy ion collisions is relatively small and expands rapidly, implying rather fast temperature changes and short fireball lifetimes. In this case, the conclusion from the static Debye screening effect may deviate from the real system, and it becomes essential to include the concrete interactions between partons and charmonia, leading to sizable inelastic reaction rates comparable to the fireball expansion (or cooling) rate. In particular, the charmonia can be destroyed below the dissociation temperature. Debye screening is still operative, by controlling the binding energy which in turn determines the phase space (and thus the width) of the dynamic dissociation reactions. An important such process in the QGP is the (leading-order) gluon dissociation process $g + J/\psi \to c + \bar{c}$, an analogy to the photon dissociation process of electromagnetic bound states. For small binding energies (i.e., when approaching the dissociation temperature), the phase space for gluon dissociation shrinks and next-to-leading order (NLO) processes take over, most notably inelastic parton scattering $g(q,\bar{q}) + J/\psi \to g(q,\bar{q}) + c + \bar{c}$. Not only partons in the deconfined phase can induce anomalous suppression, but also the secondary particles like π, ρ and ω (so-called as comovers) in a hot and dense hadron gas can interact with charmonia inelastically and cause J/ψ suppression. The cross section $\sigma_{\rm co}$ is an adjustable parameter in the calculation. In some calculations the comover densities turn out to be rather high, corresponding to energy densities well above the critical one computed in lattice QCD. Consequently, the pertinent comover-interaction cross section assumes rather small values, e.g., $\sigma_{\rm co}$ =0.65 mb, which are more suitably interpreted as partonic comover interactions.

A more detailed description of the matter evolution together with a dynamical treatment of the interactions between charmonia and comovers has been carried out in the hadronic transport models UrQMD and HSD where the J/ψ motion is traced microscopically throughout the medium. The charmonium-hadron cross sections, however, remain input parameters to these models. Alternatively, one may employ theoretical calculations of charmonium dissociation cross sections with light mesons, as computed in either quark or hadronic models. By adjusting the comover cross sections (and possibly other parameters, such as formation times), interactions at the hadron level can reproduce the SPS data of J/ψ suppression.

Motivated by the lattice QCD findings of surviving J/ψ bound states well above T_c, recent work has treated the formation and evolution of $c - \bar{c}$ correlations more microscopically. In a weakly coupled QGP (wQGP), charm quarks would fly away from each other as soon as enough energy is available, while in a strongly coupled QGP (sQGP), the strong attraction between quarks, as well as their small diffusion constant in the sQGP, opens the possibility of returning to the J/ψ ground state, leading to a substantial increase in survival probability. The charm-quark motion in the medium is described by a Langevin equation. For strongly coupled matter, the drag coeffcient characterizing the thermalization of charm quarks in the medium is large. Taking the internal energy as the heavy-quark potential (extracted from a lattice-QCD computed free energy, the survival probability of charmonia in sQGP is larger than that in wQGP. This explains why there is no large difference

between suppressions at SPS and RHIC. When using effective potentials which are identified with the free energy, F, or a linear combination the internal energy U and F, the charmonium binding is less pronounced leading to dissociation temperatures (i.e., zero binding) below 1.5 T_c even for the J/ψ, as compared to above 2 T_c when employing U. We also recall that a small charm diffusion constant can be obtained from elastic c-quark interactions based on the internal energy as a potential.

Transverse momentum distributions

All models for inclusive J/ψ yields – with and without the assumption of a QGP and with and without regeneration mechanism – describe the observed suppression after at least one parameter is adjusted. Transverse momentum distribution may depend more directly on the production and regeneration mechanisms and therefore contain additional information about the nature of the medium and J/ψ, thus helping to distinguish between different scenarios.

Anomalous suppression is not an instantaneous process, but takes a certain time depending on the mechanism. During this time the produced charmonia with high transverse momentum may "leak" out the parton/hadron plasma and escape suppression. As a consequence, low p_t charmonia are more likely to be absorbed, and consequently the average transverse momentum of the observed charmonia will show an increase which grows monotonically with the average lifetime of the plasma. A self-consistent way to incorporate the effect of leakage into the various models is through charmonium transport equation in phase space [41].

The medium created in high energy nuclear collisions evolves dynamically. In order to extract information about the medium by analyzing the J/ψ distributions, both the hot and dense medium and the J/ψ production processes must be treated dynamically. Due to its large mass, the J/ψ is unlikely fully thermalized with the medium.Thus its phase space distribution should be governed by transport equation including both initial production (incl. anomalous suppression) as well as regeneration. The charmonium distribution function, $f_\Psi(\mathbf{p}_t;\mathbf{x}_t;\tau|\mathbf{b})$ $(\Psi = J/\psi;\psi';\chi_c)$, in the central rapidity region and in the transverse phase space, $(\mathbf{p}_t;\mathbf{x}_t)$, at fixed impact parameter $\mathbf{b}$ is controlled by the classical Boltzmann transport equation

$$\frac{\partial f_\Psi}{\partial \tau} + \mathbf{v}\nabla f_\Psi = -\alpha_\Psi f_\Psi + \beta_\Psi \ .$$

The second term on the left-hand side arises from free streaming of Ψ with transverse velocity $\mathbf{v}_\Psi = \mathbf{p}_t/\sqrt{\mathbf{p}_t^2 + m_\Psi^2}$ which leads to the leakage effect. The anomalous suppression and regeneration mechanisms are reflected in the loss term α_Ψ and gain term β_Ψ, respectively. It is assumed that the medium locally equilibrates at time τ_0 after nuclear absorption of the initially produced J/ψ's has ceased. The latter effect can be included in the initial distribution, $f_\Psi(\mathbf{p}_t;\mathbf{x}_t;\tau_0|\mathbf{b})$, of the transport equation.

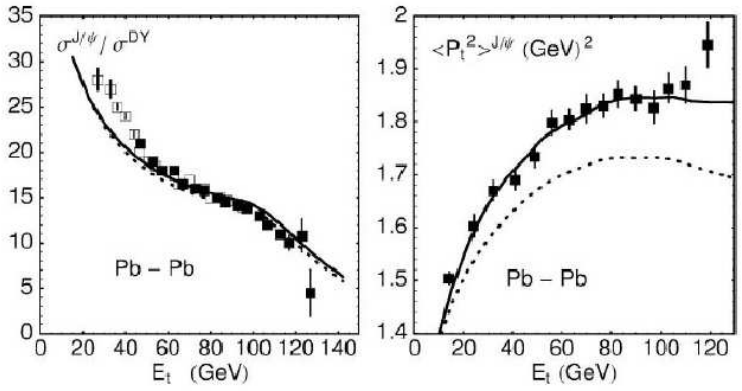

Figure 7.7: The J/ψ suppression and $< \mathbf{p}_t^2 >$ for J/ψ in Pb+Pb collisions at SPS as functions of transverse energy E_t. The dotted and solid lines are calculated in terms of comover model without and with considering the leakage effect, respectively. The figure is taken from Ref. [41].

When the loss and gain terms are known, the transport equation can be solved analytically with the result

$$f_\Psi(\mathbf{p}_t;\mathbf{x}_t;\tau_0|\mathbf{b}) = f_\Psi(\mathbf{p}_t;\mathbf{x}_t-\mathbf{v}(\tau-\tau_0);\tau_0|\mathbf{b})\ e^{\int_{\tau_0}^{\tau} d\tau' \alpha_\Psi(\mathbf{p}_t;\mathbf{x}_t-\mathbf{v}(\tau-\tau');\tau'|\mathbf{b})} + \int_{\tau_0}^{\tau} d\tau' \beta_\Psi(\mathbf{p}_t;\mathbf{x}_t-\mathbf{v}(\tau-\tau');\tau'|\mathbf{b})\ e^{\int_{\tau}^{\prime\tau} d\tau'' \alpha_\Psi(\mathbf{p}_t;\mathbf{x}_t-\mathbf{v}(\tau-\tau'');\tau''|\mathbf{b})}\ .$$

The first and second terms on the right-hand side indicate the contribution from initial production and continuous regeneration, respectively. Both suffer anomalous suppression. The coordinate shift $\mathbf{x}_t \to \mathbf{x}_t - \mathbf{v}_\Psi \Delta\tau$ reflects the leakage effect during the time period $\Delta\tau$.

At SPS energy regeneration can be neglected by setting $\beta_\Psi = 0$. In the comover-interaction model for the suppression mechanism, the J/ψ suppression and averaged transverse momentum $< \mathbf{p}_t^2 >$ are shown in Fig. 7.7. The calculation without leakage, obtained by setting $\mathbf{v}_/Psi = 0$, does not fit the data for $< \mathbf{p}_t^2 >$, even in the domain of low transverse energy, E_t (which in the NA50 experiment is used as a measure of centrality). Only when the leakage effect is taken into account, the calculation agrees well with the data. Since only high-pt charmonia are sensitive to the leakage effect, and since they are only a small fraction of the inclusive yield, both calculations with and without leakage can fit the J/ψ yield very well. The leakage effect on the transverse-momentum distribution is not sensitive to the underlying mechanism; the calculation with the threshold model as the suppression mechanism gives a similar structure of $< \mathbf{p}_t^2 >$ for J/ψ.

Charmonia in heavy-ion collisions at low energies

While in heavy-ion collisions at RHIC and LHC the formed medium is characterized by high temperatures and low (net) baryon densities, at relatively low energies, such as at NICA, highly compressed baryon matter at low temperature is anticipated. Monte Carlo simulations indicate the maximum energy and baryon density in a central Au + Au collision at NICA energy to reach $\varepsilon \sim 5$ GeV/fm^3 and $\rho/\rho_0 \sim 8$. In the following, we will give a qualitative discussion of some of the trends one might expect in the FAIR energy regime, based on the experimental and theoretical lessons at higher energies as discussed above.

Normal vs. Anomalous Suppression.

At low energies, regeneration in both the partonic and hadronic medium is expected to be small and the initial production will dominate the charmonium yield. Normal nuclear absorption of the directly produced charmonia is in the time period $t < t_{\rm d}$. At RHIC and LHC energies, where the collision time $t_{\rm d}$ is small and the lifetime of the partonic medium large, nuclear absorption is not a dominant factor, compared to anomalous suppression. However, at low energies, where the collision time $t_{\rm d}$ is much longer and the lifetime of partonic medium is much shorter, nuclear absorption becomes important, possibly the dominant effect. It has even been argued that heavy quark re-scattering in a cold nuclear medium can fully account for the observed J/ψ suppression in Pb+Pb collisions at SPS energy, without considering further suppression in the hot medium created in the later expansion stages.

Transverse-Momentum Spectra.

In comparison with the regenerated charmonia in the medium, the initially produced charmonia through hard processes have larger transverse momentum. At RHIC, the superposition of initial production and regeneration for J/ψ's leads to a roughly constant (or even slightly decreasing) average transverse momentum squared, $< \mathbf{p}_t^2 >$, with centrality. However, at NICA energy, the $< \mathbf{p}_t^2 >$ of the J/ψ's (dominated by initial production) should increase with centrality, due to the Cronin effect, i.e., the initial multiple scattering of gluons with nucleons (prior to the hard scattering leading to charmonium production).

Formation Time Effects.

The time for the medium created in heavy ion collisions to reach thermal equilibrium is short at high energies, about 0.5 fm/c at RHIC and 0.1 fm/c at LHC, and long at low energies, at least 1 fm/c at NICA (the time for full nuclear overlap is already $\sim$1.5 fm/c). Considering a finite formation time of charmonia, about 0.5 fm/c, J/ψ's are easily dissociated in the hot medium at RHIC and LHC, but might survive in the medium at low energies. Since charmonia are difficult to be thermalized at low energies, their elliptic flow at FAIR will be smaller than that at RHIC and LHC. Charmonia studies at NICA may also present a possible way to distinguish different scenarios of J/ψ suppression. For instance, when after adjusting the suppression at SPS energy, the suppression at NICA by comovers will be stronger than that by threshold melting; in addition, for the ψ/ψ' ratio, the comover scenario predicts a smooth excitation function, contrary to a step-like structure for threshold melting.

Medium Effects.

It is widely believed that chiral symmetry governs the low-energy properties and dynamics of hadrons in the vacuum and at finite temperature and density. The chiral symmetry restoration transition at high temperature (small baryon density) is a crossover, while it presumably becomes a first order phase transition at high density. Both the QCD sum rules analysis and the LO perturbative QCD calculations show that the J/ψ mass is reduced in nuclear matter due to the reduction of the gluon condensate. At SPS energy, chiral symmetry restoration reduces the threshold for charmonium break-up and could lead to a step-like behavior of the reaction rate, as suggested to account for the anomalous J/ψ suppression. The study of the ratio ψ/ψ' at SPS shows the importance of the hadronic phase for ψ' interactions, possibly related to the effect of chiral symmetry restoration. Another high density effect is the Friedel oscillation in the single-particle potential induced by a sharp Fermi surface at low temperature, which is widely discussed in nuclear matter and quark matter. The heavy-quark potential at zero baryon density, decreases monotonously with increasing temperature. In the compressed baryon matter, however, the potential may oscillate and approach the weak coupling limit very slowly. This could imply that J/ψ's survive in a wide region of high densities.

Charmed Baryons.

The importance of charmed baryons at low energies has been recently discussed. While the J/ψ and ψ' yields relative to the total number of $c\bar{c}$ pairs are roughly independent on colliding energy over a wide region from NICA to RHIC, the relative yield for charmed baryon Λ_c decreases strongly with increasing energy, exceeding the yield of D mesons at the low-energy end. This indicates that the investigation of open-charm production at low energies mandates the inclusion of charmed baryons.

7.7 Soft photons at NICA

V. V. Avdeichikov[a], E. S. Kokoulina[a,b], A. Ya. Kutov[c], V. A. Nikitin[a], I. A. Rufanov[a]

[a] *Joint Institute for Nuclear Research, Dubna, Russia;*
[b] *Gomel State Technical University, Gomel, Republic of Belarus*;
[c] *Komi SC UrD RAS, Syktyvkar, Russia.*

Experimental and theoretical studies of direct photon production in hadronic collisions essentially expand our insights about multiparticle production mechanisms [42, 43, 44]. These photons are useful probes to investigate nuclear matter at all stages of the interaction. Soft photons (SP) play a particular role in these studies. Until now we have no explanation for the experimentally observed excess SP yield. These photons have low energy transverse momenta $p_T < 0.1$ GeV/c, $|x|$ <0.01 [45, 46, 47, 48]. In this domain their yield exceeds the theoretical estimates by 5 – 8 times.

For a qualitative explanation of this effect the assumption of the formation of a cold spot of quark gluon plasma (QGP) or hadronic gas has been made in a number of theoretical papers [49, 50, 51]. It is argued that a cold spot is relatively stable and radiates soft photons. SP testify the existence of a new phenomenon connected with the collective behavior of particles [52]. One interesting option currently under discussion is the formation of a pionic condensate when a group of pions with small relative momenta can form a relatively coherent and stable system. It is known from phase shift analysis of low energy pion scattering that pions in the isotopic spin state zero have an attractive potential. In a bosonic system an attractive force is not saturated with the growth of the particle number, because all bosons can occupy one quantum state. As a consequence, the multipionic system acquires additional stability. During the formation of such a system from a hadronic gas, when single pions fall in the lowest quantum state, and an intense soft photon radiation should emerge.

We are preparing for carrying out SP investigations at U-70 (Protvino) and propose to study this unique phenomenon at JINR collider NICA. At high hadron multiplicities available in A + A collisions at collider conditions the probability to form a cold quasistationary (hadron or parton) system is higher than in previous experiments carried out at fixed target. Photons may be detected in a TPC via conversion $\gamma \to e^+e^-$. The estimated count rate of SP is 15 s^{-1} at a beam luminosity of 10^{27} $s^{-1}cm^{-2}$. Another possibility is to implement a small ($\sim$ 10 cm^2) special electromagnetic calorimeter with a low energy threshold ($\sim 1 \div 5$ MeV). This module can be incorporated into a barrel calorimeter.

Soft direct photons Direct photons (DP) by definition are not a decay product of any known particle. In accordance with quantum electrodynamics they may be emitted in the process of charged particle scattering - bremsstrahlung in a parton or hadron cascade. In particular, $q\overline{q} \to g\gamma$ and $gq \to \gamma q$ parton interactions lead to photon emission. The higher the density and the longer the system lifetime, the more DP should be emitted. The produced photons interact with the surrounding matter only electromagnetically, and therefore they bear

the information on properties of the surrounding environment during whole history of evolution.

Special attention is devoted to low energy DP (SP) whose yield surpasses the theoretical predictions by $5 \div 8$ times. This concerns K^+p and $p\bar{p}$ interactions at 70 GeV [45, 46] as well as $\pi^{\pm}p$ and K^+p interactions at 250 and 280 GeV [47, 48]. Some results are shown in Fig. 7.8. The recent results on this subject by the DELPHI collaboration [53] are devoted to studying SP inside hadronic jets originated from the $Z^0 \to q\overline{q} \to jet + X$ decay region. The authors claim a clear excess of SP as compared to the theoretical prediction by a factor 3 for charged and a factor 17 for neutral particles.

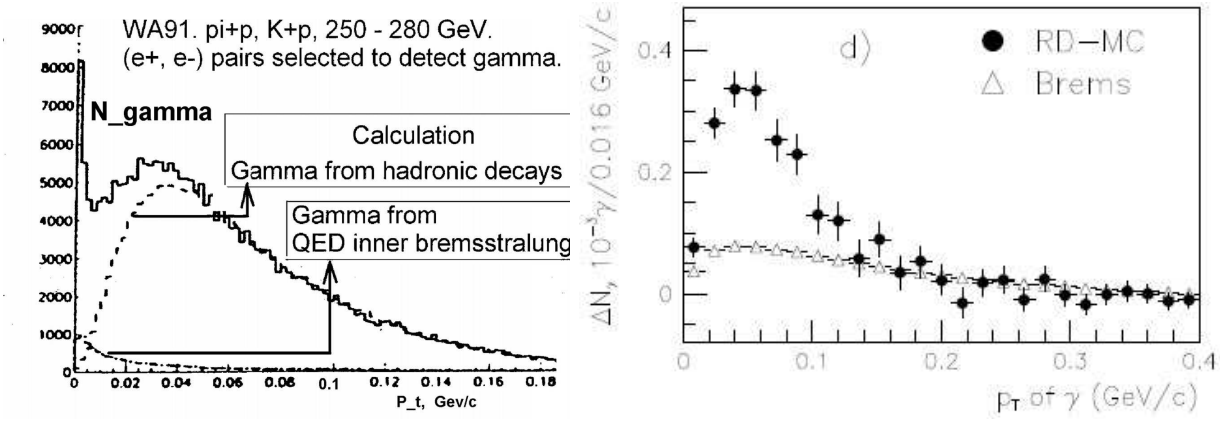

Figure 7.8: Left panel: SP p_t spectrum. The photons from decay of known particles are shown by MC histogram [47]. Right panel: Same as on Left panel, data [53]. RD-MC means real data with MC data subtracted.

The SP surplus can be assigned to unknown physical processes. In the paper [49] the formation of a cold zone of the QGP in a hadronic gas is assumed (model CQGP). The authors believe that cold partons lack energy for fast hadronization. So they recombine in hadrons rather slowly. Therefore a cold QGP droplet has a big lifetime and it reveals itself as a source of low energy DP. The idea of a cold spot of pion gas is considered in the paper [50]. Slow pions get repeatedly reflected from the border of hot and cold areas and have a large lifetime. Again at the cost of a long lifetime the cold spot radiates SP with low energy in the c.m.s.

A new interesting idea has been advanced in [54] where the analogy between expanding hadronic fireball and expanding universe was supposed. In both cases the spectrum and intensity of emerging photons can be described by a black body radiation formula. DP apear as an analogue of the cosmic microwave background radiation. A semiqualitative description of the available experimental data has been achieved.

We have designed a gluon dominance model (GDM) for describing the high multiplicity in lepton (e^+e^-) and hadron (pp, $\overline{p}p$) interactions [55, 56, 57, 58, 59, 60, 61]. We assume that the energy of colliding hadrons is transformed to internal energy of initial particles and a quark-gluon system appears. In this case a parton cascade based on QCD is possible whith quark bremsstrahlung and gluon fragmentation. This assumption has been confirmed by our recent multiplicity studies [62]. We have shown that hadron production is realized by active gluons. The comparison of the GDM predictions with experimental data in a wide energy interval shows a good agreement. Half of the active gluons ($\sim 47\%$) produce hadron jets and the remaining gluons form a quark-gluon system (QGS). We suggest that these gluons are the source of the excess rate of SP observable in a number of experiments.

We suppose that at a certain moment the QGS or excited new hadrons may be created in a near-equilibrium state within a short period or finite time. Therefore, to describe massless photons, we used the black body emission spectrum. From experimental data the inelastic cross section is equal to approximately 40 mb. The cross section of SP formation is about $4mb$, and since $\sigma_\gamma \simeq n_\gamma(T) \cdot \sigma_{in}$, the number of SP will be equal to $n_\gamma \approx 0.1$. The estimates of temperature are based on the scale for momentum transfer: $T = p \approx p_T\sqrt{2}$ (1 MeV $= 1.16 \cdot 10^{10}$ K). If $T(p_T)$ is known, using n_γ we can estimate the linear size of the radiating system ($V \simeq L^3$). The obtained linear size of the system from the SP momentum (p_T) is $L \sim 4 - 6$ fm.

It is well-known that the temperature of secondary hadrons is higher than the temperature of SP. We assume that objects with soft gluon content may not transform into hadrons but turn into SP's. The amount of such soft gluons can be estimated by the number of active gluons. The observable dependence of the yield of SP on the charged, neutral or total multiplicities can be explained the amount of partons converted to the excess

SP via QCD-processes. The differences in the excess yield for charged and neutral pions can be explained by the distinction of their constituents. The charged pions consist of different flavors ($u\overline{d}$ or $d\overline{u}$), the neutrals of the same ($u\overline{u}$ or $d\overline{d}$). They are distinguished in masses too. The excess of energy (the cooling of secondary particles) will be transformed to SP. Their yield will be higher for neutral pion (less mass) than for charged meson production.

The study of the DP seems especially interesting for the NICA project and the MPD setup [63] as it aims to deal with a high density system [64, 65]. The goal of the proposed experiment is the investigation of collective behavior of particles in the process of multiple hadron production in pp and AA interactions at the colliding beam energy $E \simeq 5$ AGeV. The domain of high multiplicity (central collisions) will be studied. Near the threshold of a reaction all particles obtain a small relative momentum.

In a thermalized cold and dense hadronic gas as a consequence of multiboson interference a number of collective effects may appear. In particular, an increase in the rate of DP results from bremsstrahlung in the partonic cascade in a dense and cold pionic gas or condensate. The production of a multipion, coherent semibound state is possible. It emits soft pions in the course of its formation. The partonic cascade leads to a high multiplicity of particles in the final state. Many of them are accompanied by bremsstrahlung radiation. At high densities an additional γ source [51] is predicted: pion annihilation $\pi^+\pi^- \to n\gamma$. Close to the region of the chiral phase transition the masses of the constituent quarks decrease which leads to an increase of radiation (bremsstrahlung and annihilation processes). This efect may serve as a more reliable tool to measure density and temperature of the system.

It is necessary to note, that the DP discussed here have energies in the c.m.s. of $E_{c.m.\ \gamma} \leq 30$ MeV or wavelength $\lambda \geq 60$ fm. Obviously, this size is much greater than the size of the formed hadron system. Therefore, such photons should be radiated by system as a whole instead of the separate particles. In this case the pion system can condense [52]. Experimental indications for Bose-Einstein condensation were obtained (Fig. 7.9) by the SVD Collaboration [66].

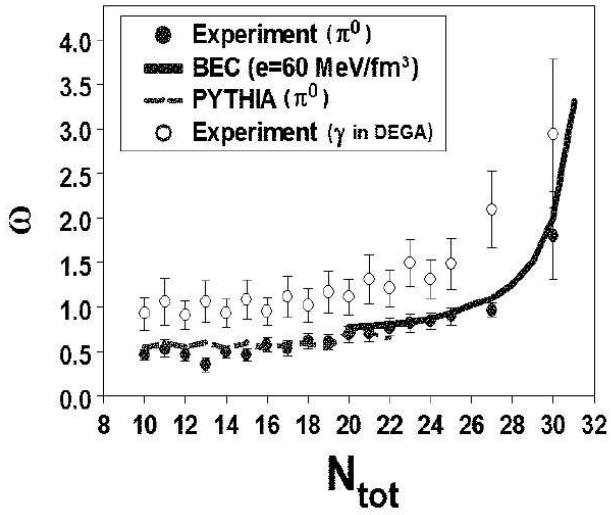

Figure 7.9: Normalized dispersion of neutral pion number as a function of the total number of pions measured in pp interactions at a proton energy of 50 GeV. $\omega = \sigma(\pi^0)^2 / < N(\pi^0) >$ [66].

Photon calorimeter with low energy threshold

A specific feature of the proposed photon detector is its capability to measure low energy deposit $E_{thresh} \leq 5MeV$ [67]. Still none of the known experiments has reached such a small value of the photon energy detection. As it has been mentioned above, it is of importance for check some exotic theoretical models. We suggest to construct an electromagnetic calorimeter (EC) from BGO scintillator. The dimension of one cell should be $\simeq 5 \times 5 \times 120$ cm^3. In this case the spatial localization of a photon is ¡ 5 cm. One should take in to account the transverse dimension of the photon shower ~ 5 cm. From this very qualitative consideration we conclude that the calorimeter transverse dimensions should be $\sim 30 \times 30$ cm^2. Four central cells with a total area of 10 cm^2 will provide a high efficiency photon detection. The longitudinal dimension should be as usual ~ 10

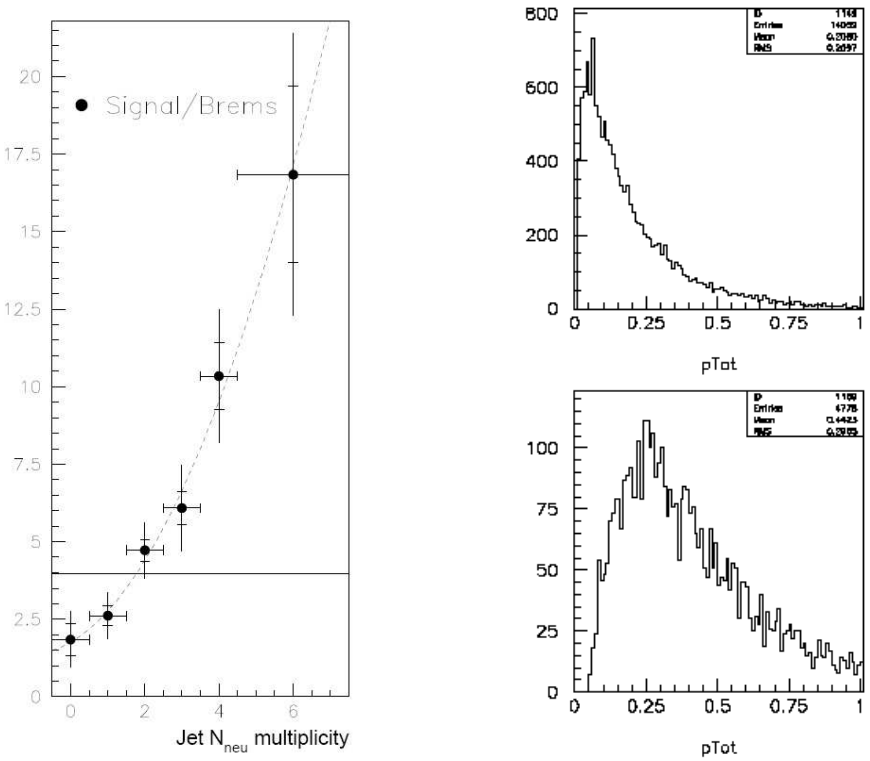

Figure 7.10: Left panel:Intensity of SP as a function of the neutral pion multiplicity in jets [53]. Right panel: MC simulation of γ and π^0 production.

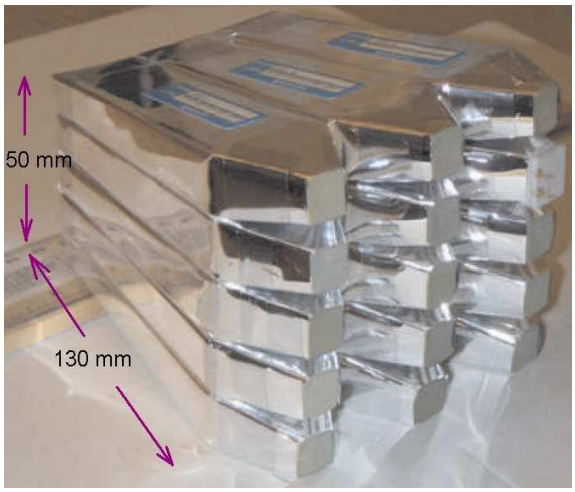

Figure 7.11: Electromagnetic calorimeter prototype [67].

radiation lengths. For BGO this is $\sim$ 12 cm. The important problem is to take into account the dissipated particle background in the experimental hall. Reduction of background may be provided by the calorimeter preshower.

According to [45, 46] the integrated cross section of the SP production in the domain $p_t \leq 0.1$ GeV/c, $-0.01 \leq x \leq 0.01$ is equal to $2 \div 4$ mb/nucleon. Assuming the SP isotropic angular distribution we get an averaged differential cross section $d\sigma/d\omega = 0.2$ mb/strad/nucleon. For a proton beam luminosity $L \simeq 10^{30}$ cm^{-2} s^{-1} the EC counting rate is equal to $\simeq 1$s^{-1}. For $Au + Au$ collisions with luminosity $L \simeq 1 \times 10^{27}$ cm^{-2} s^{-1} the count rate is equal to $\simeq 0.4$s^{-1}. During one day of runtime a statistics of $\simeq 5 \times 10^4$ SP will be accumulated. SP may convert into e^+e^- pairs in the vertex detector material and in the walls of the TPC. Thus another option is the detection of low energy e^+e^- pairs in the TPC. This leads to one order of magnitude higher statistics due to the higher angular acceptance of the TPC. But the pair detection in the TPC is subject to an additional analysis.

Assuming for the photon detector an effective area of 10^2 cm^2, set at a distance of 1.3 m from the target, leads to the following estimate of the DP count rate: 2 events per cycle. One week of runtime will provide a pretty good sample of SP: $\approx 2 \times 10^5$ events.

Let us point to the distinctive features of the present project.

- Photon spectra at several fixed angles will be measured. The lower edge of the spectra is $\sim$ 5 MeV/c.
- Each SP spectrum will be collected at a certain fixed multiplicity of secondaries in pp and AA interactions.
- We plan to study both phenomena, Bose-Einstein condensation [66] and SP yield.

Thus the inelasticity or rate of the primary energy dissipation will be known for each spectrum.

Bibliography

[1] E. V. Shuryak, Phys. Lett. **B 78,** 150 (1978).

[2] G. Agakachiev *et al.* (CERES Collaboration), Phys. Rev. Lett. **75,** 1272 (1995).

[3] R. Arnaldi *et al.* (NA60 Collaboration), Phys. Rev. Lett. **96,** 162302 (2006); Phys. Rev. **96,** 162302 (2006); Nucl. Phys. **A 774,** 715 (2006).

[4] R. Rapp, J. Wambach and H. van Hees, [arXiv:0901.3289.]

[5] Itzhak Tserruya, [arXiv:0903.0415].

[6] R. Rapp and J. Wambach, Adv. Nucl. Phys. **25**, 1 (2000); R. Rapp, G. Chanfray and J. Wambach, Phys. Rev. Lett. **76,** 368 (1996).

[7] G.E. Brown and M. Rho, Phys. Rev. Lett. **66,** 2720 (1991).

[8] M. Harada and K. Yamawaki, Phys. Rep. **381,** 1 (2003).

[9] V. V. Skokov and V. D. Toneev, Phys. Rev. **C 73,** 021902 (2006).

[10] N. S. Amelin, K. K. Gudima, S. Y. Sivoklokov and V. D. Toneev, Sov. J. Nucl. Phys. **52**, 172 (1990).

[11] N. S. Amelin, E. F. Staubo, L. P. Csernai, V. D. Toneev and K. K. Gudima, Phys. Rev. **C 44,** 1541 (1991).

[12] V. D. Toneev, N. S. Amelin, K. K. Gudima and S. Yu. Sivoklokov, Nucl. Phys. **A 519,** 463 (1990).

[13] Kh. U. Abraamyan *et al.*, Phys. Rev. **C 80,** 034001 (2009) [arXiv: 0806.2790].

[14] A. N. Sysakian, A. S. Sorin, M. K. Suleymanov, V. D. Toneev and G. M. Zinovjev [arXiv:nucl-ex/0601034]; *Proceedings of the 8th International Workshop "Relativistic Nuclear Physics: From hundreds MeV to TeV"*, (Dubna, 2006), p.306 [arXiv: nucl-ex/0511018].

[15] Kh. U. Abraamyan *et al.*, Phys. Lett. **B 323,** 1 (1994); Phys. Atom. Nucl. **59**, 252 (1996); **60**, 2014 (1997); **60**, 1843 (1997); **68**, 982 (2005).

[16] T. Matsui and H. Satz, plb 178, 416 (1986).

[17] M. C. Abreu *et al.* (NA38 Collaboration), Phys. Lett. **B 466,** 408 (1999).

[18] B. Alessandro *et al.* (NA50 Collaboration), Eur. Phys. J. **C 35,** 335 (2005).

[19] M. C. Abreu *et al.* (NA50 Collaboration), Phys. Lett. **B 477,** 28 (2000).

[20] R. Arnaldi *et al.* (NA60 Collaboration), Phys. Rev. Lett. **99,** 132302 (2007).

[21] A. Adare *et al.* (PHENIX Collaboration), Phys. Rev. Lett. **98,** 232301 (2007).

[22] L. Kluberg, Eur. Phys. J. **C 43,** 145 (2005).

[23] B. Alessandro et *al.* (NA50 Collaboration), Eur. Phys. J. **C 33,** 31 (2004).

[24] P. Cortese *et al.* (NA50 Collaboration), Nucl. Phys. **A 715,** 679 (2003).

[25] M. C. Abreu *et al.* (NA50 Collaboration), Phys. Lett. **B 553,** 167 (2003).

[26] E. Scomparin, R. Arnaldi (NA60 Collaboration), *Quark Matter 2009*, (Knoxvill, TN, USA, March 30-April 4), 2009.

[27] M. J. Leitch, J. Phys. G. **34,** S453 (2007).

[28] M. E. Peskin, Nucl. Phys. **B 156,** 365 (1979); G. Bhanot and M. E. Peskin, Nucl. Phys. **B 156,** 391 (1979).

[29] D. Kharzeev and H. Satz, Phys. Lett. **B 334,** 155 (1994).

[30] D. Kharzeev and H. Satz, Phys. Lett. **B 356,** 365 (1995).

[31] K. Martins, D. Blaschke and E. Quack, Phys. Rev. **C 51,** 2723 (1995).

[32] S. Matinyan and B. Müller, Phys. Rev. **C 58,** 2994 (1998) [nucl-th/9806027].

[33] R. Vogt, Phys. Rep. **310,** 197 (1999).

[34] C. Gerschel and J. Hufner, Annu. Rev. Nucl. Part. Sci. **49**, 225 (1999).

[35] P. Cortese *et al.* (NA50 Collaboration), J. Phys. G. **31,** S809 (2005).

[36] C. Y. Wong and H. W. Crater, Phys. Rev. **D 75,** 034505 (2007).

[37] F. Karsch, D. Kharzeev, and H. Satz, Phys. Lett. **B 637,** 75 (2006).

[38] A. Capella, E. J. Feireiro and A. B. Kaidalov, Phys. Rev. Lett. **85,** 2080 (2000).

[39] E. L. Bratkovskaya, W. Cassing, and H. Stoecker, Phys. Rev. **C 67,** 054905 (2003).

[40] J. P. Blaizot, P. M. Dinh and J. Y. Ollitrault, Phys. Rev. Lett. **85,** 4010 (2000).

[41] J. Hüfner and P. Zhuang, Phys. Lett. **B 559,** 193 (2003).

[42] J. F. Owens Rev. Mod. Phys.**59**, 465 (1987).

[43] W. Vogelsang *et al.*, J. Phys. G: Nucl. Part. Phys. **23**, A1 (1997).

[44] M. M.Aggarwal *et al.*, [nucl-ex /0006007].

[45] P. V. Chlapnikov *et al.*, Phys. Lett. **B 141,** 276 (1984).

[46] M. N. Ukhanov *et al.*, IHEP preprint 86-195, Protvino, (1986).

[47] S. Banerjee *et al.*, Phys. Lett. **B 305,** 182 (1993); A.Belogianni *et al.*, Phys. Lett. **B 408,** 487 (1997).

[48] F. Botterwerk *et al.*, Z. Phys. **C51**, 541 (1991).

[49] P. Lichard and L. Van Hove, Phys. Lett. **B 245,** 605 (1990).

[50] E. V. Shuryak, Phys. Lett. **B 231,** 175 (1989).

[51] M. K. Volkov, E. A. Kuraev, D. Blaschke, G. Röpke, S. M. Schmidt, Phys. Lett. **B 424,** 235 (1998).

[52] S. Barshay, Phys. Lett. **B 227,** 279 (1989).

[53] J. Abdallah (DELPHI Collaboration), Eur. Phys. J. **C 47,** 273 (2006); **57**, 499 (2008).

[54] M. K. Volkov, E. S. Kokoulina, E. A. Kuraev, Ukr. Jour. of Physics. 48, 1252 (2003).

[55] E. S. Kokoulina and V. A. Nikitin, *The International School-Seminar The Actual Problems of Microworld Physics*, (Gomel, Belarus), Dubna, 1 (2004) 221;

[56] E. S. Kokoulina and V. A. Nikitin, *Proceedings of Baldin Seminar on HEP Problems "Relativistic Nuclear Physics and Quantum Chromodynamics"*, (JINR, Dubna, Russia), 319 (2005).

[57] P. F. Ermolov *et al.*, *Proc. of Baldin Seminar on HEP Problems "Relativistic Nuclear Physics and Quantum Chromodynamics"*, (JINR, Dubna, Russia), 327 (2005).

[58] V. V. Avdeichikov *et al.*, *Proposal "Termalization"* (in Russian), JINR-P1-2004-190 (2005).

[59] E. Kokoulina, Acta. Phys. Polon. **B 35,** 295 (2004).

[60] E. Kokoulina and A. Kutov, Phys. Atom. Nucl. 71, 1543 (2008).

[61] E. S. Kokoulina *et al.*, Nucl. Phys. (Rus.) 72, 189 (2009).

[62] *SVD Collaboration, Preprint IHEP*, 2011-4.

[63] V.A. Nikitin, *Nonlinear Phenomena in Complex Systems*, 12, 202 (2010); http://theor.jinr.ru/twiki-cgi/view/NICA/WebHome.

[64] J. Cleymans and K. Redlich, Phys. Rev. **C 60,** 054908 (1999).

[65] F. Becattini, J. Manninen and M. Gazdzicki, Phys. Rev. **C 73,** 044905 (2006).

[66] *SVD Collaboration, Preprint IHEP*, 2011-5.

[67] D. D. Dijulio, V. Avdeichikov *et al.*, NIM, **A612**, 127 (2009).

8 Local $\mathcal{P}$ and $\mathcal{CP}$ violation in hot QCD matter

The existence of topological solutions is a very important property of QCD. Topological solutions arise due to the non-Abelian nature of this theory, and lead to a number of important consequences for the properties of the vacuum and hadrons. In hot hadronic matter, the topological fluctuations near the critical temperature can create the space-time domains with locally broken $\mathcal{P}$ and $\mathcal{CP}$ invariances. The local violation of parity can manifest itself in heavy ion collisions through the separation of positive and negative hadrons with respect to the reaction plane; this charge separation would induce an electric dipole moment of the produced hot quark-gluon matter. The charge separation stems from the interplay of strong magnetic field (and/or the angular momentum) in the early stage of the heavy ion collision and the presence of topological configurations in hot matter ("the chiral magnetic effect"). Recent result from RHIC [8] provides an experimental evidence for this phenomenon in heavy ion collisions. This effect should be enhanced in the deconfined quark-gluon plasma phase because it requires the separation of quarks over a large ("macroscopic" on the scale of hot matter size) distance. As discussed in this section, there are reasons to expect that the asymmetry will have a peak at some energy, possibly within the energy range of the NICA collider. It should be emphasized that at high baryon density one can also expect the phenomenon of spontaneous parity violation with a number of unique signatures. The high-energy and low-energy scans at RHIC and the dedicated programs at NICA and FAIR would thus provide a necessary and complementary to each other experimental information.

8.1 Topologically induced local $\mathcal{P}$ and $\mathcal{CP}$ violation in hot QCD matter

D. Kharzeev

Physics Department, Brookhaven National Laboratory, Upton, NY, USA

It has been established experimentally that there is no global violation of $\mathcal{P}$ and $\mathcal{CP}$ invariances in QCD. However, the issue of $\mathcal{P}$ and $\mathcal{CP}$ symmetries in QCD is highly nontrivial because of the existence of topological solutions and the presence of axial anomaly in this theory ("the strong $\mathcal{CP}$ problem"). Even in the absence of global $\mathcal{P}$ and $\mathcal{CP}$ violation, topological fluctuations in QCD vacuum are believed to play an important role in the chiral symmetry breaking, thus being responsible for many properties of hadrons. In hot hadronic matter, the topological fluctuations near the critical temperature can create the bubbles with locally broken $\mathcal{P}$ and $\mathcal{CP}$ invariances [1, 2].

It was suggested in [7] that the local violation of parity can manifest itself in heavy ion collisions at RHIC through the separation of positive and negative hadrons with respect to the reaction plane; this charge separation would induce an electric dipole moment of the produced hot quark-gluon matter. The charge separation stems from the interplay of strong magnetic field (and/or the angular momentum) in the early stage of the heavy ion collision and the presence of topological configurations in hot matter ("the chiral magnetic effect") [8, 5, 6]. The gradients of the topological charge distribution at the boundaries of the domain induce an electric charge [5], and the variation of topological charge with time induces an electric current [8, 6]. Therefore in the presence of very intense magnetic fields, topological fluctuations in hot QCD matter can be observed directly through the spatial separation of positive and negative electric charge signaling a **local** violation of $\mathcal{P}$ and $\mathcal{CP}$ symmetries.

The experimental observable that is sensitive to the local violation $\mathcal{P}$ and $\mathcal{CP}$ invariances has been proposed in [7]. Because the sign of the electric dipole moment is expected to fluctuate from event to event, and one needs to sum over many events to acquire the necessary statistics, the observable is $\mathcal{P}$-even but largely insensitive to the statistical fluctuations [7]. Recent result from RHIC [8] provides an experimental evidence for this phenomenon in heavy ion collisions. This effect should be enhanced in the deconfined quark-gluon plasma phase because it is requires the separation of quarks over a large ("macroscopic" on the scale of hot matter size) distance.

The energy dependence of the local $\mathcal{P}$ and $\mathcal{CP}$ violation is driven by two factors:

- the energy density of the produced hadronic matter and
- the strength and variation with time of the produced magnetic field.

While the initial value of the magnetic field at the time of collision of course increases with energy, the produced field falls off faster at higher energies [8] reflecting a faster separation of the charged spectators and particles produced in the collision. As a result, one expects an increase of the charge asymmetries towards lower energies. On the other hand, at some threshold collision energy the deconfined matter will no longer be produced, and

so the asymmetry should significantly decrease in magnitude. It would be extremely important to explore this behavior in low-energy heavy ion collisions. The low-energy scan at RHIC and the dedicated programs at NICA and FAIR would thus provide a necessary and complementary to each other experimental information.

8.2 Magnetic effects in QCD vacuum: lattice view

P.V. Buividovich[a,b], M.N. Chernodub[b], E.V. Luschevskaya[b] and M.I. Polikarpov[c]

[a] *JIPNR, Minsk, Belarus;*
[b] *ITEP, Moscow, Russia;*
[c] *CNRS, Tours, France*

Chiral magnetic effect

Generation of electric current along the direction of magnetic field takes place on local fluctuations of chirality (= difference between densities of left-handed and right-handed quarks). Can be observed in $\mathcal{CP}$-even quantities only! Observables which can be calculated on the lattice: $\langle j_\mu j_\nu \rangle$, $\sigma^2_{\mu\nu}$, ... Lattice results for quenched vacuum and overlap Dirac fermions:

- Confinement phase: the current along the magnetic field $\langle j^2_\parallel \rangle$ is enhanced with respect to the perpendicular component $\langle j^2_\perp \rangle$ when the magnetic field grows (see Fig. 8.1)
- Deconfinement phase: the current along the magnetic field $\langle j^2_\parallel \rangle$ stays constant, while the perpendicular component $\langle j^2_\perp \rangle$ is suppressed (see Fig. 8.1)

This current can be observed as enhanced emission of charged particles perpendicular to the reaction plane!

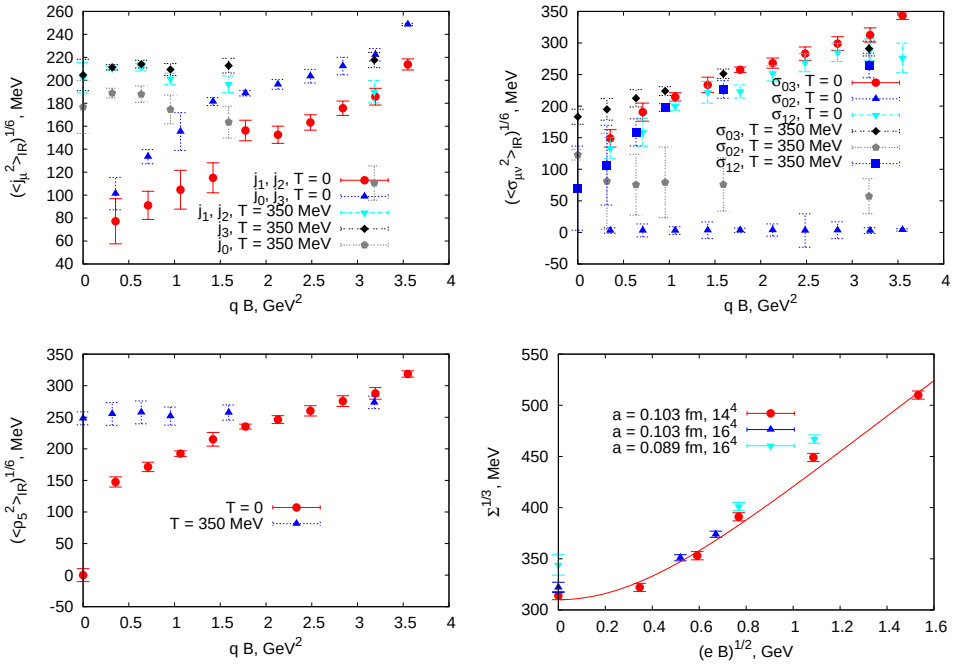

Figure 8.1: Upper panels: Induced fluctuations of electric current and electric dipole moment along and perpendicular to the magnetic field. Magnetic field is directed along the 3rd axis. Lower panels: The dependence of the induced fluctuations of chirality and of the chiral condensate on the magnetic field.

Generation of electric dipole moment (EDM) along the direction of magnetic field

An observable quantity is the square of different components of the EDM associated with spin: $\sigma_{\mu\nu} = i/2\,\bar{q}\,[\gamma_\mu, \gamma_\nu]\,q$. We see a strong enhancement of the fluctuations of moth magnetic moment and the EDM with magnetic field, which are almost equal. In contrast to current, EDM behaves similarly in both confinement and deconfinement phases (see upper panels of Fig. 8.1)

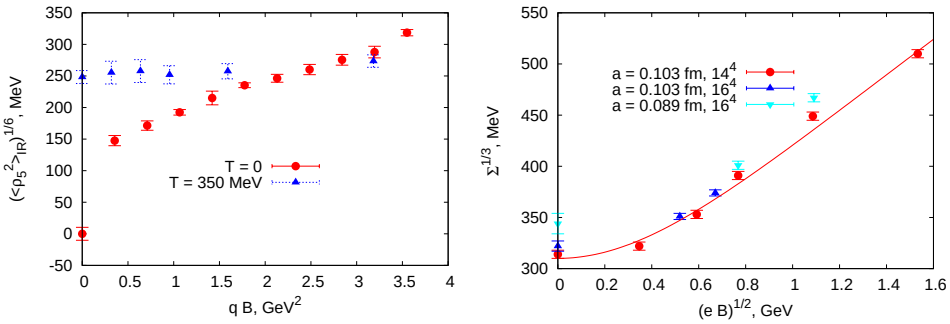

Figure 8.2: The dependence of the induced fluctuations of chirality and of the chiral condensate on the magnetic field. Magnetic field is directed along the 3rd axis.

Enhanced fluctuations of chirality

Magnetic field, as well as temperature, enhances the fluctuations of the difference of the densities ρ_5 of left and right quarks. This, in turn, enhances the chiral magnetic effect (see lower left panel of Fig. 8.2).

Enhancement of the chiral symmetry breaking.

The magnetic field stabilizes the chirally broken (low-temperature) phase of QCD enlarging the value of the chiral condensate and enhancing the chiral symmetry breaking (see lower panels of Fig. 8.2). According to the Gell-Mann-Oakes-Renner relation, the pion mass is proportional to the chiral condensate, which gives a possibility to measure this enhancement.

8.3 Rich physics of non-central heavy-ion collisions

S. Voloshin

Wayne State University, Detroit, Michigan, USA

The idea of the local strong parity violation (due to quark interaction with topologically non-trivial gluonic configuration: topology induced parity violation) has received a lot of developments in the recent years starting from paper [1, 2]. Originally it was noticed that such an effect can lead to difference in the reaction plane reconstructed from positive and negative particles [11], but no effect has been observed at that time. More recently it was noticed [7, 8, 5, 6] that in the presence of the strong magnetic of non-central nuclear collision, it could result in the charge separation along the direction magnetic field (or the system angular momentum). The corresponding experimental techniques has been developed in [7] and first results from STAR Collaboration [12] indeed are consistent with theoretical expectations. The effects is expected to depend strongly on the existence of the deconfinement stage. Also, the charge separation depends linearly on the strength of magnetic field, more exactly on the time integral of the magnetic field. It is predicted that the latter is increasing at lower energies. Combined with effect of deconfinement it could lead to a threshold behavior. In this sense the study of the local strong parity violation at NICA become extremely important. At this point I would also mention, that if observed, for the further study of the effect one might need good particle identification and also possibility to collide different nuclei, in particular isobaric nuclei.

The most interesting measurements of the anisotropic flow from my point of view would be

- elliptic flow of charge particles and possible observation of the wiggle in v_2 behavior, in particular in the region of possible deconfinement transition [13, 14, 15, 16],
- checking constituent quark number scaling in elliptic flow of identified particles [15, 17], again as an indicator of deconfinement, and
- directed flow of identified particles which is sensitive to the dynamics of baryon stopping and system expansion [18].

Femtoscopy of the system asymmetries, first proposed in [19] and for non-identical particles in [20] (for a review, see [21]), obviously would be necessary to understand the entire picture of the system evolution.

Finally, I mention on interesting possibility of the system global polarization (transfer of the orbital angular momentum into particle spin) [5, 23]. Although at RHIC energies it was found to be consistent with zero within experimental uncertainties [24] it will be exciting to repeat these measurements at lower energies

8.4 Spontaneous $\mathcal{P}$-violation in dense matter accessible with NICA

A. Andrianov[a], V. Andrianov[a] and D. Espriu[b]

[a] *St.Petersburg State University, Russia;*
[b] *University of Barcelona, Spain*

Parity violation in QCD can take place spontaneously under extreme conditions due to condensation of neutral pseudoscalar matter. Its detection would constitute an important breakthrough for the understanding of strong interactions at high density and a considerable achievement for heavy-ion experiments. It is conjectured [25] that such a parity breaking phase may be present for densities ranging from 3 to 10 times the normal nuclear density ρ_0 and moderate temperatures. This is sketched in Fig. 8.3

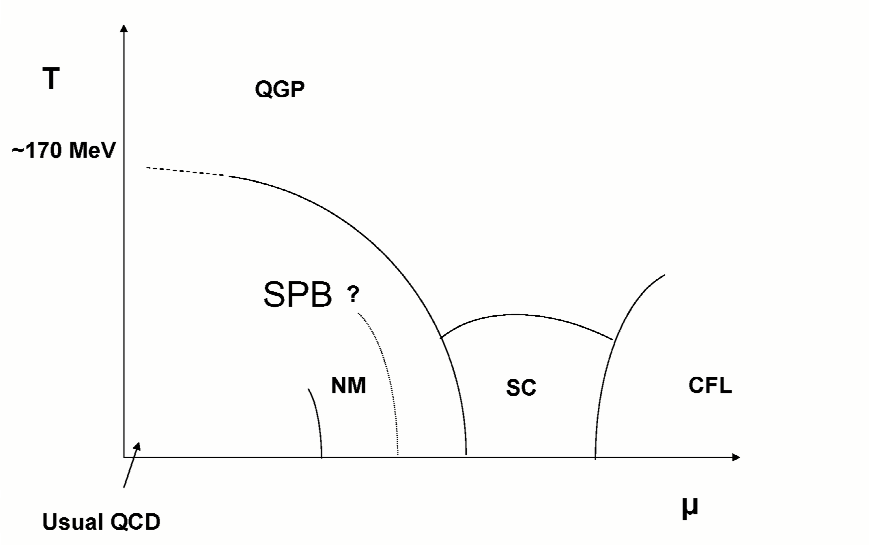

Figure 8.3: Tentative location of the hypothetical parity breaking phase in QCD.

The possibility of spontaneous parity breaking (SPB) may be accessible in the range of nuclear densities where the hadron phase persists and quark percolation does not occur yet (see Fig. 8.4). Since, as it is known, pion condensation is believed to be impossible in models with only one scalar/pseudoscalar isomultiplet, it will be necessary to include the two lowest lying, scalar/pseudoscalar resonances in each channel. While this is not the most general model, it contains the sufficient ingredients for spontaneous parity breaking.

The "pion" condensate may arise as a relative complex phase factor between the two scalar condensates. We arrive at the conclusion that such an effect takes place by using an effective Lagrangian for low-energy QCD that retains the two lowest lying states in the scalar and pseudoscalar sectors. We include [26] a chemical potential for the quarks that corresponds to a finite density of baryons, implement the bound state of normal nuclear matter and investigate the pattern of symmetry violation in its presence. In general this phase is bound by a divide line and it extends across a range of chemical potentials that correspond to nuclear densities where more exotic phenomena such as CFL or CS may occur.

Within this model the expectation values of the two scalar condensates $\langle\sigma_1\rangle$ and $\langle\sigma_2\rangle$ and of the pseudoscalar one $\rho = \langle\Pi\rangle$ has the following qualitative behaviour as the chemical potential is increased.

The mass spectrum differs considerably from the familiar one as seen in Fig. 8.5. At the phase transition point where spontaneous parity breaking occurs three massless states (Goldstone bosons) appear. Throughout the parity breaking phase two charged states remain massless while the third Goldstone boson is light, but not massless.

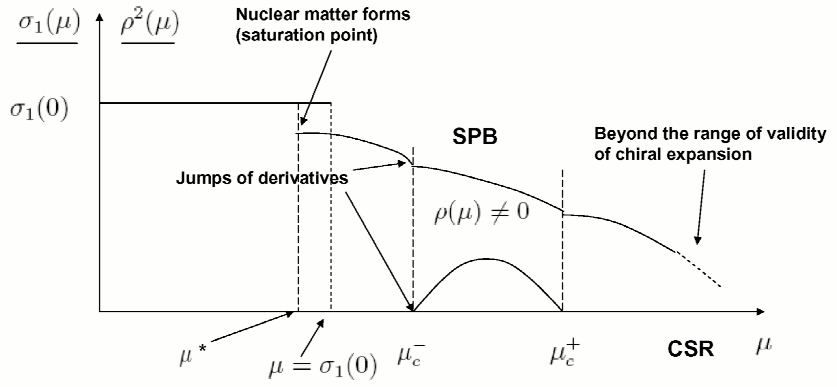

Figure 8.4: The figure shows the dependence of the various expectation values on μ. Notice the *only partial* restoration of chiral symmetry at the saturation point, a considerable achievement of this model

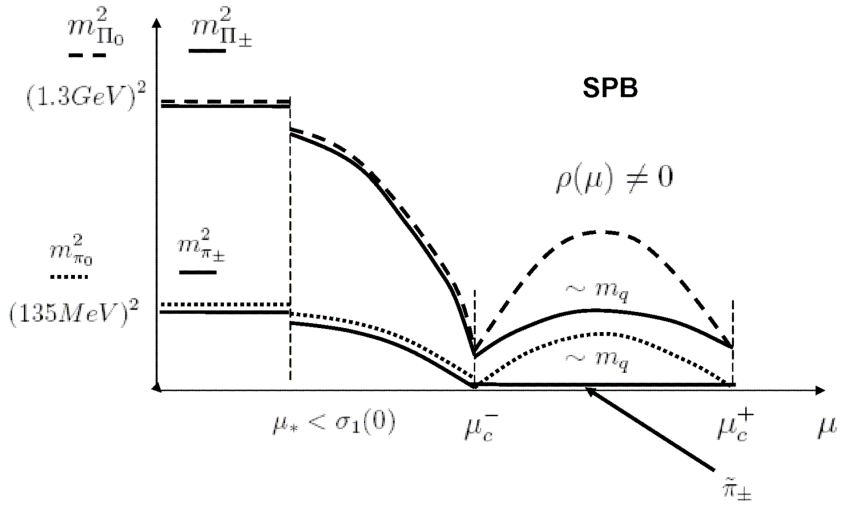

Figure 8.5: The lines indicate the evolution of the usual pion and the heavy pion (1300) multiplets as the chemical potential evolves

A salient characteristics of this phase would be the spontaneous violation of the vector isospin symmetry $SU(2)_V$ down to $U(1)$ as is made evident by the generation two additional massless charged pseudoscalar mesons. The latter cause substantial changes in the nuclear equation of state. The signature of the spontaneous parity breaking is a strong mixing between scalar and pseudoscalar states that translate spontaneous parity violation into meson decays. The mass eigenstates will decay both in odd and even number of pions simultaneously. Isospin violation can also be visible in decay constants.

While parity violation in QCD would lead to striking consequences [25, 26], detecting the changes of characteristics such as the same in-medium resonance being able to decay into even and odd number of pions, isospin violation and the like may be very difficult because the observation of in-medium particle properties is a difficult task. More signatures are wanted which could be detected outside the reaction region and would be suitable to discriminate the SPB phenomenon from other processes going on in ordinary nuclear matter.

Let us focus on central collisions. Then one can expect a pion condensate (if any) $\langle \Pi \rangle$ arising in a rather space-homogeneous configuration but essentially depending on the collision time $\langle \dot{\Pi} \rangle \equiv \eta \neq 0$ (first increasing then decreasing). Then a remarkable phenomenon shows up [27], namely, due to the presence of parity odd interaction, the term $\Pi \, F_{\mu\nu} \, \widetilde{F}^{\mu\nu}$ appears in the Lagrangian relevant for this situation. This term describes the

neutral pion decay into two photons. And in the presence of pion condensation it distorts the photon spectrum via a modification of Maxwell Electrodynamics with a Chern-Simons interaction $\eta\vec{A}\cdot\vec{B}$. As a consequence, the two transversal, circularly polarized, photons obtain different effective masses. When $\eta > 0$ one of them becomes massive $m^2_{\gamma,+} = \eta|\vec{k}|$ with a mass growing with photon momentum $\vec{k}$ and another one appears as a tachyon with negative mass squared $m^2_{\gamma,-} = -\eta|\vec{k}|$. For the opposite sign of the condensate time derivative $\langle\dot{\Pi}\rangle$ the polarizations are interchanged.

As a result, photons with momenta $|\mathbf{k}| > \frac{4m_l^2}{\eta}$ start to decay into lepton pairs $\gamma \to l^+l^-$. A hierarchy of thresholds appear for different leptons (mostly electrons and muons). An additional feature of his type of decay is the creation of dileptons in a rather narrow cone when $\eta \ll m_l$. The decay width $\sim \alpha\ \eta$ is suppressed by the fine structure constant α but may be considerably enhanced if the pion condensate derivative η rapidly increases. If parity breaking occurs spontaneously as a second order phase transition then at the very critical line indeed η increases unboundly, see the Fig. 8.6.

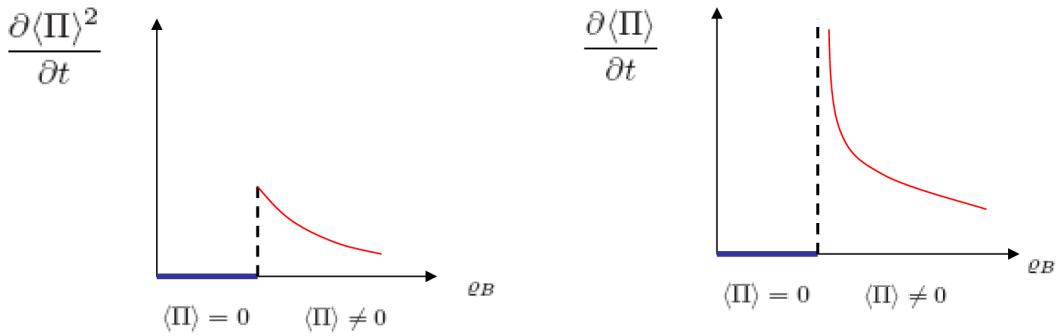

Figure 8.6: The figure shows the evolution of the time derivative of the pseudoscalar condensate $\langle\Pi\rangle$ in the vicinity of the critical density.

However for finite nuclei one should not expect a divergence, but a large enhancement. The decay width will also become large enough to produce abnormal excess of dileptons in spite of being an electromagnetic process.

A still open question is to what extent the $\mathcal{P}$-breaking phase can last with increasing temperatures. It is conceivable that the $\mathcal{P}$-breaking divide line points out directly to the QCD tricritical point. Thus the experimental studies with the NICA facilities of the QCD tricritical point may well detect a more complicated phase structure due to the interplay with the parity violation phase.

8.5 On $\mathcal{CP}$ violation in heavy-ion collisions at the NICA energy

V. Skokov and V. Toneev

Gesellschaft für Schwerionenforschung mbH, Darmstadt, Germany;
Joint Institute for Nuclear Research, Dubna, Russia

In QCD, chiral symmetry breaking is due non-trivial topological effect. Topological transitions have never been observed directly (*e.g.* at the level of quarks in DIS). The best evidence of this physics would be event-by-event strong parity violation.

One of the most exciting signals of the deconfinement and the chiral phase transitions in heavy-ion collisions, chiral magnetic effect, suggested in [8], predicts an observable effect of preferential emission of charged particles along the direction of angular momentum in the case of non-central heavy-ion collisions due to presence of a non-zero chirality. As it was stressed in [8, 6] both deconfinement and chiral phase transitions are essential requirements for chiral magnetic effect to take place. The first one is needed, since only in this case soft quarks can separate over distances greater than the radius of nucleon. The second is also required [8, 6], since non-zero values of chiral condensate drives asymmetry between the number of right- and left-handed quarks to zero. Here we compare these conditions at the RHIC and NICA energies.

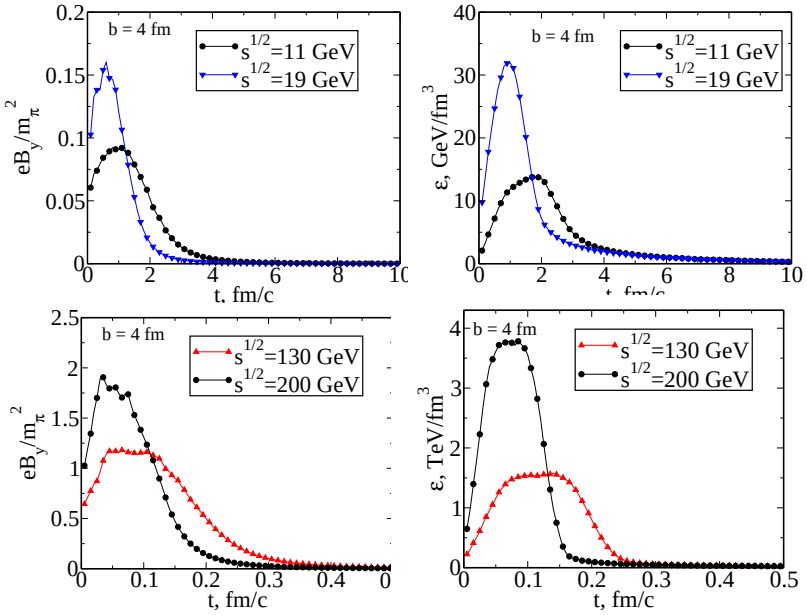

Figure 8.7: Upper panels: The time evolution of the magnetic field strength eB_y (left) and energy density (right) at the central point. The UrQMD calculations are carried out for Au + Au collisions with impact parameter, $b = 4$ fm for $\sqrt{s_{\rm NN}} = 11$, 19 GeV. The symbols are plotted with the step $\delta t = 0.2$ fm/c. Lower panels: the same upper panels for $\sqrt{s_{\rm NN}} = 130$ and 200 GeV, with the time step $\delta t = 0.01$ fm/c.

We focus our calculations [9] on the magnetic field in the central point O of the created fireball (symmetric with respect to the reaction plane $x - z$ in the transverse $x - y$ plane) and energy density of nuclear matter in the Lorentz-contracted box with 2 fm site-length centered around O. Nuclei are colliding along z-axis.

The magnetic field strength at a position $\vec{x}$ and time t is defined by the Lienard-Wiechert potentials

$$e\vec{B}(t,\vec{x}) = \alpha_{\rm EM} \sum_n Z_n \frac{1-v_n^2}{\left(R_n - \vec{R}_n\vec{v}_n\right)^3} \left[\vec{v}_n \times \vec{R}_n\right], \tag{8.1}$$

where the fine-structure constant $\alpha_{\rm EM} \approx 1/137$, Z_n is the electric charge of the nth particle (in units of the electron charge), $\vec{R_n} = \vec{x} - \vec{x}_n$ is a radius vector of particle, $\vec{v}_n$ is particle velocity. The quantities $\vec{v}_n$ and $\vec{x}_n$ are taken at the time moment t' defined implicitly by the following equation

$$|\vec{x} - \vec{x}_n(t')| + t' = t. \tag{8.2}$$

Summation is to be done over all charged particles.

On the basis of the expression (8.1) one can draw several conclusion for the main properties of the magnetic field at the origin O. First of all, from symmetry reasons it is evident that the magnetic field will be negligible for collision with small impact parameter. From the same symmetry considerations one obtains that the field will have only non-zero B_y-component. Second, the field will be negligible for low collision energies, because the field strength is proportional to the particle velocity. On the other hand for very high, ultrarelativistic energies of the collision the contribution to the magnetic field is feasible only for for particles close to transverse plane $\left(R_n - \vec{R}_n\vec{v}_n\right) \sim 0$. The contribution from particles away from transverse plane is suppressed by factor of $(1 - v^2)$.

In the left panels of Fig. 8.7 , the time evolution of the magnetic field strength is shown for RHIC and NICA energies. The magnetic field is created in non-central Au + Au collision with impact parameter $b = 4$ fm. The resulting field strength is averaged over 100 events to reduce statistical fluctuations. It is clear, however, that magnetic field fluctuation in a single event can be significant for an observable effect.

The key quantity of these effects is a value of a background magnetic field strength created in heavy-ion collisions. The results obtained within the UrQMD very close to the early estimate [8] where it was shown that

the field may reach very high values $eB \sim 3 \cdot m_\pi^2 \sim 3 \times 10^{18}$ Gauss (Note we measure the magnetic field strength in units of squared pion mass, using for definiteness $m_\pi = 140$ MeV. However the magnetic field strength can be translated into cgs system by the following identity $m_\pi^2 = 140^2 \times 0.512 \cdot 10^{14}$ Gauss $\approx 10^{18}$ Gauss).

The large value of the magnetic field strength itself does not guarantee possible observable effects, but additional requirements are needed, *e.g.* for chiral magnetic effect the system should be in deconfinement and chiral restored phase. To demonstrate that matter in central region is, presumably, in QGP phase we calculated the energy density. It is done in the center region of created fireball. The calculated time evolution of energy density in the center region is shown in the right panels of Fig. 8.7. Even for bombarding energy $\sqrt{s_{\rm NN}} = 11$ GeV and impact parameter $b = 4$ fm the energy density in the central region is sufficient to reach QGP phase. However, the question whether the system is in local equilibrium and can it be described by temperature and chemical potential(s) is still open.

Values of magnetic field strength and energy density play an important role in estimations of possible observable effects of deconfinement and chiral phase transition in heavy-ion collisions. Going down from the RHIC to NICA top energy in Au + Au collision at $b = 4$ fm, the magnetic field strength B_y decreases approximately by 17 times which is not too small as would naively expect. However, as compared to RHIC, the peak energy density ϵ, being above the deconfinement transition one, decreases by a factor of ~ 250. This reduces substantially the possibility of appearance of non-zero winding number configurations at the NICA energies. In both limiting energy regions the deconfined state defined as $\varepsilon \gtrsim 1$ GeV/fm^3 is inside the range of the maximal magnetic field strength but at the NICA energy the system stays there longer by a factor of $\sim$20 as compared to the RHIC one. Thus, taking into account theoretical uncertainties, it is still not excluded that a small effect of the charge separation can be observed at the top NICA energy [10].

8.6 Chiral vortaic effect and neutron asymmetries at NICA

O. Rogachevsky[a,b], A. Sorin[a,c] and O. Teryaev[a,c]

[a] *JINR Dubna, Dubna, Russia;*
[b] *PNPI RAS, Leningrad district, Russia;*
[c] *Dubna International University, Dubna (Moscow region), Russia*

We study the possibility of testing experimentally signatures of P-odd effects related with the vorticity of the medium. The Chiral Vortaic Effect is generalized to the case of conserved charges different from the electric one. In the case of baryonic charge and chemical potential such effect should manifest itself in neutron asymmetries at the NICA accelerator complex measured by the MPD detector. The required accuracy may be achieved in a few months of accelerator running. We also discuss polarization of the hyperons and P-odd correlations of particle momenta (handedness) as probes of vorticity.

We dedicate this section to the memory of Academician Alexei Norairovich Sissakian

The local violation [6] of discrete symmetries in strongly interacting QCD matter is now under intensive theoretical and experimental investigations. The renowned Chiral Magnetic Effect (CME) uses the (C)P-violating (electro)magnetic field emerging in heavy ion collisions in order to probe the (C)P-odd effects in QCD matter.

There is an interesting counterpart of this effect, Chiral Vortaic Effect (CVE)[28, 29] due to coupling to P-odd medium vorticity. In its original form [28] this effect leads to the appearance of the same electromagnetic current as CME. Here we suggest a straightforward generalization of CVE resulting in generation of all conserved-charge currents. In particular, we address the case of the *baryonic* charge and the corresponding asymmetries of baryons, especially neutrons (not affected by CME), which can be measured by the MultiPurpose Detector (MPD) [30] at the Nuclotron-based Ion Collider fAcility (NICA) [31] at the Joint Institute for Nuclear Research (JINR).

Chiral Magnetic and Vortaic effects

The basic point in the emergence of CME is the coupling of the topological QCD field θ to the electromagnetic field A_α controlled by the triangle axial-anomaly diagram. Similar interaction of θ with the velocity field V_α exists in relativistic hydrodynamics due to the new coupling

$$e_j A_\alpha J^\alpha \Rightarrow \mu_j V_\alpha J^\alpha \tag{8.3}$$

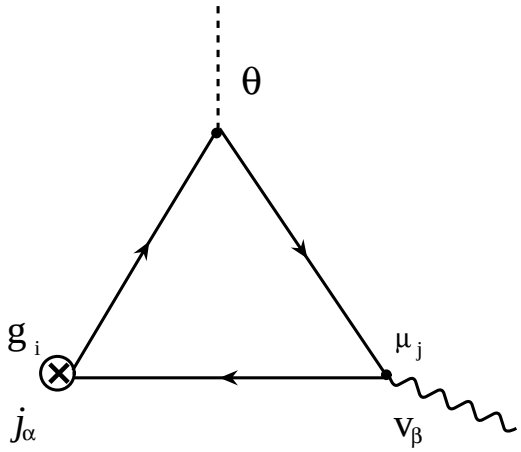

Figure 8.8: The generation of the current of the conserved charge g_i by the chemical potential μ_j.

involving the chemical potentials μ_j (for various flavours j) and the current J^α. It provides also the complementary description [32] of the recently found contribution of fluid vorticity to the anomalous non-conserved current [33]. Note that the similarity between the effects of the magnetic field and the rotation mentioned in [28] is very natural as the rotation is related by the Equivalence Principle to the so called *gravitomagnetic* field (see e.g. [34] and references therein).

CVE leads to similar (to CME) contribution to the electromagnetic current:

$$J_e^\gamma = \frac{N_c}{4\pi^2 N_f}\varepsilon^{\gamma\beta\alpha\rho}\partial_\alpha V_\rho \partial_\beta(\theta \sum_j e_j\mu_j) \ , \tag{8.4}$$

where N_c and N_f are the numbers of colours and flavours, respectively. If variation of the chemical potential is neglected, the charge induced by CVE for a given flavour can be obtained from that due to CME by substitution of the magnetic field with the curl of the velocity: $e_j\vec{H} \to \mu_j\vec{\nabla}\times\vec{V}$.

On one hand, CVE provides another source for the observed consequences of CME, relating with both light and strange [35] quarks (regarded as the heavy ones [36]). On the other hand (this is the basis of our following discussion), CVE leads also to the separation of charges different from the electric one. This becomes obvious if the current is calculated from the triangle diagram, where quark flavours j carry various charges $g_{i(j)}$ (see Fig. 8.8). The calculation may also be performed, following [28], by variation of the effective Lagrangian with respect to the external vector field. In that case this vector field can be not only the electromagnetic potential [28] (entering the Lagrangian describing the interaction with the real electromagnetic field) but also an arbitrary (auxiliary) field coupled to any conserved charge.

If variation of the chemical potential in Eq. (8.4) is neglected, the current of that charge g_i selecting the specific linear combination of quark triangle diagrams is related to electromagnetic one as follows (see Fig.1):

$$J_i^\nu = \frac{\sum_j g_{i(j)}\mu_j}{\sum_j e_j\mu_j}\ J_e^\nu \ . \tag{8.5}$$

In another extreme case of dominance of chemical potential gradients (assumed to be collinear) one get the relation

$$J_i^0 = \frac{|\vec{\nabla}\sum_j g_{i(j)}\mu_j|}{|\vec{\nabla}\sum_j e_j\mu_j|}\ J_e^0 \tag{8.6}$$

which might be useful e.g. for the mixed phase [42] description.

In particular, the large baryonic chemical potential (actually the largest one which is achievable in accelerator experiments [37]), appearing in the collisions at comparatively low energies at the FAIR and NICA (and possibly SPS and RHIC at low energy scan mode) facilities, may result in the separation of the baryonic charge. Of

special interest are manifestations of this separation in *neutron* asymmetries with respect to the production plane, as soon as the neutrons, from the theoretical side, are not affected by CME and, from the experimental side, there is a unique opportunity to study neutron production and asymmetries by MPD at NICA. Besides that, the noticeable strange chemical potential at the NICA energy range (see e.g. [38] and references therein) might result in the strangeness separation.

Experiments at NICA and neutron asymmetries

The numerical smallness of such expected vortaic effect makes it highly improbable to search it on an event-by-event basis. To collect statistics from different events one needs to construct a quadratic variable which does not depend on the varying sign of topological field fluctuations.

This problem was solved in the experimental studies of CME [39, 40, 41] by consideration of the angular asymmetries of *pairs* of particles with the same and opposite charges with respect to the reaction plane. Moreover, one can use three-particle correlations as well in order to avoid the necessity of fixing the reaction plane.

We suggest to use the similar correlations for baryonic charge. However, this method is not directly applicable in the case of baryon charge separation because of the very small number of produced antibaryons, in particular, antineutrons[5]. Nevertheless, the two-particle correlation for neutrons still might be used as one of the probes of CVE. In the case of three-particle correlations the third particle should not necessarily be the neutron and could also be a charged particle.

Note that the comparison of above-mentioned correlations for various particles could be very useful. Namely, CVE is negligible for pions, due to the rather small chemical potential, so that only CME contributes. On the other hand, for neutrons the correlations are entirely due to CVE, while for protons one should have both such effects. In case the correlations emerged due to other reasons than CVE and CME to quadratic order, then their simultaneous observation would be an important test of their actual existence.

For the studies of CVE we suggest the collider NICA[6] which is expected to operate with average luminosity $L \sim 10^{27} cm^{-2} s^{-1}$ for Au + Au collisions in the energy range $\sqrt{s_{\rm NN}} = 4 \div 11$ GeV/n (for Au^{79+}). In one of the collision points of NICA rings the Multi Purpose Detector (MPD) [30] will be located. MPD is proposed for a study of dense baryonic matter in collisions of heavy ions over the wide atomic mass range $A = 1 \div 197$. Inclusion of neutron detectors is also considered in the conceptual design of the MPD. The multiplicity of the neutrons in these collisions, predicted by the UrQMD model [43], will be about 200 in a full solid angle. The number of registered neutrons in each event depends on the event centrality and varies on the range $10 \div 150$ with a reasonable efficiency $\sim 80\%$ for neutron detection. With the proposed interaction rate for the detector MPD of about 10 kHz [30], it will be possible in a few months of accelerator running time to accumulate $\sim 10^9$ events with different centralities and measure CVE with comparable accuracy to CME or set an upper limit on the value of CVE. For the estimation of CVE we could explore the same three-particle correlator

$$\langle cos(\phi_\alpha + \phi_\beta - 2\phi_c) \rangle \tag{8.7}$$

which was used for the calculation of CME [39, 40, 41].

The possible magnitude of the statistical errors for the three-particle correlator with this number of collected events from the UrQMD model collisions of Au + Au at $\sqrt{s_{\rm NN}} = 9$ GeV is shown in Fig.8.9. The error points were obtained by taking two of the neutrons (α and β in Eq. (8.7)) from the mid-rapidity range ($|\eta| < 1$) and a third one (c in Eq. (8.7)) was taken from the ZDC rapidity range ($|\eta| > 3$). We should mention that the number of neutrons in each event within the mid-rapidity range is much smaller than the number of charged particles. Hence, in order to determine CVE with the same value of precision as in the CME case at RHIC [41], we need a much larger number of events. Precisely while $\sim$ 15M of events were sufficient at RHIC for targeted precision in the CME case, at NICA we need $\sim 1000M$ of events for the same precision in CVE measurements, which could be accumulated in a few months of NICA/MPD running time. More detailed estimates taking into account also neutron detector acceptances and efficiencies will be discussed elsewhere.

Conclusions and outlook

We discussed the new tests of P-odd effects in heavy ions collisions due to vorticity in the specific conditions of the MPD detector at NICA. Special attention was paid to the generalization of the Chiral Vortaic Effect to the case of separation of the baryonic charge and its manifestation in neutron asymmetries.

[5]Note that the opposite sign charge correlations for CME are also very small [41].

[6]The value of CME at NICA is under intensive discussion [42].

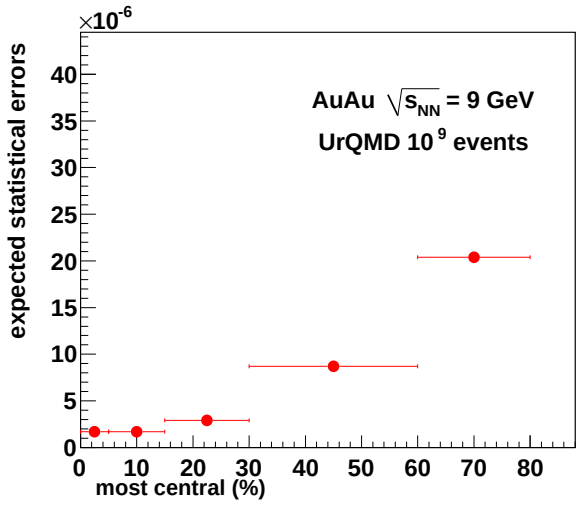

Figure 8.9: Estimation of statistical errors.

We proposed to study the two- and three-particle correlations similar to those used in studies of CME. We compared the required accuracies and found that CVE could be studied with the data collected in a few months of NICA running.

As an outlook, let us first mention that the non-perturbative (in particular, lattice QCD [44]) studies of vorticity effects are very important. Let us also note that the large chemical potential might result in meson decays forbidden in the vacuum, like C-violating $\rho \to 2\gamma$ [45, 46] or recently considered CP-violating $\eta \to 3\pi$ [47].

Vorticity is related to the global rotation of hadronic matter, an interesting observable by itself. Its manifestation in the polarization of Λ particles was suggested some time ago in [5] although the experimental tests at RHIC [39] did not show any significant effect. One may think that such a polarization can emerge due to the anomalous coupling of vorticity to the (strange) quark axial current via the respective chemical potential, being very small at RHIC but substantial at FAIR and NICA energies. In that case the Λ polarization at NICA [42] due to triangle anomaly can be considered together with other probes of vorticity [48] and recently suggested signals [49] of hydrodynamical anomaly. This option may be explored in the framework of the program of polarization studies at NICA [42] performed in the both collision points.

To collect the polarization data from different events one need to supplement the production plane with a sort of orientation. For this purpose one might use the left-right asymmetry of *forward* neutrons as it was done at RHIC [39, 40] or another observable, interesting by itself. The last comment regards handedness [50], namely, the P-odd multiparticle momenta correlation. Its exploration in heavy ion collisions provides a way of orienting the event plane and collecting data for Λ polarization and other P-odd observables.

Finally, let us mention the possibility [42] to study P-even angular distributions of dileptons [51] which might be used as probes of quadratic effects of CME [52] and, quite probably, CVE.

Bibliography

[1] D. E. Kharzeev, R. D. Pisarski and M. H. G. Tytgat, Phys. Rev. Lett. **81,** 512 (1998) [arXiv:hep-ph/9804221].

[2] D. Kharzeev and R D. Pisarski, Phys. Rev. **D 61,** 111901 (2000).

[3] D. Kharzeev, Phys. Lett. **B 633,** 260 (2006)

[4] D. Kharzeev, L. McLerran and H. Warringa, Nucl. Phys. **A 803,** 227 (2008), [arXiv:0711.0950].

[5] D. Kharzeev and A. Zhitnitsky, Nucl. Phys. **A 797,** 67 (2007).

[6] K. Fukushima, D. Kharzeev and H. Warringa, Phys. Rev. **D 78,** 074033 (2008), [arXiv:0808.3382].

[7] S.A. Voloshin, Phys. Rev. **C 70,** 057901 (2004), [arXiv:hep-ph/0406311].

[8] S. A. Voloshin, [arXiv:0806.0029].

[9] V. Skokov, A. Illarionov, and V. Toneev, [arXiv:0907.1396].

[10] D. Kharzeev, *talk at the NICA Round Table III*, (Dubna, 2008), http://theor.jinr.ru/ meetings/2008/roundtable/ .

[11] S. A. Voloshin, Phys. Rev. **C 62,** 044901 (2000) [arXiv:nucl-th/0004042].

[12] S. A. Voloshin (STAR Collaboration)*, talk at QM2009*.

[13] S. A. Voloshin, A. M. Poskanzer and R. Snellings, [arXiv:0809.2949].

[14] S. A. Voloshin and A. M. Poskanzer, Nucl. Phys. **B 474,** 27 (2000), [nucl-th/9906075].

[15] S. A. Voloshin, Nucl. Phys. **A 715,** 379 (2003), [nucl-ex/0210014].

[16] H. Satz, Nucl. Phys. **A 715,** 3 (2003) [hep-ph/0209181].

[17] D. Molnar and S. A. Voloshin, Phys. Rev. Lett. **91,** 092301 (2003) [nucl-th/0302014].

[18] R. J. M. Snellings, H. Sorge, S. A. Voloshin, F. Q. Wang and N. Xu, Phys. Rev. Lett. **84,** 2803 (2000), [nucl-ex/9908001].

[19] S. A. Voloshin and W. E. Cleland, Phys. Rev. **C 53,** 896 (1996) [nucl-th/9509025]; **54**, 3212 (1996), [nucl-th/9606033].

[20] S. Voloshin, R. Lednicky, S. Panitkin and N. Xu, Phys. Rev. Lett. **79,** 4766 (1997) [nucl-th/9708044].

[21] M. A. Lisa, S. Pratt, R. Soltz and U. Wiedemann, Ann. Rev. Nucl. Part. Sci. **55**, 357 (2005).

[22] Z. T. Liang and X. N. Wang, Phys. Rev. Lett. **94,** 102301 (2005) [nucl-th/0410079]; **96**, 039901 (2006).

[23] S. A. Voloshin, [arXiv:nucl-th/0410089].

[24] B. I. Abelev *et al.* (STAR Collaboration), Phys. Rev. **C 76,** 024915 (2007), [arXiv:0705.1691].

[25] A. A. Andrianov and D. Espriu, Phys. Lett. **B 663,** 450 (2008).

[26] A. A. Andrianov, V. A. Andrianov and D. Espriu, Phys. Lett. **B 678,** 416 (2009) [arXiv:0904.0413].

[27] A. A. Andrianov, D. Espriu, P. Giacconi and R. Soldati, JHEP **09**, 057 (2009) [arXiv: 0907.3709].

[28] D. Kharzeev and A. Zhitnitsky, Nucl. Phys. **A 797,** 67 (2007), [arXiv:0706.1026 [hep-ph]].

[29] D. Kharzeev, *Talk at the Round Table Discussion IV "Searching for the mixed phase of strongly interacting matter at the Nuclotron-based Ion Collider fAcility (NICA): Physics at NICA (White Paper)"*, (JINR Dubna, September 9 - 12 (2009)), http://theor.jinr.ru/meetings/2009/roundtable/

[30] *MPD Conceptual Design Report*, http://nica.jinr.ru

[31] *NICA Conceptual Design Report*, http://nica.jinr.ru

[32] F. V. Gubarev, V. I. Zakharov, *Talk at JINR/ITEP seminar on heavy ion collisions*, (February 15, 2010).

[33] D.T. Son and P. Surowka, Phys. Rev. Lett. **103,** 191601 (2009), [arXiv:0906.5044 [hep-th]].

[34] Y. N. Obukhov, A. J. Silenko and O. V. Teryaev, Phys. Rev. **D 80,** 064044 (2009), [arXiv:0907.4367 [gr-qc]].

[35] O. V. Teryaev, *Proceeding of SPIN-09 Workshop* (Dubna, September 1-5 2009), p. 147-150.

[36] M. V. Polyakov, A. Schafer and O. V. Teryaev, Phys. Rev. **D 60,** 051502 (1999), [arXiv:hep-ph/9812393].

[37] J. Randrup and J. Cleymans, Phys. Rev. **C 74,** 047901 (2006).

[38] V. D. Toneev, E. G. Nikonov, B. Friman, W. Norenberg and K. Redlich, Eur. Phys. J. **C 32,** 399 (2003), [arXiv:hep-ph/0308088].

[39] I. Selyuzhenkov [STAR Collaboration], J. Phys. G. **32,** S557 (2006), [arXiv:nucl-ex/0605035].

[40] B.I. Abelev *et al.* (STAR Collaboration), [arXiv:0909.1717 [nucl-ex]].

[41] S. A. Voloshin, [arXiv:1003.1127 [nucl-ex]].

[42] *NICA White Paper*, http://nica.jinr.ru , http://theor.jinr.ru/twiki-cgi/view/NICA/WebHome

[43] M. Bleicher, E. Zabrodin, C. Spieles *et al.*. J. Phys. G: Nucl. Part. Phys. **25** (1999) 1859

[44] P. V. Buividovich, M. N. Chernodub, E. V. Luschevskaya and M. I. Polikarpov, [arXiv:0909.1808 [hep-ph]].

[45] O. Teryaev, Chin. J. Phys. **34**, 1074 (1996).

[46] A. E. Radzhabov, M. K. Volkov and V. L. Yudichev, J. Phys. G. **32,** 111 (2006), [arXiv:hep-ph/0510329].

[47] R. Millo and E. V. Shuryak, [arXiv:0912.4894 [hep-ph]].

[48] B. Betz, M. Gyulassy and G. Torrieri, Phys. Rev. **C 76,** 044901 (2007), [arXiv:0708.0035 [nucl-th]].

[49] B. Keren-Zur and Y. Oz, [arXiv:1002.0804 [hep-ph]].

[50] A.V. Efremov, L. Mankiewicz and N.A. Tornqvist, Phys. Lett. **B 284,** 394 (1992).

[51] E. L. Bratkovskaya, O. V. Teryaev and V. D. Toneev, Phys. Lett. **B 348,** (1995) 283.

[52] P. V. Buividovich, M. N. Chernodub, D. E. Kharzeev, T. Kalaydzhyan, E. V. Luschevskaya and M. I. Polikarpov, [arXiv:1003.2180 [hep-lat]].

9 Cumulative processes

Cumulative processes are the processes that are kinematically forbidden for (quasi-)free nucleons. Therefore, they necessarily involve collective properties of the nuclear constituents and allow to extract unique information about the short-distance correlations of quarks and gluons in cold and hot hadronic matter. The study of cumulative processes was pioneered at Dubna; these studies can be extended at NICA at a new level. This section details the measurements that can be performed, and discusses the physics issues that can be addressed on the basis of the new data.

9.1 New forms of QCD matter and cumulative processes

A. Kaidalov

Institute for Theoretical and Experimental Physics, Moscow, Russia

It is emphasized that investigation of cumulative processes in nucleus-nucleus collisions can provide an important information on new forms of QCD matter at high baryon density. Properties of cumulative processes are shortly discussed and possible experiments for NICA facility are proposed. It was realized in recent years that the phase diagram of QCD has a rich structure. Besides the confinement-deconfinement phase transition there is a possibility of the color super-conductivity phase at very large baryon densities (see review [1]). On the other hand a structure of the phase diagram for baryon densities, which are several times larger than the usual nuclear density, is poorly known.

A very important question is: how to investigate the phase diagram of QCD and new forms of quark-gluon matter in laboratory? Here I would like to suggest to investigate these problems for the region of large baryon densities in experiments with nucleus-nucleus collisions in the kinematical region forbidden for interactions of quasi-free nucleons (the so called cumulative processes).

Cumulative processes have been discovered in early seventies [2] and were studied in interactions of hadrons and leptons with nuclei [3, 4, 5]. Existing experimental information is usually described in terms of dense multi-quark configurations in nuclei ("fluctons" [6]) or short-range correlation of nucleons [7, 8, 9, 10, 11, 12]. Such configurations can be considered as small drops of a new QCD phase in nuclei. These configurations exist in fast moving nuclei and may represent a new form of QCD matter.

Let me remind some characteristic properties of cumulative processes, which indicate that they are related to intrinsic properties of nuclei and reflect a new form of QCD matter.

- Universality of spectra in cumulative region. Spectra of hadrons in cumulative region $x > 1$ have a form $E\ d^3\sigma^a_{hA}/d^3p = exp(-\beta^a_A x)$ and the slope of the distribution β^a_A practically does not depend on initial energy, atomic number A and type of the produced hadron a.

- Average transverse momenta of produced hadrons increase as x increases. For pions $< p^2_T >$ reach values $\sim 2\ GeV^2$ at $x \sim 4$ [4]. These values are much larger than average transverse momenta of particles produced in interactions of hadrons and nuclei at high energies. Strange particle suppression is practically absent in cumulative region. There are many other characteristic features of cumulative processes, which can be interpreted as manifestation of dense multi-quark systems in nuclei. An information on cumulative particle production in nucleus-nucleus collisions is very limited and new facilities like NICA can considerably enlarge information on these interesting processes. It is worth to emphasize that colliders of very high energy like RHIC and LHC are not suitable for a study of these processes and the best region for investigation of non-nucleonic configurations in nucleus-nucleus collisions is the intermediate energy region $\sqrt{s_{\rm NN}} \sim 5$ GeV relevant for NICA.

Several observables, which can be studied in nucleus-nucleus collisions, sensitive to the effects considered above, are discussed below:

- It is important to study inclusive spectra of hadrons $E\ d^3\sigma^a_{A_1A_2}(b)/d^3p$ in the cumulative regions of both colliding nuclei. Broadening of spectra can be caused by multiple production of "drops" of a new phase and it is possible to search for a phase transition to the new phase. Deviations from the universality indicated above can be also due to "stopping" of produced fast hadrons by other nucleus. This effect leads to a faster decrease of spectra with x. It would be interesting to study spectra as functions of centrality.

- Is there an extra strangeness enhancement in cumulative region for nucleus-nucleus collisions? How it depends on atomic numbers and collision geometry? Very rich information can be obtained from a study of correlations for particles produced in cumulative regions:

  a) Production of two particles in the fragmentation region of the same nucleus. Here one can study BE-correlations and determine the sizes of production region. It is very interesting to study production of resonances in cumulative region (say ρ, ω, ϕ mesons). A study of multi-baryon resonances from decays of multi-quark configurations looks promising.

  b) Correlations between particles in the opposite fragmentation regions. One can look for interaction of two or more dense fluctuations. Production of particles with large transverse momenta, which can be due to such interactions is studied now at ITEP. To conclude, there is a very interesting and practically unexplored region of dense QCD medium, which can be studied in nuclear collisions at intermediate energies. Investigation of kinematical regions forbidden for quasi-free nucleon-nucleon interactions is the most suitable for these purposes. A rich experimental program of investigation of dense fluctuation for nuclei is formulated and can be realized at NICA.

9.2 The study of dense cold nuclear matter with cumulative trigger

A. Stavinskiy, O. Denisovskaya, Yu. Zaitsev, K. Mikhailov, P. Polozov, M. Prokudin, V. Stolin, R. Tolochek, S. Tolstoukhov and G. Sharkov

Institute for Theoretical and Experimental Physics, Moscow, Russia

It is important to study the phase diagram of nuclear matter and find out signals of phase transitions. The region of large density and small temperature is hardly accessible experimentally but strongly motivated by new theoretical results (see for example [13, 14, 15, 16, 17]. Cumulative effect [18] can be considered in terms of dense local multinucleon fluctuations (fluctons [19]), but some problems prevent the interpretation of such fluctons as dense nuclear matter droplet. First of all, flucton is a dynamical fluctuation with zero lifetime. Second it is a virtual configuration. And the last one, it is a small few-nucleon system.

We propose to study light ions collisions (from HeHe to CC) with high p_{T} midrapidity photon trigger(see figure). The maximum possible photon momentum corresponds to maximum c.m.s. collision energy and select a flucton-flucton interaction. High p_{T} process guarantee the locality (system size r of the order of 1 fm). It means that we can expect a dense real multinucleon ($6 - 7$ nucleons) system in the final state. Kinematical restriction will result in relatively small internal energy of the final multibaryon system with its relatively long lifetime. High density of the system just after collision ($20 \div 40\ \rho_0$) results in small mean-free path length $l << r \sim 1$ fm. It means that multinucleon system in the final state can be considered as a dense nuclear matter droplet [20].

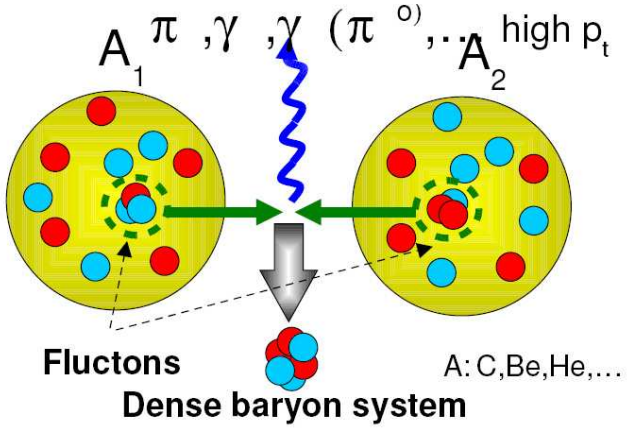

Figure 9.1: Artist's view of the flucton-flucton interaction process.

For the selected events we propose the wide analysis program to study dense nuclear system properties. Some analysis tasks are

- Relative momenta distribution study to check momentum space locality of the system due to kinematical properties of the proposed trigger
- Femtoscopy measurements (two particles correlations at small relative velocity) to check coordinate space locality of the system [21, 22, 23, 24, 25]
- Particle ratio ($n/p, \pi^+/\pi^-$) measurements to study the expected izosymmetrization effect [26]
- Strangeness production measurements (strangeness enhancement predicted for a hot QGP [27], expected also for cold dense matter)
- Vector meson production measurements (vector meson enhancement predicted in [28]; it is also interesting to check vector meson properties in dense matter)
- Search for exotic (like dibaryons or pentaquarks [29, 30, 31]). Fraction of exotic hadrons expected to be much higher than that for unselected events due to expected saturation of the nucleonic degrees of freedom.
- Search for direct photons (c.m.s. energy for flucton-flucton interactions will be much higher than that for NN collisions at the same beam momenta)
- Search for expected multifermion effects. It was shown that multiboson effects will modify standard meson femtoscopy at high density [32]. We also expect additional analysis items in the proposed program due to theoretical progress during the detector construction period. Program is proposed for MPD. Some program tasks need additional detector components (can be discussed separately; ITEP group responsibility also can be discussed). Trigger rate have being estimated base on real experimental data accumulated by FLINT collaboration in ITEP [33] and proved to be reasonable (see Table 9.2).

	Q1+Q2∼5	Q1+Q2∼6	Q1+Q2∼7
NICA	10^5(CC) 10^4(HeHe)	3.10^3(CC) 3.10^2(HeHe)	10^2(CC) 10^2(HeHe)
RHIC	10^3(CC) 10^2(HeHe)	3.10^1(CC)	

Table 9.1: Estimated data sample for 4π detector (expected number of accumulated events as a function of $Q_1 + Q_2$ for 10^6 sec run; preliminary)

In the table Q_1 and Q_2 are minimal numbers of nucleons in interacting fluctons. Estimate was done for CC (upper row) and HeHe (lower row) collisions at luminosity $L = 10^{30}\ cm^{-2}sec^{-1}$ (NICA) and $L = 10^{28}cm^{-2}sec^{-1}$ (RHIC).

Bibliography

[1] K. Rajagopal and P. Wilczek, [hep-ph/0011333]; T. Schafer and E. Shuryak, [nucl-th/0010049]; D. Rischke and R. Pisarsky, [hep-ph/0004016].

[2] A. M. Baldin, EPAN **8**, 429 (1971).

[3] V. S. Stavinsky, EPAN **10**, 949 (1979).

[4] S. B. Boyarinov *et al.*, Yad. Fiz. **34**, 119 (1991); S. B. Boyarinov *et al.*, Yad. Fiz. **57**, 1452 (1994).

[5] K. S. Egiyan *et al.*, Phys. Rev. Lett. **96,** 082501 (2006); E. Piasetsky *et al.*, Phys. Rev. Lett. **97,** 162504 (2006).

[6] D. I. Blokhintsev, JETP **33**, 1295 (1957).

[7] A. V. Efremov, Yad. Fiz. **24**, 1208 (1976).

[8] V. K. Lukyanov and A. I. Titov, EPAN **10**, 815 (1979).

[9] V.V. Burov, V.K. Lukyanov and A.I. Titov, EPAN **15**, 1249 (1984).

[10] A. V. Efremov, A. B. Kaidalov, V. T. Kim *et al.*, Sov. J. Nucl. Phys. **47**, 868 (1988);

[11] A.V. Efremov, A.B. Kaidalov, G.I. Lykasov and N.V. Slavin, Yad. Fiz. **7**, 932 (1994).

[12] M. I. Strikman and L. L. Frankfurt, EPAN **11**, 571 (1980).

[13] B.Barrois, Nucl. Phys. **B 129,** 390 (1977).

[14] D. Bailin and A. Love, Phys. Rep. **107,** 325 (1984).

[15] M. Alford, K. Rajagopal and F. Wilczek, Phys. Lett. **B B422,** 247 (1988).

[16] R. Rapp, T. Schafer, E. V. Shuryak and M. Velkovsky, Phys. Rev. Lett. **81,** 53 (1988).

[17] M. Alford, K. Rajagopal, T. Schafer and A. Schmitt, Rev. Mod. Phys. **80**, 1455 (2008).

[18] A. M. Baldin *et al.*, *JINR Preprint* P1-5819 (1971); Yad. Fiz. **18**, 79 (1973).

[19] D. I. Blokhintsev, JETP **6**, 995 (1958).

[20] D. Seibert, Phys. Rev. Lett. **63,** 136 (1989); R.S. Bhalerao and R.K. Bhaduri, [hep-ph/0009333].

[21] G. I. Kopylov and M. I. Podgortski, Yad. Fiz. **15**, 392 (1972).

[22] S. E. Koonin, Phys. Lett. **B 70,** 43 (1977).

[23] P. Lednitski and V. L. Ljuboshitz, Yad. Fiz. **35**, 1316 (1982).

[24] B. K. Jennings, D. W. Boal and C. J. Shillcock, Phys. Rev. **C 33,** 1303 (1986).

[25] Yu. D. Bajukov *et al.*, Yad. Fiz. **50**, 1023 (1989).

[26] Yu. D. Bajukov *et al.*, Yad. Fiz. **42**, 185 (1985); L.S.Vorobijov *et al.*, Yad. Phys. **59**, 694 (1996).

[27] J. Rafelski and B. Muller, Phys. Rev. Lett. **48,** 1066 (1982).

[28] A. M. Baldin and S. B. Gerasimov, *JINR communication* E2-11804 (1978).

[29] L. A. Kondratjuk *et al.*, Yad. Fiz. **45**, 1252 (1987).

[30] A. A. Grigirjan and A. B. Kaidalov, JETP Letters **28**, 318 (1978); Nucl. Phys. **B 135,** 93 (1978).

[31] D. Diakonov, Prog. Nucl. Phys. **51**, 173 (2003); R.L. Jaffe, [hep-ph/0409362].

[32] R. Lednicky *et.al.*, Phys. Rev. **C 61,** 034901 (2000).

[33] I. Alekseev *et al.*, Yad. Fiz. **71**, 1879 (2008).

10 Polarization effects and spin physics

This section contains the discussion of two important issues: i) polarization effects in heavy ion collisions and ii) the spin program with polarized beams. The studies of polarization effects in heavy ion collisions have just began. The conversion of the huge initial angular momentum available in a heavy ion collision into the angular momentum carried by dense matter, and possibly by the spins of produced particles is an extremely interesting problem. Understanding it will undoubtedly allow to penetrate deeper into the collision dynamics. A number of observables are proposed in this section – most of them have never been studied before in heavy ion experiments. The physics issues include the dynamics of the collision, the chiral properties of the produced medium, and of the possible local violation of $\mathcal{P}$ and $\mathcal{CP}$ invariances discussed above.

The spin program is an important and integral part of the NICA project. Indeed, ever since the "spin crisis" of 1987, the composition of the nucleon's spin in terms of the fundamental constituents – quarks and gluons – remains in the focus of attention of many physicists. This section contains the discussion of the physics goals and perspectives of the spin program at NICA. The highlights of the NICA spin program include the measurements of Drell-Yan processes with longitudinally polarized proton and deuteron beams, spin effects in the inclusive and exclusive production of baryons, light and heavy mesons and direct photons, and the studies of helicity amplitudes and double spin asymmetries in elastic scattering. This section also addresses the issue of the competitiveness of the NICA spin program – it appears that the SPD detector at NICA would allow to contribute significantly to the current and planned international program in spin physics.

10.1 Polarization effects in heavy ions collisions at NICA

A. Efremov, O. Teryaev and V. Toneev

Joint Institute for Nuclear Research, Dubna, Russia

Spin effects are known to be the most sensitive tests of the the adequacy of theoretical description of high energy processes. Their investigation in heavy ion collisions is currently not very well developed, probably because of the experimental difficulties of the polarization measurements having the large number of produced particles. The exploration of spin effects in the new generation of experiments with heavy ions, including NICA, offers a new opportunities for the detailed studies of the patterns of hadronic phases.

The polarization observable which can be studied in the easiest way is the hyperon (in particular, Λ) polarization revealing itself via the angular asymmetry in the parity violating decay. Due to the parity conservation in the case of binary or inclusive reaction it can be only transverse (like all Single Spin Asymmetries in QCD [1]), i.e. directed normally to the scattering plane providing the only available pseudovector. If any kind of (isotropic) hadronic medium is formed and the direction of the colliding beams is "forgotten", the transverse polarization should be diluted. At the same time, the longitudinal polarization emerging in the parity-violating weak Σ decays should be preserved. Such changes in the Λ polarization were suggested [2, 3, 4] as a signal for hadronic medium formation. The observation of the effect of dilution of transverse polarization at NICA may be an important complementary probe of the mixed phase.

In order to observe the transverse polarization together with the longitudinal one it is possible to choose its direction normal to the reaction rather than production plane. The latter may be identified in event-by-event analysis. It is also important to have this plane oriented, which was achieved by the identification of left-right asymmetry of forward neutrons. Nevertheless the RHIC data showed that the polarization is compatible with zero. This contradicts to the model [5] of the coupling of the collective orbital momentum of the produced medium to the hyperon spin. This may not be surprising as this orbital momentum is distributed among a large number of hadrons and its amount coupled to the polarization of a single hadron is quite small. One may therefore use various types of the transverse handedness [6] to probe the orbital momentum of the matter.

As soon as Single Spin Asymmetries are $\mathcal{T}$-odd observables, they may emerge due to the effects of spontaneous $\mathcal{CP}$-violation in dense matter. Therefore, the correlations of Λ polarization with with the charge separation (see [7, 8] and references therein) may be used for the search of this effect.

The $\mathcal{T}$-even polarization observables are represented, first of all, by the anisotropy of dileptons [9, 10] probing the tensor polarization of virtual photon. The formation of isotropic matter provides the important restrictions to its form, depending only on polar angle in Collins-Soper frame and being sensitive to mechanisms of dilepton productions [11]. The existence of the preferred direction, like the normal to the production plane may give

rise also to azimuthal asymmetries, providing another probe for collective orbital momentum. There are also much more strong effects [12] if the directions of colliding ions momenta are somehow remembered which may be studied in the correlation analysis together with the other observables.

To conclude, the following polarization observables at NICA may be studied:

- Polarization of Λ as a probe of formation of isotropic matter.
- Correlations of Λ polarization with charge sepration as a complementary signal for $\mathcal{CP}$-violation in dense matter.
- Transverse handedness as a probe for collective orbital momentum of the matter.
- Tensor polarization of dileptons as a complementary probe of matter formation, dilepton production mechanisms and collective orbital momentum.

10.2 Spin physics

A. Efremov, A. Nagaytsev, I. Savin, O. Shevchenko and O. Teryaev

Joint Institute for Nuclear Research, Dubna, Russia

The composite nature of the nucleon spin structure has been studied for a long time by means of Deep Inelastic Scattering (DIS) of leptons and production of Drell-Yan (DY) [13] lepton pairs in the Bjorken regime. As a consequence of the high scale Q, scattering occurs in a collinear configuration between the incident lepton and a single parton in the nucleon. The factorization theorem allows the inclusive DIS and DY cross section to be expressed as a convolution of two contributions: one corresponds to the hard process occurring at short distance between probe and parton; the other accounts for the coherent long-distance interactions between parton and target, and is described in terms of parton distributions. In the leading order (leading twist) the variable x can be interpreted as a fraction of the longitudinal momentum of the parent (fast-moving) nucleon carried by the active parton, and one may distinguish three kinds of Parton Distributions Functions (PDF). Two of them are well-known structure functions measured in DIS and other processes: f_1^α (α is a parton flavor, often suppressed) is the density of unpolarized partons with longitudinal momentum fraction x in an unpolarized nucleon, and $g_1(x)$ giving the net helicity of partons in a longitudinally polarized nucleon. The third one, the transversity $h_1(x)$, describing the density of partons with polarization parallel to that of a transversely polarized nucleon minus the density of partons with antiparallel polarization, is chiral-odd and requires a quark helicity flip that cannot be achieved in hard subprocess. Other parts of the cross section have to be explored for that. They are either chiral-odd Fragmentation Function (FF) (e.g. Collins fragmentation function $H_1^\perp$ in semi inclusive DIS (SIDIS) or another transversity of the second polarized incident hadron in the DY).

However, in addition to the information on the longitudinal behaviour in momentum space along the direction in which the nucleon is moving, a complete three-dimensional picture of the nucleon also requires knowledge of the transverse motion of partons [14, 15]. A full account of the orbital motion, which is also an important issue to understand the spin structure of the nucleon, can be given in terms of Transverse-Momentum Dependent parton distribution functions (TMDs). There are eight leading-twist TMDs: $f_1(x, p_\mathrm{T})$, $f_{1T}^\perp(x, p_\mathrm{T})$, $g_{1L}(x, p_\mathrm{T})$, $g_{1T}(x, p_\mathrm{T})$, $h_1(x, p_\mathrm{T})$, $h_{1L}^\perp(x, p_\mathrm{T})$, $h_{1T}^\perp(x, p_\mathrm{T})$, $h_{1L}^\perp(x, p_\mathrm{T})$. Two of them, the Boer-Mulders and Sivers function, $h_1(x, p_\mathrm{T})$ and $f_{1T}^\perp(x, p_\mathrm{T})$ [16, 17], are $\mathcal{T}$-odd, *i.e.* they change sign under naive time reversal, which is defined as usual time reversal, but without interchange of initial and final states. The other six leading-twist TMDs are $\mathcal{T}$-even. In order to be sensitive to intrinsic transverse parton momenta, it is necessary to measure adequate transverse momenta of the produced hadrons in the final state, e.g., in processes like semi-inclusive lepton-nucleon DIS (SIDIS), hadron production in e^+e^- annihilation [14, 15, 16, 17] or the transverse momentum lepton pair in the Drell-Yan processes in hadron-hadron collisions. Here, factorization has been proved at leading twist [18, 19, 20] allowing to access information on TMDs as well as on fragmentation functions (FFs) describing the hadronization process of the hit quark decaying into the detected hadrons. At leading twist, the fragmentation of unpolarized hadrons is described in terms of two fragmentation functions, $D_1(z, K_\mathrm{T})$ and $H_1^\perp(z, K_\mathrm{T})$, where z is the energy fraction taken out by the detected hadron and $K_T = |\vec{K}_\mathrm{T}|$ its transverse momentum. The function $D_1(z, K_\mathrm{T})$ describes the decay of an unpolarized quark, whereas the Collins function $D_1(z, K_\mathrm{T})$ describes a left-right asymmetry in the decay of a transversely polarized quark [6]. By measuring the angular distribution of produced hadrons in SIDIS or lepton pairs in DY, it is possible to access information

on all eight leading-twist TMDs in combinations with the two leading-twist FFs. Restricting ourselves to the one-photon approximation and considering spin degrees of freedom such as the beam helicity and the target spin, the contraction between the lepton and hadron tensors in the cross section can be decomposed in a model-independent way in terms of eighteen structure functions, thus exhibiting a non trivial azimuthal dependence of the detected hadron in SIDIS [21] or lepton pairs in the DY [22]. According to factorization, each of the leading-twist structure functions can be conceived as a convolution between one TMD and one FF in SIDIS or two TMDs (for quark and antiquark) in the DY. Since structure functions enter the cross section with a defined angular coefficient, they can be accessed by looking at specific azimuthal asymmetries. This has become now a powerful tool for studying the three-dimensional structure of the nucleon [23, 24] and many more data are expected to come in the future. The remarkable experimental progress was accompanied by and motivated numerous theoretical and phenomenological studies in literature.

Concerning the Drell-Yan process. During the past decades dilepton production in high-energy hadron-hadron collisions [13, 25] has played an important role in order to pin down parton distributions (PDFs) of hadrons. While the main focus was on PDFs of the nucleon, also information on the partonic structure of the pion was already obtained through Drell-Yan measurements. The crucial tool, required for the extraction of PDFs, is the QCD-factorization theorem if the invariant mass of the dilepton pair is sufficiently large. Experimentally, the Drell-Yan process is quite challenging because of the relatively low counting rates. On the other hand, from the theoretical point of view it is the cleanest hard hadron-hadron scattering process. The fact that no hadron is detected in the final state simplifies the proof of factorization in comparison to hadron-hadron collisions with hadronic final states. This important point is one of the main reasons for the continued interest in the Drell-Yan reaction. Currently, not less than six programs for future Drell-Yan measurements are pursued. These plans comprise dilepton production in nucleon-nucleon collisions (at RHIC [26], J-PARC(KEK) [27, 28], IHEP(Protvino) [29], and at the JINR (Dubna) [30], in antiproton nucleon collisions (at FAIR (GSI) [31], as well as in pion-nucleon collisions at COMPASS (CERN). Past measurements exclusively considered the unpolarized cross section, but all future programs are also aiming at polarization measurements. Including polarization of the incoming hadrons opens up a variety of new opportunities for studying the strong interaction in both the perturbative and the nonperturbative regime. Enough to mention, the opportunities to access the transversity distribution of the nucleon [32, 33] and to other TMDs describing the strength of various intriguing spin-spin or spin-orbit correlations of the parton-hadron system [34, 35] for more information on TMDs.

In order to analyze upcoming and planning new data from polarized Drell-Yan measurements it is necessary to have a general and concise formalism at hand. This step is most conveniently done in a dilepton rest frame like the Collins-Soper frame [36] with z-axis in direction in the sum of incident hadrons momenta. However, to the best of our knowledge, a complete formalism for the polarized Drell-Yan process has not been worked out yet. This is a challenge to theory and availability of the experimental data is very important for this purpose.

In addition to model-independent results, the process in the parton model approximation is usually considered. In the latter case TMDs enter in the parton model description and in a full QCD treatment [19, 20].

The parameters of the NICA collider allows to perform the important spin and polarization effect studies of:

- Drell-Yan (DY) processes with longitudinally and transversely polarized p and d beams. Extraction of unknown (poor known) Parton Distribution Functions (PDFs);
- PDFs from J/ψ production processes;
- Spin effects in baryon, meson and photon production;
- Effects in various exclusive reactions;
- Diffractive processes;
- Cross sections, helicity amplitudes and double spin asymmetries (Krisch effect) in elastic reactions;
- Spectroscopy of quarkonium.

The preliminary design of the SPD detector for spin effects studies is based on the requirements set by the DY and J/ψ productions studies. These requirements are the following:

- almost 4π geometry for secondary particles;

- precision vertex detector;
- precision tracking system ;
- precision momentum measurement of secondary particles;
- good particle identification capabilities for (μ, π, p, e etc.);
- high trigger rate capabilities.

The most of these requirements are also good for other studies mentioned in previous sections. Basing on these requirements several possible scheme of SPD are considered, one of them is similar to the detector of PAX experiment (close to NICA in kinematics) at FAIR GSI, the second one is the SPD of limited possibilities, providing the muon pair detection only and the third is the scheme of SPD based on so-called Muon Range System, which is considered as detector for PANDA muon system. The final version of the SPD will be defined after detailed Monte-Carlo simulations and consideration of requirements for other spin effects studies. The purpose is to have the simple universal detector.

Since the famous "spin crisis" in 1987, the problem of the nucleon spin structure remains one of the most intriguing puzzle of high energy physics. The central component of this problem attracting for many years enormous both theoretical and experimental efforts, is a search for answering the questions, how the spin of the proton is build up from spins and orbital momenta of its constituents. The searches brought up a concept of the parton distribution functions in nucleon, at the beginning two of them, one, f_1, for unpolarized and second, g_1, for polarized nucleons. Now we know that about 50 different parton distributions functions are needed for a complete description of the nucleon structure. While today a part of the polarized distributions can be considered as sufficiently well known, there is a number of PDFs which are either absolutely unknown or poorly known, especially the spin dependent ones, These are longitudinally polarized distributions of valence light sea, strange quarks and gluons, both sea and valence transversely polarized distributions of all flavours. This new class of PDFs is characterized by its non-trivial dependence on a transverse quark momentum. The most significant among them are Sivers and Boer-Mulders PDFs. The studies of these open questions of the nucleon structure is the first priority task for the scientific program of the second IP the NICA facility.

10.3 Polarization of Λ^0 hyperons in nucleus-nucleus collisions at MPD

V. Ladygin, A. Jerusalimov and N. Ladygina

Joint Institute for Nuclear Research, Dubna, Russia

One of the new signature of the phase transition from ordinary nuclear matter to a quark gluon plasma (QGP) can be the change of in the polarization properties of the secondary particles in the nucleus-nucleus collisions compared to the nucleon-nucleon collisions. A number of polarization observables have been proposed as a possible signature of phase transition, namely, decreasing of the Λ^0 transverse polarization in central collisions [37, 38], non-zero $\bar{\Lambda}^0$ longitudinal polarization [2, 3, 4, 39], non-zero J/ψ polarization at low $p_{\rm T}$ [12], anisotropy in di-electron production from vector mesons decay [40] (and references therein), global hyperon polarization [5] and spin-alignment of vector mesons [41] in non-central events etc.

However, at the moment there are only few results on the Λ^0 polarization in nucleus-nucleus interaction [42, 43, 44, 45]. The precise measurements of Λ^0 polarization in nucleus-nucleus collisions at $\sqrt{s_{\rm NN}}$ of several GeV can be performed using the high luminosity MPD/NICA setup [46].

A significant amount of the data on Λ^0 polarization in pp- and pA-collisions has been accumulated at different nucleon initial energies between 6 and $\sim$2000 GeV. The data show large effect as a function of transverse momenta $p_{\rm T}$ and $x_{\rm F}$. Most of the models explain the Λ^0 polarization by the recombination of a polarized s-quark with an unpolarized (ud) spectator diquark. For instance, in the framework of the semiclassical recombination model of DeGrand-Miettinen [47] the Λ^0 polarization is defined by the slow s-quark spin precession.

In the case of relativistic nucleus-nucleus collisions, the expectation is that, Λ^0's coming from the region where the critical density for QGP formation has been achieved, are produced through the coalescence of independent slow sea u, d and s quarks. Therefore, the plasma creates Λ^0 with zero polarization [38]. Finally, in the case of QGP formation the depolarization effect compare to proton-induced reaction should be observed.

One expect up to 30–40% of the depolarization effect for the central events [38]. It is shown that the measurable depolarization effect can be observed at the Λ^0 transverse momenta $p_T \geq (0.6 - 0.8)$ GeV/c.

Another novel phenomena is so called global polarization [5, 41]. System in the noncentral collisions have large orbital angular momentum, which manifests in the polarization of secondary particles along the direction of the system angular momentum. Parton interaction in noncentral relativistic nucleus-nucleus collisions leads to the global polarization of the produced quarks.

The main method to measure Λ^0 polarization in nucleus-nucleus collisions is the measurement of the emission angle distribution of the decay proton with respect to the system orbital momentum L (reaction plane). Feasibility of Λ^0 polarization measurement at high energies can be estimated from UrQMD transport model. One can expect production of approximately 20 Λ^0's decaying into $p\pi^-$ pair in the central Au + Au collisions at the energies $\sqrt{s_{NN}}$ of several GeV·A. The collider mode provides more symmetrical acceptance for Λ^0 hyperons than fixed target experiments, that is significant for the proper reconstruction of the polarization. Also, the important feature of MPD setup is quite large acceptance for the detection of the both protons and pions. Therefore, it is possible to detect the Λ^0- hyperons with large transverse momenta p_T, where maximal effect in polarization properties is expected. The $y - p_T$ ideal acceptance for Λ^0's from Au + Au central collisions at $\sqrt{s_{NN}}$= 7.1 GeV for the collider mode (assuming the axial symmetry of MPD) is show in Fig. 10.1.

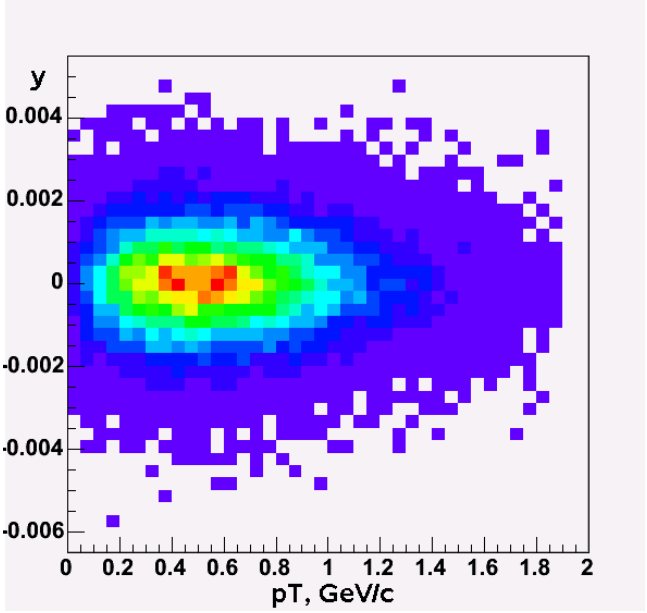

Figure 10.1: The $y - p_T$ acceptance for Λ^0's from Au + Au central collisions at $\sqrt{s_{NN}}$= 7.1 GeV for the collider mode.

Since no particle identification is required the transverse momenta p_T achieved can be large enough to measure sizable polarization effects for Λ^0's production. In this case the main source of the background is K^0_S meson decaying into $\pi^+\pi^-$ pair. The measurement of the Λ^0 polarization requires good knowledge of the kinematical parameters of the Λ^0, as well as the reaction plane and centrality value, which can be measured with zero degree calorimeter PSD or via charged particles energy flow reconstructed in the time-projection chamber.

The measurement of the Λ^0 polarization in nucleus-nucleus collisions at the energies of NICA can be a new important tool in addition to the traditional ones to study the features of mixed phase and phase transition. The study of the polarization effects in hyperon production for the collider mode can be performed at MPD setup and has certain advantages compared to the fixed target experiments.

10.4 Possible effect of mixed phase and deconfinement upon spin correlations in the $\Lambda\bar{\Lambda}$ pairs generated in relativistic heavy-ion collisions

V.L. Lyuboshitz and V.V. Lyuboshitz

Joint Institute for Nuclear Research, Dubna, Russia

Spin correlations for the $\Lambda\Lambda$ and $\Lambda\bar{\Lambda}$ pairs, generated in relativistic heavy ion collisions, and related angular correlations at the joint registration of hadronic decays of two hyperons with nonconservation of space parity are analyzed. Within the conventional model of one-particle sources, correlations vanish at enough large relative momenta. However, under these conditions, in the case of two non-identical particles ($\Lambda\bar{\Lambda}$) a noticeable role is played by two-particle annihilation (two-quark, two-gluon) sources, which lead to the difference of the correlation tensor from zero. In particular, such a situation may arise when the system passes through the "mixed phase" .

Generalities

The spin density matrix of the $\Lambda\Lambda$ and $\Lambda\bar{\Lambda}$ pairs, just as the spin density matrix of two spin-1/2 particles in general, can be presented in the following form [**?**, 48, 49]:

$$\hat{\rho}^{(1,2)} = \frac{1}{4}\left[\hat{I}^{(1)}\otimes\hat{I}^{(2)} + (\hat{\boldsymbol{\sigma}}^{(1)}\mathbf{P}_1)\otimes\hat{I}^{(2)} + \hat{I}^{(1)}\otimes(\hat{\boldsymbol{\sigma}}^{(2)}\mathbf{P}_2) + \sum_{i=1}^{3}\sum_{k=1}^{3} T_{ik}\hat{\sigma}_i^{(1)}\otimes\hat{\sigma}_k^{(2)}\right]; \tag{10.1}$$

in doing so, $tr_{(1,2)}\hat{\rho}^{(1,2)} = 1$.

Here $\hat{I}$ is the two-row unit matrix, $\hat{\boldsymbol{\sigma}} = (\ \hat{\sigma}_x,\ \hat{\sigma}_y,\ \hat{\sigma}_z\ )$ is the vector Pauli operator ($x, y, z \to 1, 2, 3$), $\mathbf{P}_1$ and $\mathbf{P}_2$ are the polarization vectors of first and second particle ($\mathbf{P}_1 = \langle\hat{\boldsymbol{\sigma}}^{(1)}\rangle$, $\mathbf{P}_2 = \langle\hat{\boldsymbol{\sigma}}^{(2)}\rangle$), $T_{ik} = \langle\hat{\sigma}_i^{(1)}\otimes\hat{\sigma}_k^{(2)}\rangle$ are the correlation tensor components . In the general case $T_{ik} \neq P_{1i}\,P_{2k}$. The tensor with components $C_{ik} = T_{ik} - P_{1i}P_{2k}$ describes the spin correlations of two particles .

It is essential that any decay of an unstable particle may serve as an analyzer of its spin state .

Let us consider the double angular distribution of flight directions for protons formed in the decays of two Λ particles into the channel $\Lambda \to p + \pi^-$, normalized by unity (the analyzing powers are $\boldsymbol{\xi}_1 = \alpha_\Lambda\mathbf{n}_1$, $\boldsymbol{\xi}_2 = \alpha_\Lambda\mathbf{n}_2$). It is described by the following formula [**?**, **?**]:

$$\frac{d^2\,w(\mathbf{n}_1,\mathbf{n}_2)}{d\,\Omega_{\mathbf{n}_1}\,d\,\Omega_{\mathbf{n}_2}} = \frac{1}{16\,\pi^2}\left[1 + \alpha_\Lambda\mathbf{P}_1\,\mathbf{n}_1 + \alpha_\Lambda\mathbf{P}_2\,\mathbf{n}_2 + \alpha_\Lambda^2\sum_{i=1}^{3}\sum_{k=1}^{3} T_{ik}n_{1i}n_{2k}\right], \tag{10.2}$$

where $\mathbf{P}_1$ and $\mathbf{P}_2$ are polarization vectors of the first and second Λ particle, T_{ik} are the correlation tensor components, $\mathbf{n}_1$ and $\mathbf{n}_2$ are unit vectors in the respective rest frames of the first and second Λ particle, defined in the common (unified) coordinate axes of the c.m. frame of the pair ($i, k = \{1, 2, 3\} = \{x, y, z\}$) .

The polarization parameters can be determined from the angular distribution of decay products by the method of moments [48, 49] – as a result of averaging combinations of trigonometric functions of angles of proton flight over the double angular distribution .

The angular correlation, integrated over all angles except the angle between the vectors $\mathbf{n}_1$ and $\mathbf{n}_2$ and described by the formula [48, 49, 50, 51]

$$d\,w(\cos\theta) = \frac{1}{2}\,(\,1 + \frac{1}{3}\,\alpha_\Lambda^2 T\,\cos\theta)\sin\theta d\,\theta = \frac{1}{2}\,[\,1 - \alpha_\Lambda^2\,(W_s - \frac{W_t}{3})\cos\theta]\sin\theta d\,\theta, \tag{10.3}$$

is determined only by the "trace" of the correlation tensor $T = W_t - 3W_s$ (W_s and W_t are relative fractions of the singlet state and triplet states, respectively), and it does not depend on the polarization vectors (single-particle states may be unpolarized).

Due to CP invariance, the coefficients of P-odd angular asymmetry for the decays $\Lambda \to p+\pi^-$ and $\bar{\Lambda} \to \bar{p}+\pi^+$ have equal absolute values and opposite signs: $\alpha_{\bar{\Lambda}} = -\alpha_\Lambda =$
$-\,0.642$. The double angular distribution for this case is as follows [48, 49]:

$$\frac{d^2\,w(\mathbf{n}_1,\mathbf{n}_2)}{d\,\Omega_{\mathbf{n}_1}\,d\,\Omega_{\mathbf{n}_2}} = \frac{1}{16\,\pi^2}\left[1 + \alpha_\Lambda\mathbf{P}_\Lambda\,\mathbf{n}_1 - \alpha_\Lambda\mathbf{P}_{\bar{\Lambda}}\,\mathbf{n}_2 - \alpha_\Lambda^2\sum_{i=1}^{3}\sum_{k=1}^{3} T_{ik}n_{1i}n_{2k}\right], \tag{10.4}$$

(here $-\alpha_\Lambda = +\alpha_{\bar\Lambda}$ and $-\alpha_\Lambda^2 = +\alpha_\Lambda\alpha_{\bar\Lambda}$) .

Thus, the angular correlation between the proton and antiproton momenta in the rest frames of the Λ and $\bar\Lambda$ particles is described by the expression:

$$d\,w(\cos\theta) = \frac{1}{2}\,(\,1 - \frac{1}{3}\,\alpha_\Lambda^2 T\,\cos\theta)\sin\theta d\,\theta = \frac{1}{2}\,[\,1 + \alpha_\Lambda^2\,(W_s - \frac{W_t}{3})\cos\theta]\sin\theta d\,\theta, \tag{10.5}$$

where θ is the angle between the proton and antiproton momenta.

Spin correlations at the generation of $\Lambda\,\Lambda$ pairs in multiple processes

We will use the model of one-particle sources [52], which is the most adequate one in the case of collisions of relativistic ions .

Two Λ particles are identical particles. Spin and angular correlations in this case arise due to the Fermi statistics and final-state interaction.

Indeed, it is easy to see that the Fermi-statistics effect leads not only to the momentum–energy $\Lambda\,\Lambda$-correlations at small relative momenta (correlation femtoscopy), but to the spin correlations as well.

The following relation holds, in consequence of the symmetrization or antisymmetrization of the total wave function of any identical particles with nonzero spin (bosons as well as fermions) [53]:

$$(-1)^{S+L} = 1. \tag{10.6}$$

Here, S is the total spin and L is the orbital momentum in the c.m. frame of the pair. At the momentum difference $q = p_1 - p_2 \to 0$ the states with nonzero orbital momenta "die out", and only states with $L = 0$ and even total spin S survive.

Since the Λ-particle spin is equal to $1/2$, at $q \to 0$ the $\Lambda\,\Lambda$ pair is generated only in the singlet state with $S = 0$.

Meantime, at the 4-momentum difference $q \neq 0$ there are also triplet states generated together with the singlet state.

Within the conventional model of one-particle sources emitting unpolarized particles, the triplet states with spin projections $+1$, 0, and -1 are produced with equal probabilities. If correlations are neglected, the singlet state is generated with the same probability – the relative "weights" are $\widetilde{W}_t = 3/4$, $\widetilde{W}_s = 1/4$.

When taking into account the Fermi statistics and s-wave final-state interaction, which is essential at close momenta (at orbital momenta $L \neq 0$ the contribution of final-state interaction is suppressed), the fractions of triplet states and the singlet state are renormalized .

We will perform here the analysis of spin $\Lambda\Lambda$ correlations in the c.m. frame of the $\Lambda\Lambda$ pair . In the c.m. frame, we have: $q = \{0, 2\mathbf{k}\}$, where q is the difference of 4-momenta of the Λ particles, $\mathbf{k}$ is the momentum of one of the particles. In doing so, the momentum $\mathbf{k}$ is connected with the relative momentum $\mathbf{q}$ in the laboratory frame by the Lorentz transformation [54],(we use the unit system with $\hbar = c = 1$):

$$\mathbf{k} = \frac{1}{2}\,\left[\mathbf{q} + (\gamma - 1)\frac{(\mathbf{qv})\mathbf{v}}{|\mathbf{v}|^2} - \gamma\mathbf{v}\,q_0\right]; \tag{10.7}$$

here, $\mathbf{v} = (\mathbf{p}_1 + \mathbf{p}_2)/(\varepsilon_1 + \varepsilon_2)$ is the velocity of the $\Lambda\Lambda$ pair in the laboratory frame, $\gamma = (1 - v^2)^{-1/2}$ is the Lorentz factor, $\mathbf{q} = \mathbf{p}_1 - \mathbf{p}_2$ and $q_0 = \varepsilon_1 - \varepsilon_2$ are the laboratory relative momentum and energy, respectively .

The Lorentz transformations of 4-coordinates are given by the expressions:

$$\mathbf{r}^* = \mathbf{r} + (\gamma - 1)\,\frac{(\mathbf{rv})\mathbf{v}}{|\mathbf{v}|^2} - \gamma\mathbf{v}\,t, \qquad t^* = \gamma(t - \mathbf{vr}), \tag{10.8}$$

where $\mathbf{r} = \mathbf{r}_1 - \mathbf{r}_2$ and $t = t_1 - t_2$ are the differences of coordinates and times for one-particle sources in the laboratory frame .

The interference term connected with identity (quantum statistics) is determined by the expression:

$$\langle\cos 2\mathbf{kr}^*\rangle = \int W_{\mathbf{v}}(\mathbf{r}^*)\cos(2\mathbf{kr}^*)d^3\mathbf{r}^*, \tag{10.9}$$

where

$$W_{\mathbf{v}}(\mathbf{r}^*) = \int W(x)\,d\,t^* = \int W(\mathbf{r}^*, t^*)\,d\,t^*$$

is the distribution of coordinate difference between two sources in the c.m. frame of the $\Lambda\Lambda$ pair.

Meantime, the contribution of s-wave final-state interaction is expressed as follows (at the sizes of the generation region in the c.m. frame, exceeding the effective radius of interaction of two Λ particles):

$$B_{\rm int}(q) = B^{(\Lambda\Lambda)}(\mathbf{k},\mathbf{v}) = \int W_{\mathbf{v}}(\mathbf{r}^*)\, b(\mathbf{k},\mathbf{r}^*) d^3\mathbf{r}^*, \tag{10.10}$$

where the function $b(\mathbf{k},\mathbf{r}^*)$ has the structure [48, 54, 55]:

$$b(\mathbf{k},\mathbf{r}^*) = |f^{(\Lambda\Lambda)}(k)|^2 \frac{1}{(r^*)^2} + 2\,{\rm Re}\left(f^{(\Lambda\Lambda)}(k)\,\frac{e^{ikr^*}\cos\mathbf{kr}^*}{r^*}\right) - 2\,\pi\,|f^{(\Lambda\Lambda)}(k)|^2\, d_0^{(\Lambda\Lambda)}\delta^3(\mathbf{r}^*). \tag{10.11}$$

Here, $k = |\mathbf{k}|$, $r^* = |\mathbf{r}^*|$, $f^{(\Lambda\Lambda)}(k)$ is the amplitude of low-energy $\Lambda\Lambda$ scattering. In the framework of the effective radius theory [53, 56]:

$$f^{(\Lambda\Lambda)}(k) = a_0^{(\Lambda\Lambda)}\left(1 + \frac{1}{2}\,d_0^{(\Lambda\Lambda)}\,a_0^{(\Lambda\Lambda)}\,k^2 - i\,k\,a_0^{(\Lambda\Lambda)}\right)^{-1}, \tag{10.12}$$

where, by definition, $(-a_0^{(\Lambda\Lambda)})$ is the length of s-wave scattering and

$$d_0^{(\Lambda\Lambda)} = \frac{1}{k}\,\frac{d}{d\,k}\left({\rm Re}\,\frac{1}{f^{(\Lambda\Lambda)}(k)}\right)$$

is the effective radius.

The integral (11), with expression (12) inside, approximately takes into account the difference of the true wave function of two interacting Λ particles with the momenta $\mathbf{k}$ and $(-\mathbf{k})$ at small distances from the asymptotic wave function of continuous spectrum [**?**, **?**].

Information about the parameters of $\Lambda\Lambda$ scattering is contained in the works studying double hypernuclei and pair correlations in the reactions with formation of two Λ particles (see, for example, [58, 59, 60]). Analysis of the experimental data leads to the conclusion that the length of $\Lambda\Lambda$ scattering is comparable by magnitude ($\approx (-20)$ fm) with the length of neutron–neutron scattering [60].

Spin correlations at the generation of $\Lambda\bar{\Lambda}$ pairs in multiple processes

In the framework of the model of independent one-particle sources, spin correlations in the $\Lambda\bar{\Lambda}$ system arise only on account of the difference between the interaction in the final triplet state ($S = 1$) and the interaction in the final singlet state . At small relative momenta, the s-wave interaction plays the dominant role as before, but, contrary to the case of identical particles ($\Lambda\Lambda$), in the case of non-identical particles ($\Lambda\bar{\Lambda}$) the total spin may take both the values $S = 1$ and $S = 0$ at the orbital momentum $L = 0$. In doing so, the interference effect, connected with quantum statistics, is absent .

If the sources emit unpolarized particles, then, in the case under consideration, the correlation function describing momentum-energy correlations has the following structure (in the c.m. frame of the $\Lambda\bar{\Lambda}$ pair):

$$R(\mathbf{k},\mathbf{v}) = 1 + \frac{3}{4}\,B_t^{(\Lambda\bar{\Lambda})}(\mathbf{k},\mathbf{v}) + \frac{1}{4}\,B_s^{(\Lambda\bar{\Lambda})}(\mathbf{k},\mathbf{v}). \tag{10.13}$$

The components of the correlation tensor for the $\Lambda\bar{\Lambda}$ pair are as follows:

$$T_{ik} = \frac{B_t^{(\Lambda\bar{\Lambda})}(\mathbf{k},\mathbf{v}) - B_s^{(\Lambda\bar{\Lambda})}(\mathbf{k},\mathbf{v})}{4 + 3\,B_t^{(\Lambda\bar{\Lambda})}(\mathbf{k},\mathbf{v}) + B_s^{(\Lambda\bar{\Lambda})}(\mathbf{k},\mathbf{v})}\,\delta_{ik}; \tag{10.14}$$

here the contributions of final-state triplet and singlet $\Lambda\bar{\Lambda}$ interaction are determined by the expression (analogously to Eqs.(11),(12) for the $\Lambda\Lambda$ interaction [48, 55], with the replacement $\cos\mathbf{kr}^* \to e^{i\,\mathbf{k}\,\mathbf{r}^*}$ in Eq.(12) owing to the non-identity of the particles Λ and $\bar{\Lambda}$ [54]) :

$$B_{s(t)}^{(\Lambda\bar{\Lambda})}(\mathbf{k},\mathbf{v}) = |f_{s(t)}^{(\Lambda\bar{\Lambda})}(k)|^2\,\langle\frac{1}{(r^*)^2}\rangle + 2\,{\rm Re}\left(f_{s(t)}^{(\Lambda\bar{\Lambda})}(k)\,\langle\frac{e^{ikr^*}e^{i\,\mathbf{kr}^*}}{r^*}\rangle\right) -$$

$$-\frac{2\pi}{k}\,|f_{s(t)}^{(\Lambda\bar{\Lambda})}(k)|^2\,\frac{d}{d\,k}\left(\mathrm{Re}\,\frac{1}{f_{s(t)}^{(\Lambda\bar{\Lambda})}(k)}\right)\,W_{\mathbf{v}}(0), \tag{10.15}$$

where $f_{s(t)}^{(\Lambda\bar{\Lambda})}(k)$ is the amplitude of the s-wave low-energy singlet (triplet) $\Lambda\bar{\Lambda}$ scattering.

At sufficiently large values of k, one should expect that [55]:

$$B_s^{(\Lambda\bar{\Lambda})}(\mathbf{k},\mathbf{v})=0, \qquad B_t^{(\Lambda\bar{\Lambda})}(\mathbf{k},\mathbf{v})=0.$$

In this case the angular correlations in the decays $\Lambda\to p+\pi^-$, $\bar{\Lambda}\to\bar{p}+\pi^+$, connected with the final-state interaction, are absent :

$$T_{ik}=0, \qquad T=0.$$

Angular correlations in the decays $\Lambda\to p+\pi^-$ and $\bar{\Lambda}\to\bar{p}+\pi^+$ and the "mixed phase"

Thus, at sufficiently large relative momenta (for $k\gg m_\pi$) one should expect that the angular correlations in the decays $\Lambda\to p+\pi^-$ and $\bar{\Lambda}\to\bar{p}+\pi^+$, connected with the interaction of the Λ and $\bar{\Lambda}$ hyperons in the final state (i.e. with one-particle sources) are absent . But, if at the considered energy the dynamical trajectory of the system passes through the so-called "mixed phase", then the two-particle sources, consisting of the free quark and antiquark , start playing a noticeable role . For example, the process $s\,\bar{s}\to\Lambda\bar{\Lambda}$ may be discussed .

In this process, the charge parity of the pairs $s\bar{s}$ and $\Lambda\bar{\Lambda}$ is equal to $C=(-1)^{L+S}$, where L is the orbital momentum and S is the total spin of the fermion and antifermion . Meantime, the CP parity of the fermion–antifermion pair is $CP=(-1)^{S+1}$.

In the case of one-gluon exchange, $CP=1$, and then $S=1$, i.e. the $\Lambda\bar{\Lambda}$ pair is generated in the triplet state; in doing so, the "trace" of the correlation tensor $T=1$.

Even if the frames of one-gluon exchange are overstepped, the quarks s and $\bar{s}$, being ultrarelativistic, interact in the triplet state ($S=1$) . In so doing, the primary CP parity $CP=1$, and, due to the CP parity conservation, the $\Lambda\bar{\Lambda}$ pair is also produced in the triplet state. Let us denote the contribution of two-quark sources by x. Then at large relative momenta $T=x>0$.

Apart from the two-quark sources, there are also two-gluon sources being able to play a comparable role. Analogously with the annihilation process $\gamma\gamma\to e^+e^-$, in this case the "trace" of the correlation tensor is described by the formula (the process $g\,g\to\Lambda\bar{\Lambda}$ is implied):

$$T=1-\frac{4\,(1-\beta^2)}{1+2\,\beta^2\,\sin^2\theta-\beta^4-\beta^4\,\sin^4\theta}, \tag{10.16}$$

where β is the velocity of Λ (and $\bar{\Lambda}$) in the c.m. frame of the $\Lambda\bar{\Lambda}$ pair, θ is the angle between the momenta of one of the gluons and Λ in the c.m. frame (see [**?**]). At small β ($\beta\ll 1$) the $\Lambda\bar{\Lambda}$ pair is produced in the singlet state (total spin $S=0$, $T=-3$), whereas at $\beta\approx 1$ – in the triplet state ($S=1$, $T=1$). Let us remark that at ultrarelativistic velocities β (i.e. at extremely large relative momenta of Λ and $\bar{\Lambda}$) both the two-quark and two-gluon mechanisms lead to the triplet state of the $\Lambda\bar{\Lambda}$ pair ($T=1$).

In the general case, the appearance of angular correlations in the decays $\Lambda\to p+\pi^-$ and $\bar{\Lambda}\to\bar{p}+\pi^+$ with the *nonzero* values of the "trace" of the correlation tensor T at large relative momenta of the Λ and $\bar{\Lambda}$ particles may testify to the passage of the system through the "mixed phase" (see also [62]).

Summary

So, it is advisable to investigate the spin correlations of $\Lambda\Lambda$ and $\Lambda\bar{\Lambda}$ pairs produced in relativistic heavy ion collisions .

The spin correlations are studied by the method of angular correlations – method of moments .

The spin correlations, as well as the momentum-energy ones, make it possible to determine the space-time characteristics of the generation region and, besides, the parameters of low-energy scattering of Λ on Λ and Λ on $\bar{\Lambda}$. They should be investigated jointly with the momentum-energy correlations.

One should expect the sufficient statistics for (anti)baryon pairs production at very high energies only. Thus the suggested observables may be considered as a reference point for the studies of phases of lower (NICA) energies.

Bibliography

[1] A. V. Efremov and O. V. Teryaev, Phys. Lett. **B 150,** 383 (1985).

[2] M. Jacob, Z. Phys. **C38**, 273 (1988).

[3] M. Jacob and J. Rafelski, Phys. Lett. **B 190,** 173 (1987).

[4] B. Betz, M. Gyulassy and G. Torrieri, Phys. Rev. **C 76,** 044901 (2007), [arXiv:0708.0035].

[5] Z.T. Liang and X.N. Wang, Phys. Rev. Lett. **94,** 102301 (2005) [nucl-th/0410079].

[6] A.V. Efremov, L. Mankiewicz and N.A. Tornqvist, Phys. Lett. **B 284,** 394 (1992).

[7] D. Kharzeev, Phys. Lett. **B 633,** 260 (2006).

[8] D. Kharzeev, L. McLerran and H. Warringa, Nucl. Phys. **A 803,** 227 (2008), [arXiv:0711.0950].

[9] P. Hoyer, Phys. Lett. **B 187,** 162 (1987).

[10] E.L. Bratkovskaya, O.V. Teryaev and V.D. Toneev, Phys. Lett. **B 348,** 283 (1995).

[11] R. Arnaldi *et al.* (NA60 Collaboration), [arXiv:0812.3100].

[12] B. L. Ioffe and D. E. Kharzeev, Phys. Rev. **C 68,** 061902(R) (2003), [hep-ph/0306176].

[13] S. D. Drell and T. M. Yan, Phys. Rev. Lett. **2,** 316 (1970); **25**, 902 (1970).

[14] J. C. Collins, Acta. Phys. Polon. **B 34,** 3103 (2003).

[15] J. C. Collins, T. C. Rogers and A. M. Stasto, Phys. Rev. **D 77,** 085009 (2008).

[16] D. Boer and P. J. Mulders, Phys. Rev. **D 57,** 5780 (1998).

[17] D. W. Sivers, Phys. Rev. **D 41,** 83 (1990); **43**, 261 (1991).

[18] J. C. Collins and D. E. Soper, Nucl. Phys. **B 193,** 381 (1981); **213**, 545 (1983)].

[19] X. D. Ji, J. P. Ma and F. Yuan, Phys. Rev. **D 71,** 034005 (2005); Phys. Lett. **B 597,** 299 (2004).

[20] J. C. Collins and A. Metz, Phys. Rev. Lett. **93,** 252001 (2004).

[21] A. Kotzinian, Nucl. Phys. **B 441,** 234 (1995).

[22] S. Arnold, A. Metz and M. Schlegel, [arXiv:0809.2262].

[23] A. Airapetian *et al.* (HERMES Collaboration), Phys. Lett. **B 648,** 164 (2007).

[24] R. Seidl, M. Grosse-Perdekamp and A. Ogawa (Belle Collaboration), Phys. Rev. **D 78,** 032011 (2008).

[25] S. D. Drell and T. M. Yan, Annals Phys. **66**, 578 (1971); **281**, 450 (2000).

[26] G. Bunce *et al.*, http://spin.riken.bnl.gov/rsc/report/spinplan_2008/ spinplan08.pdf, *Plans for the RHIC Spin Physics Program.*

[27] J. C. Peng *et al.*, http://j-parc.jp/NuclPart/pac_0606/pdf/p04-Peng.pdf, J-PARC Proposal P04 (2006).

[28] Y. Goto *et al.*, http://j-parc.jp/NuclPart/pac_0801/pdf/Goto.pdf, J-PARC Proposal P24 (2007).

[29] V. V. Abramov *et al.*, [hep-ex/0511046].

[30] A. Sissakian, O. Shevchenko, A. Nagaytsev, and O. Ivanov, [arXiv:0807.2480].

[31] V. Barone *et al.*, (PAX Collaboration), [arXiv:hep-ex/0505054].

[32] M. Anselmino, V. Barone, A. Drago and N. N. Nikolaev, Phys. Lett. **B 594,** 97 (2004).

[33] A. V. Efremov, K. Goeke and P. Schweitzer, Eur. Phys. J. **C 35,** 207 (2004).

[34] U. D'Alesio and F. Murgia, Progr. Part. Nucl. Phys. **61,**394 (2008).

[35] V. Barone, A. Drago and P. G. Ratcliffe, Phys. Rep. **359,** 1 (2002).

[36] J. C. Collins and D.E. Soper, Phys. Rev. **D 16,** 2219 (1977).

[37] A. D. Panagiotou, Phys. Rev. **C 33,** 1999 (1986).

[38] A. Ayala, E. Cuautle, G. Herrera and L. M. Montano, Phys. Rev. **C 65,** 024902 (2002).

[39] G. Herrera, G. Magnin and L. M. Montano, Eur. Phys. J. **C 39,** (2005) 95.

[40] E. L. Bratkovskaya, W. Cassing and U. Mosel, Z. Phys. **C75**, 119 (1997).

[41] Z.-T. Liang and X.-N. Wang, Phys. Lett. **B 629,** 20 (2005).

[42] J. Harris *et al.*, Phys. Rev. Lett. **47,** 229 (1981).

[43] M. Anikina *et al.*, Z. Phys. **C25**, 1 (1984).

[44] R. Bellwied *et al.*, Nucl. Phys. **A 698,** 499 (2002).

[45] B. I. Abelev *et al.*, Phys. Rev. **C 76,** 024915 (2007).

[46] V. P. Ladygin, A. P. Jerusalimov and N. B. Ladygina, [arXiv:0806.3867].

[47] T. A. DeGrand and H. I. Miettinen, Phys. Rev. **D 23,** 1227 (1981); **24**, 2419 (1981); **31**, 661(E) (1985).
bibitemlyu1 V. L. Lyuboshitz and M. I. Podgoretsky, Yad. Fiz. **60**, 45 (1997).

[48] V. L. Lyuboshitz, *Proceedings of XXXIV PNPI Winter School . Physics of Atomic Nuclei and Elementary Particles*, St-Petersburg (2000), p.402.

[49] R. Lednicky and V. L. Lyuboshitz, Phys. Lett. **B 508,** 146 (2001).

[50] G. Alexander and H.J. Lipkin, Phys. Lett. **B 352,** 162 (1995) .

[51] R. Lednicky, V. V. Lyuboshitz and V. L. Lyuboshitz, Yad. Fiz. **66**, 1007 (2003)

[52] M. I. Podgoretsky, Fiz. Elem. Chast. At. Yadra **20**, 628 (1989)

[53] L. D. Landau and E. M. Lifshitz, *Quantum Mechanics. Nonrelativistic Theory* (in Russian), (Nauka, Moscow, 1989).

[54] V. L. Lyuboshitz and V. V. Lyuboshitz,*Proceedings of XXXVII and XXXVIII Winter Schools of the Petersburg Institute of Nuclear Physics. Physics of Atomic Nuclei and Elementary Particles*, St.-Petersburg (2004), p.390 .

[55] R. Lednicky and V.L. Lyuboshitz, Yad. Fiz. **35**, 1316 (1982)

[56] H. A. Bethe and P. Morrison, *Elementary Nuclear Theory* (New York, 1956) p.10.

[57] V. L. Lyuboshitz, Yad. Fiz. **41**, 820 (1985) [Sov. J. Nucl. Phys. **41**, 529 (1985)].

[58] S. Iwao and M. Shako, Progr. Theor. Phys. **48**, 1412 (1972).

[59] A. O. Ohnishi *et al.*, Nucl. Phys. **A 670,** 297 (2000).

[60] I. R. Afnan, Nucl. Phys. **A 639**, 55c (1998).

[61] W. H. McMaster, Rev. Mod. Phys. **33**, 8 (1961).

[62] V. L. Lyuboshitz and V. V. Lyuboshitz, Yad. Fiz. **73**, 836 (2010); Phys. At. Nucl. **73**, 805 (2010).

11 Related topics

11.1 Determination of the equation of state of dense matter

S. Fantoni[a], *S. Gandolfi*[b], *A. Illarionov*[c], *F. Pederiva*[c,d] *and K. Schmidt*[e]

[a] *International School for Advanced Studies, SISSA, Italy and INFN, Trieste, Italy;*
[b] *Theoretical Division, Los Alamos National Laboratory, Los Alamos, USA;*
[c] *Dipartimento di Fisica dell'Universitá di Trento, Trento, Italy;*
[d] *INFN, Gruppo Collegato di Trento, Trento, Italy;*
[e] *Department of Physics, Arizona State University, USA*

In order to understand the properties of matter at intermediate densities and temperatures, it is important to gather knowledge on the regime defined by densities of the order $n_0 < n < (3-4)n_0$, and temperatures between 0 and 10 – 20 MeV. This regime is particularly challenging. At such densities it is completely not obvious that the knowledge on the nucleon-nucleon and many-nucleon interactions, that has been developed essentially fitting properties of small nuclei, is s till applicable. On the other hand, this regime is at present completely unaccesible to QCD.

The constraints coming from astrophysical observations (in particular on the properties of neutron stars) have been partly supplied with information coming from heavy-ion collisions. However, the present situation does not allow for a definitive discrimination among the variety of proposed models that have been developed in the last two decades.

The development of a facility allowing for reaching dense matter conditions might help to improve the situation of uncertainty that permeates the field.

Recent methodological developments allowed for a more systematic approach to the study of the properties of high density nucleonic matter. In particular, by means of the Auxiliary Field Diffusion Monte Carlo (AFDMC) method [1], it is possible to solve with extremely high accuracy the Schrodinger equation with realistic potentials for numbers of nucleons A which might be of order 100, allowing therefore to make predictions on the properties of nuclear [2] and neutron[3] matter.

This is a big step forward, because the limits on number of nucleons that can be treated efficiently has been moved forward by at least one order of magnitude. Even more important, however, is the fact that for a given interaction (more or less phenomenological), it is possible to obtain solutions which are not plagued by uncontrolled approximations. It is therefore possible to start discussing with no ambiguity the portability of current interactions (like Argonne-Urbana AV18+UIX or Illinois ILX potentials) to the high density regime, and to possibly develop alternatives that might at least give phenomenological input for attacking important problems.

In this context, for instance, we have recently developed a density-dependent interaction (DDI) following the initial intuition of Lagaris and Pandharipande [4] which, after fitting three parameters on basic properties of symmetrical nuclear matter (saturation density, energy and compressibility at saturation density), yields an equation of state (EOS) which is by far softer than the celebrated Akmal, Pandharipande and Ravenhall [5] EOS, both for symmetrical nuclear matter and pure neutron matter, and consequently gives estimates of Neutron Star properties (such as Mass/Radius ratio, momentum of inertia, and others) that are much better reconciled with observations, and closer to extrapolated constraints.

Once more, the importance of such an approach is that a sound starting point for phenomenological discussion and further developments is now available. In particular we want to mention two future developments which might be relevant for the regime of densities and temperatures of matter that should be reached in NICA. The study of the occurrence of a transition to a mixed nucleon-hyperon phase. Despite there is a large amount of literature present on the subject, the determination of the onset of the presence of hyperons depends on two unknowns: the hyperon-nucleon interaction (about which the amount of experimental information is very limited) and the equation of state of nuclear/neutron matter.

The presence of these two unknowns at the same time generated a wide variety of predictions. The use of AFDMC and DDI can help to narrow down the range of such predictions, allowing for a more stringent comparison with possible new constraints that should emerge from experiments as exemplified in Fig. 11.1.

The second issue concerns the temperature effects on the equation of state. Once more, the information available is very limited. From the point of view of microscopic calculations the neater approach would be the development of a code capable to compute the expectation of operators in the Quantum Canonical Ensemble

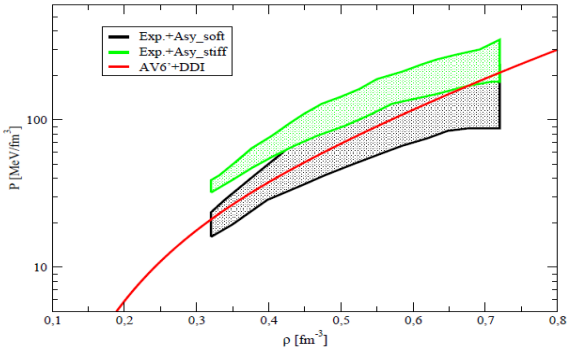

Figure 11.1: Zero-temperature EOS for neutron matter. The upper and lower shaded regions for neutron matter consistent with the experimental of data of heavy-ion collision after inclusion of the pressures from asymmetry terms with strong and weak density dependence, respectively [6]. The line shows our prediction for neutron matter EOS.

(always neglecting relativistic effects) by means of Path Integral Monte Carlo techniques. In principle this would allow for a rigorous study of nuclear/neutron matter up to temperatures and densities very close to the phase transitions of interest in NICA. However, approximated approaches based on the extrapolation of the temperature behavior from Fermi Hypernetted Chain calculations [7] could be used in order to include temperature dependence up to 20 – 25 MeV. This fact is important because it provides a guide the corrections necessary to have a sensible comparison between $T = 0$ results yielded by AFDMC calculations. Work along this line has been already in progress.

We believe that the availability of a facility like NICA will be important to clarify important issues not only from the QCD point of view, but also for as concerns some obscure points that are still present in the understanding of the nucleon-nucleon interactions and of the phase transitions that matter undergoes at medium densities and relatively low temperatures, a physics that is extremely relevant for a theoretical analysis of dense stars, in particular for the properties of the inner crust and of the exterior core.

11.2 Relativistic nuclear fusion reactions and QED of strong fields: novel possibilities at the NICA facility

A. Kovalenko, A. Sissakian and A. Sorin

Joint Institute for Nuclear Research, Dubna, Russia

The main goal of the proposed two storage rings of the NICA facility is to provide head-on collisions of heavy ions [8]. This short remark is aimed at discussing of the proposal for extending the research program at NICA to investigate the interactions of relativistic multi-particle systems having a small difference in the momentum. In other words we would like to consider interactions (collisions) of **relativistic co-moving particles**. Different ion-ion spices, light polarized nuclei with different orientation of spin or even electron-ions can be used as interacting objects. The construction of a facility to study electron-ion collisions was proposed at JINR in 1989 [9]. The electron-ion mode of operation was proposed for the RIKEN facility at Japan [10], nevertheless the maximum ion energy was limited to about 0.8 GeV/A. The peak energy of electron beam was chosen at 2.5 GeV to produce highly brilliant X-rays, if necessary. As it has been shown [11], the optimization of the collider lattice can make it possible to reach practically the same luminosity of ion-ion collisions for the case of co-moving beams as those for head-on collisions.

The use of co-moving particle interactions make it possible to study the interactions of heavy ions near and below the Coulomb barrier, the momentum transfer can be controlled by adjustment of the machine parameters. The observation of ultra-peripheral interactions of different highly charged ions is also possible. The production of e^+e^--pairs can be observed.

The technical realization of the co-moving ion-ion interaction mode appears to be feasible. Several conditions should be taken into account:

- beam crossing angle is not zero in this case to provide necessary separation between the beams after

crossing point;

- beam crossing angle is chosen in some range, let say, between 10 mrad $< \theta <$ 150 mrad.
- the collider magnets power supply system should be flexible enough and provide necessary changing of supply current direction and independent power supplies of the magnetic elements of the insertions near the beam intersection points;
- longitudinal momentum of the reaction products will dominate over the transverse one, thus forward detector and particle separation channel are needed. It is important that in the case of non-zero crossing angle we don't need to work with bunched beams.

Thus, the stochastic cooling will operate well. The conditions for electron cooling system are also very comfortable. The total number of stored particles in the coasting beams can be increased.

The case of co-moving particle interactions is most reasonable to consider in the range of beam kinetic energy of 2 GeV/A. The Coulomb forces in the circulating beams is suppressed by a factor of 10, the transverse component of ion momentum due to non-zero crossing angle will be in the range from 20 MeV/A to 300 MeV/A. The difference between longitudinal momentum of the interacting particles can be varied in fine steps over the range of ± 0.5 GeV/A and wider. Note that it is possible to use co-moving collision mode at large difference of the particles longitudinal momentum to increase the luminosity of heavy ion collisions at the lowest requested energies at NICA. The luminosity of co-moving particle interaction is estimated to $10^{27} cm^{-2} s^{-1}$ for heavy ions and to $10^{31} cm^{-2} s^{-1}$ for the light ions including polarized ones.

11.3 Development of highly charged ion sources for NICA injector and its possible applications for nanofabrication and in medicine

D.E. Donets, E.D. Donets, E.E. Donets, V.V. Salnikov V.B. Shutov

Veksler&Baldin Laboratory of High Energy Physics, JINR, Dubna, Russia

Novel type of highly charged ions sources – Electron String Ion Sources (ESIS) is under development in JINR in framework of NICA project. This ion sources produce intense beams of highly charged ions of heavy elements, up to gold. Two major applications of this ion sources: for nanofabrication and for cancer therapy are briefly discussed.

Novel type of ion sources - Electron String Ion Source of highly charged ions is for injector complex of NICA project. According to the Project parameters this new ion source Krion-6T (which is under construction now) should produce up to $3 \cdot 10^9$ ppp of Au^{32+}. However, this ion source also could produce higher charge states: up to Au^{69+} for Krion-6T. The operational ion source of ESIS type – Krion-2 ESIS has produced ion beams up to Au^{54+} in stand laboratory conditions in 2009 (see [12] and refs therein). In February-March 2010 Krion-2 ESIS was successfully used as injector of highly charged Xe^{42+} ions during 41-st Nuclotron run. Krion-2 ESIS has produced up to 3x10^8 Xe^{42+} ions per pulse; this ion beams were accelerated in LU-20 LINAC and further in Nuclotron up to relativistic energies and used for physics experiments.

As a result, the high ionization efficiency as well as the reliability and stability of Electron String Ion Source Krion-2 in an automatic regime of it's work have been demonstrated. The present status of studies and the tests on a synchrotron show that Electron String Ion Source has become a new and useful tool for accelerator facilities.

However, highly charged ions of heavy elements, produced and slowly extracted from the ion source could be used in many interesting applications. Nonaccelerator physics of highly charged ion is relatively new developing branch. We would like to describe only two possible applications which could be considered in parallel to the main stream of the NICA project development.

Production of nanostructures by slow highly charged ions for information storage and processing at nanometer range

A highly charged ion (HCI) reacts intensely with matter through deposition of its large potential energy. The potential energy is equal to the summation of ionization energy to produce the HCI concerned and increased rapidly with the ion charge. For example, potential energy of Xe^{44+} reaches 48 keV while singly charged Xe^{+1} ion has only 12 eV of potential energy. Another feature is that HCI has a large number of unoccupied orbitals. When HCI approaches to a solid surface, the HCI captures a lot of electrons to the orbitals and releases the

large potential energy with in a short time (< 100 fs) onto a small region of the surface. Such interaction of the HCI with the surface (previously called as "Coulomb explosion") give two important charactersitics; one is a high yield of secondary electron emission and the other is terrawatts power flux deposition onto nanoregion. This effect is essentially different from that induced by irradiation of energetic low charged ions, where the kinetic energy of the primary particles plays a major role.

A nanoscopically modified materials (such as HOPG – highly oriented pyrolithic graphite, Si(111) and others) by slow highly charged ions, such as Xe^{44+}, I^{51+} have craters and hillocks of a typical size of 5 – 10 nm in diameter and about 1.5 nm in depth/height. Such surface modifications result from deposition of huge potential energy of HCIs to a nanometer sized region of the surface within a short time, which corresponds to a power flux density of > 1 TW/cm^2. Although Terawatt power density is also achieved with a short pulsed laser, the laser beam waist is about 500 nm in a diameter at least, while HCI can deposit terawatts power flux onto a nanoregion. Usually images of the surface nanomodifications by HCI are obtained with use of scanning tunneling microscope (STM) [13].

Surface modification by HCI opens possibility to create large-scale devices with dimensions in the 10 nm range. First application could be information storage. The extremely small size of ion damage sites (1-10 nm) suggests that the ultimate limit for information density using this technique is about 10^{12} bits/cm^2, or 1000 Gb/cm^2 that is few order of magnitude higher than the best modern devices.

In order to perform the HCI based nano-processes efficiently, HCI beams should have high flux density and intensity. Therefore HCIs have to be efficiently extracted from the ion source and transported precisely in a beam line with well designed ion optical elements. Nano-sized capillares seem to be one of the efficient tools for precise ion steering transportation [14].

Several areas need to be explored before ion nanofabrication can be exploited: the ion/surface interaction and the nature of the damage; materials and (possibly?) chemical processing; the limits of size and density of independent devices; development of ion sources to higher flux of HCI ions of heavy elements; steering the ions to nanometer precision; information processing in nanometer range et cetera...

The planned development of the ESIS-type ion sources in framework of the NICA project could give an excellent opportunity to develope this area since this ion sources provide intense beams of heavy HCI's up to gold, which are mostly applicable for the described nano-applications.

Resonant combination cancer therapy – newly proposed method with use of highly charged ion source of highest intensity

The new scheme of cancer therapy includes source of highly charged heavy ions of highest intensity only and no any accelerators. Conceptual basis of this scheme is following [15]. Well-tested technology already exists to deliver 1.9 nm gold particles to achieve considerable concentration of gold in tumor, while maintaining an order of magnitude less concentration in the normal tissue due to the trapping of the gold nanoparticles within the tumor vasculature.

The scheme proposed involves impacting slow bare or hydrogen-like heavy ions onto a surface, resulting in one high energy photon (> 30 keV) per K-shell vacancy with the energy of these photons being dictated by the atomic number (Z) of the highly charged ions used. A particular ion is selected so that these photons lie just above the K-edge of a heavy ion species (gold) preferentially incorporated into the tumor leading to a large local dose as required. **Radiation in the 'Desired Radiation Window' efficiently produces K-shell holes in the gold nanoparticle. After a radiative transisition, this system stabilises predominantly by Auger decay that should destroy tumor cells in surroundings of gold nano-particle due to electron flux during fs.**

An example of the set up for the proposed from of radiotherapy is following: ions are transported from a high intensity ion source (ESIS or EBIS) which has been configured to produce predomimantly bare ot hydrogen-like heavy ions, chosen so that the K-alpha radiation from these ions lies just above the K-edge of a heavy atom dopant (gold) previously incorporated into the tumor. These ions are transported through rotatable guntry and focused onto a thin aluminium window (0.25 – 0.5 mm width). This window acts both as an electron rich target, generating the high energy photons and also as a high-pass filter, attenuating low energy (< 20 keV) x-rays. The resultant x-rays are then collimated using s multileaf collimator so as to target tumor.

The ion source requirements for this scheme are following: 10^{11} – 10^{12} ions/second for highly charged (like Au^{78+}) heavy ions. These requirements are still beyond present ion source capabilities. However, ions source development toward more highly charge states and intensity should give a real chance for successful realization of this new, safe and relatively cheap form of nonaccelerator cancer therapy.

Basic and applied researches with highly charged intense ion beams of heavy elements, produced with ESIS-type ion sources have a very wide area for applications in nano-sceiences and medicine. Ion source development program in framework of the NICA project has a great potential for various nonaccelerator applications as well.

Bibliography

[1] K. E. Schmidt and S. Fantoni, Phys. Lett. **B 446,** 99 (1999).

[2] S. Gandolfi, F. Pederiva, S. Fantoni and K. E. Schmidt, Phys. Rev. Lett. **99,** 022507 (2007).

[3] S. Gandolfi, A. Yu. Illarionov, K. E. Schmidt, F. Pederiva and S. Fantoni, Phys. Rev. **C 79,** 054005 (2009).

[4] I. E. Lagaris and V. R. Pandharipande, Nucl. Phys. **A 359,** 331 (1981).

[5] A. Akmal, V. R. Pandharipande and D. G. Ravenhall, Phys. Rev. **C 58,** 1804 (1998).

[6] P. Danielewicz, R. Lacey, W. G. Lynch, Science **298**, 1592 (2002).

[7] K. E. Schmidt and V. R. Pandharipande, Phys. Lett. **B 87,** 11 (1979).

[8] A. N. Sissakian *et al.*, *The Project NICA/MPD at JINR: Search for the Mixed Phase of Strongly Interacting Matter at Nuclotron-based Ion Collider fAcility. XXIII International Symposium on Lepton and Photon Interactions at High Energy, LP07.* (August 13-18, 2007, Daegu, Korea).

[9] A. D. Kovalenko. *On a possible conception of a relativistic nucleus and electron beam facility. JINR Communication* , P9-89-26, JINR, 1989.

[10] T. Katayama, Yu. Batygin *et al.*, Nucl. Phys. **A 626,** 545 1997.

[11] Yu. Batygin and T. Katayama. *Merging Beam-Beam Interactions. Proc. PAC99*, p.1737.

[12] D. E. Donets *et al.*, Rev. Sci. Instrum. **80**, 063304 (2009)

[13] M. Tona *et al.*, Eds. R. W. McCullough *et al.*, *Proceedings of the 13th International Conference on the Physics of Highly Charged Ions* (2007), Journal of Physics conference series **58** 379.

[14] N. Stolterfoht *et al.*, Phys. Rev. Lett. **88,** 133201 (2002)

[15] A. P. Kavanagh *et al.*, Eds. R. W. McCullough, *et al.*, *Proceedings of the 13th International Conference on the Physics of Highly Charged Ions* (2007), Journal of Physics conference series **58**, 439

12 Fixed Target Experiments

With the completion of the booster system in 2014, there will be the possibility to have ion beams with a good quality starting from the year 2015. These beams which are extracted to the experimental hall can be used for experiments full time before the NICA/MPD experiment is ready for operation. Therfore, it is actual to discuss in this section the physics potential of possible experiments using the extracted ion beams with laboratory energies up to 5.5 AGeV.

12.1 Measurement of Elementary Cross Sections

J. Aichelin[1], M. Bleicher[2], E. Bratkovskaya[2], C. Hartnack[1]

[1] *SUBATECH, Laboratoire de Physique Subatomique et des Technologies Associées, Université de Nantes, Nantes, France;*

[2] Frankfurt Institute for Advanced Studies (FIAS), Frankfurt am Main, Germany

Today heavy ion reactions are not made any more to discover single particle spectra of hadrons. These spectra have since long been analysed and for the most frequent particles reproduced by simulation programs like QMD [2, 1], HSD [3] or URQMD [4]. The present goal of heavy ion experiments is much more ambitious. One aims to study in medium properties of particles, the nuclear equation of state, the transition toward a quark gluon plasma or reaction mechanisms which are only present in heavy ion collisions like those reactions which involve a Δ in the initial state. To extract this desired information the experimental results have to be compared with these computer programs which predict observables for different assumptions of the in medium properties, the cross sections etc. The assumption which fits best is than used to predict other observables in order to cross check whether it reflects really the properties of the system. Using this method remarkable progress has been made in the last decade on strangeness production close to the threshold, on the nuclear equation of state and other properties of hadrons in matter.

The problem with these simulation programs for heavy ion reactions is the fact that they use measured elementary cross sections as input quantities. Up to beam energies of around 1.5 GeV these elementary cross sections have been measured in the sixties and seventies by bubble chamber experiments.Therefore many of them suffer from low statistics. In addition, already at 2 GeV yet unknown elementary cross sections limit the predictive power of the heavy ion simulation programs. A good example is the dilepton production in CC at 2 AGeV which has been measured by the HADES collaboration. The experimental data show an enhancement of the dileption yield at an invariant mass corresponding to the mass of the ρ and ω but since the experimental cross sections

$$\begin{aligned} np &\to \rho + x \\ pp &\to \rho + x \\ np &\to \omega + x \\ pp &\to \omega + x \end{aligned} \tag{12.1}$$

are either unknown or known only with large error bars (and theoretical prediction differ by up to a factor of 5) it is difficult to interpret these data yet. One simply cannot say whether the measured yield can be reproduced using free production cross sections or whether the data give a hint that properties of these mesons, like their mass, have changed in the medium, not to talk about more ambitious ideas like to verify experimentally the off-shell propagation of the baryon resonances and mesons in a nuclear environment. This has been discussed extensively at the last collaboration meeting of HADES.

In addition, it would be very important to know the role of nuclear resonances for the meson production (which could in principle be analysed by kinematics) but there almost no information is available presently. This excludes an interpretation of the enhanced dilepton cross section in large systems for intermediate invariant masses observed by the HADES collaboration. Even worse, for mesons like the η, which is one of the candidates for this enhancement,the production in np reactions in unknown in the energy regime of interest . Therefore this enhancement is not accessible for theoretical studies presently.

All the people who are implied in the development of these simulation programs, agree that the present limitation of their predictive power is the lack of knowledge on the cross section.

Today TPCs or similar devices are very effective to measure the complete kinematics of charged particles with a high frequency and, tagging the p in dp reactions, would allow for studying the np collisions. The multiplicity in these elementary reactions is small and therefore the detection does not require sophisticated devices.

Therefore we think that a program "measurement of elementary cross sections from 1.5 GeV upwards" would be extremely helpful for the later coming heavy ion reactions, or, to be more precise, without such a program it will be impossible to extract the physics of the heavy ion reaction in a convincing way.

In addition, this energy regime is also very interesting. At 2 GeV we see that the particles in the exit channel in reactions like $NN \to NNK^+$are distributed according to the three dimensional phase space. At 80 GeV and probably also well below, in order to describe the data one has to assume that strings are formed and the distribution of the particles is governed by the 1-dim longitudinal phase space. In transverse direction the particles have about a pt of 300 MeV. Therefore the transition between a description of the reaction in nuclear degrees of freedom and in quark degrees of freedom takes place in this energy regime and it would by very interesting to identify precisely the energy where the transition takes place.

We would therefore recommend that the experimental program at DUBNA starts out from this proposal of elementary collisions.

12.2 Search for scaling onset in exclusive reactions with lightest nuclei at NUCLOTRON using fixed target.

Yu.N. Uzikov

Joint Institue for Nuclear Researches,LNP, Dubna, Moscow reg. Russia

Search for transition region from hadron to quark-gluon degrees of freedom in nuclear structure at short distances between nucleons ($r_{\rm NN} < 0.5$ fm) is a challenging problem of particle and nuclear physics. This transition is expected to occur in processes at enough high transferred momenta allowing to probe dense fluctuations of nuclear matter in nuclear structure [5].

A possible signature for this transition is related with the constituent counting rules (CCR) [6, 7]. According to CCR the differential cross section of a binary reaction $AB \to CD$ at (asympthoticaly) high incident energy $\sqrt{s}$ and transferred momentum t can be parameterized for a given c.m.s. scattering angle $\theta_{\rm cm}$ as

$$\frac{d\sigma}{dt}(AB \to CD) = \frac{f(t/s)}{s^{n-2}}, \tag{12.2}$$

where $n = N_{\rm A} + N_{\rm B} + N_{\rm C} + N_{\rm D}$ and N_i is the minimum number of point-like constituents in the *i-th* hadron (for a lepton and photon one has $N_l = 1$), $f(s/t)$ is a function of $\theta_{\rm cm}$. The CCR follows from the hypothesis of self-similarity [6] and perturbative QCD (pQCD) [7].

Existing high energy data for many measured hard processes with free hadrons appear to be consistent with the CCR [8]. The CCR derived for asympthoticaly high values of kinematical variables $s \to \infty$ and $t \to \infty$, surprisingly, turned out to be valid at moderate energies $\sim$ few GeV in many reactions with **free hadrons** when the condition $\theta_{\rm cm} = const$ is used [8].

For exclusive reactions with **lightest nuclei** at high Q^2, CCR can give a definite signal for transition to the valence quark region. Indeed, the s^{-11} behaviour of the cross section $d\sigma/dt$ of the reaction $\gamma d \to pn$, observed at SLAC/Jlab at $E_\gamma = 1 - 4$ GeV and large scattering angles $\theta_{\rm cm} = 90^\circ$, perfectly follows the CCR (see [9] and references therein, Fig.12.1). A similar behaviour was observed in the reaction $^3{\rm He}(\gamma, pp)n$ [10] with much lower cross section. On the other hand, the reaction $pp \to d\pi^+$ at very similar kinematics does not demonstrate the CCR behaviour s^{-12} [12].

Further study of this phenomenon, however, is very limited *by small cross sections* of the electromagnetic interactions. Recently, the precise CCR dependence s^{-22} was found in the **pure hadronic reactions** $dd \to {}^3{\rm H}p$ and $dd \to {}^3{\rm He}n$ measured at SATURNE at $T_{\rm d} = 0.5 - 1.2$ GeV and large scattering angles $\theta_{\rm cm} = 50 - 60^\circ$ [12] (see Fig.12.2). The $pd \to pd$ cross section demonstrates the s^{-16} dependence but with worse χ^2 [12]. At lower scattering angles, i.e. lower transferred momenta, this behaviour is absent both in the $dd \to {}^3{\rm H}p$, $pd \to pd$ and $\gamma d \to pn$ reactions.

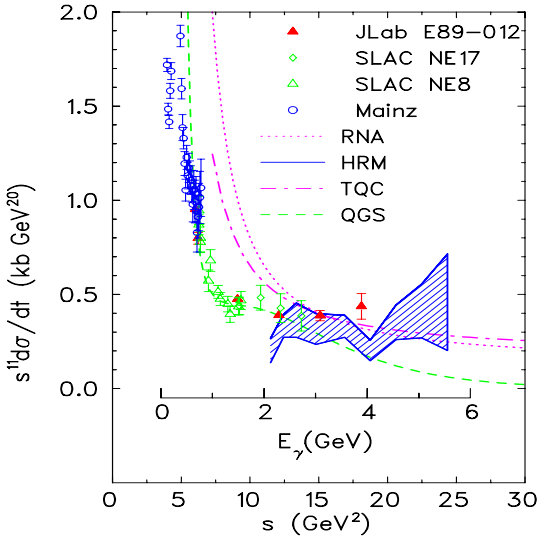

Figure 12.1: The invariant cross section of the reaction $\gamma d \to pn$ at $\theta_{\rm cm} = 90^\circ$ multiplied by s^{11} in comparison with different theoretical models. The figure is taken from Ref.[11]

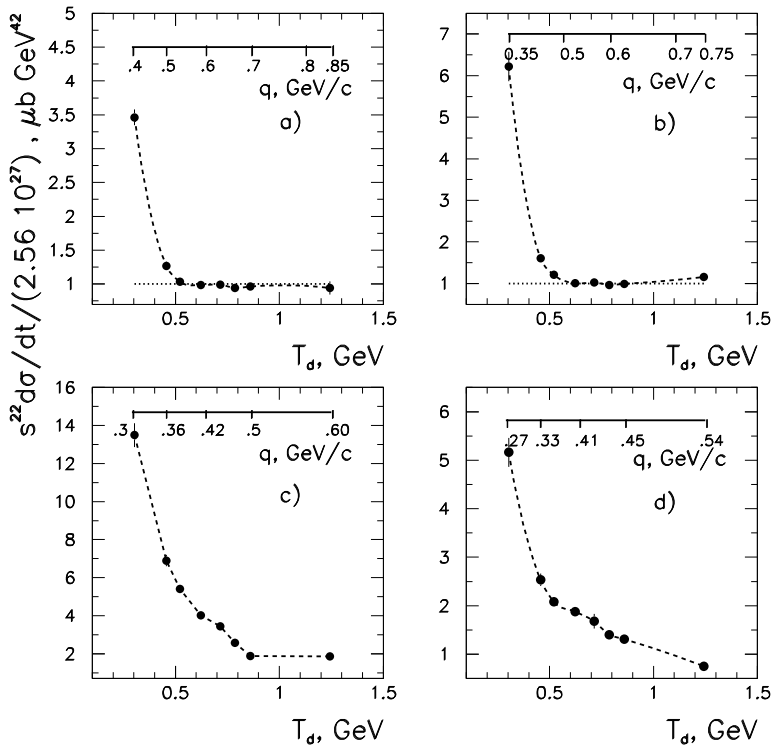

Figure 12.2: The invariant cross section of the $dd \to {}^3Hen$ and $dd \to {}^3Hp$ reactions multiplied by s^{22} versus the deuteron beam energy at different scattering angles $\theta_{\rm c.m.}$: $a - \theta_{\rm c.m.} = 60^o$; $b - 50^\circ - 52^\circ$; $c - 33^\circ - 35^\circ$; $d - 28^\circ$. On the upper scale is shown the minimal relative momentum (GeV/c) between nucleons in the deuteron for the ONE mechanism. The data are taken from Ref. [14]. At lower scattering angles the plateau is not visible in this data, maybe, except for $\theta_{\rm cm} = 33^\circ - 35^\circ$. The figure is taken from Ref.[12]

All these reactions involve nuclear wave functions at very high internal momenta between nucleons $q \sim 1$ GeV/c. The perturbative QCD, however, can be hardly applied at these rather low energies. **New data on these and other exclusive reactions are required to clarify the underlying dynamics. One of the most important task is determination of the scaling onset for different reactions.** Measurement of energy dependence of the differential cross section of the reaction $dd \to {}^3\mathrm{He}\,n$ in the interval $T_\mathrm{d} = 1 - 3$ GeV at fixed cms scattering angles within $\theta_\mathrm{cm} = 30^\circ - 90^\circ$ would be very important to confirm the SATURNE data.

The JINR *Nuclotron with fixed target* facility provides unique possibility to perform this study in dd and pd collisions above 1 GeV. A broad experimental program will include other exclusive reactions with lightest nuclei: $dd \to dd$,$pd \to pd$, $pd \to {}^3\mathrm{H}\pi^+$, $pd \to {}^3\mathrm{He}\eta$, $dd \to {}^4\mathrm{He}\eta$, $pp \to d\rho^+$, $d^3\mathrm{He} \to {}^4\mathrm{He}\,p$.

12.3 Measurement of strange particle production in the NICA fixed-target program

V. Friese

GSI Helmholtzzentrum für Schwerionenforschung mbH, Darmstadt, Germany

The production of strange particles is considered a sensitive probe of the dynamics of nuclear collisions and of the state of the produced matter since the early days of heavy-ion physics, the original perception being that strangeness is more easily produced in parton-parton interactions than in hadronic interactions, and is thus more abundant in the final state should a deconfined phase be transiently reached [15]. This "strangeness enhancement" was indeed observed [16], but it was soon realised that the measured particle abundances, including those of strange particles, can be described in terms of an equilibrium hadron gas model [17].

The apparent chemical equilibrium was interpreted to be a consequence of the phase transition from deconfined to confined matter, either by phase-space dominance [18] or by multi-particle collisions [19] which become effective near the phase boundary, which, for high collision energies like at SPS or RHIC, is expected to coincide with chemical freeze-out. However, the statistical model was also successfully applied to the final state hadrons emerging from nuclear collisions at lower energy like at AGS or even at SIS, where the creation of deconfined matter is not likely, and where, as suggested by results from lattice QCD calculations, the chemical freeze-out is separated from the deconfinement phase transition by a stage of dense hadronic medium. This observation led recently to the proposal of an additional QCD phase, the "quarkyonic phase", where confinement still holds, but chiral symmetry is restored [20]. The phase transition from this "quarkyonic" medium to hadrons could then act as a "thermaliser" in the same way as the transition from deconfined to confined matter does for higher collision energies.

The energy regime of the Nuclotron and the future FAIR facility, creating a baryon-dense but moderately hot initial state, is uniquely suited for the study of this part of the QCD phase diagram and the hypothetical quarkyonic phase. A prime tool are again strange particles, the production features of which still bear open questions. Recently, the HADES experiment reported a large deviation of the measured Ξ^- yield from the statistical model in Ar+KCl at 1.76 A GeV beam energy [21]. The same is true for the η meson yield measured by the TAPS collaboration (Fig. 12.3). The particle abundances measured by FOPI in Ni+Ni collisions at SIS energies can be fitted thermally, but the extracted temperature is below that deduced from the transverse momentum spectra, i.e. at kinetic freeze-out. Fixed-target experiments at the Nuclotron should shed light on these puzzles by the study of strangeness production at energies above SIS and for heavy collisions systems, where the currently available experimental data are either missing, scarce, or cover only a small fraction of the phase space.

Of particular interest, besides the bulk strangeness carriers K and Λ, are multi-strange hyperons. A measurement of the Ξ^- excitation function in heavy-ion reactions near the elementary threshold would provide substantial input to the understanding of the collision dynamics and the strangeness production processes (strangeness exchange, multi-step processes). Even more spectacular would be the observation of deep subthreshold Ω production. K^0_S, Λ, Ξ and Ω are all detected by their weak decay topology; these channels can thus be studied by a spectrometer consisting of a magnet and a high-precision tracking device. Such a compact experiment would allow to characterise the major part of the total strangeness content of the final state. The fixed-target geometry allows to cover a large rapidity range and facilitates the detection of the displaced decay vertices because of the Lorentz boost from CM to laboratory frame. The same detection principle can also be applied for the search of the hypothetical multi-strange di-baryons [22].

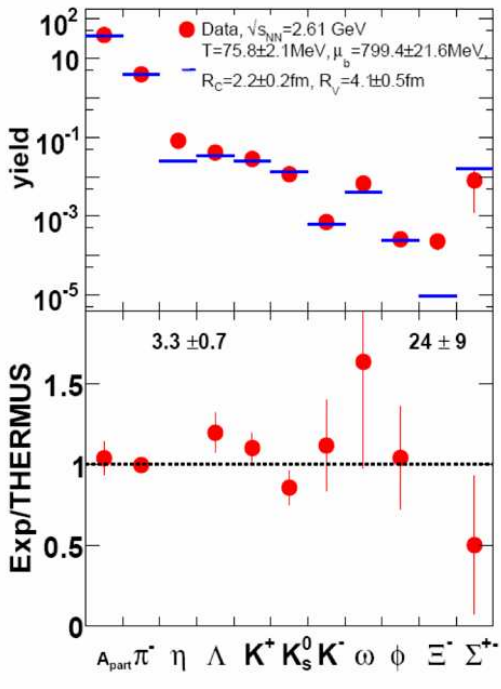

Figure 12.3: Comparison of hadron abundances measured by the HADES experiment and the hadron gas model fit [21]. The Ξ^- yield differs by more than an order of magnitude from the model. A large deviation is also observed for the η meson measured by TAPS.

As the measurement of the rare probes Ξ and Ω requires high event rates, large-volume gas drift chambers are not applicable. The choice could be a Silicon tracker, covering a large part of the forward hemisphere. The development and construction of such a device is consumptive in terms of budget, manpower and time, but possible synergy effects exist with similar detector developments for the MPD project and for the CBM experiment at FAIR.

A complete characterisation of the final state requires in addition the measurement of protons, charged pions and charged kaons. This task can be covered by a time-of-flight detector which, given the moderate momenta of the produced particles at Nuclotron energies, can be located at about 5 m downstream of the interaction point. State-of-the-art Resistive Plate Chambers can equip this device, but for high interaction rates, their rate capabilities become an issue. Again, a possible experiment could profit from developments at FAIR, where the CBM project faces similar problems.

In the context of strangeness in heavy-ion reactions, the ϕ meson plays an important role, as it carries a strange quark pair but is strangeness-neutral as a hadron. At SPS energies, ϕ meson production is not well described by the statistical model [23], while HADES at SIS reports no deviation from the thermal fit. In contrast, the microscopic transport model UrQMD describes the ϕ yield at lower energies reasonably well, while it starts to fail a higher energies. The experimental situation at RHIC energies in unclear. At SPS, different yield were claimed to be observed in the hadronic and in the muonic decay channels [24]. Data from the Nuclotron, just above threshold, would be highly desirable for an understanding of these features. In the setup outlined above, the ϕ meson can be observed in its decay into charged hadrons. This also requires the selection of decay candidates by time-of-flight to reduce the combinatorial background, but the required precision of kaon identification is lower than for the measurements of direct kaons since the final identification of ϕ is done by invariant mass.

In summary, the production of strangeness at Nuclotron energies (up to 5.5AGeV incident beam energy) can be studied by a compact detector setup with magnet and tracking system. A time-of-flight detector with moderate size can extend the range of observables towards charged pions and kaons. Emphasis should be put on good coordinate resolution of the tracking system, large acceptance coverage and capabilities for high interaction rates to cover also the rare multi-strange hyperons and possible exotic states.

It should be noted that the experimental programme discussed above is in large parts concurrent to the planned activities of the CBM experiment, which will start taking data at the SIS-100 accelerator at beam energies from $2A$ to $10A$ GeV from 2018 on. However, the physics focus of CBM is the energy domain from $10A$ to $45A$ GeV to be covered by the SIS-300 synchroton in a later stage of the realisation of FAIR, whereas an experiment at the Nuclotron will be optimised to the specific energy range of this accelerator. The two activities hence provide complementary approaches to the study of high- density QCD matter.

12.4 Fixed target mode: correlations in relative 4-velocity space

V.A. Okorokov

National Research Nuclear University ?MEPhI?, Moscow, Russia

Investigation of a mixed phase associated with the transition from meson-nucleon to quark-gluon degrees of freedom is one of the hottest topics in the world program of research into the field of strong interactions. Experiments studying hadron interactions at intermediate energies may furnish important information about the emergence of new (color) degrees of freedom.

A relativistically invariant method was proposed in [25, 26] for studying collective effects in multiparticle production processes. Large experimental material for various interaction types was analyzed at intermediate energies (see, for example [27, 28]). In particular, in was observed that the values of mean square of soft jet size in 4-velocity space are significantly smaller for hadron-hadron reactions at $\sqrt{s} \sim 3$ GeV than those in other interactions at slightly higher energies. Moreover the energy dependence of mean kinetic energy of particles in the jet rest frame shows a sharp growth in a narrow interval of initial energies $\sqrt{s} \sim 3 - 5$ GeV with further smoother behavior [29]. The observations allow to assume that these effects may be due to the involvement of new degrees of freedom in the production of soft pion jets and to the respective transition from the description of these processes in terms of meson?nucleon degrees of freedom to the use of color (quark?gluon) degrees of freedom. But additional experimental investigations with high statistics and better particle identification are important for more detail study these effects at intermediate ener-gies.

In various realms of physics, the onset of manifestations of new degrees of freedom and transition processes is accompanied by the presence of self-affine and fractal effects in collective phenomena. In [30], it was proposed to study geometric properties of pion jets in the space of 4-velocities with the aid of the cluster dimension, which is determined by the relation between the number of particles in the jet and its radius in the relative 4-velocity space. For a number of the reactions investigated in the range $\sqrt{s} \sim 3-20$ GeV the cluster dimensions have fractional values, and this gives sufficient grounds to assume that pion jets have fractal properties [29]. Special features found in the energy dependence of cluster (fractal) dimension for hadron?hadron reactions are compatible with the qualitative assumption made above that new degrees of freedom arise in the region around $\sqrt{s} \sim 3 - 5$ GeV.

Thus, investigations of collective and geometric (fractal) properties in soft hadron reactions at intermediate energies $\sqrt{s} \sim 3 - 5$ GeV with high statistics at modernized Nuclotron can provide new important information about the hadronization mechanism, non-perturbative physics, and the way in which color degrees of freedom become operative in collective phenomena.

Bibliography

[1] C. Hartnack, R. K. Puri, J. Aichelin, J. Konopka, S. A. Bass, H. Stoecker and W. Greiner Eur. Phys. J. **A 1,** 151 (1998), [arXiv:nucl-th/9811015]

[2] J. Aichelin, Phys. Rep. **202,** 233 (1991).

[3] W. Cassing and E. L. Bratkovskaya, Phys. Rep. **308,** 65 (1999).

[4] S. A. Bass *et al.*, Progr. Part. Nucl. Phys. **41,**255 (1998); **41**, 225 (1998), [arXiv:nucl-th/9803035].

[5] G. A. Leksin, Yad Fiz. **65** 2042 (2002).

[6] V. A. Matveev, R. M. Muradyan and A. N. Tavkhelidze, Lett. Nuovo Cim. **7**, 719 (1973).

[7] S. J. Brodsky and G. R. Farrar, Phys. Rev. Lett. **31,** 1153 (1973).

[8] C. White *et al.*, Phys. Rev. **D 49,** 59 (1994).

[9] J. Napolitano, *et al.*, Phys. Rev. Lett. **61,** 2530 (1988); P. Rossi *et al.*, Phys. Rev. Lett. **94,** 012301 (2005).

[10] I. Pomerantz, Phys. Lett. **B 684,** 106 (2010).

[11] S.J. Brodsky *et al.*, Phys. Lett. **B 578,** 69 (2004).

[12] Yu.N. Uzikov, JETP Lett. **87** 387 (2005).

[13] Eds. A. N. Sissakian, V. V. Burov, A. I. Malakhov *Proc. of 18 Int. Baldin Seminar on High Energy Physics Problem* (Dubna, 25-30 Sept., 2006), V.I p.51.

[14] G. Bizard, J.L. Laville, C.Le Brun *et al.*, Phys. Rev. **C 22,** 1632 (1980).

[15] P. Koch, B. Müller and J. Rafelski, Phys. Rep. **142,** 167 (1986).

[16] E. Andersen *et al.*, Phys. Lett. **B 417,** 202 (1999).

[17] see e.g. F. Beccattini, J. Manninnen and M. Gadzdicki, Phys. Rev. C **73**, 044905 (2006).

[18] R. Stock, Phys. Lett. **B 456,** 277 (1999).

[19] P. Braun-Munzinger, C. Wetterich and J. Stachel, Phys. Lett. **B 596,** 61 (2004).

[20] A. Andronic *et al.*, Nucl. Phys. **A 837,** 65 (2010).

[21] A. Rustamov (HADES Collaboration), *Proceedings of the 6*$^{\text{th}}$ *International Workshop on "Critical Point and Onset of Deconfinement"*, (Dubna, Russia, August 22 - 28, 2010), to appear.

[22] J. Schaffner-Bielich, R. Matiello and H. Sorge, Phys. Rev. Lett. **84,** 4305 (2000).

[23] C. Alt *et al.*, Phys. Rev. **C 78,** 044907 (2008).

[24] B. Alessandro *et al.*, Phys. Lett. **B 555,** 147 (2003).

[25] A. M. Baldin, Sov. Phys. Dokl. **20**, 418 (1975).

[26] A. M. Baldin, Sov. Phys. Dokl. **29**, 1031 (1984).

[27] A. M. Baldin and L. A. Didenko, Fortschr. Phys. **38**, 261 (1990).

[28] V. I. Mikhailichenko *et al.*, Phys. At. Nucl. **62**, 1665 (1999).

[29] V. A. Okorokov *et al.*, Phys. At. Nucl. **73**, 1963 (2010).

[30] V. A. Okorokov *et al.*, *Proceedings of the Scientific Session MEPhI-2000*, MEPhI. V.7, 218 (2000); ibid 220.